Imperial College
OF SCIENCE, TECHNOLOGY AND MEDICINE


UNIVERSITY OF LONDON

# DESIGN AND TESTING OF A HIGH PRESSURE CHAMBER FOR DIESEL SPRAY STUDIES

By

**NIALL McGLASHAN**

Thesis submitted for the degree of
Doctor of Philosophy
in the University of London

September, 1997

# ABSTRACT

The thesis describes in detail the design, manufacture and testing of a novel combustion chamber for Diesel spray studies. The chamber consists of a cylindrical pressure vessel capable of withstanding the high pressures and temperatures present in Diesel engine combustion chambers. By supplying high pressure gas to this chamber from a compressor and heating the gas as it enters the chamber, the thermodynamic conditions found within a Diesel engine can be reproduced. The chamber has optical access, allowing laser diagnostic techniques to be applied to a Diesel spray injected into the chamber.

A second part of the thesis describes the calibration of three different Diesel pumps; a Lucas DPC, a Bosch MW and a Bosch EPVE. A further subsection describes the design, construction and testing of a skip-firing valve that enables single shot injections to be produced. This valve is necessary for future studies on vaporising and combusting sprays.

Testing of the chamber was performed by investigating the structure of the sprays generated by two fuel injection systems based on in-line pumps. This was achieved by using Phase Doppler Anemometry to measure diameter and velocity of the droplets in the spray, and imaging to examine the spray's cone angle and tip penetration. Parameters investigated included, pump speed, load and chamber pressure.

# ACKNOWLEDGEMENTS.

Firstly I would like to thank my supervisor, Professor Dinos Arcoumanis, for his constant support during the whole of my PhD. In particular, he has supported an extensive project, at considerable expense and over a long period, with little or no external financial support.

I would like to thank Dr Shaun Crofton, who gave me a great deal of technical support during the design stages of the combustion chamber and also for the pragmatic advice that he has given me on many other matters.

Perkins Technology Ltd., have given me support both financially and with equipment during the last stage of the PhD. I would particularly like to thank Dr Nigel McKinley for his help and advice during this time.

Many members of the Thermofluids section, have helped me during the last four years, but in particular may I thank the following for their time and patience: Paul Bruni, Yong-Seok Choi, Dr Paul Cutter, Marek Duszynski, Alan Finch, Harminder Flora, Fred Hall, Dr Andy Heyes, John Laker, Phil Proctor and Ian Wright.

I would also like to thank the various members of the technical staff in the college who have aided me, particularly with the construction of the combustion chamber, specifically: Bob Gammond, John Gavin, Barry Jasjew, Chris Jerrard, Dave Lincoln, Alex Noorbhai, John Pickett, Chris Stafford and Glen Wallington.

Lastly I would like to thank my mother and father for their continuous support over the last four years, without which I could not have completed the PhD.

# TABLE OF CONTENTS.

# LIST OF FIGURES

# LIST OF PLATES

# LIST OF TABLES

# NOMENCLATURE

## ABBREVIATIONS

| | |
|---|---|
| ASI | [Time] After Start of Injection. |
| CD | Coefficient of Discharge. |
| CN | Cavitation Number. |
| DI | Direct Injection |
| LDA | Laser Doppler Anemometry. |
| PDA | Phase Doppler Anemometry. |
| SMD | Sauter Mean Diameter. |
| VCO | Valve Covered Orifice. |

## ROMAN SYMBOLS

| | |
|---|---|
| d | Diameter (μm). |
| n | Exponent used in spray cone angle prediction. |
| K | Constant used in spray cone angle prediction.. |
| P | Pressure (bar). |
| R | Radius of window (mm) |
| r | Distance right of spray's centre line. |
| S | Spray tip penetration (mm). |
| V | Radial velocity of droplets at nozzle exit (m/s). |
| t | Time (ms). |
| x | Thickness of window (mm) |
| Z | Distance from nozzle (mm). |

## GREEK SYMBOLS

| | |
|---|---|
| $\theta$ | Cone angle (°). |
| $\rho$ | Density (kg /m$^3$). |
| $\sigma$ | Stress (MPa). |

## SUBSCRIPTS

| | |
|---|---|
| cha | Chamber. |
| f | Fluid. |
| Inj | Injection. |
| Max | Maximum. |
| o | Nozzle hole. |
| Vap | Vapour. |

# CHAPTER 1

# INTRODUCTION AND LITERATURE SURVEY

## 1.1 INTRODUCTION.

Reducing Diesel engine exhaust emissions has become a major issue in recent years with the mounting scientific evidence of the harm being done, particularly to the local environment, by Diesel engines. Of particular importance is the possibility that particulate emissions from Diesels have contributed to the increased instance of respiratory disorders among city dwellers, especially the young and elderly. Although the absolute responsibility of Diesel engines for this problem is, to say the least, questionable, it is unfortunately politically convenient to blame the Diesel for what is really the wider problem of societies excessive consumption. For this reason our legislators are producing stricter and stricter emissions targets. Whatever the logic behind these regulations, pragmatically they have to be considered as a fact of life by the engine industry and complied with.

Fortunately the imposition of these regulations has occurred at a fortuitous time for the industry. With the advent of laser diagnostic techniques and computational fluid dynamics in the last twenty years, it has become possible, for the first time, for a detailed and fundamental analysis to be made of the processes occurring inside the engine combustion chamber. With this improved understanding, at least in principle, cleaner engines can be designed. This is the hope of the industry and explains the increased research activity in this area in recent years.

There is of course the possibility that there is a finite limit to the improvements that can be made in the cylinder no matter how well we understand the processes. Because of this, post exhaust valve solutions, such as catalysts and traps, were introduced to reduce engine emissions. Nonetheless knowledge has to be better than ignorance.

What then are the areas of interest in a Diesel engine? The least well understood aspect is probably the fuel atomisation process. Spray atomisation undoubtedly has a strong influence on the subsequent mixing and combustion processes which occur inside the chamber. Perhaps more fundamentally, from an engineering perspective, it is one area where by changing certain design parameters of the injection system the engine designer can have a significant influence on the spray atomisation and hence the subsequent combustion, which determines the performance of the engine. Unfortunately for engine designers, though there are numerous models of fuel atomisation none of them can be said to give a satisfactory explanation of Diesel spray break-up.

However, it would be naive to think that this was the limit of our ignorance. The enormously complex four dimensional nature of Diesel combustion makes mathematical modelling exceptionally difficult, even well away from the atomisation region. For modelling to be at all practical, an extensive database of all of the various parameters of Diesel combustion and spray break-up needs to be established. This will entail the work of numerous researchers over a number of years.

How and what are these researchers going to measure? The pragmatic answer is everything which helps our understanding of the engine. This will include all aspects of fuel vaporisation and oxidation, fuel-air mixing and combustion, including soot formation and oxidation, but more crucially the initial spray characteristics which is the main determinant of combustion. The characteristics of a particular spray can be reduced to a map in space and time of droplet size and velocity and, if possible, liquid flux.

All of these various measurements have only become possible due to the advent of laser diagnostics. A description of the different methods is outside the scope of this thesis. There is, however, one common aspect to optical techniques, namely the need for specialised 'optical' measuring equipment.

## 1.2 ATMOSPHERIC EXPERIMENTS AND OPTICAL ENGINES.

The simplest form of experimental set up is an atmospheric rig, where the Diesel spray is injected into open air [*Arcoumanis and Cutter,* 1995]. Optical access is essentially unlimited as there are no windows, cylinder liners, pistons etc. to obstruct the view of the spray, see Figure 1.1. The technique is also relatively cheap in comparison to the more sophisticated constant volume combustion chambers and optical engines. Atmospheric experiments are therefore popular methods of studying spray characteristics, though are obviously less useful for combustion work. And because of the unrestricted access, all of the available optical techniques are applicable. The main problem however, is the lack of realistic 'combustion chamber' conditions, and in particular the low gas densities. Gas density in the combustion chamber is an important factor in the atomisation and break-up of the spray. Atmospheric experiments should not, however, be dismissed as being wholly unrealistic, as much has been learned from them. And with their unlimited optical access, atmospheric experiments are often the only feasible method for investigating sprays when using some optical techniques.

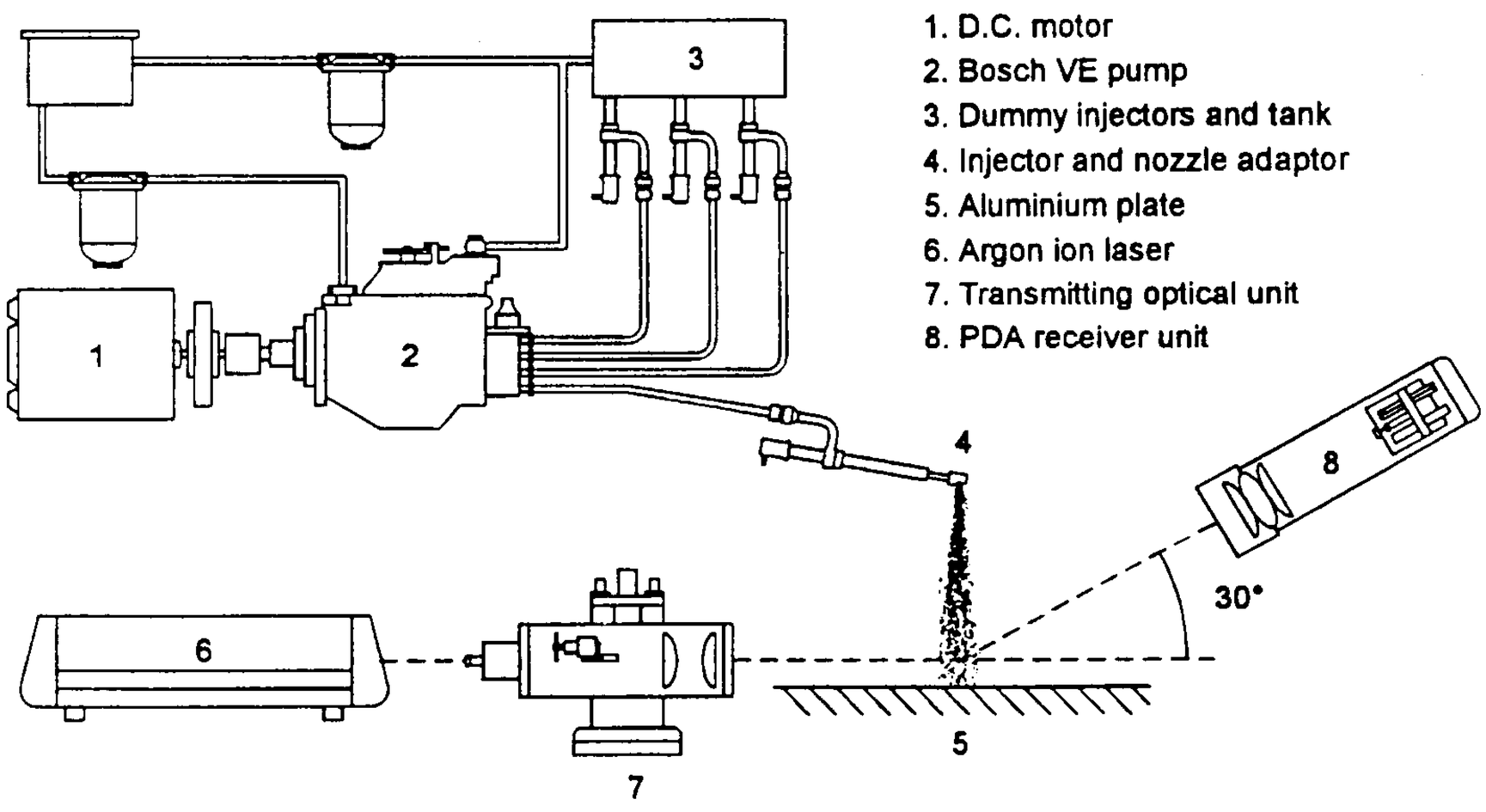


**Fig 1.1** Typical atmospheric set-up for PDA studies of spray surface interaction. [*Arcoumanis and Cutter,* 1995]

Clearly atmospheric tests have their limitations and it is for this reason that engine experiments are desirable. With these there is, however, the obvious problem of optical access, there being no readily available optical path into the combustion chamber of a production engine. The optical engine, which has been more or less perfected in recent years, remains the solution [*Arcoumanis,* 1994] despite its disadvantage of causing some modifications to the engine geometry.

Optical engines, it could be said, are as old as the internal combustion engine itself. The first practical engine, patented by Street in 1794 [*Wrangham,* 1960], had manual ignition, an operator opened a side hatch and ignited a vaporised mixture of turpentine and air with a taper, the hatch was closed and the cycle proceeded much as

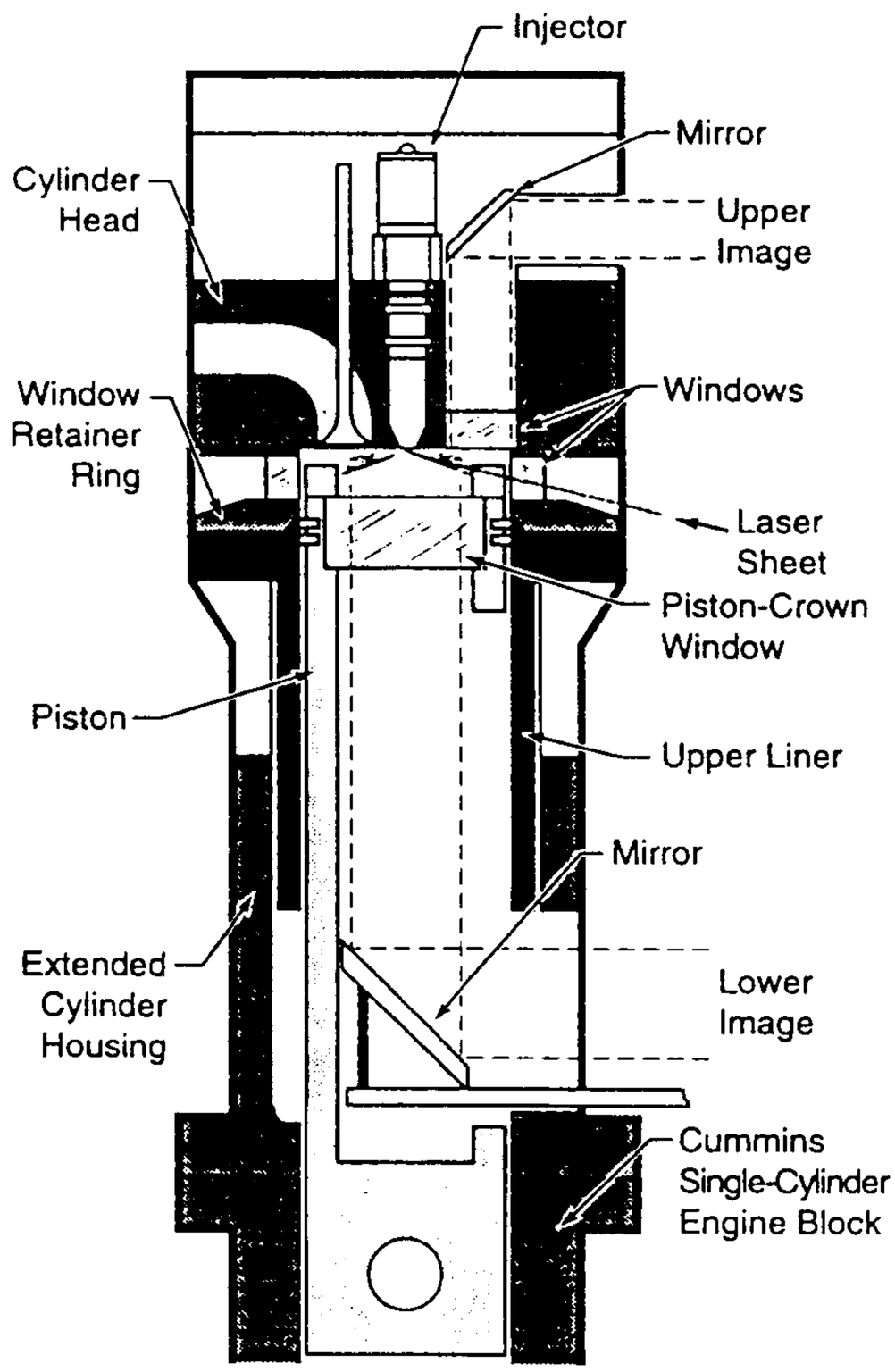


**Fig 1.2** Picture of optical engine showing windows in piston bowl, cylinder head and cylinder liner [*Dec and Espey,* 1995]

with the much later Lenoir engine. It seems plausible that the operator might have delayed closing the hatch and observed the combustion merely to satisfy his curiosity. Modern optical engines and experimental techniques are clearly more sophisticated than this early primitive device, but the need to satisfy Man's curiosity remains.

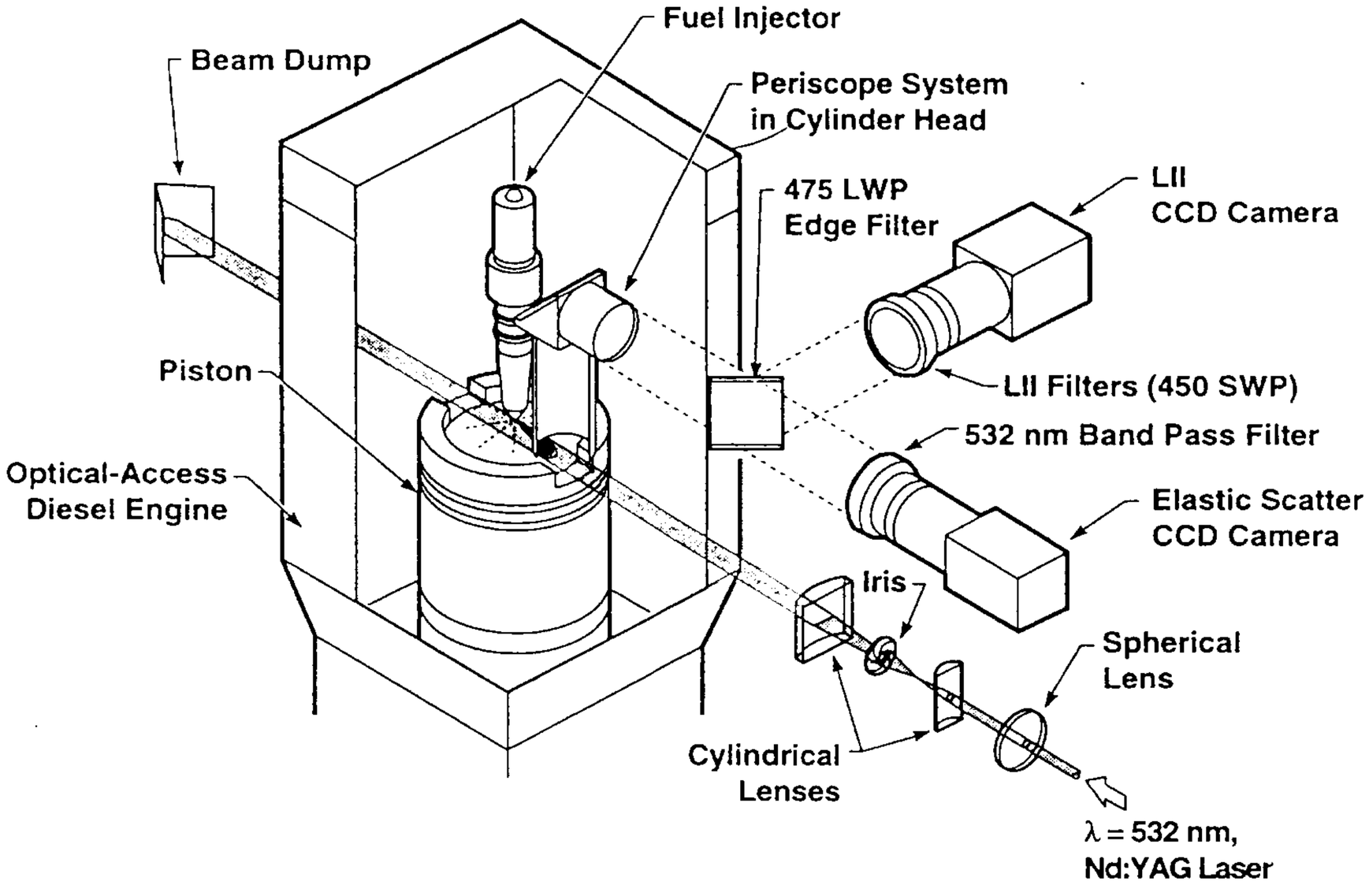


**Fig 1.3** Pictorial view of optical engine showing set-up for simultaneous laser induced incandescence and elastic scatter imaging, with the laser sheet passing through the side windows and the images being taken through the cylinder head window. The use of cut-outs in the top of the piston crown for the laser sheet is also shown [*Dec and Espey,* 1995]

Optical engines today typically have three types of optical access, side windows mounted at the top of the cylinder which allow a view at right angles to the cylinder axis, piston crown windows which view along the cylinders axis, which requires the addition of a mirror and extended pistons, much like in a periscope, and lastly cylinder head windows which also view along the axis, these can either be relatively small additions to one side of the cylinder, or, if inlet and exhaust ports or formed in the liner as in a two stroke engine, can extend right across the cylinder

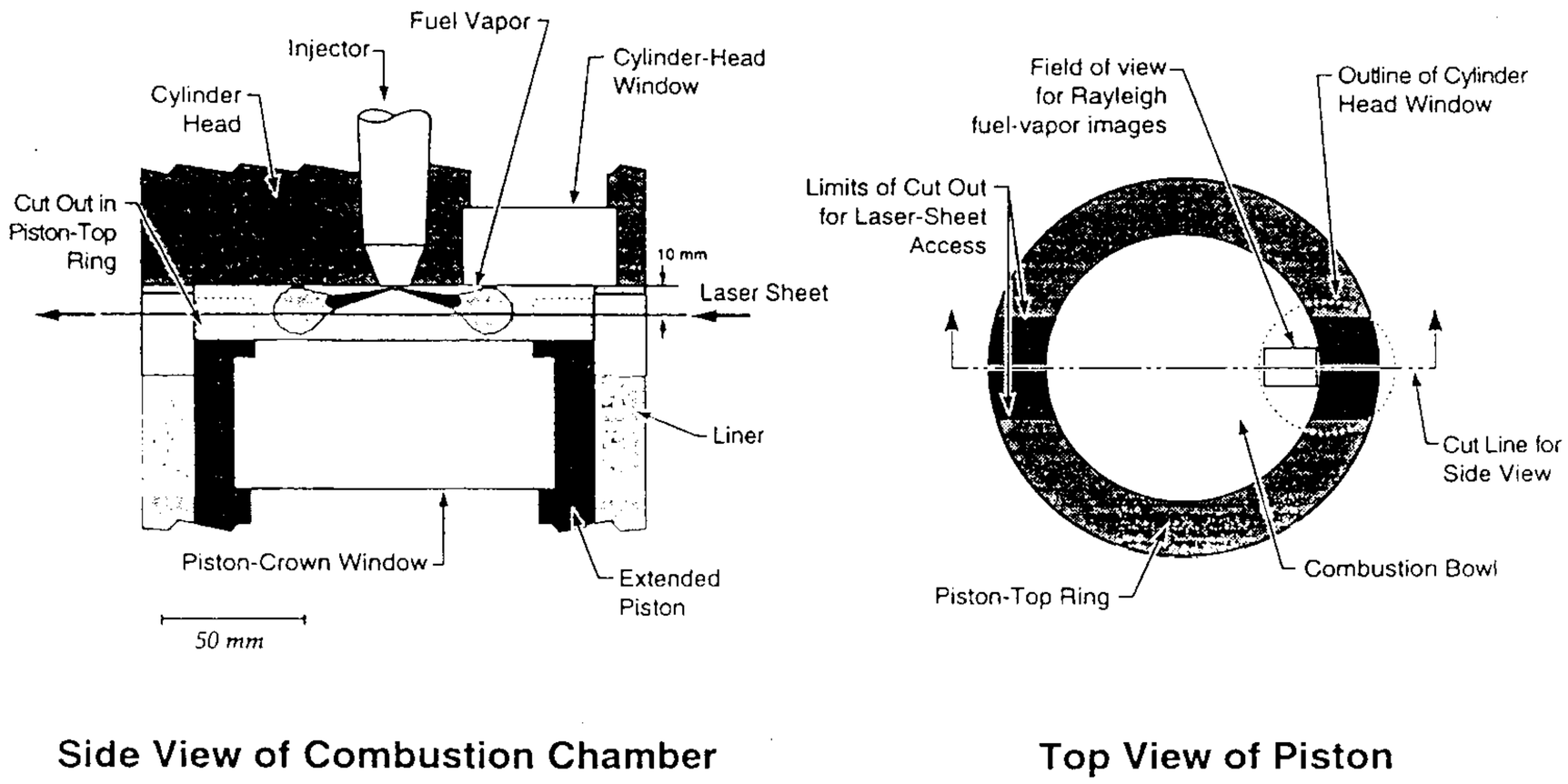


**Fig 1.4** Cross section of optical engine with piston crown cut-outs to allow side access. Cylinder head and piston crown windows and their field of view are also shown. [*Dec and Espey,* 1995]

giving very good optical access. All of these window types are shown in a cross section of a typical optical engine in Figure 1.2, while Figure 1.3 shows the same engine with a typical experimental set-up using the side and cylinder head windows.

Optical engines are the preferred method in engine research when realism of the flow field is important. One might argue that realism is always required, the problem is that it comes at a price of poor optical access, mechanical complexity, vibration and financial expense. Optical access from the side in particular is often limited at TDC where the piston obscures the side windows view of the combustion chamber, although an unimpeded view of the combustion chamber is still available throughout the head or piston crown window, many optical techniques (any laser sheet method) need side access as well. This difficulty can be partly overcome by either slots in the piston bowl rim (see Figure 1.4), or small windows in the side of the piston which line up with the side windows at TDC. Both of these methods still have a limited degree of optical access and have a definite effect on the flow field within the piston bowl. To overcome this difficulty optical engines with completely transparent piston bowls have been constructed which may be used in engines with or without transparent liners, the one problem with this type, apart from their cost, is that if the piston bowl has a shape similar to a production engine then there is likely to be

a great deal of distortion of light travelling through the piston crown. This may not be a problem if a short parallel portion of the piston bowl can be arranged, which is particularly useful if laser sheet methods are used.

The most advanced type of optical engines have a completely transparent cylinder liner [*Bates,* 1988; *Richman and Reynolds,* 1984]. Although these liners allow excellent optical access they are expensive and fragile, and therefore the engines are often limited to non-combustion studies. This is especially true in Diesel research where the pressures and temperatures during combustion would impose very high mechanical and thermal stresses on such a liner. There is also the risk of the liner being scratched by the piston rings, which eventually may lead to failure and more so because optical engines usually employ 'dry' lubrication. An additional problem is that the piston may still obscure the piston bowl at TDC and hence piston cut-outs, piston windows or transparent piston crowns are still needed in the piston.

Optical engines are also inflexible as parameters like compression ratio, swirl number, injector type cannot be altered easily, as often the whole cylinder head needs to be changed. This is both expensive and laborious and only a limited number of different conditions can be tried. A further disadvantage is the often tedious exercise of window cleaning as it is difficult to design an easily cleaned optical engine. One last difficulty is that optical engines do not allow studies of the spray to be made without combustion, as once auto-ignition has taken place observation of spray development is difficult with the available optical techniques due to light obscuration or window fouling; such studies are desirable if a full investigation of spray break-up and fuel vaporisation is to be made.

## 1.3 CONSTANT-VOLUME CHAMBERS.

It might be thought that with optical engines and atmospheric test rigs the full range of experiments would be possible. This is untrue, as both have serious limitations which are not necessarily solved by each other. What is required is a third device which bridges between the two, having the versatility and optical access of an

atmospheric rig but with the realistic gas densities and flow field of an optical engine. The constant volume combustion chamber neatly fits this specification.

A combustion chamber consists in its simplest form of a sealed pressure vessel into which high pressure gas can be introduced. For Diesel work, an injector is fitted and windows are placed in different positions to allow for various optical techniques. Experiments consist of a sequence of filling the chamber to a particular pressure, then injecting a certain quantity of fuel. Depending on the optical technique being used data is acquired during this period. The sequence is repeated many times so that sufficient data for statistical purposes can be collected. This may be a few cycles or perhaps many hundreds depending on the optical technique being used. This describes the simplest form of chamber and with suitable design, semi-continuous operation can be achieved.

The principle advantage of constant-volume combustion chambers over the alternative atmospheric test rigs and optical engines is that realistic gas conditions can be achieved but with very good optical access. Unfortunately combustion chambers are expensive as they often have to be purpose built within research laboratories and can require a great deal of auxiliary equipment such as compressors, air heaters etc. Since these are not off-the-shelf items, there is a natural reluctance to invest time and money in new untried equipment and this has limited their more widespread adoption.

Before starting the design of the chamber, a review of existing design practices was undertaken. A summary of the various combustion and pressure chambers being used around the world is given in Table 1.1. This table is not exhaustive but includes chambers representative of each of the different types. In general, there are three types of pressure chamber: rapid compression machines, single shot and continuous flow. These will be described in the first section of this chapter.

The rapid compression machine can be seen as a compromise between the optical engine and the constant-volume chamber and consists of a long cylinder fitted with a piston. The piston can be driven, usually by a pneumatic cylinder, compressing the charge into a combustion space at the end of the cylinder, much as in an engine. At first sight there seems to be no advantage over an optical engine, indeed as the device is only capable of one compression stroke at a time, the frequency of experiments is much more limited than in an optical engine. The main advantage lies

| Paper. | Authors. | Chamber Type. | Max. Press. (bar). | Max. Temp. Prior to Combustion (°C). | Window Cleaning Arrangement. | Flow Field. | Optical Technique Used. | Remarks. |
|---|---|---|---|---|---|---|---|---|
| *"Air Fuel Ratio Visualisation in a Diesel Spray"*, Paper presented winter annual meeting of ASME, 1993. | K. D. Carabell, P. V. Farrell. | Rapid Cycling Machine. | 100 | 700 | Window removed by unscrewing flange retaining bolts. | Swirling. | Imaging - Laser Induced Fluorescence. | The chamber is fitted to the side of a large single cylinder engine, which simply acts as a pump; the chamber is rather like a Ricardo swirl chamber, fitted to the side of the engine. Operation is therefore continuous until window fouling occurs. |
| *"High-Speed Photography of Fuel Spray and Combustion Events in a Production Diesel Engine and Combustion Bomb"*, Proc. I.Mech.E., Vol. 203, pp 269, 1989. | E. R. Karimi. | Single Shot. | 55 | 600 | Windows removed by unscrewing retaining ring. | Swirling or quiescent. | Imaging of fuel spray with combustion. | Chamber is filled from a high pressure bottle and then heated internally by electrical heaters. To simulate swirl a drum within the chamber can be rotated before the experiment, to 'spin' the air charge. |
| *"Design of Combustion Bomb used for High Resolution Photography of Diesel Sprays"*, Royal Institute of Technology. | M. Hallberg, H-E. Ångström. | Single Shot. | 200 | 730 | Window in housing is unscrewed from chamber as one complete unit. | Quiescent. | Imaging of combusting spray. | Gas from high pressure bottles is admitted to the chamber by a manually actuated valve. There is no air heating. |
| This Thesis. | N. R. McGlashan. | Continuous Flow. | 100 | 800 | Breech loading mechanism - head window is withdrawn in holder. | Quiescent, swirling or turbulent. | Imaging and droplet sizing with and without combustion. | The chamber is fed with pressurised air from compressor which is heated prior to entry into chamber. The tubing and the chamber itself are lined with ceramic to reduce heat losses. Optical access is provided specifically for PDA with a scattering angle of 70°. |
| *"Effects of Gas Density and Vaporisation on Penetration and Dispersion of Diesel Sprays"*, SAE 960034. | J. D. Naber, D. L. Siebers. | Single Shot. | 350 | 250 | Windows removed by unscrewing retaining ring. | Quiescent. | Imaging and Schlieren Shadowgraphy. | The chamber is filled with an inert gas mixture from high pressure bottles. |
| *"The Design and Operation of a High-Pressure Combustion System for Study of Soot Formation"*, SAE 922206. | M. A. A. Nazha, R. J. Crookes. | Rapid Compression Machine. | 100 | 825 | Not stated. | Quiescent, cross flow or turbulent | Not stated. | The chamber consists of a long tube made up from sections, the number of which can be selected to suit the experiment. Air is delivered to the chamber from a high pressure receiver charged from a compressor. |

**Table 1.1** Table of optical and experimental rigs reported in the literature.

| Paper | Authors | Chamber Type | Max. Press. (bar). | Max. Temp Prior to Combustion. (°C) | Window Cleaning arrangement. | Flow Field | Optical Technique Used. | Remarks. |
|---|---|---|---|---|---|---|---|---|
| *"A Diesel Combustion Bomb: Proof of Concept"*, SAE 841358. | D. C. Oren, S. Wahiduzzaman, C. R. Ferguson. | Single Shot. | | | Four air actuated clamping pistons hold the window flange in place. These can be quickly unscrewed once de-pressurised. | Quiescent. | Combustion studies. | The combustion bomb is heated up to 200°C prior to the experiment by electrical heaters. End of compression temperatures are achieved by combustion of an air-acetylene mixture in the chamber. |
| *"Velocity and Dropsize Measurements in Fuel Sprays in a Direct Injection Diesel Engine"*, International Symposium on LDA, 1994. | G. Pitcher, G. Wigley. | Rapid Cycling Machine. | 56 | N/A | Windows removed by unscrewing retaining ring. | Quiescent. | Droplet velocity and size measurements on combusting spray - PDA. | The chamber is fitted on top of Single cylinder engine much like a top hat combustion chamber. Good optical access is achieved through side windows which are not obscured by the piston at TDC. |
| *"Two Component Velocity and Size Measurements for a Non-Combusting Fuel Spray in a Diesel Swirl Combustion Chamber"*, Sixth International Conference on Liquid Spray Atomisation and Spray Systems, 18-22 July., 1994. | G. Pitcher, G. Wigley. | Rapid Cycling Machine. | 58 | N/A | Windows removed by unscrewing retaining ring. | Swirling. Tangential velocities of 30 M/s are possible. | Droplet velocity and size measurements on non-combusting spray - PDA. | As for the Carabell/Farrell chamber the bomb is fitted to the side of a large single cylinder engine. Optical access is designed to enable PDA measurements using a scattering angle of 70°. |
| *"Effects of Ambient Gas Conditions and Turbulence on Vaporising Sprays"*, GM. Research, Fluid Mechanics Dept., January 28, 1988. | R. D. Reitz. | Continuous Flow Spray Tunnel. | 250 | 830 | | Cross flow with varying amounts of turbulence | Droplet velocity and size measurements on combusting spray - PDA. | High pressure air from a compressor is supplied to the chamber (tube) through a gas fired heat exchanger. A catalytic converter on the exit oxidises any unburned fuel to avoid atmospheric pollution. |
| *"Spray Structure of Automotive Injectors"*, International Symposium on advanced Spray Combustion, July 6-8, Hiroshima, Japan, 1994. | G. Renner, R. R. Maly. | Single Shot. | 60 | N/A | Window retaining flange is removed after unscrewing flange retaining bolts. | Quiescent. | Imaging - Laser Shadowgraphy. | The chamber is Nitrogen filled and of sufficient volume to allow a number of single shot injections before cleaning is necessary. |

**Table 1.1** (cont.)

| Paper | Authors | Chamber Type | Max. Press. (bar). | Max. Temp Prior to Combustion. (°C) | Window Cleaning arrangement. | Flow Field | Optical Technique Used. | Remarks. |
|---|---|---|---|---|---|---|---|---|
| *"Pressure Chamber Experiments for Fuel Spray Model Development"*, Report to the European Energy Commission, 1988. | Th. Schmidt, W. Esser-Schmittmann, P. Roosen, E. Hassel, H. Xu, U. Reuter, E. Scheid. | Continuous Flow. | 60 | 650 | Window retaining flange is removed after unscrewing flange retaining bolts. | Quiescent or cross flow. | Imaging of spray with and without combustion - Schlieren Shadowgraphy. | A continuous flow of air is supplied to the chamber through an electrical heater. The tubing and the chamber itself are lined with ceramic to reduce heat losses. |
| *"Temperature Effects on Fuel Sprays from a Multi-Hole Nozzle Injector"*, SAE 962005. | C. B. Warrick, T. S. Su, P. V. Farrell. | Rapid Cycling Machine. | 100 | 330 | Window in housing is unscrewed from chamber as one complete unit. | Swirling. | Imaging with and without combustion. | As for the Carabell/Farrell chamber the bomb is fitted to the side of a single cylinder engine. The chamber can be operated as a single shot chamber, if cold non-combustion studies are required, by feeding the chamber with gas from high pressure bottles with the engine piston at TDC.. |

**Table 1.1** (cont.)

in the much improved optical access and the increased flexibility. More specifically parameters like the end of compression temperature and pressure can be varied by adjusting the pressure and temperature of the initial charge in the cylinder and possibly the stroke. Also the 'cylinder head' can be changed easily as there is no valve gear. This enables not just different combustion chamber shapes to be examined but also heads with different optical access. Figure 1.5 shows a schematic of a typical example of a rapid compression machine [*Rife and Heywood,* 1974].

There are a number of disadvantages of the rapid compression machine, principally it is a single shot device, that is capable of producing only one injection at a time. This has two main consequences. Firstly the frequency of experiments is low; this is not important for many of the imaging techniques for which rapid compression

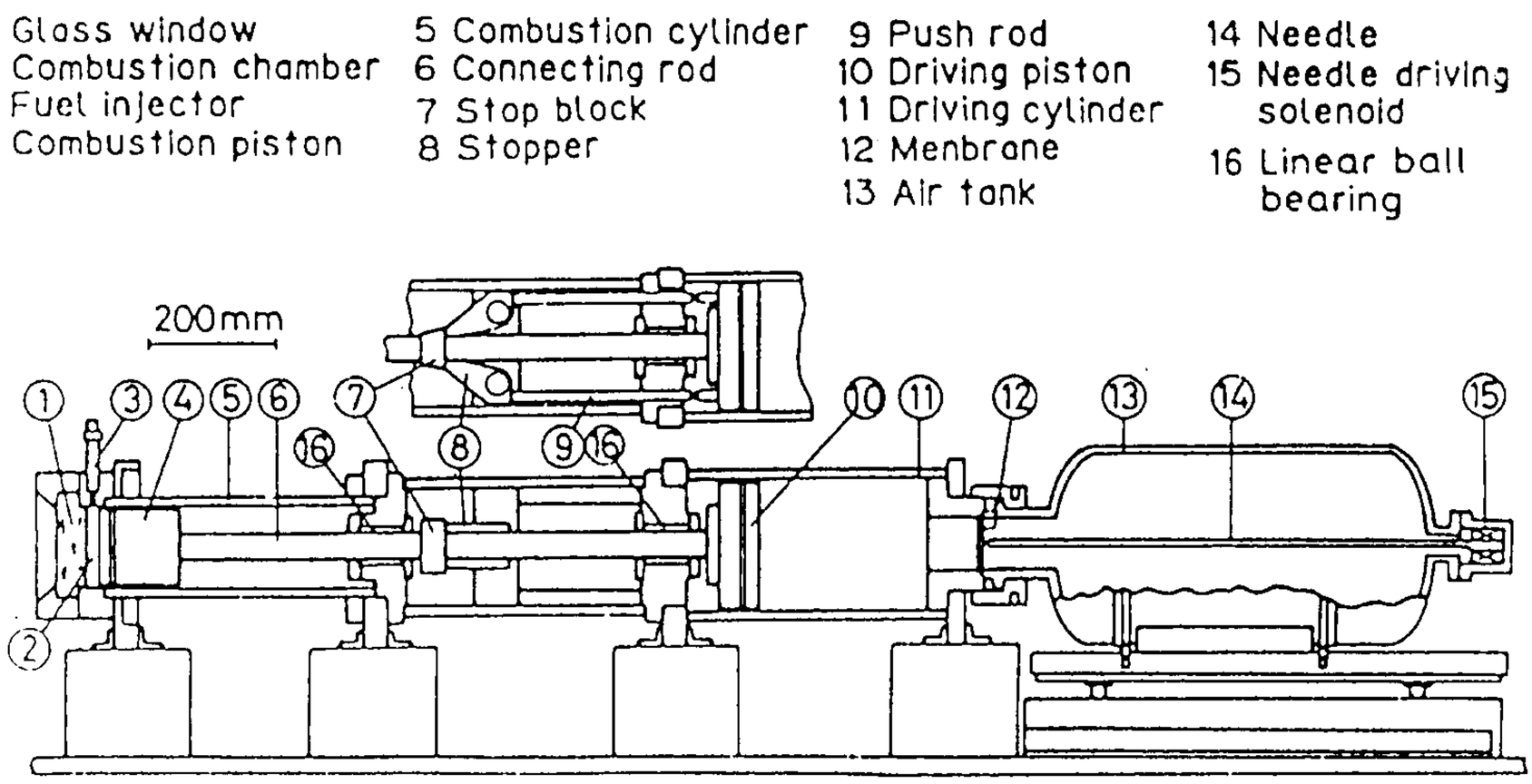


**Fig 1.5** Rapid compression machine [*Rife and Heywood,* 1974]

machines are used extensively, however, for PDA and LDA many hundreds or even thousands of cycles are required at a number of different grid points. To complete such a test matrix in a rapid compression machine would be impractical. Secondly because the gas is quiescent at the start of compression, it is difficult to reproduce realistic flow fields in the combustion chamber. This is not necessarily a major

disadvantage, as for many of the more fundamental investigations quiescent conditions are more than adequate. However, the ability to produce realistic flow fields has to be a feature of any optical chamber.

The single shot chamber can be seen as a further development of the rapid compression machine, even though it existed before the latter. Like a rapid compression machine there is a combustion chamber with extensive optical access, the difference lies in the method by which high pressure gas is introduced. Rather than having a dedicated piston and cylinder to compress the gas into the chamber, gas is introduced from an external supply. Single shot chambers consist of a sealed pressure vessel into which a charge of high pressure gas is admitted through some type of fast acting valve, for example see Figure 1.6 from *Oren et al* [1984]. A single injection is then admitted into the chamber and, depending on the technique used, measurements are taken of this spray. The gas is typically supplied from a high pressure gas cylinder and may be air or an inert gas of some kind. The gas may also be heated before its entry into the chamber if studies of combustion or fuel vaporisation are required.

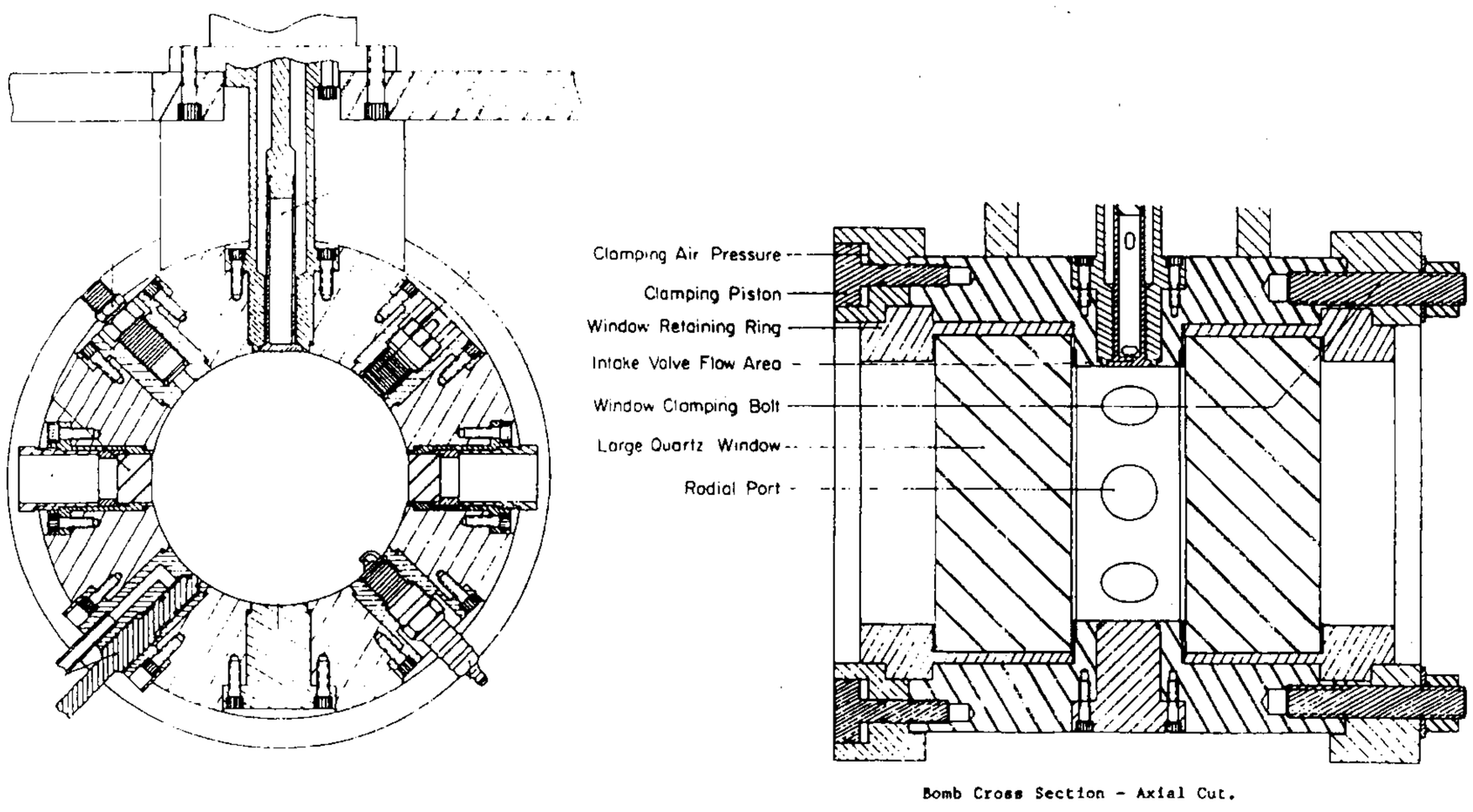


**Fig 1.6** Single shot constant-volume combustion chamber [*Oren et al,* 1984]

Fundamentally there is little difference between the rapid compression machine and a single shot chamber. Just as with a rapid compression machine, the chamber has to be evacuated and cleaned before another experiment can take place and there are the same limitations on the flow field. The difference between the two is an engineering difference, namely the means by which high pressure gas is charged into the combustion space. As far as the optical experimentalist is concerned, they are almost identical in the scope of experiments that can be undertaken.

Continuous flow chambers are different from both of the above in that the pressurised gas flows through the chamber continuously, purging the chamber of unburned fuel or combustion products and allowing experiments to continue over a long period. In their simplest form they consist of a long pipe through which pressurised gas flows [*Reitz,* 1988; *Nazha and Crookes*, 1992]; windows are fitted into the side of the pipe at appropriate positions for spray characterisation with the injector being fitted opposite the windows and a typical example is shown in Figures 1.7 and 1.8. The principle of operation can be seen from the schematic; air from a high

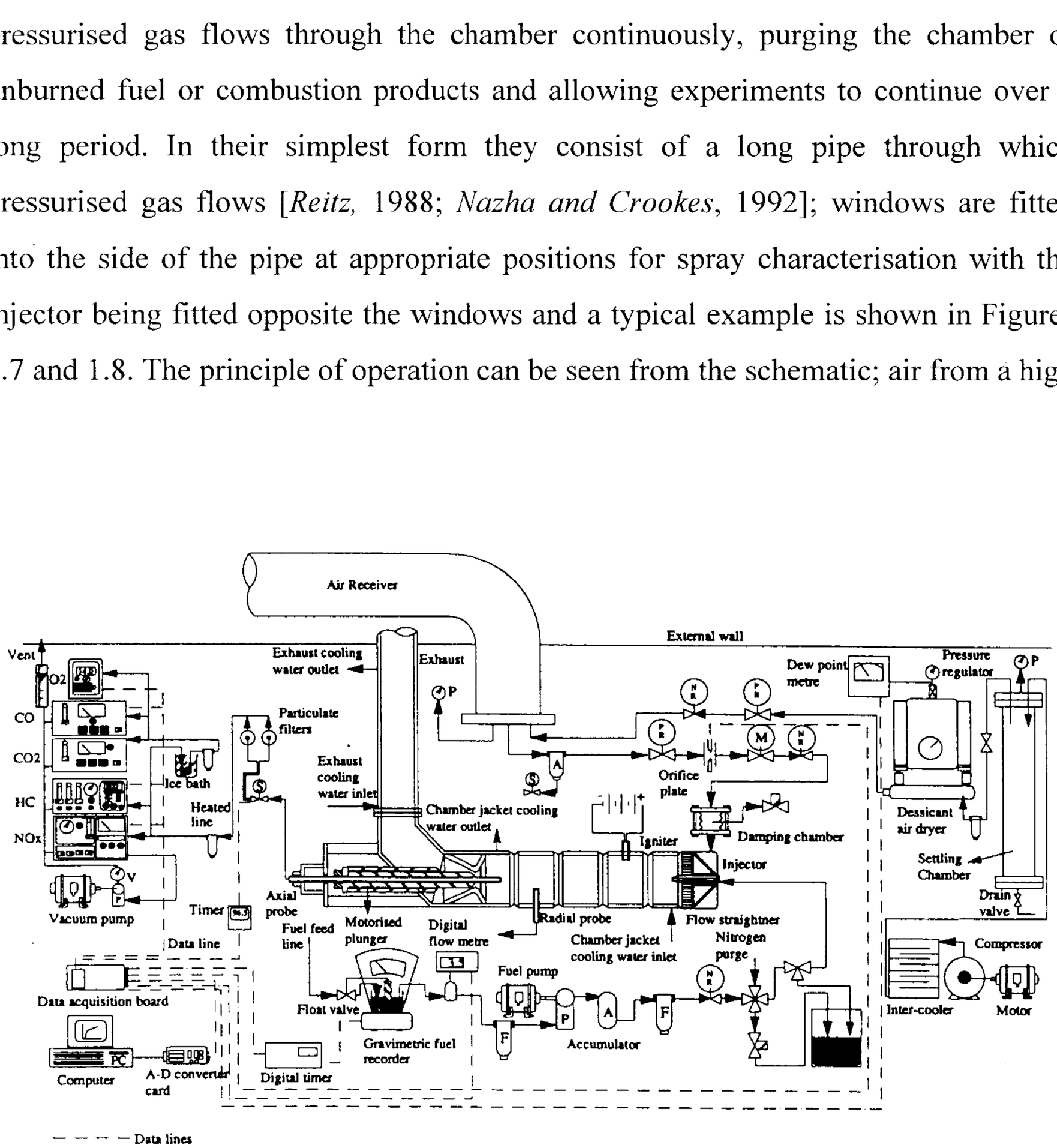


**Fig 1.7** Schematic layout of high-pressure steady-state combustion installation. [*Nazha and Crookes,* 1992].

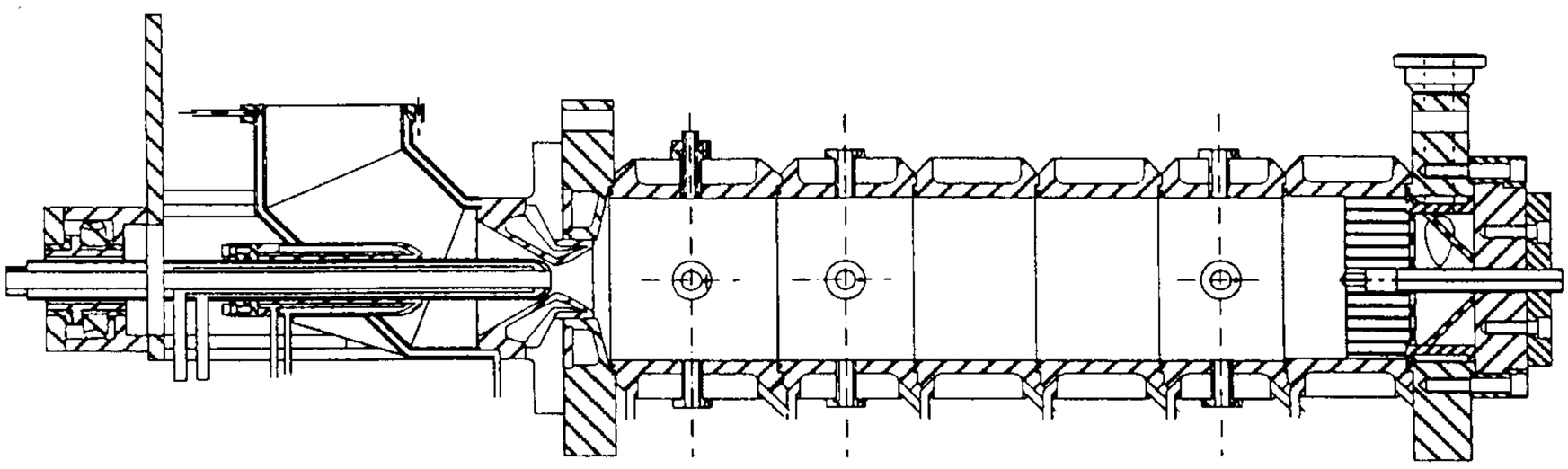

**Fig 1.8** Cross section of high-pressure combustion chamber. [*Nazha and Crookes,* 1992]

pressure receiver is admitted to the chamber through a reducing valve which, along with a reducing valve on the outlet, can be adjusted to give a range of chamber pressures. In the diagram the air stream passes through a 'flow straightener', but different flow fields (such as swirl) can be produced by using ducts and baffles. A hydraulic pump pressurises fuel which is sprayed into the air stream continually from the injector shown. For combustion studies an ignitor is used to initiate combustion and the fuel then burns much like in a gas turbine combustion chamber. Optical access is gained through windows in the removable sections which make up the body of the chamber, though none are shown in the figures. This specific chamber is designed principally for a steady-state flame, but could be adapted for Diesel spray studies if required. The major disadvantage with chambers of this type is that their combustion chamber does not resemble that of a real engine, however, they give good optical access and the Diesel pump can be run at realistic speeds as the scavenging can be quite efficient.

Figure 1.9 [*Schmidt et al,* 1988] describes a particularly advanced version of the continuous flow chamber that is used widely in Germany, with several chambers of similar design based at Aachen University. The design is compact and allows a variety of optical techniques to be used, including phase Doppler anemometry (PDA), but there are two major drawbacks. Firstly the flow field is unrealistic and unable to represent the swirl velocities and turbulence levels present in Diesel engines; in many cases levels are low enough for the flow to be assumed to be quiescent. This may not

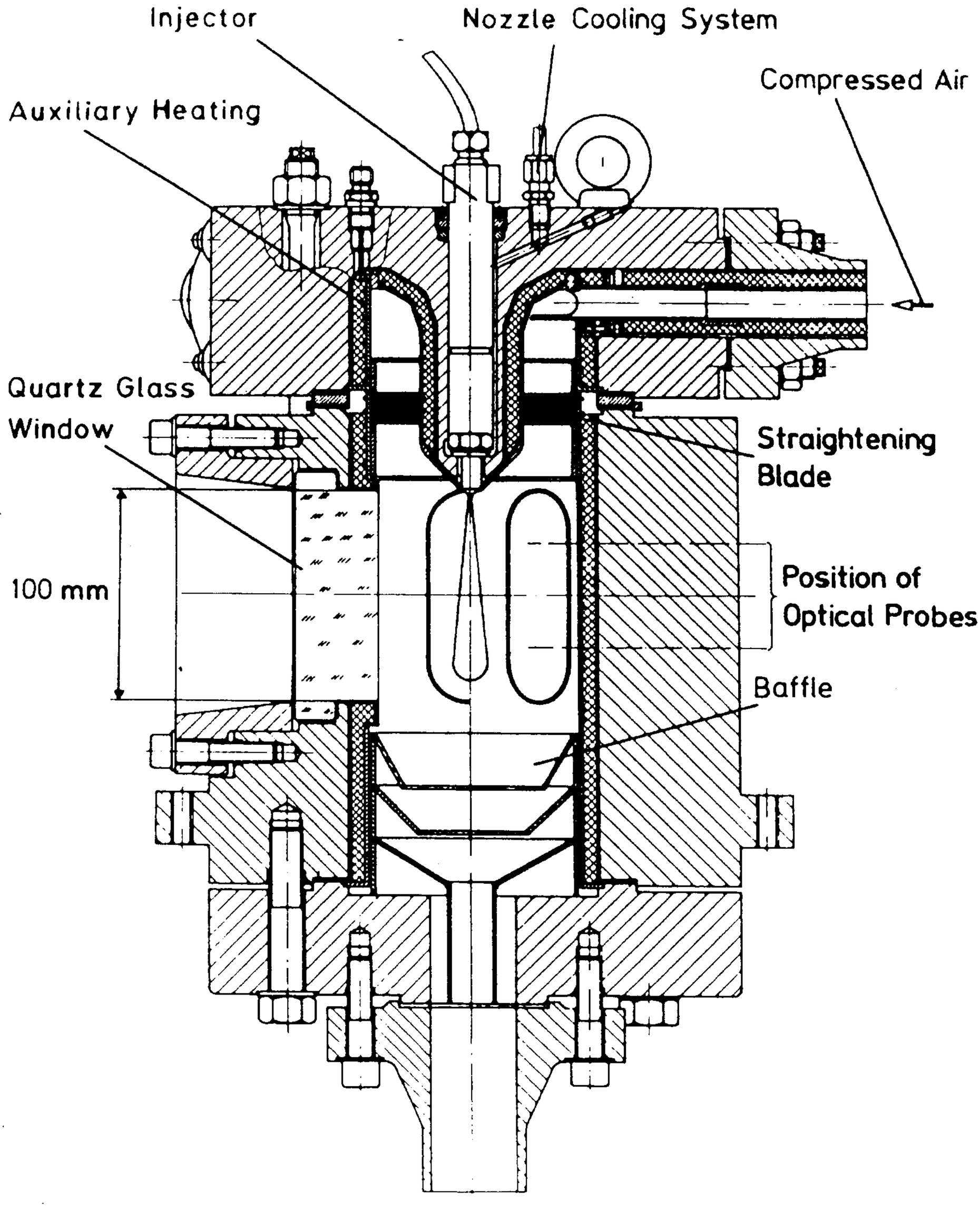


**Fig 1.9** Continuous flow constant-volume combustion chamber [*Schmidt et al,* 1988]

be a problem if work of a fundamental nature concerning the spray development is being done, but potential industrial sponsors invariably expect the flow conditions to simulate Diesel engines as closely as possible, the flow field being the most important parameter. The second limitation is that the chamber is designed to take prototype injectors with a single axially directed spray. These have to be specially made and are hence expensive; also there is considerable doubt that the sprays produced by these special injectors are representative of production ones as cavitation effects are severely restricted.

More recently work with standard injectors has been done in these chambers, the injector being mounted from the side of the chamber through a side window port [*Wiartalla, et al* 1995]; this is to allow spray/wall interaction to be studied. Advantage is also gained as there is a cross flow past those sprays which are perpendicular to the chamber axis. This is useful when looking at the effects of swirl on the spray structure. However, if PDA measurements are to be taken, at least one of the sprays must be coaxial with the chamber, which implies that PDA cannot be used to study the spray in the presence of the cross flow of air.

Constant volume chambers have been in existence for many years, but with laser diagnostics becoming more common, the need has grown for every Diesel research laboratory to have some sort of combustion chamber. With this in mind the internal combustion engine group at Imperial College, which lacked such a device, decided to have one built.

## 1.4 THESIS OUTLINE.

Chapter 2 of this thesis describes the basic design, manufacturing and preliminary testing of the system including the auxiliary equipment. Calibration of the fuel injection equipment and the design of a 'skip firing valve' is described in Chapter 3, followed by results and discussion in Chapter 4. Chapter 5 summarises the main conclusions of the research program and offers recommendations for future work.

# CHAPTER 2

# DESIGN AND CONSTRUCTION OF A CONSTANT-VOLUME CHAMBER.

## 2.1 DESIGN SPECIFICATION.

After it had been decided to build a combustion chamber, the first task was to arrive at some suitable specifications. The chamber was primarily intended for work on Diesel sprays so the maximum working pressure and temperature were set by considering the thermodynamic conditions present in production engines; using an appropriate margin, a pressure of 100 bar and a temperature of 750°C. were decided upon. These are the most important parameters in the stress analysis of the chamber, particularly that of the optical windows.

Due to the limitations of the flow field generated in many combustion chambers, it was decided that a design requirement would be the ability to produce different flow fields. This would be a unique feature of the chamber and would increase the scope of possible future experiments. At the same time there is still a need to produce quiescent conditions for some test cases, so the design would have to be capable of producing both high and low flow velocities in the region of the spray.

The ability to study spray/wall interaction inside the chamber was also made a design requirement. This would allow the work already being done using atmospheric rigs [*Arcoumanis and Cutter,* 1995] to be extended to combustion chamber conditions. To facilitate this work the injector must be capable of being positioned accurately to a specified distance from a surface and, ideally, with a variable impingement angle.

Another common problem in optical experiments is the fouling of windows. This is inevitable when combustion occurs and where there is spray impingement on the window surface, with the windows often becoming completely obscured after just a few injection cycles. This liquid film must be removed and to facilitate this the

chamber must be opened to give access to cleaning tools. In many optical engines and combustion chambers this is a time consuming exercise. The ability to complete the cleaning of the windows quickly and without any damage to them was seen as an important design feature.

Finally due to the widespread use of PDA in the Thermofluids section and its application to spray characterisation, optical access allowing the use of PDA was considered essential for measuring the axial or radial components of droplet velocity together with droplet sizing. This would allow sprays to be sized with a component of velocity either axial or perpendicular to the chamber axis, thus placing no restriction on the type of fuel injection equipment (FIE) used (both multi-hole and pintle type nozzles could be characterised).

## 2.2 DETAIL DESIGN.

### 2.2.1 Combustion chamber.

#### 2.2.1.1 General arrangement and optical access.

The 'Schmidt' chamber described in section 1.3 seemed to offer a good starting point in the design process representing a compact and flexible measuring tool. Despite this, it was felt that the unrealistic flow field produced in this type of chamber and the restrictions on PDA measurements justified a different design capable of producing a more realistic cylinder flow field with improved optical access.

Figure 2.1 shows a preliminary design, while Figure 2.2 shows the final design arrived at after extensive development; the parentage of these designs from the 'Schmidt' chamber can clearly be seen. The basic arrangement consists of a plug representing the piston crown placed at the head of the chamber. Pressurised gas, introduced through a side port, flows along the cylinder and hence past the injector into an annular duct through holes in a liner, before being discharged through a

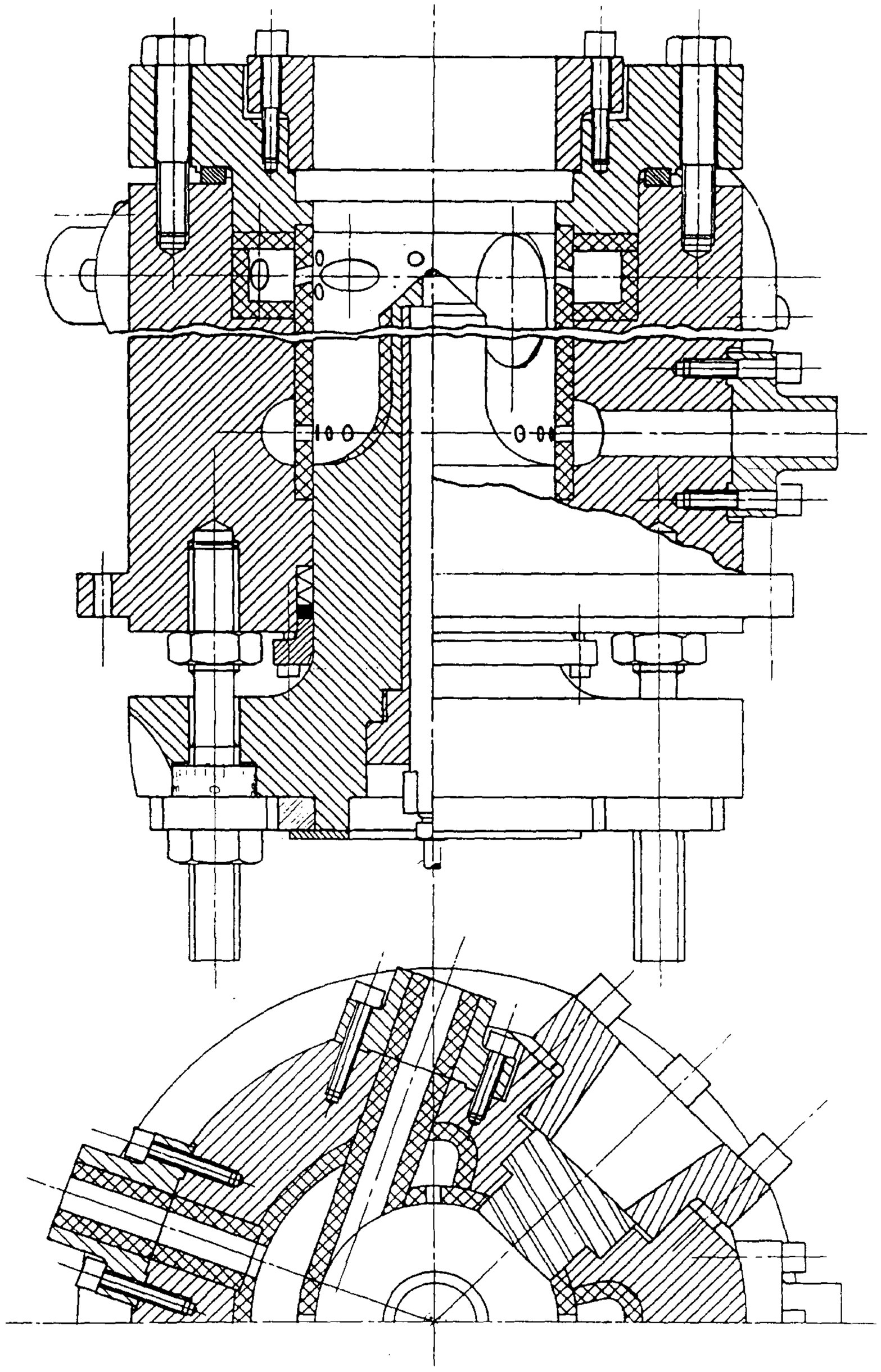

**Fig 2.1** Preliminary design drawing.

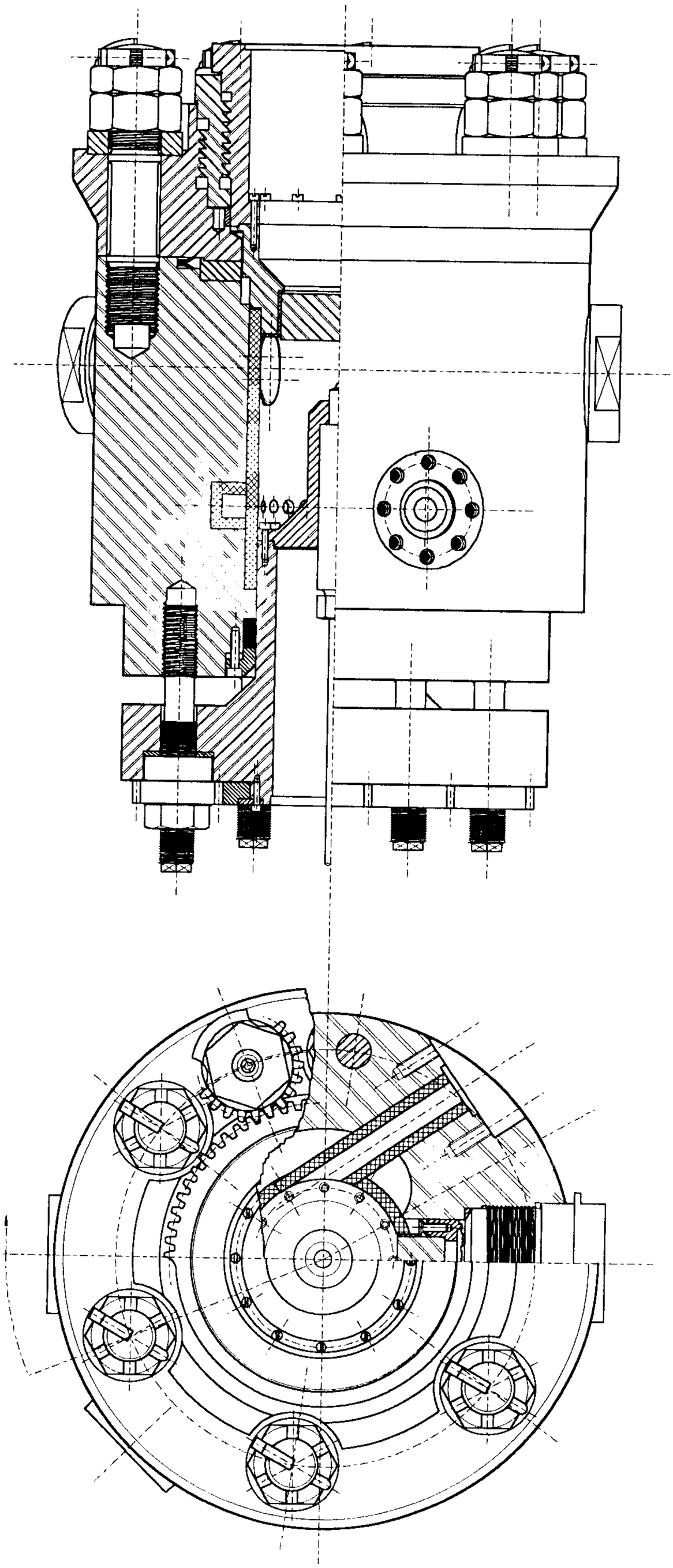

**Fig 2.2** Finished design of chamber.

throttling valve. The continuous gas flow purges the chamber sufficiently well to allow the injector pump to be run at full speed - at least for the non combusting experiments.

The injector is mounted on a moveable cross head which can be used to position the injector relative to the dummy piston crown. This is particularly useful for spray/wall interaction studies as the distance the spray travels before hitting the dummy piston crown can be varied.

The dummy piston can either be a quartz window as shown in the drawings or a steel plug fitted in its place. As the plug can be changed at will, there are no restrictions on the possible shape of the surface. This makes possible even the modelling of piston bowl shapes. Alternatively, sensors can be fitted into the plug or even a heater, any arrangement in fact, as long as the plug can withstand the gas pressure and fits into the adapter.

The desire for a more realistic flow field led to a further feature of the chamber design. Gas can either be admitted via a tangential port, thus producing a swirling flow, or through a 'sieve plate' arrangement. The 'sieve' consists of holes drilled through a special liner; a second liner being required for the tangential port. These holes are supplied with pressurised gas via annular recesses machined into the top of the body of the chamber and can be seen in Plate 1. With this arrangement it was hoped that a relatively quiescent chamber could be achieved but without reducing the degree of scavenging.

### 2.2.1.2 Breech head design.

The head, which can be seen in Plate 2, forms the front end of the combustion chamber. It consists of a steel flange bolted to the body of the chamber by means of six high tensile studs, which can be seen in many of the photographs. In between the head and the body of the chamber (described later) there is a high pressure seal. The seal is of all metal construction as it needs to withstand the high flash temperatures which may occur during combustion; a rubber seal would easily contain the pressure but would perish under these temperature conditions.

The main task of the head is to contain the breech loading mechanism, this mechanism enables the rapid removal and replacement of the dummy piston holder. The breech is useful purely to facilitate access to the inside of the chamber to change injectors, remove windows or liners etc. Its main purpose, however, is to enable the rapid cleaning of the windows. This is often a wearisome experience on many optical engines and chambers. Many minutes or even hours being required to complete the process and windows are often broken by being constantly removed and replaced into tight sockets. The breach mechanism affords an elaborate but otherwise completely satisfactory method of quick window removal. Perhaps the only objection being the space occupied by the mechanism itself restricting the available optical access.

**Plate 1**. Front end of chamber's body as machined, with annular recesses for connection with sieve-plate liner.

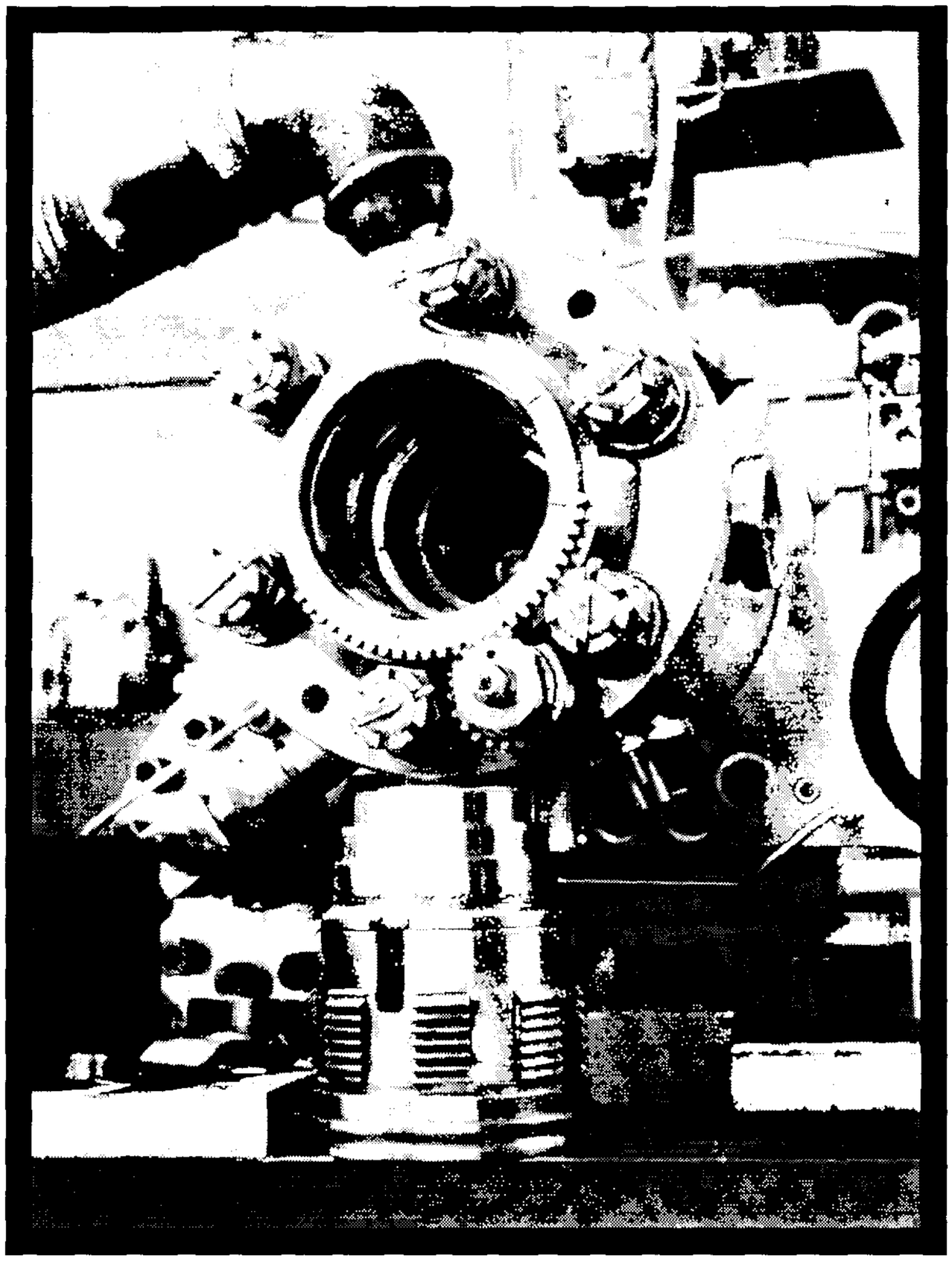

**Plate 2**. Front end of assembled chamber, illustrating breech loading mechanism for securing head window in chamber.

Reference to Plate 2 shows the workings of the mechanism, the slotted threads of the breech being clearly shown. There are three basic components of the breech; the dummy piston holder, the tightening ring and the breech head itself. The piston holder screws into the tightening ring which in turn screws into the breech head. Both sets of threads are right-hand and of buttress form. However, the thread between head and ring has a smaller pitch- 5 Tpi (5.08 mm) than that between the ring and holder - 4½Tpi (5.64 mm). The threads between the ring and holder are slotted so as to allow the removal of the holder after merely an eighth of a turn. To lock the holder in position, the holder is inserted into the tightening ring up against the seal in the head. The tightening ring is then rotated anti-clockwise one eighth of a turn, whilst the

holder is prevented from turning by a key fixed to the breech head. This causes the slotted threads of the ring and holder to engage, locking the holder in position. As both sets of threads are right-handed, the locking action stems from the difference in pitch between the two threads, equivalent to a thread of 45 Tpi (pitch 0.56 mm). This gives a large mechanical advantage, the only limiting factor on the degree of tightness achieved being friction. The rotation of the ring to achieve this locking is made by a pinion actuated by a specially made spanner; this pinion engages with the gear teeth cut into the periphery of the tightening ring, see Figure 2.2 or Plate 2.

An important feature of the breech is the means of making the initial tightening adjustment. This adjustment is needed as the axial position of the window holder at the end of the tightening sequence can be such that there is a gap between the sealing faces. To make the adjustment the angular position of the key, which prevents rotation of the holder whilst tightening takes place, is adjusted until the correct amount of preload is achieved between the sealing faces. Plate 3 shows the

**Plate 3**. Front end of chamber with tightening ring removed to show vernier key ring, with the numbered holes shown clearly. The locking pin prevents the rotation of the key ring and hence stops rotation of the window holder when the breech is being tightened.

mechanism used to effect this adjustment. A thin ring to which the key is fitted can rotate within the breech head. A series of dowel holes, machined half into the head and half into the key ring, are clearly seen in the plate. These holes allow the fitting of a dowel which locks the key ring in position. To provide for a fine adjustment these half holes are machined in a vernier arrangement, there being seventeen half holes in the head and only sixteen in the key ring. This vernier allows the key to be positioned in approximately 1.5° steps.

Although the breech looks complicated, by far the greatest challenge has been in the design of the breech seal. Like the seal between the head and body, it has to take high pressures and temperatures, but in addition must be capable of sealing and resealing many thousands of times. All of this must be achieved with a small end load produced by the hand operated mechanism described above. Making any seal work over such a large diameter presents problems, but with these specifications this was probably the most difficult problem in the design of the whole chamber.

Two attempts were made before satisfactory sealing was achieved. At first a plain soft metal seal was adopted, but was found to leak badly at even moderate pressures, the problem being strain of the breech mechanism causing the seal to 'lift off'. To prevent this 'lift off', a self acting metal-to-metal seal was used. Here the gas pressure itself is used to press sealing lips outwards onto the sealing face, using a purpose built seal which was specially made for the chamber. Great care must be taken not to damage the seal, as the slightest mishandling and consequent damage may render it useless; a new seal would then need to be made at great expense.

Subsequent to the success of this type of seal, a number of self acting seals of similar nature have been used in many other parts of the chamber and ancillary equipment. These are unquestionably the best type of seal for the high temperatures and pressures required in the present research program.

### 2.2.1.3 Injector carriage.

The injector carriage or cross head serves the purpose of holding the injector in position within the chamber. As different injectors and FIE systems will be used, this mounting needs to be able to accept various shapes and sizes of injector. An additional purpose of the carriage is to position the injector at varying axial positions along the chamber to facilitate spray/wall interaction studies and PDA measurements.

As Figures 2.1 and 2.2 show, the injector is held with an adapter which is bolted onto a flange joint at the end of the carriage. One such adapter needs to be made for each different injector, though as injectors are often of standard sizes, these can be reused. The carriage itself consists of a cylindrical part of the same diameter as the nominal chamber cylinder bore. This has a flange fitting for the injector adapter on its end. The cylinder slides in and out of the chamber, thereby positioning the injector. A stuffing box type seal prevents leakage past the carriage.

On the other end of the carriage is a large flange which carries six nuts. These nuts, along with their studs, which are screwed into the body of the chamber, carry the end load caused by pressure in the chamber. The nuts are seated in cup type bearing bushes of gunmetal, each nut having a journal bearing fitting in the bush. Positioning of the carriage is achieved by turning the nuts thereby moving the hole assembly. To avoid uneven load between the six nuts a novel device has been used. Each of the six nuts has a 20 teeth gear cut in its periphery. These gears each engage with a central 'Sun' gear- see Plate 4. One of the nuts has an additional set of hexagon flats and by turning this 'Master' nut with a spanner, the five remaining nuts are turned simultaneously and at an equal rate. By this means each nut contributes an equal share to the combined end load.

To aid the accurate positioning of the injector, the studs were screwcut to a fine pitch and micrometer graduations are marked on the journal portion of the 'Master' nut- see Figure 2.1. By this means positioning of the injector with an accuracy of at least +/-0.05 mm can be achieved.

### 2.2.1.4 Main body.

The main body consists of a thick walled cylindrical pressure vessel, forming the combustion chamber itself- see Plates 1,5 and 6. The body forms the heart of the chamber to which are fixed the breech head and the injector carriage. The three side windows are fitted into the body and both inlet and outlet ports are machined into it.

Plate 1 shows the front end which accepts the Breech head. Six tapped holes take the studs which hold the head to the body. A recess is machined in the front end for the head seal between the main body and Breech head; this consists of a steel ring ground flat. By virtue of the fine finish between the sealing faces, an adequate seal capable of withstanding high pressures was achieved. This was only a temporary

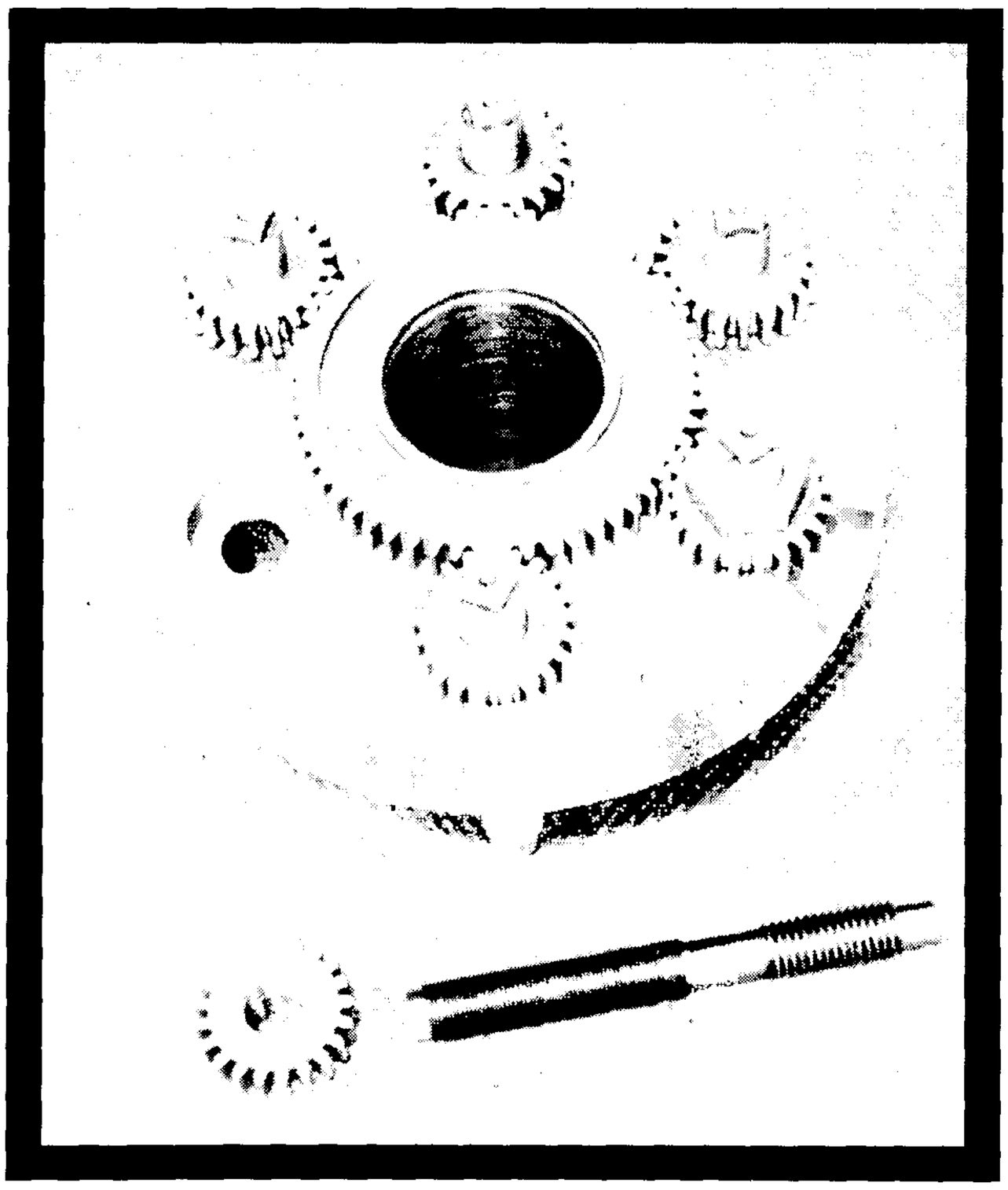

**Plate 4**. End view of injector carriage with sun and planet gear nuts for providing even tightening load on each stud.

solution, however, to enable a pressure test to be completed, as this arrangement has a major design flaw. A gap is necessitated between the flange faces, which adds flexibility to the whole joint and hence increases the cyclic loading on the studs [*Bickford,* 1990]. To avoid any possibility of consequent fatigue failure, with inspection of the studs being difficult, it was decided to use a seal which would allow the flanges to be bolted together to improve their fatigue life. Just as with the breech seal, a self acting, metal-to-metal, 'V' type seal was chosen; 'V' rings are commonly used in industry when high temperatures and pressures are experienced.

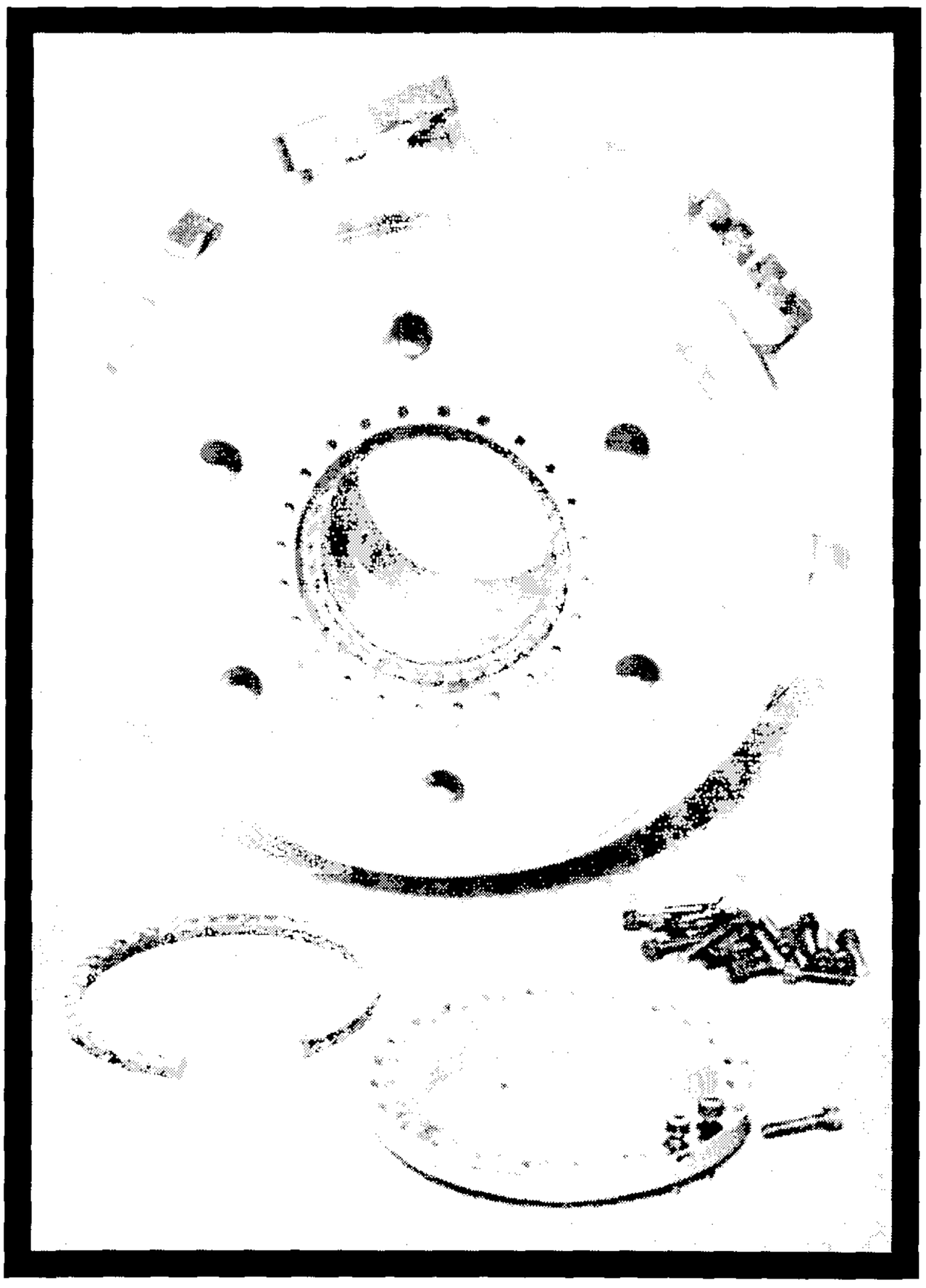

**Plate 5**. Body as machined showing 'stuffing box' gland for sealing the moveable injector carriage.

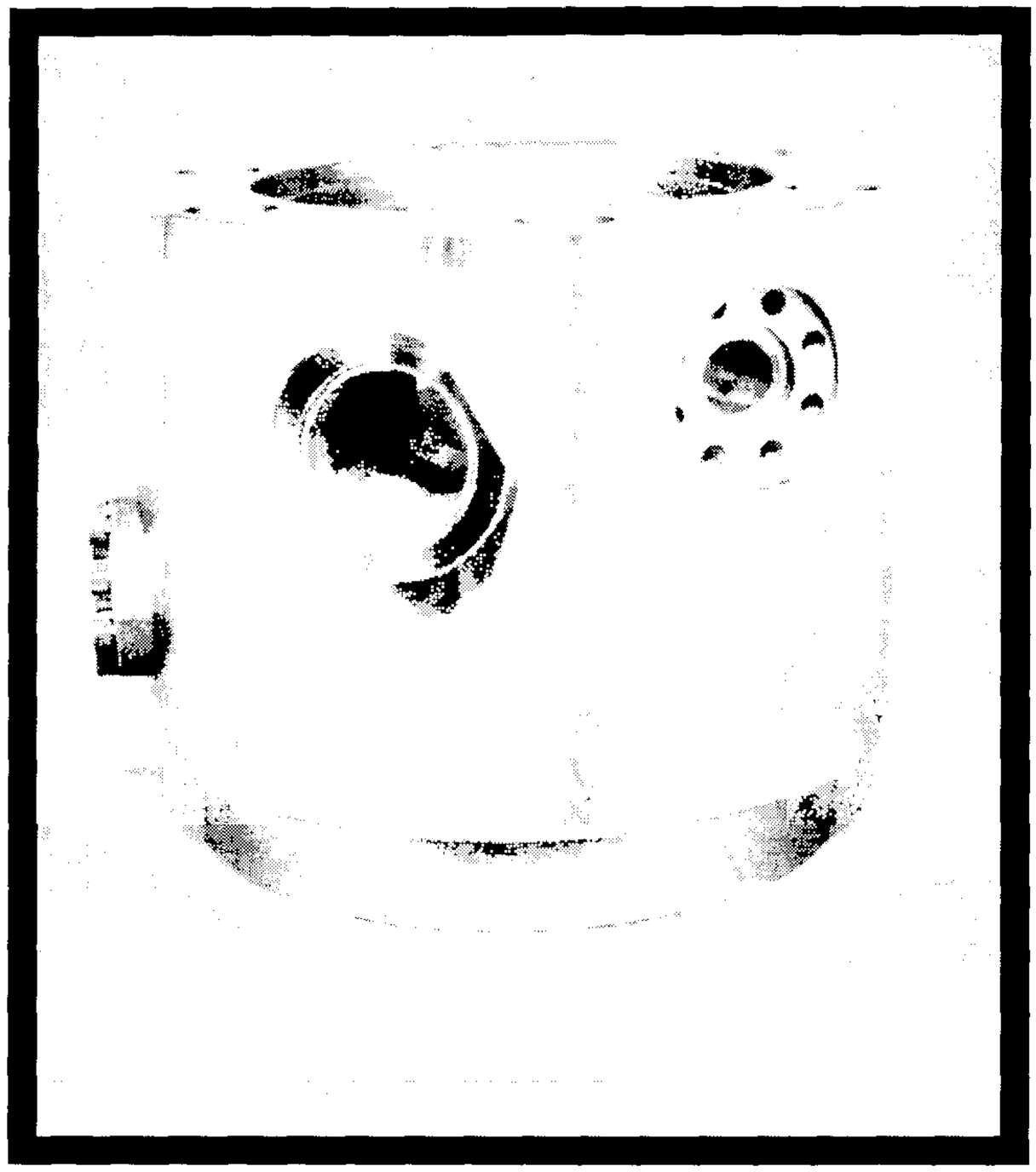

**Plate 6**. Side view of body showing one side window and inlet port.

To further increase safety, leak out grooves were added onto the face of the Breech head's flange. If a complete failure of the seal occurred, these would vent off the gas, avoiding a situation where high gas pressure acts over a considerable portion of the flange, as the studs are not designed for such a high loading. These grooves are not shown in the plates as they were added at a later stage after the photographs were taken.

One further refinement was the accurate grinding flat of the head and body flanges. This enables the two faces to bed together over a large area, rather than on a few high spots, thereby increasing the stiffness of the joint and further reducing cyclic stresses on the studs. There is also an additional benefit of the grinding, a lower pre-stress in the studs can be used while still maintaining the required end load. This will improve their fatigue life further.

The opposite end of the body takes the injector carriage, as shown in Plate 5. The end of the body has a 'stuffing box' type of seal to prevent blow-by past the

injector carriage. This is designed to maintain a seal whilst allowing the carriage to move in and out of the chamber for positioning of the injector. The seal consists of a recess formed between the body and the carriage. This accepts the graphite packing rings shown in the plate. Sealing is effected by a top hat gland ring which squashes the packing into the recess when a series of bolts are tightened. In operation these bolts are progressively tightened until a seal is obtained.

The barrel of the chamber is machined to accept a liner; Plate 7 shows one such liner. The liner forms the supposed bore of the engine cylinder. Machined into the liners are cut-outs for the side windows, inlet port and towards the end, the ring of holes forming the gas outlet. These outlet holes connect with an annular grove which itself connects with the outlet port. The annular grove can just be seen in Plate 1, towards the end of the body's bore. The outlet port connection can be seen in Plate 6, it is plugged at the side of the body. An adapter fits onto this connection for the outlet reducer, which will be described later. Due to the outlet port being on one side of the chamber, it was felt that the flow field close to the outlet might become asymmetric since air would be sucked to one side as it flows out of the chamber. To reduce this effect the size of the outlet holes in the liner varies. Those close to the outlet port being proportionally smaller than those on the other side of the chamber; these holes can be seen in Plate 7.

The liner shown in Plate 7 is designed to take a tangential inlet port which can be seen along-side the liner in the plate. The inlet port connects to a 'feed in barrel' also shown in the plate. This barrel seals onto the inlet port with a 'ball and socket' seat. A spring forces this seat together as the relative position of the inlet port cannot be accurately controlled. The inlet ports themselves can be removed without having to dismantle any pipework, simply by turning them through 180 degrees and removing them with the breech open. This feature greatly reduces the time taken to change from one liner to another, as the port effectively pins the liner in position and needs to be removed before the liner can be taken out.

The liner shown is of the swirl type, but a non-swirl type can also be used. As yet none have been made but in principle they will have a sieve-plate, rather than a tangential port, as the gas inlet. This sieve-plate will simply be a series of holes, perhaps many hundreds, fed from the gas supply. To give a more uniform flow field

this sieve will extend around the circumference of the liner. Gas will enter the chamber therefore from all directions and at relatively low velocity giving an approximation to a quiescent chamber condition. To supply gas to all of this sieve, annular ducts machined in the top of the body connect the holes with the gas supply; these annular ducts are shown in Plate 1.

**Plate** 7. Liner with swirl inlet port and feed pipe all made from machineable ceramic. The liner and pipe are relieved over long portions of their length so that they only touch the chamber over a narrow area, in this way an air gap is maintained and excessive heat transfer avoided.

### 2.2.1.5 Window mounts and stress analysis.

The design of the windows can be broken into two areas, stress analysis and optical access. These are in many ways mutually exclusive as optical access requires as large a window as possible whereas to reduce stresses to a minimum windows should be as small as possible. The first decision to be taken, however, was the window material. There are basically only two main contenders, quartz and sapphire; for a thorough review of the mechanical properties of these two materials see *Richman and Reynolds,* [1984]. Sapphire has the advantage of high tensile strength but also has a high coefficient of thermal expansion. This makes it unsuitable when high temperatures and hence high thermal stresses are involved. Quartz on the other hand has a very small coefficient of expansion, but also has a low tensile strength. Perhaps the determining factor in the choice of material is that of price. Quartz windows are easier to fabricate and are typically ten to twenty times cheaper. For these reasons quartz was chosen for the chamber's windows.

A full description of the failure modes of glass is outside the scope of this thesis. However, the interested reader is referred to the numerous works in the literature on the fracture mechanics of glass [*Zarzycki,* 1982]. In principle there are two major points about glass as a structural material. Firstly its tensile strength is about an order of magnitude less than its compressive strength, and, secondly, glass of any kind suffers from stress fatigue.

The quartz windows are the weakest point in the pressure vessel and as such constitute the largest risk of failure. The thickness of the windows has to be increased disproportionately as the working pressure is raised, due to the low tensile strength of glass; consequently thick windows are often necessary in optical chambers. Because of this, great care was taken in their design and particularly the method of mounting them. The ideal window mount would only impose the minimum of load to prevent the window from blowing out of the pressure vessel. In particular, point loading onto the window of any kind has to be avoided, as this will inevitably lead to high tensile or shear stresses and consequent failure. Another common source of failure is frictional forces where high contact pressures are accompanied by movement between the window and its mounting. This movement can be due to differences in thermal

expansion or even the different values of Young's Modulus. The frictional forces caused by the sliding resolve into shear stresses which, if high enough, can cause shear cracks which may grow to cause total failure.

The stress analysis of the windows used in the combustion chamber is given below. There are two sizes of window fitted in the combustion chamber, only the analysis for the large circular window is given, as this experiences the highest stresses.

The relevant formula for the stress in a simply supported short cylinder under uniform end pressure is given by [*Roark and Young,* 1975]:

$$\sigma_{Max} = \frac{3PR^2(3+\nu)}{8x^2} \qquad (2.1)$$

This formula is for thin disks, and will safely overestimate the stress in our 'thick' window. A typical value of limiting stress for quartz is 50 MPa. For the present head window's dimensions of diameter 63.5 mm and thickness 25 mm, the window is expected to fail when the following chamber pressure is applied:

$$P = \frac{8x^2\sigma_{Max}}{3R^2(3+\nu)} = \frac{8\times 0.025^2 \times 50\times 10^6}{3\times 0.03175^2 \times (3+0.16)} = 26.2\text{Mpa} = 262\text{bar}$$

With a maximum working pressure of 100 bar, at first sight, this gives a quite adequate factor of safety. However, one further aspect of the stress analysis of quartz is that of stress fatigue. Work done by NASA [*Weiderhorn et al,* 1974] for the 'Skylab' has indicated that over a period of time cracks will grow in glass which is experiencing steady stress well below the ultimate failure stress. Thus the problem for the designers of optical equipment is that proof testing of the device under an

increased test pressure does not guarantee that the window will not fail after a period of use at a lower working pressure. This may well explain why a window suddenly fails after months or years of experimenting for no apparent reason, even though these failures are usually put down to rough handling and edge chips.

Figure 2.3 below shows a Weibull plot produced by NASA to help their designers produce safe window designs without excessive weight. To use the chart the chosen working stress is first found on the 'x' axis and a vertical line is drawn from this. A horizontal line is then drawn from the desired life of the window found on the 'y' axis; where the two lines cross on the map, a proof test ratio can be read off. To guarantee that the window will not fail before the chosen life time, it must be pressure

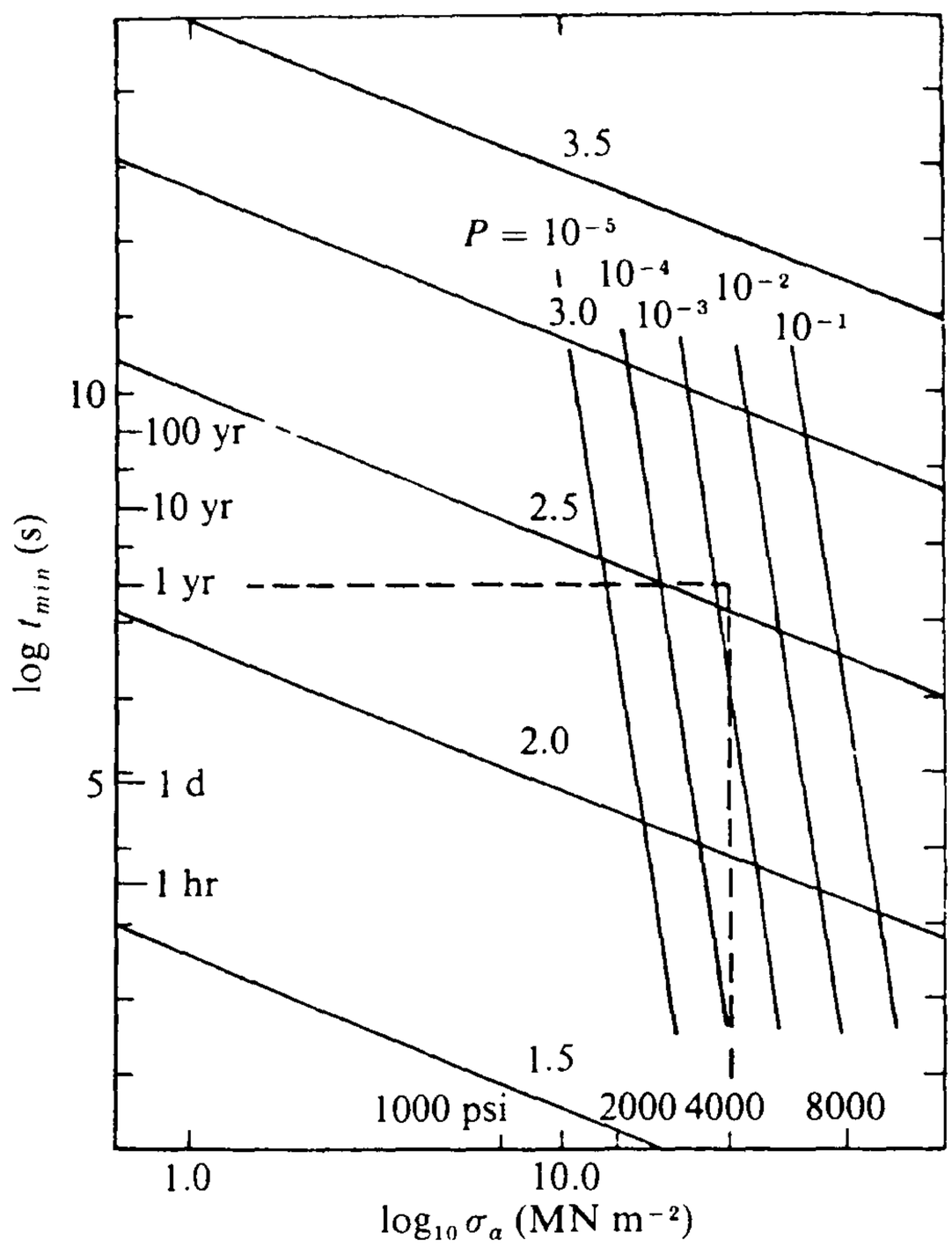


**Fig 2.3** Estimation of the life-time of window glass in the spacecraft Skylab as a function of working stress $\sigma_a$. The lines of equal probability P from $10^{-1}$ to $10^{-5}$ correspond to estimates following the Weibull method. The straight lines marked 1.5 to 3.5 correspond to the proof test ratios $\sigma_P/\sigma_a$ [Zarzycki, 1982].

tested to a stress equal to the working stress multiplied by this ratio.

For the head window, with a chosen life time of 10 years, this factor was found to be 3.0; so the maximum safe working pressure is one third of the hydraulic test pressure, which was 150 bar (the hydraulic test is described in detail in section 2.3). Consequently the maximum safe working pressure of this window is only 50 bar, which is much lower than the failure pressure calculated using the static stress formula and also much lower than the allowable pressure on the rest of the combustion chamber. However, to design a window to withstand the chamber's maximum working pressure of 100 bar would necessitate a thicker window, providing less optical access with smaller aperture, a critical factor in PDA studies. In addition, the particular set of experiments that were conducted did not need chamber pressures above 50 bar, therefore it was decided to opt for a thin, large diameter window with good optical access. If higher chamber pressures are needed in the future, a new window and mounting can be designed, and a thicker window fitted; this is a simple matter, as the breech mechanism is designed to accept a number of different window mounts, so a selection of different windows for different applications and pressures can be made when required.

All of the above stress analysis assumes that the windows are operating under cold conditions. If hot gas is used inside the chamber and especially in the presence of combustion, thermal stresses may become a problem. As it is likely that pressures would exceed the maximum safe pressure under combustion conditions, a new window would have to be designed in this case as well.

### 2.2.2 Chamber mount and traverse.

To enable optical techniques to be used, there must be a means of moving, with reasonable precision, the optics relative to the combustion chamber. This position must then be maintained during the measurement with the minimum of vibration.

Clearly there are two options, either the chamber is held stationary while the optics move or vice-versa. Fixing the chamber was decided to be the most convenient

option. The chamber with all the ancillaries weighs nearly a quarter of a ton. Moving the much smaller weight of an optical bench seemed more practical, despite its much greater length. Despite that a rigid traverse was considered essential due to the multiplicity of sources of vibration and the still considerable weight of the bench.

A specially made traverse was considered, but the normal practice of using an old milling machine was adopted. This was both much cheaper and offered a higher specification due to the massive construction of the milling machine used (see Plate 8).

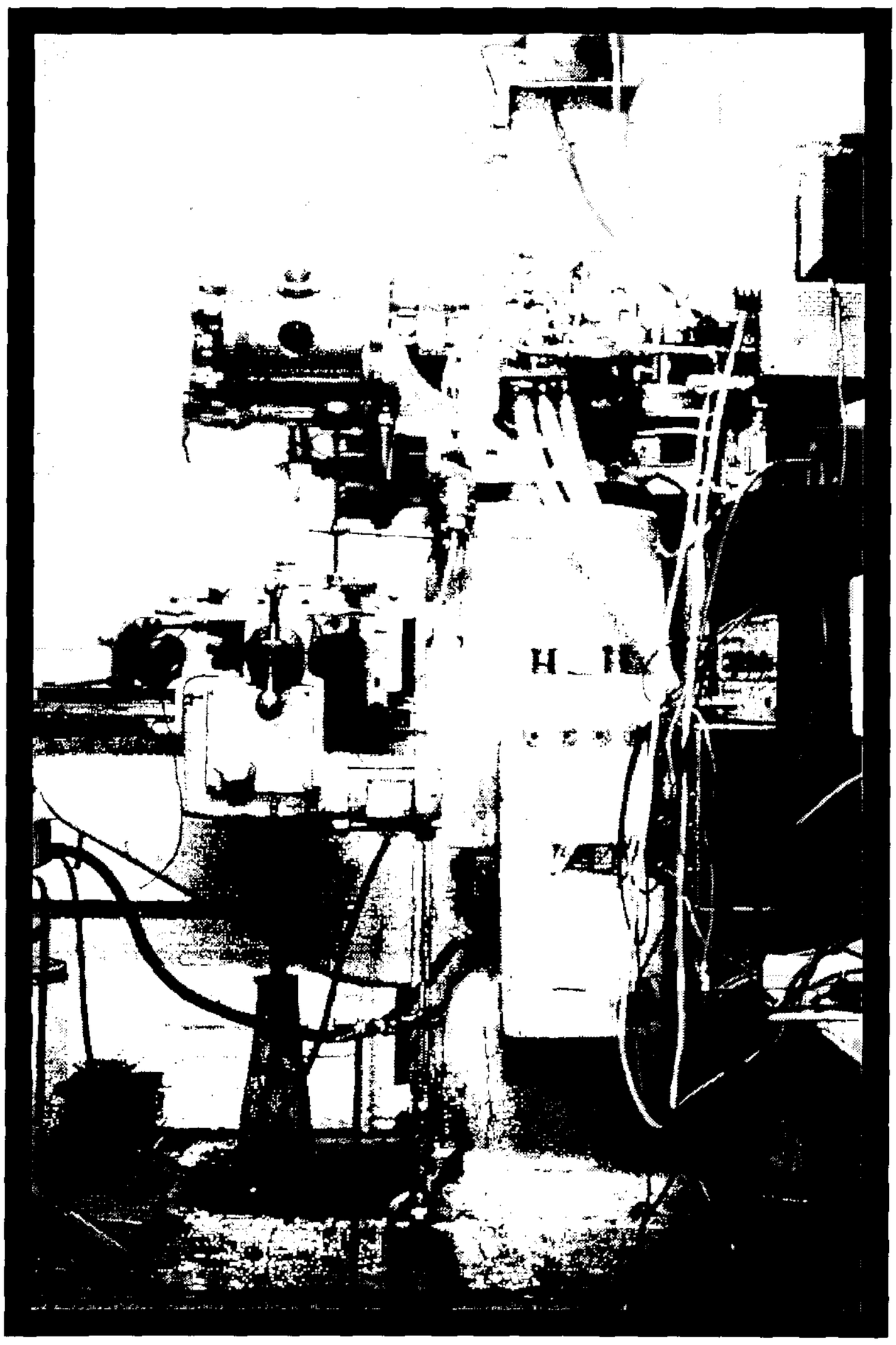

**Plate 8**. Side view of chamber on its mounting, the XYZ table can clearly be seen. On top of the mounting is fixed the DPC pump whilst it was being calibrated.

As the plate shows, the chamber is mounted on a substantial bracket. The bracket also holds the heater in position and offers a platform for the tray in which the FIE is fitted. The bracket has a dovetail slide which fits a female dovetail machined into a swivel casting. This casting fits on the top of the body of the milling machine, and originally accepted the milling machine's turret arm. Thus the whole combustion chamber can be swivelled about a vertical access. A scale marked in degrees allows the chamber to be positioned with some accuracy to any required angle relative to the axis of the bench (see Plate 9). This feature has been particularly useful for the PDA set-up, which will be described later.

The optical bench fits onto the milling table and due to the considerable length of the table, support is given to the bench avoiding excessive strain. Accurate positioning of the bench is achieved using the normal micrometer screws of the milling machine. These are graduated in metric units and despite the wear on them, positioning within 50 μm is possible over a considerable distance.

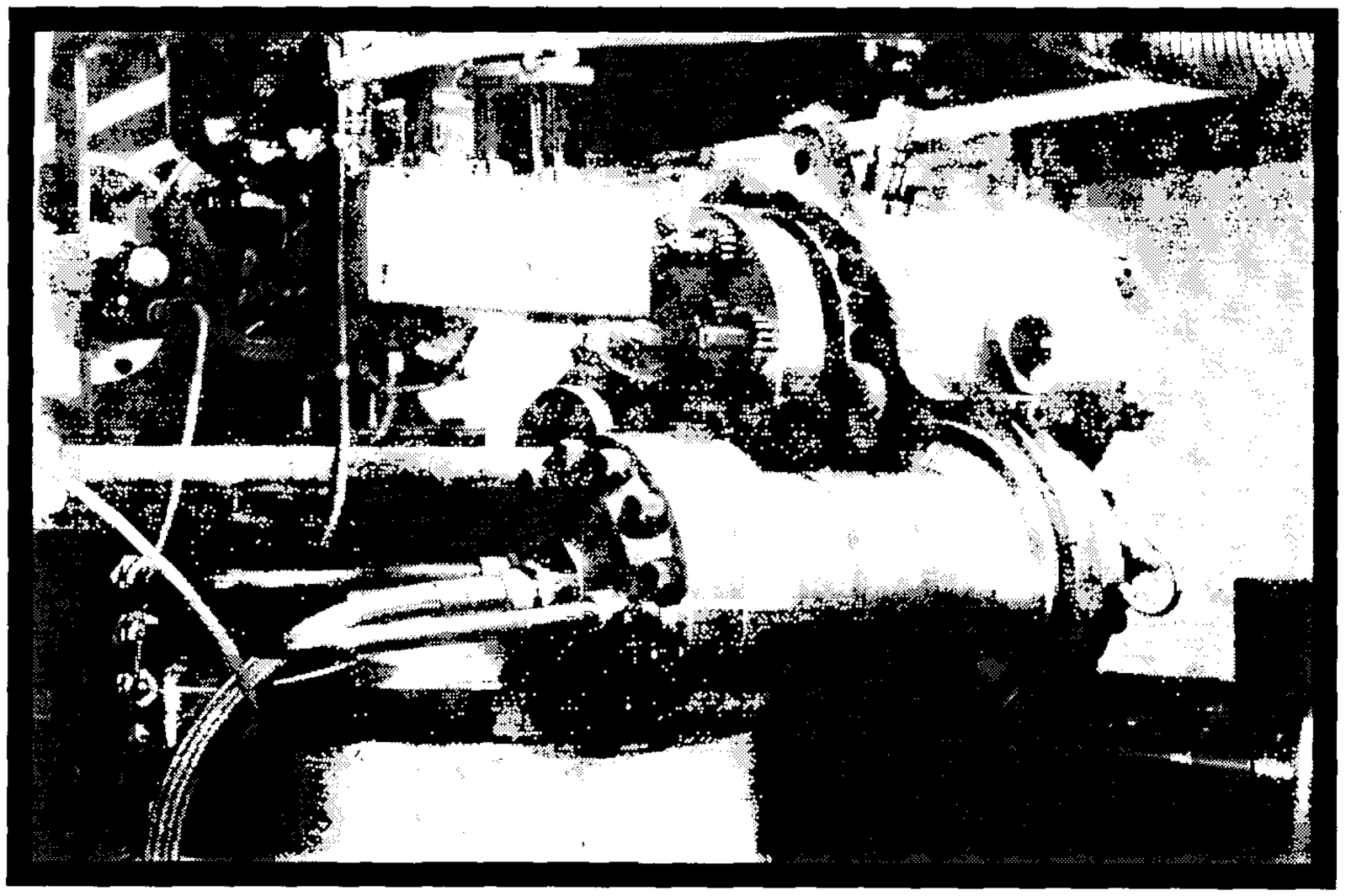

**Plate 9**. Side view of chamber showing: the heater's pressure vessel, the 'Pyro' cables feeding the electrical heater inside and the flexible air pipe used to supply air from the reducing panel. Also shown is the scale, graduated in degrees, used to position the chamber at any angle relative to the XYZ table's axis.

The whole unit comprising the combustion chamber, optical bench and milling machine is mounted on an existing engine test bed in one of the laboratory test cells. This engine bed has vibration dampers which damp vibrations produced by external equipment, like the compressor and other engines, and also equipment attached to the chamber itself, principally FIE. Thus a relatively vibration free platform is maintained facilitating optical work. Freedom from vibration is one advantage that the combustion chamber has over optical engines which cannot be overstated.

### 2.2.3 Air heater.

Heating the air or gas entering the chamber is a major feature of the constant volume chamber. It enables both combustion work to be undertaken, with air being heated to simulate the end of compression temperatures of an engine, as well as fuel vaporisation studies in the absence of combustion using inert gases instead of air. This last feature is not yet available, and additional equipment will be needed to achieve this.

The first consideration in the design of the heater was whether to use electrical or some kind of fuel-fired heater. The latter offers the advantage of lower running cost and higher potential heat input. On the other hand electric heating is much cleaner, simpler and more controllable than fuel firing. In addition fuel firing by external combustion, namely indirect heating, is complicated by the need for a high pressure heat exchanger, as these would require special materials to withstand both the high pressures and temperatures involved. An alternative might be direct firing of fuel into the air stream. Leaving aside the difficulties of maintaining flames in a high pressure environment, there is the objection that the gas entering the combustion chamber will be contaminated with combustion products. Although in experiments needing EGR to be simulated this would have been desirable, overall fuel firing was considered too complicated and electrical heating was chosen.

The next consideration was the required power input into the heater. This clearly relates to the flow rate of gas, its specific heat and the temperature rise required. Another consideration was the amount of electricity available, as due to

supply problems in the engine laboratory this was limited to 60 kW, with the compressor and auxiliaries needing a further 25 kW.

To calculate whether the available 60 kW was sufficient, some specifications had to be decided. First that the peak temperature needed was 750°C. This was arrived at both from metallurgical limitations on the outlet valve, which is not insulated like the rest of the chamber, and as a sensible approximation to the end of compression temperatures in Diesels. The flow rate through the chamber was less easy to determine, and at the end a figure of 5 Kg/min was decided after consideration of the delivery of the compressor and the maximum flow rate through the reducing valves in the system.

With the flow rate and temperature rise set, a simple calculation shows that the power consumption of the heater needs to be at least 40 kW, which meets the requirement for the maximum permissible electrical demand. After some searching a suitable proprietary heater was found, with a nominal rating of 36 kW which is less than the required value. However, due to the low duty cycle of the heater, and the nature of the experiments being intermittent and of limited duration, by purchasing a heater designed for lower voltages than the supply voltage, the necessary increase in the maximum power output could be achieved by overrunning the heater at the higher voltage; this is standard practice in industry where duty cycle is low.

The heater was manufactured by the company Sylvania and a general assembly drawing is shown in Figure 2.4. It consists of six spiral wound elements each in their own ceramic tube. The six tubes are held in a cage which fits inside a stainless steel outer casing; this casing is designed to hold only limited pressures far below that necessary for this application. Consequently a pressure vessel was designed to contain the heater which can be seen in Plate 9 and in Figure 2.5.

Although the peak rating of the heater is important, for many experiments at low temperatures and flow rates, a reduced power consumption is necessary. To be able to cope with these varying power demands, a power controller for the heater was used. Although a large variable transformer was available in the department, unfortunately it had no means of feedback control, a necessary feature to maintain an accurate gas temperature. Therefore some form of solid state power control was

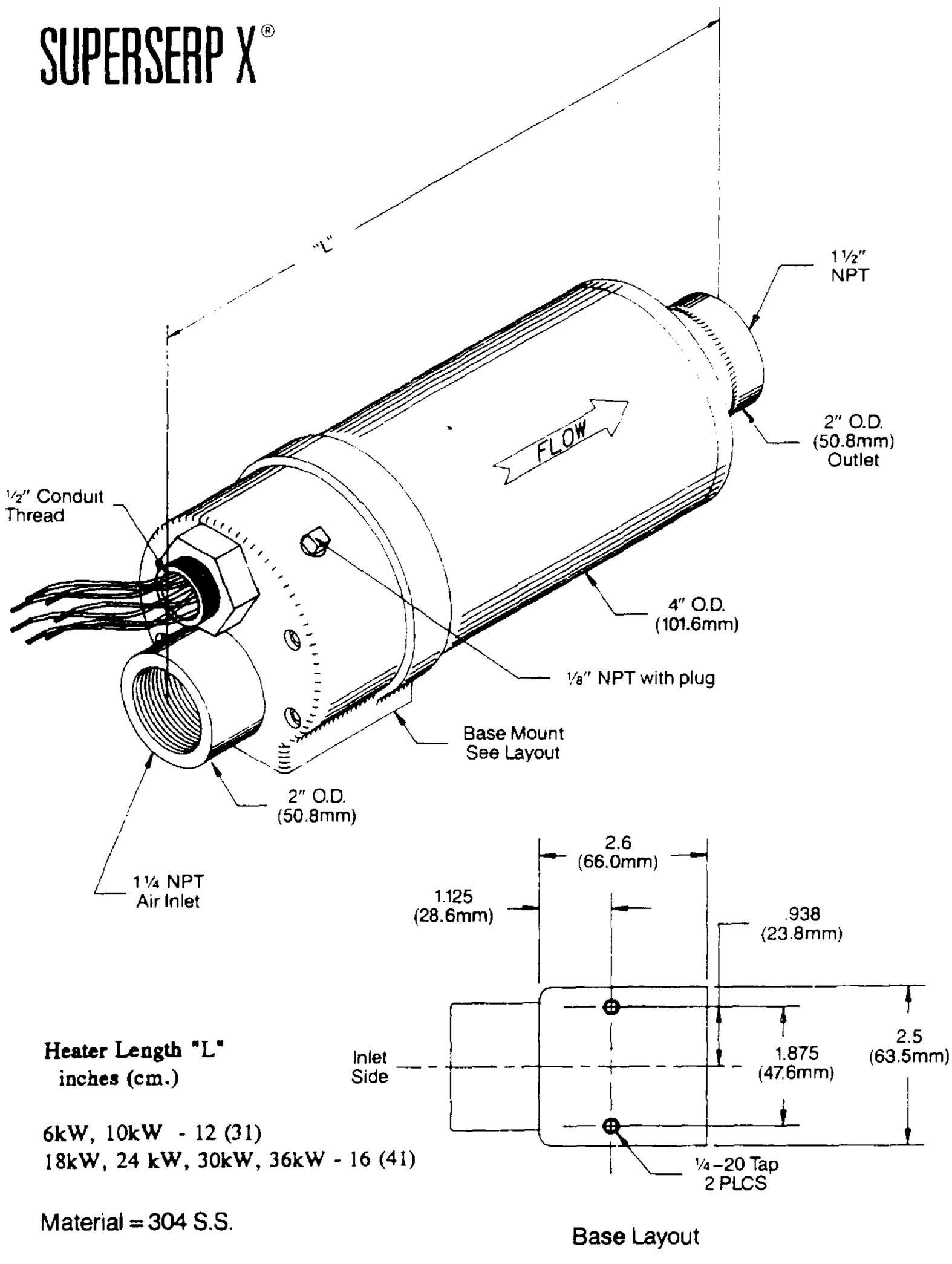


**Fig 2.4** General assembly of 'Sylvania' 36 kW heater.

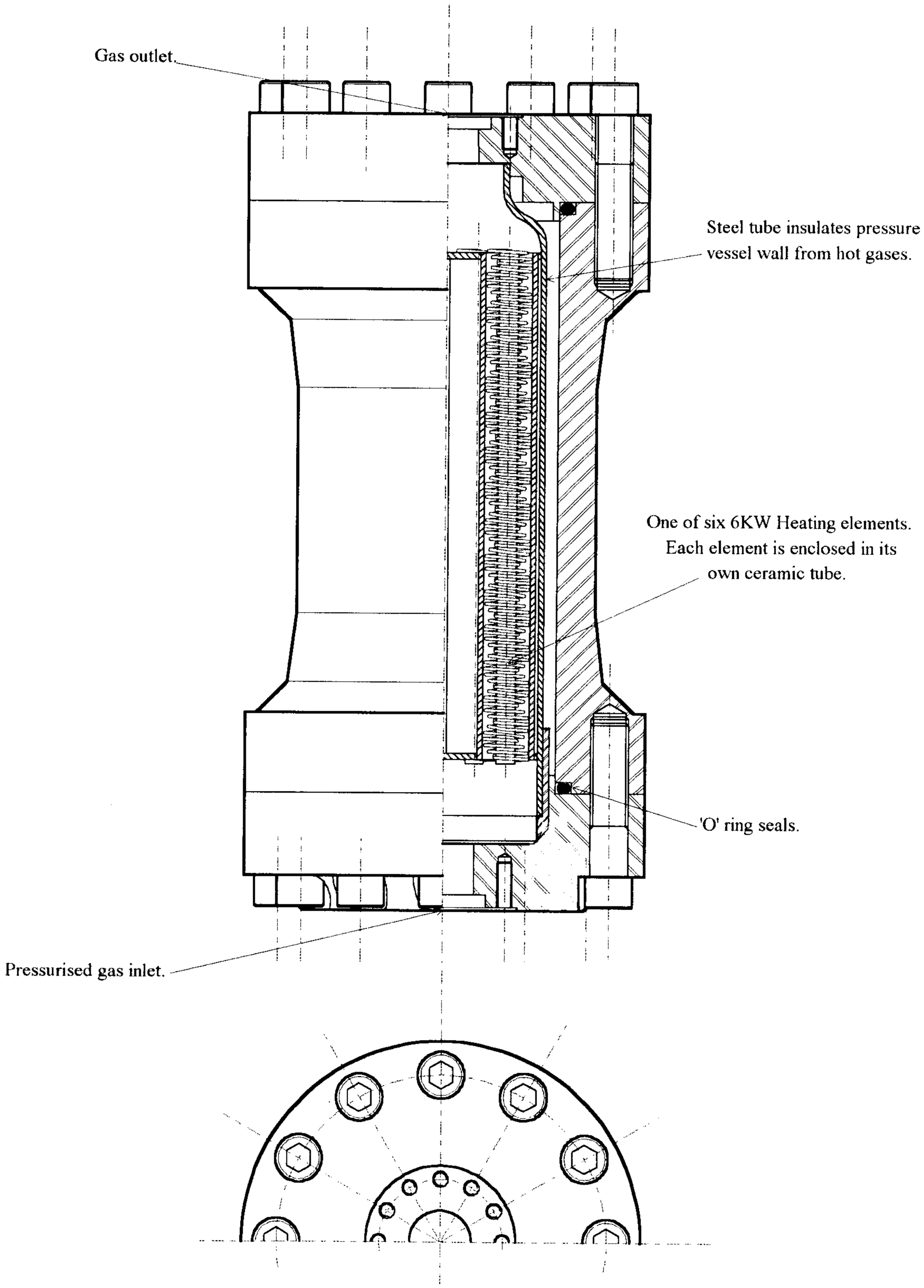


**Fig 2.5** Cross section of heater pressure vessel showing 'Sylvania' heater inside.

considered. In the end a thyristor-based phase angle control system was chosen. This type has good transient response and enables feedback to be used. The controller was constructed from discrete components as proprietary controllers were expensive and had no advantage over a purpose built version.

A feedback control has been added to enable a constant temperature to be maintained. This consists of a Eurotherm controller purpose designed for interfacing with an external phase angle thyristor controller. A thermocouple installed in the system between the heater and the chamber was used to measure the gas flow temperature. The thermocouple was connected directly to the controller which has a display of the measured temperature. In operation a set temperature is programmed into the controller, which then maintains the gas temperature close to this setting by varying the power delivered to the heating elements.

A complication of this design is the difficulty in bringing electrical current through a metal pressure vessel to the heater inside. This problem was solved by the use of a special type of cable called 'Pyro', which is designed for use in fire alarm systems, but is commonly used for the purpose of 'leading through' electricity into pressure vessels in industry. The cable consists of a copper tube inside which are the conductors. To insulate these conductors from the outer tube, magnesium oxide is compacted around the conductors. Due to this method of manufacture, the degree of compactness is so great that very high pressures are required to force out the conductors and insulation (though a minimum length of cable is required as friction alone is holding the pressure). Consequently if the outside tube of the cable is sealed using a standard tube fitting, as long as there is a sufficient length of cable, the internal gas pressure cannot escape. The cables, which can be seen in Plate 9, are the two copper tubes entering the rear of the pressure vessel. Two cables are required as all six wires of this three phase heater are accessible, the 'Pyro' only being available in a maximum of three cores.

## 2.2.4 Compressed air supply.

### 2.2.4.1 Compressor.

Compressed air is needed in large quantities and at high pressure for the operation of the combustion chamber. Though high pressure bottles were considered as a source of supply, it was quickly realised that the demands of the chamber would require tens of bottles of air per day for certain experiments. Apart from the cost, handling so many bottles would be impractical. So a high pressure compressor was considered as the only option, which should be capable of supplying air at a pressure of at least 100 bar and, if temporary storage was not used, at a flow rate of 5 Kg/min, which is the design maximum flow for the chamber.

Since no such compressor existed in the laboratory, one had to be purchased. It was quickly realised that a reservoir was not only necessary but desirable. Firstly, as the experiments in the chamber are intermittent with a compressor running continuously charging a bottle, a compressor of nominally lower delivery than needed by the chamber could be used; the periodic high flow rates being met by emptying of the reservoir. This system has the additional advantage that, if only for short periods, very high flow rates would be possible, by discharging the reservoir, much higher than could be achieved by direct supply from even a very large compressor. In fact the flow is only limited by the choking of the supply pipework. Combustion experiments would not be possible at these flows due to the limitation of the heater power output, but non combustion experiments could be undertaken.

After some preliminary inquiries it was realised that the purchasing of a new compressor was impossible because of its high price. So a second hand compressor was obtained from the Royal Navy. The finished installation is shown in Plates 10,11 and 12.

The compressor, shown in Plate 10, is a four stage, intercooled reciprocating type, with a discharge of 1 kg/min (35 SCFM) at a pressure of 270 bar (4000 psi). A 35 hp electric motor powers the compressor so the unit is self contained. All that is additionally required is cooling water for the jackets and intercoolers, which is supplied from the department's economy water system. A further refinement is the

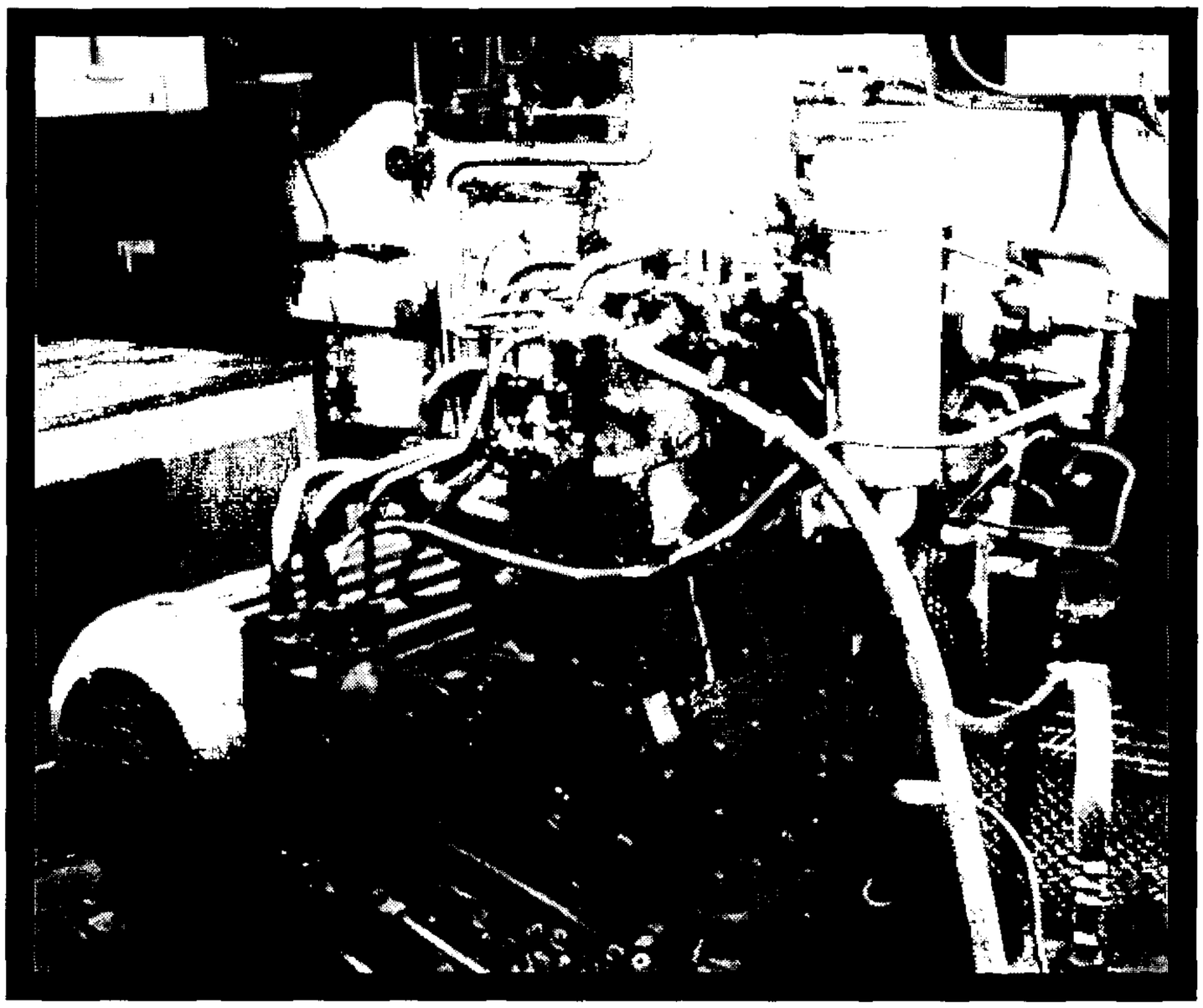

**Plate 10**. Picture of 4-stage high pressure compressor, which is capable of discharging 1 Kg/min of air at a pressure of 270 bar.

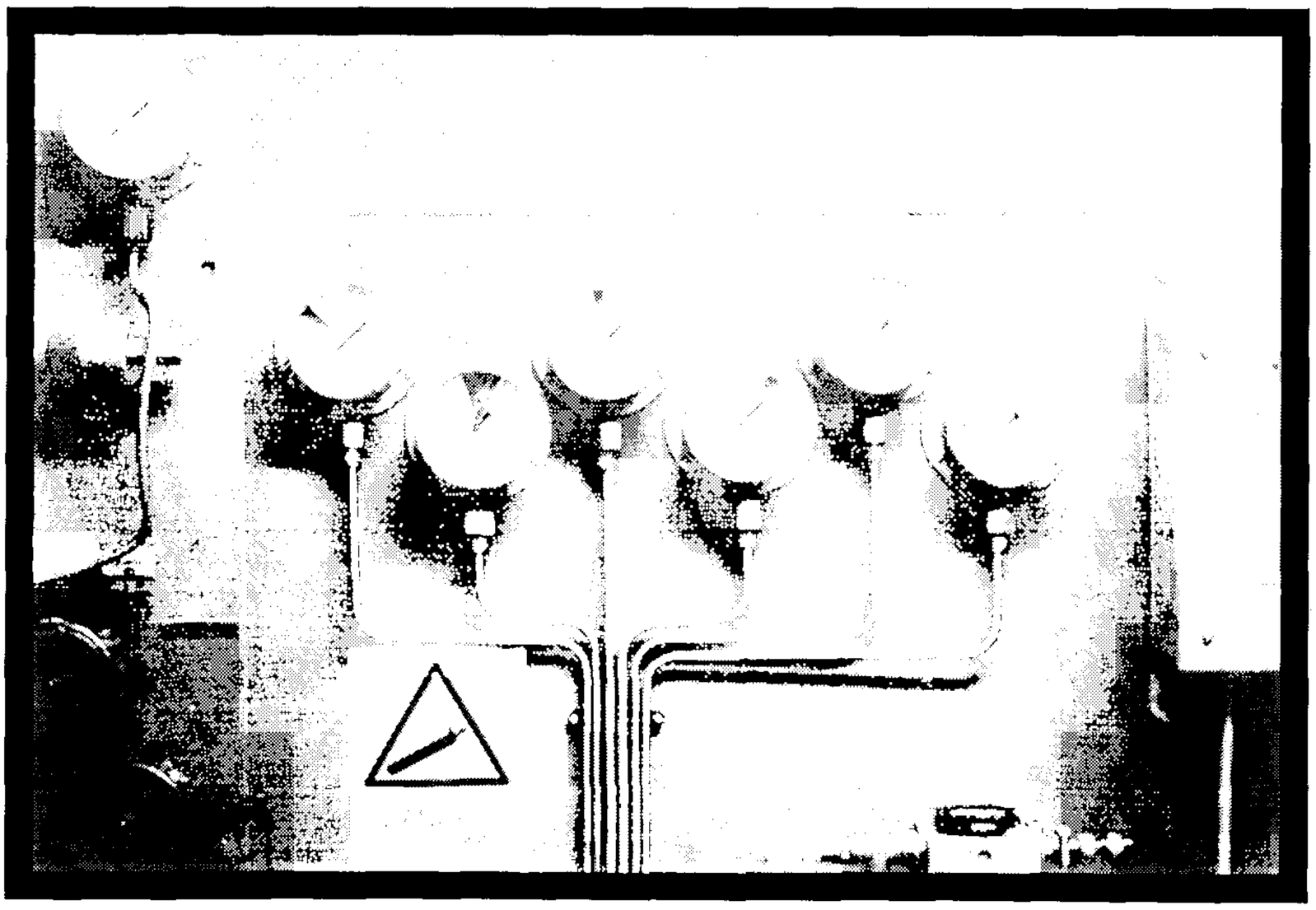

**Plate 11**. Pressure gauges on test cell wall used to monitor the operation of the compressor.

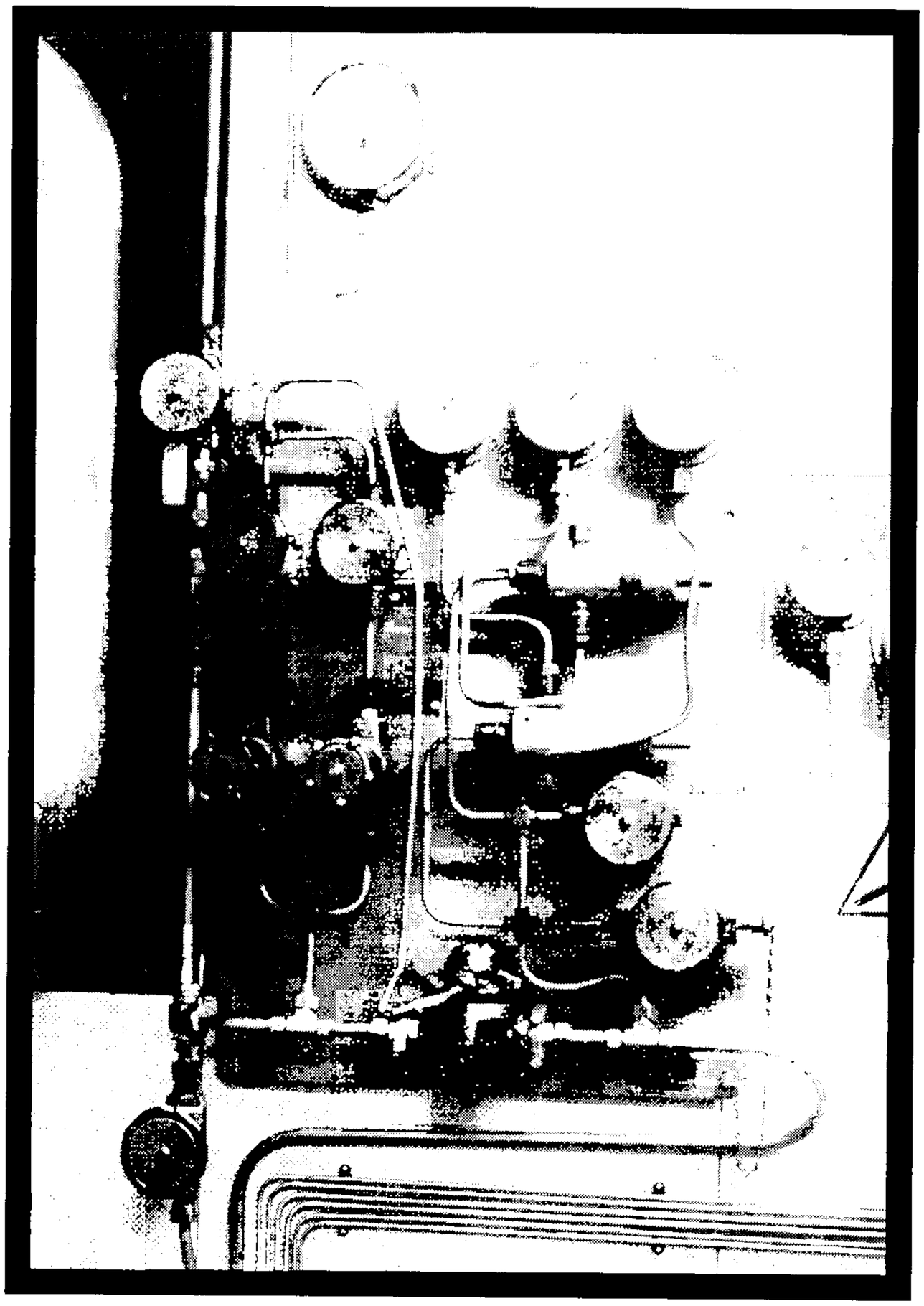

**Plate 12**. Reducing panel used to reduce the pressure of the air supplied to the chamber, from bottle pressure (typically over 200 bar) down to that required for experiments. This panel can supply air at any pressure from less than 1 bar to full bottle pressure at flow rates of over 20 Kg/min.

fitting of separators after each of the stages, except the last, which remove the water and oil that precipitates out of the air as it is compressed. The separators are purged every 40 minutes automatically. These separators are vital as they remove matter which would otherwise be entrained in the air of the system and hence flow through the chamber. This 'matter' would firstly foul the heater and secondly might be confused for droplets or soot and hence invalidate the experiments which require known inlet conditions.

The compressor is equipped with six pressure tappings for oil, water and the discharge pressure of the four stages. These tappings are connected to gauges mounted on the wall (see Plate 11) and enable the performance of the compressor to be monitored; they would also be the first indicators of any malfunction. A full description of the compressor and its operation is given in the manufacturers manual [*Compair Reavel,* 1990]. This manual also includes a trouble-shooting section which should be referred to if the compressor gives any problems.

### 2.2.4.2 Air storage and pressure reducing equipment.

The output from the compressor is taken under the floor through a non-return valve to a large receiver (at the left hand edge of Plate 12). This has a nominal capacity of 115 litres. which at the maximum pressure of 270 bar equates to some 40 kg of air. Only about 30 Kg is available, however, since some pressure must remain in the reservoir. A secondary purpose of the receiver is as a settling tank. This is required to avoid entrained oil and water from entering the chamber as there is no final stage separator on the compressor. A drain valve is placed at the bottom of the receiver inlet pipe which must be opened periodically. Air is drawn from the top of the bottle where it should be relatively clear of contamination.

From the bottle the air flows through a stop valve to the reducing panel, see Plate 12. The main item on this panel is a dome regulating valve, which is capable of maintaining a set pressure with a large variation of flow rate. The valve needs an external pilot regulating valve to maintain the pressure on one side of a diaphragm at the required outlet pressure. This is done by one of the two regulating valves, mounted vertically, on the left of the panel. On the right of the panel are some venting valves and pressure gauges for monitoring the outlet pressure.

After being regulated to the required pressure, the air flows through a high pressure tube under the floor to the rear of the combustion chamber where it rises and ends in a standpipe. This standpipe has a pipeline relief valve, a pressure gauge and a stop valve. The relief valve is designed to ensure that the pressure in the pipe does not rise above 100 bar. This is a protective measure against excessive pressure in the

flexible piping running from the stop valve to the chamber, the maximum working pressure of this pipe being lower than the connecting pipework. It also prevents air being fed to the chamber at above its working pressure, though the chamber's own relief valve would prevent any dangerous over-pressure.

In the run of flexible piping to the chamber is the main stop valve for controlling air flow into the chamber. This is an air-actuated stop valve which is maintained in the closed position while the chamber is at idle. When experiments begin, the control system which will be described later reverses the air pressure in the actuator that opens the stop valve. High pressure air is then free to flow through the chamber and experiments can proceed.

After flowing through the chamber the air is exhausted into the laboratory's exhaust gas system. This is done through a restriction, with air flowing from the high pressure environment of the chamber to the low pressure environment of the large bore tube of the exhaust system. Because of this large pressure drop choking is guaranteed in the restriction and it is a relatively simple matter to select the flow rate through the chamber by setting the area of this restriction. Various different sizes of restriction have been made and they are simply screwed in place into the outlet adapter of the chamber. Due to the restriction at the outlet of the chamber, the pressure in the chamber is almost identical to that of the pipeline, with the flowrate and hence pressure drop along the pipework being relatively low since most of the pressure drop occurs in the restriction.

For the moment this method of regulating the outlet flow is considered satisfactory, however, a much better way would be to use a throttling valve. The objection to this is its high cost and the requirement that such a valve has to take the full temperature of the exhaust whilst resisting very high pressures. To do this with a comfortable factor of safety involves the use of expensive materials and hence the price of a proprietary valve was unacceptably high.

## 2.2.5 Control and electrical system.

Electrical power for the compressor, combustion chamber and auxiliaries comes from a distribution board (see Plate 13), which has the additional feature of an emergency stop system. A large contactor needs to be energised for any electricity to be supplied to equipment in the test cell. If the stop buttons are pressed, the contactor de-energises, removing power to all equipment; however, lasers, computers and other measuring equipment are powered from the labs ring-main and are not disconnected. This emergency stop is considered an essential safety feature. After the contactor there are two individually fused circuits; one for the compressor and the other for the control panel, with cabling for both units running under the floor.

The control panel is shown in Plates 14, the box to the left of the panel is a 12 volt supply for proprietary automotive parts. The inside of the panel has three main sections. On the right side, are the power input, fuses and connector blocks. There are also two separate dc power supplies for powering various parts of the control system. At the top is the power control for the heater. As can be seen, there is a large heatsink for the power semiconductors- thyristors. The small black box above the heatsink is the phase angle controller which triggers the thyristors. This takes an analogue input from the Eurotherm controller described earlier, and controls the power output of the thyristors in proportion to this input voltage. Underneath the power controller are the relays which control the air supply, pump motor, pump fuel solenoid, and switch the heater on and off. These provide for semi-automatic control of the various parts of the chamber. The relays are primarily intended to increase the safety of operation through providing interlocking. They also have the advantage of relieving the user of routine operations and are much faster than manual operation.

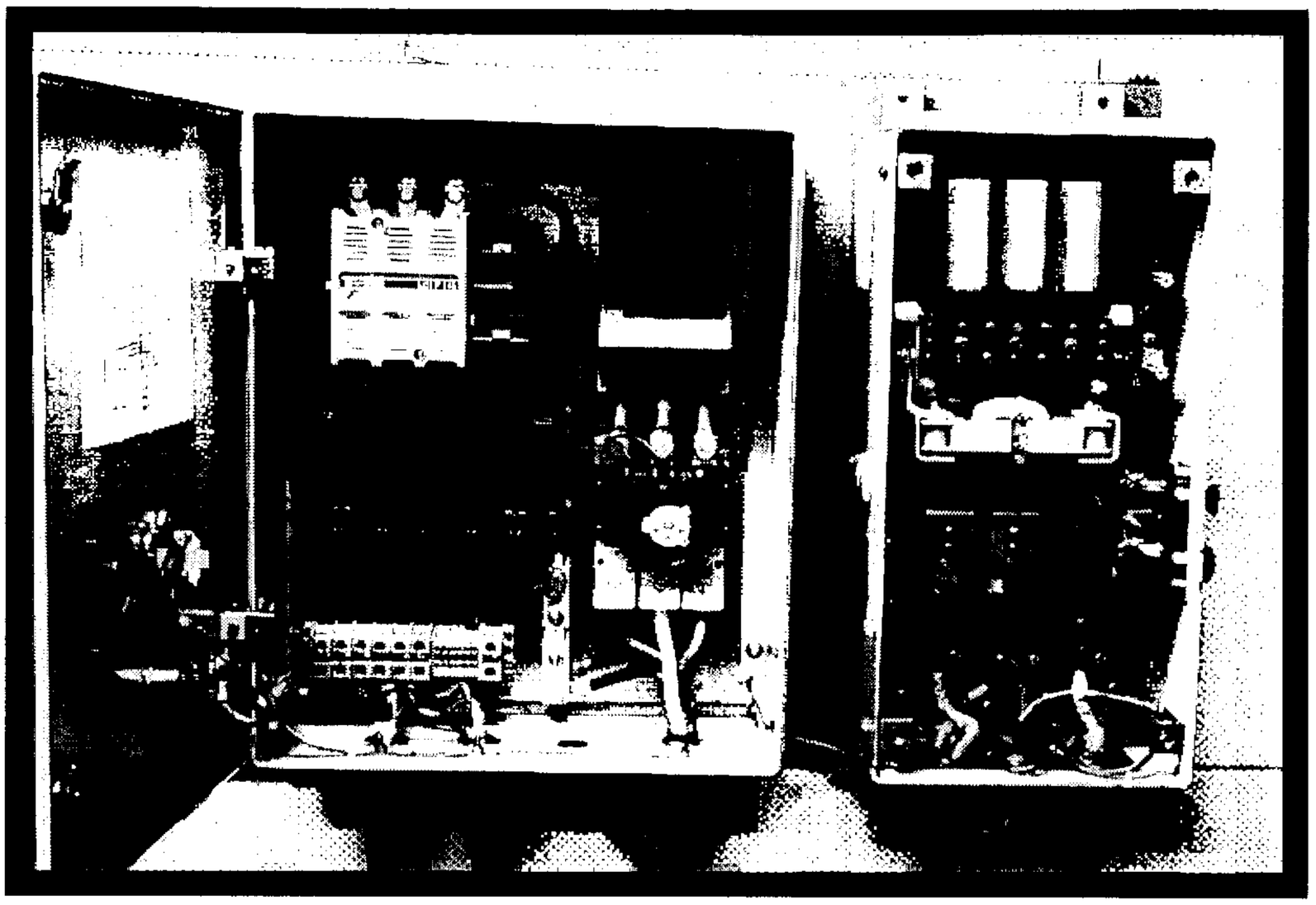

**Plate 13**. Distribution board with 'emergency stop' contactor which is designed to cut electrical power to all the equipment in the test cell in an emergency.

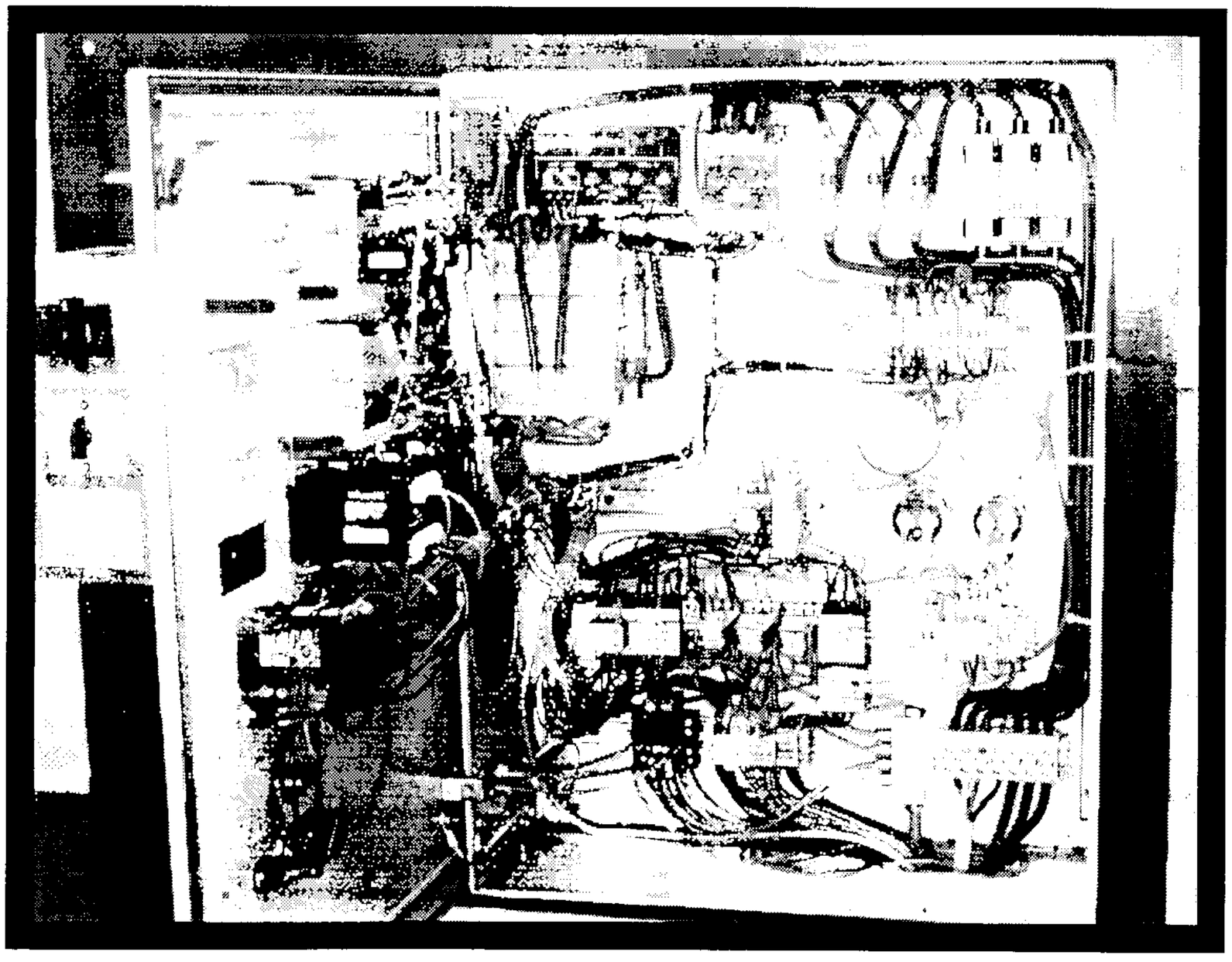

**Plate 14**. Control panel which provides semi-automatic control of the chamber and includes the heater power controller.

## 2.3 PRESSURE TESTING OF THE COMBUSTION CHAMBER.

After the assembly of all the various parts of the system, all that remained was to test the equipment. Pressure testing of the chamber, compressor and air reservoir was the most important task. Hydraulic testing of pressure vessels is clearly necessary for personnel safety, apart from being a requirement of the College's insurance policy.

Tests were made on all of the pressure vessels in the system (pipework is not covered by insurance) under the supervision of an inspector from the College's insurance company At first they were filled with either water or oil, care being taken to exclude as much air as possible. A hydraulic pump was then used to pump in oil through a suitable high pressure connection. The pressure applied to the particular vessel was measured with a test pressure gauge in the pipe leading from the pump to the vessel. By this means each of the components of the system was raised to a pressure of at least one and a half times its working pressure. In the case of the combustion chamber itself, the test was done with the quartz windows fitted, these being the most likely point of failure; all of the vessels passed the hydraulic test without any problems.

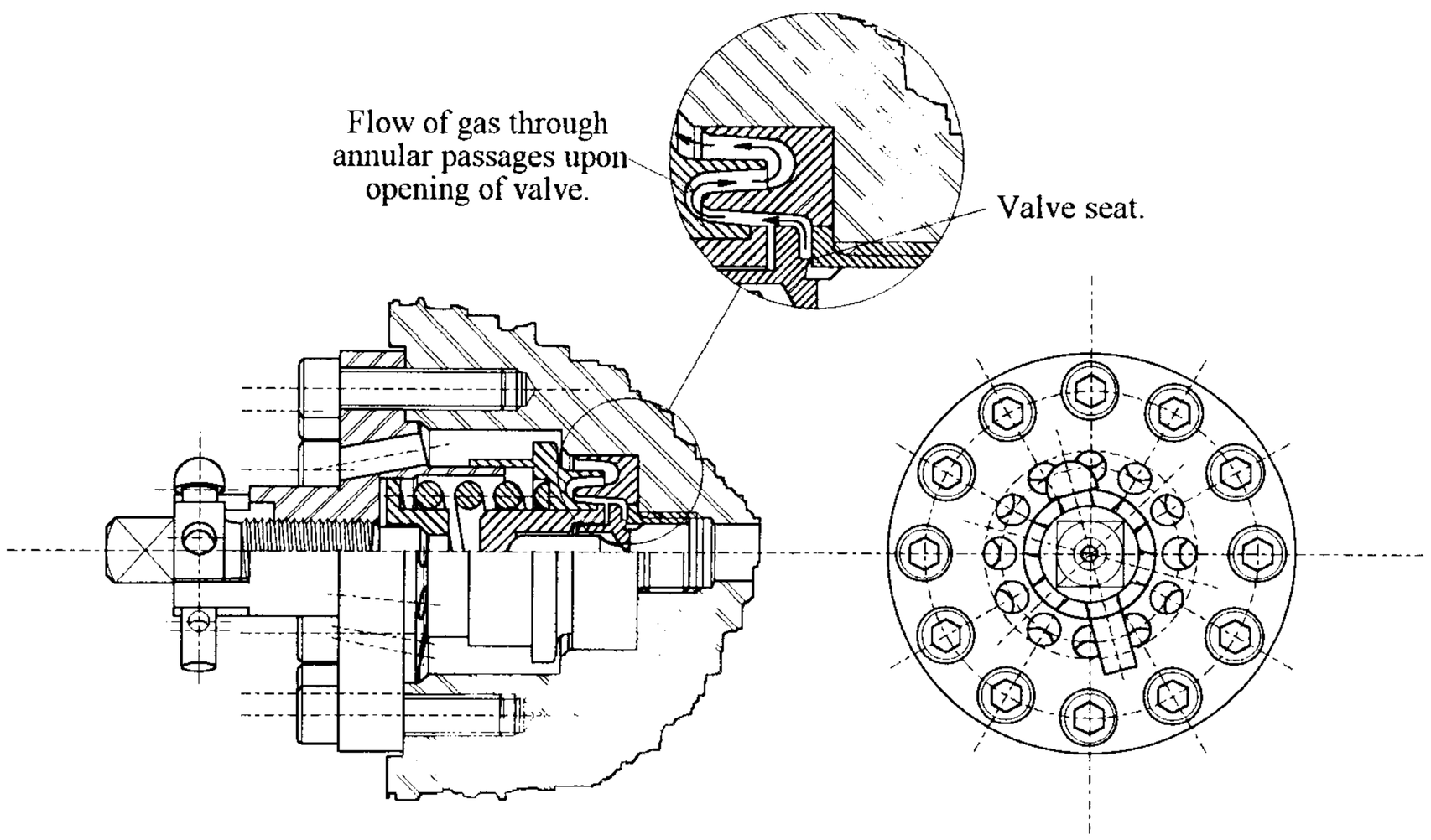


**Fig 2.6** Cross section of combustion chamber safety valve.

A second stage of testing, also supervised by the inspector, was the 'cracking' of the numerous safety valves in the system; it should be noted that during the hydraulic tests these were jammed closed to allow the necessary test pressure to be reached. The valves were set to crack at 105% of the working pressure which is a standard percentage used in industry.

The most important of these valves is that fitted to the chamber itself. Here, due to the presence of quartz windows, the chamber pressure must be relieved as quickly as possible should the pressure exceed a safe value due to the safety factors being lower than elsewhere in the design. The relief valve is of the 'pop' type, which has a very rapid response. This valve was designed and purpose-built in the laboratory. The outside of the valve is shown in Plate 2 on the underside of the chamber. Figure 2.6 shows a cross section of the valve fitted into the chamber. The rapid action of the valve is achieved by using the escaping gas to augment the force lifting the spring. This is done by using the impulse of the gas flowing through shaped passages which are labelled in Figure 2.6. In addition to impulse, there is also a degree of reaction as the gas is expanding radially, much like in a Lungström turbine. In operation the gas begins to leak slowly at the set pressure, but, with the slightest increase in pressure the valve 'pops' open. This 'pop' is in fact a very loud bang, and those operating the equipment for the first time should test the valve so that they know what to expect should the valve open when the chamber is being operated. It is good practice anyway for the safety valves to be cracked periodically to ensure their continued operation at the rated pressure.

## 2.3 GENERAL SAFETY PRECAUTIONS.

There is no substitute for experience when using such a potentially dangerous piece of equipment as this combustion chamber. For this reason any person wishing to use the equipment should be thoroughly familiarised with its operation by someone competent in the use of the chamber. However, there are certain basic rules which should always be followed.

The most dangerous part of the chamber is the breech mechanism. It is possible for the air pressure to be applied without this being closed; in the long run the best solution is the fitting of an interlock. But while there is no such interlock, before each experiment the user should make sure that the breech is definitely closed; this is easily done by observing the mark machined in the side of the window holder which should line up with one of the six marks on the locking ring (see Plate 15), thus ensuring that the threads are fully engaged.

**Plate 15**. Close up view of alignment marks used to check if breech mechanism is closed.

After the breech has been checked, a visual inspection of the chamber should be made with particular attention being paid to the windows, making sure they have no cracks. It may be possible to use a cracked window, but only if the crack is on the compression side (i.e. inside the chamber), and only if it is a side window. The head window is too large and the potential damage caused by its failure too great for such a risk to be taken. Nonetheless even with a side window, if cracked it should be

removed and inspected before any decision about its continued use is made. In general, if in doubt, it is safer to discard the window and use a new one.

Another source of danger in the system is the high pressure gas itself. Jets of air escaping from valves or from leaks can be travelling at high velocity and have a great deal of momentum. The hazard is caused by the possibility of these jets cutting skin or even piercing parts of the body. For this reason all such jets should be treated with care and direct contact of jets with any part of the body, particularly close to the leaking orifice, should be avoided.

## 2.4 FUTURE IMPROVEMENTS TO THE CHAMBER.

Despite the thorough design process, because of the prototypical nature of the design there are a number of shortcomings. This section will outline those which the author considers serious enough to warrant alterations at a later date.

### 2.4.1 Larger side windows.

As will be explained in the section on PDA, optical access at present rather restricts the extent to which PDA measurements can be undertaken. The experimenter is forced to use 70° as a scattering angle which, although it has some advantages, gives rise to low intensity of scattered light that makes measurement more difficult. Due to the difficulty of characterising Diesel sprays even under optimised conditions, this is a serious limitation. Ideally a scattering angle of 30° should be used, but any reduction from 70° will increase the light intensity and help taking measurements.

For this reason it will be highly desirable for the side windows to be increased in size. Figure 2.7 shows a cross section of the chamber with the proposed design which demonstrates much longer windows. This would allow the beams to cross the chamber at a more obtuse angle; a scattering angle of 45° could be obtainable with the

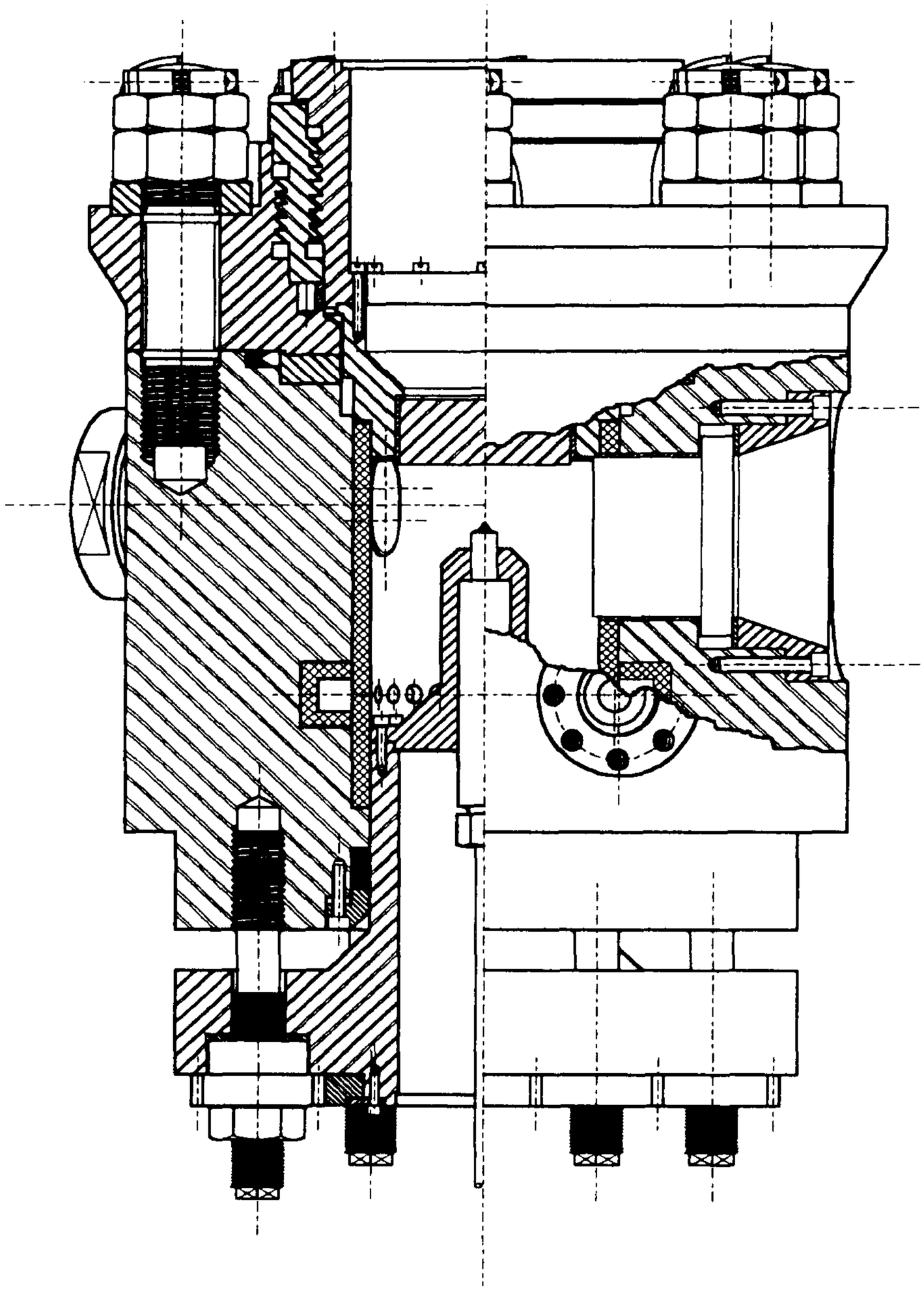

**Fig 2.7** Cross section of combustion chamber with new design of side windows for increased optical access, facilitating the use of smaller scattering angles for PDA studies.

design shown. One added benefit of this is that the injector would have to be moved along the chamber, away from the head window, to bring it in line with the crossing beams. At present the window suffers from spray impingement and the consequent bad fouling due to the proximity of the injector.

The proposed design, however, entails a great deal of metalwork on the chamber. New sockets for the side windows would need to be machined into the body

which would involve the chamber being removed from its mounting to allow the machining to take place. Although this is quite involved, the advantages are thought to far outweigh the expense.

The new design uses flange fittings for the side windows, however, this is not the preferred method of window fixing as there is always the possibility of tightening the flange bolts unevenly and hence cracking the windows. Nevertheless, it is the only feasible design as a screwed retaining ring, like that used at present, would be of too large a diameter to fit in the chamber. In defence of the flange fitting, this is the method adopted on many other chambers.

### 2.4.2 Outlet reducing valve.

At present the mass flow rate through the chamber is determined by a restriction on the outlet pipe. As this is always choked (except at very low chamber pressures of less than 5 bar) the flow rate is a linear function of chamber density. The restrictions are of fixed diameter and hence one restriction is needed for each flow rate at each pressure. When quiescent conditions are required in the chamber the flow rate is largely unimportant as long as it is sufficient to scavenge the chamber; the variation in flow velocity is rather small. However, when flow velocities are high enough to affect the spray, an infinitely adjustable throttling valve is necessary so that the mass flow can be controlled independently of pressure.

Such a valve must be capable of withstanding the high pressures present in the chamber and at the same time the high temperatures of the gas flow. Two options were considered: first the valve could be water-cooled, which would allow it to be manufactured from relatively low cost materials such as stainless steel. Alternatively a non water-cooled valve constructed from materials capable of withstanding high stresses at high temperature could be used. Materials with such 'red hardness' are expensive, however, the advantage is that the complication of water cooling can be avoided and there is no risk of the valve being operated without adequate cooling.

Because of the simplicity of a non-cooled valve, a proprietary valve was sought. 'Autoclave' manufacture high pressure valves designed for high temperatures

which have a special gland with an integral heat sink to avoid high temperatures at the sealing rings; these have to run at a lower temperature than the rest of the valve body. In addition the valves are manufactured with specially shaped needle tips which give a linear variation of mass flow rate upon adjustment. Although these valves are expensive, which has prevented their purchase, they are essential when gas temperatures are significant.

### 2.4.3 Interlocked breech mechanism.

The lack of interlocking of the breech could potentially result in the chamber being opened under pressure. Such an accident would certainly damage the chamber and cause injuries. For this last reason alone some form of interlocking needs to be fitted to the chamber. This can be achieved quite simply by fitting a pressure sensor or switch sensitive enough to measure very low, almost barometric pressures inside the chamber; it should be noted that even a pressure of less than 0.5 bar is sufficient to push out the window holder with considerable force. The sensor must also be capable of withstanding the high pressures found in the chamber during the experiments. Unfortunately these two requirements are mutually exclusive and it has been impossible to date to find a proprietary sensor. One solution is to use an isolating valve between the sensor and the pressure tapping which prevents pressure over a certain level from reaching and damaging the sensor. This would allow a cheap and sensitive low pressure diaphragm switch to be used.

In addition to prevent the breech from being opened whilst pressure is applied to the chamber, a locking pin engaging with the tightening ring of the breech is necessary. This could be actuated pneumatically with a small pneumatic cylinder, using the signal from the pressure sensor to control the solenoid valve.

# CHAPTER 3

# TESTING AND CALIBRATION OF FUEL INJECTION EQUIPMENT.

## 3.1 PRELIMINARY TESTS AND SKIP-FIRING VALVE.

### 3.1.1 Calibration of DPC pump.

Before any measurements of a spray can be done, the characteristics of the injection system need to be ascertained. This involves the simultaneous measurement of needle lift, line pressure and injection rate, all timed relative to the angular position of the pump. This is a fairly standard procedure so only moderate detail will be given here.

Preliminary experiments were done with a Lucas DPC pump which was mounted on a base plate, itself mounted on the top of the chamber bracket (see Plate 8, Chapter 2). This base plate has a fuel tank and filter and the pump is driven by a DC electric motor, equipped with speed control. The coupling between the pump and the motor was of a flexible type to allow for any slight misalignment. A flywheel on the pump shaft was necessary as, although the motor had more than enough inertia, the coupling's backlash would allow an unacceptable amount of pump speed fluctuations. The flywheel had a ring of 36 equi-spaced holes in its periphery which were used with a magnetic pick-up to provide the necessary timing for the data acquisition system. An additional single hole in the flywheel was also used to provide a 'once per revolution' starting pulse for the timing circuit.

All four injectors were connected to the pump, one being fitted into a Bosch type injection rate meter [*Bosch,* 1966]. The three remaining injectors discharged into flexible tubes for fuel recirculation. The injector connected to the rate meter had an inductive needle lift sensor and a bridge type Kistler pressure sensor was installed in the pipe line as close as possible to the injector. The signal from these two sensors and

the rate meter were simultaneously sampled by a National Instruments, EISA-2000 data acquisition card fitted to a PC. Time based sampling was used, the pulses from the flywheel pick-up merely being used to determine the starting point for the on board clock.

Measurements were performed at full load, half load and idle and at two different pump speeds of 600 and 1200 rpm (the conditions are given in Table 3.1). At each condition there were 10 tests and in each case the data from the three sensors was sampled at a rate of 50 kHz and stored over 15 injections. After completing the experiments the data was ensemble averaged and the results are shown in Figures 3.1, 3.2, 3.3 and 3.4.

| **Speed (rpm)** | **Load** | **Delivery ($mm^3$/Inj)** |
|---|---|---|
| 1200 | Full | 21.88 |
| 1200 | Half | 9.82 |
| 1200 | Idle | 2.17 |
| 600 | Full | 21.48 |
| 600 | Half | 10.03 |
| 600 | Idle | 2.48 |

**Table 3.1** Test conditions for calibration of DPC pump and tests of skip-firing valve.

## 3.1.2 Skip-firing valve.

### 3.1.2.1 Purpose of skip-firing.

Skip-firing or to use the older term 'hit and miss firing', refers to the intermittent injection of fuel and subsequent combustion. This mode of operation is highly desirable for certain types of experiment, particularly in combustion chambers. One example is combustion tests where there is insufficient air flow to purge the.

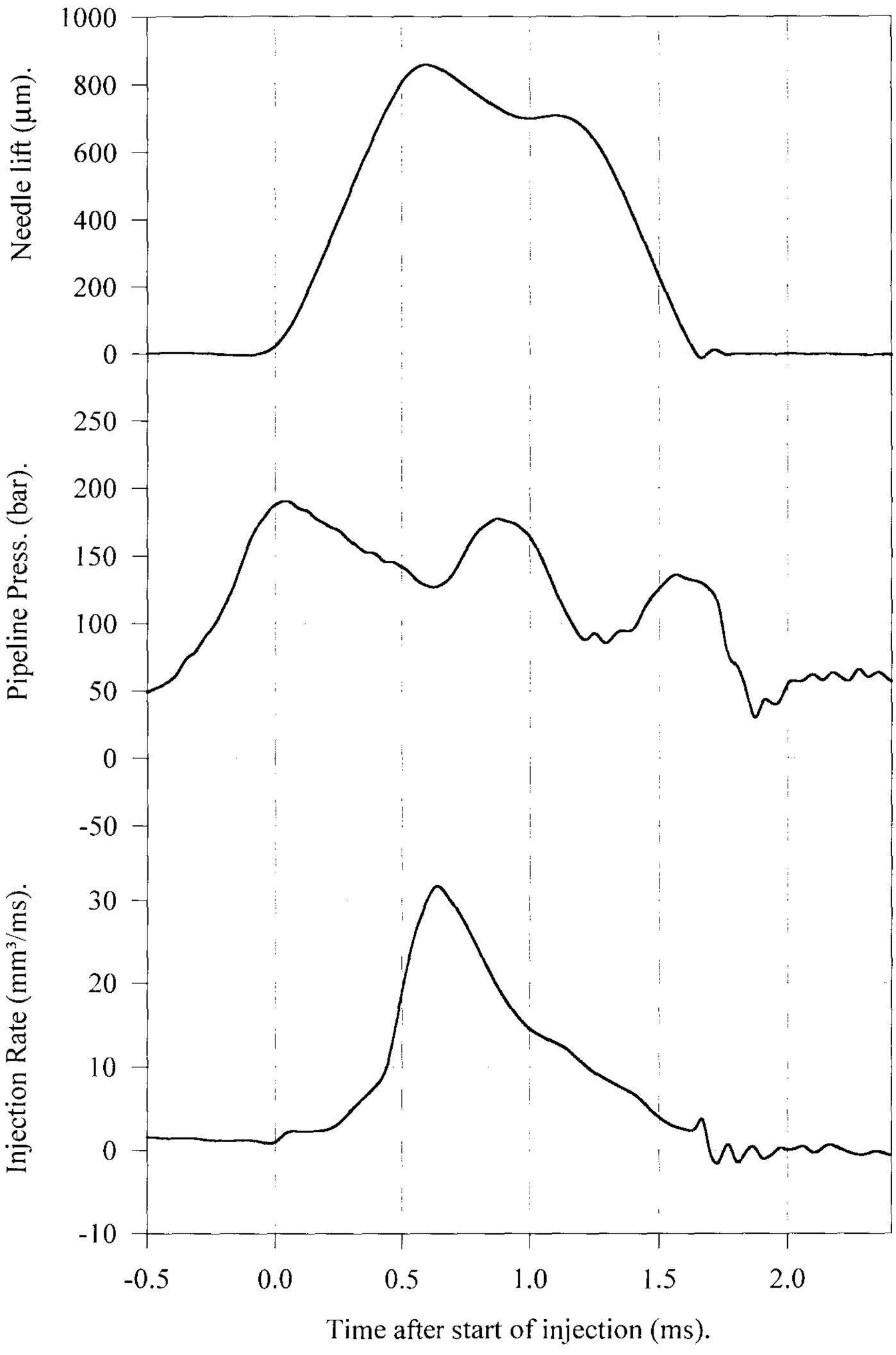


**Fig 3.1** Graphs of needle lift, line pressure and injection rate, of DPC pump FIE.
1200 rpm, full load.

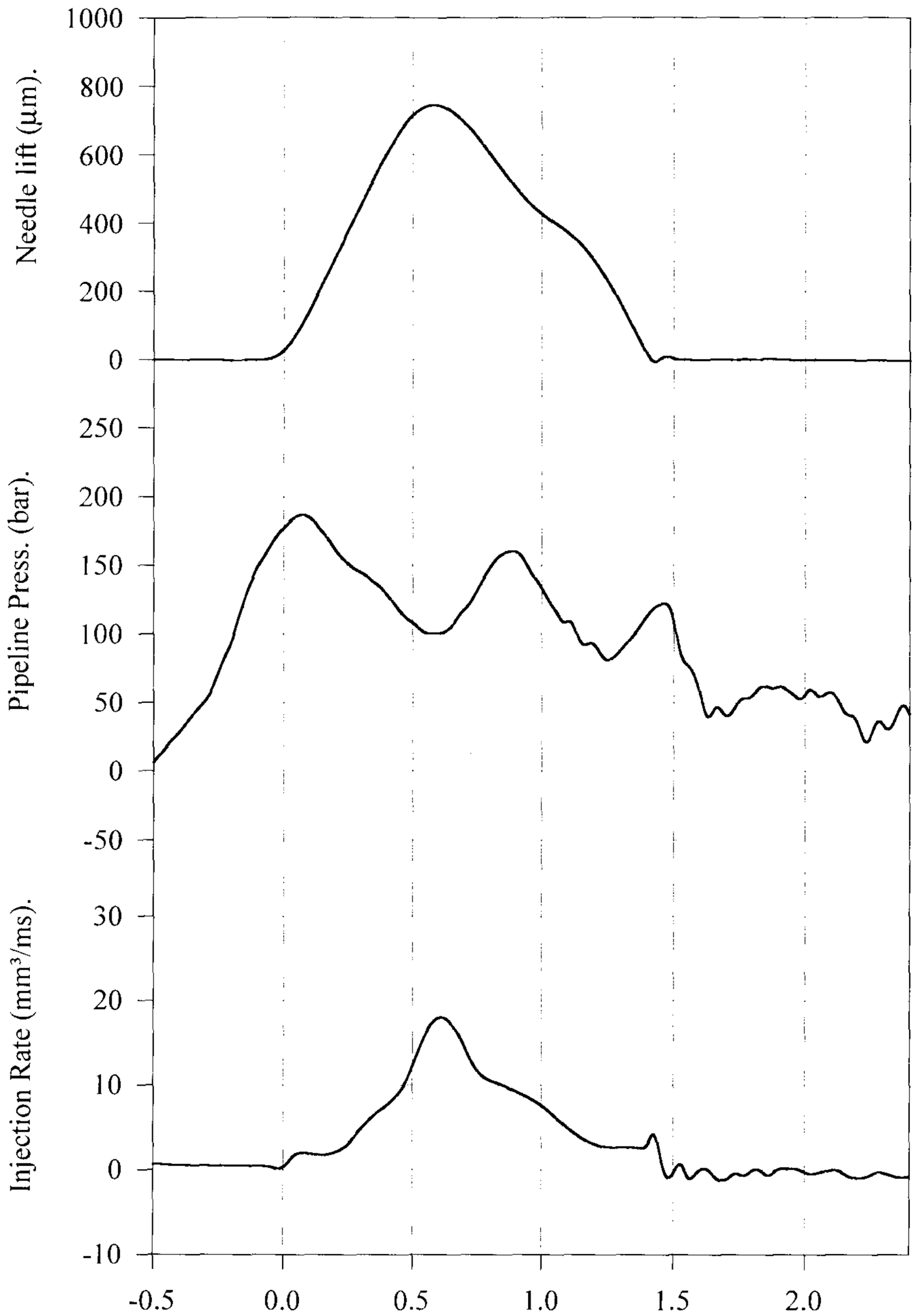


**Fig 3.2** Graphs of needle lift, line pressure and injection rate, of DPC pump FIE.
1200 rpm, half load.

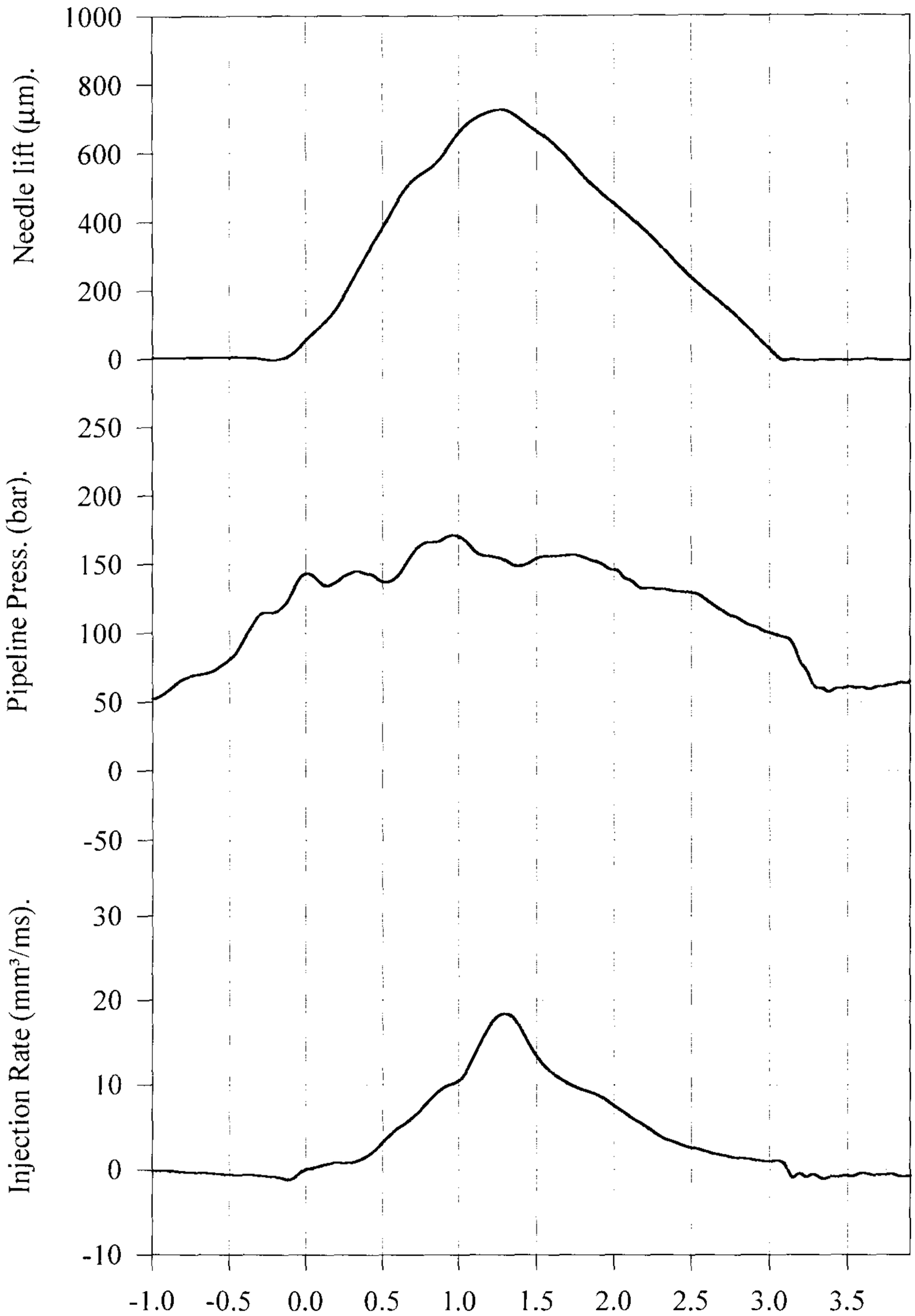


**Fig 3.3** Graphs of needle lift, line pressure and injection rate, of DPC pump FIE.
600 rpm, full load.

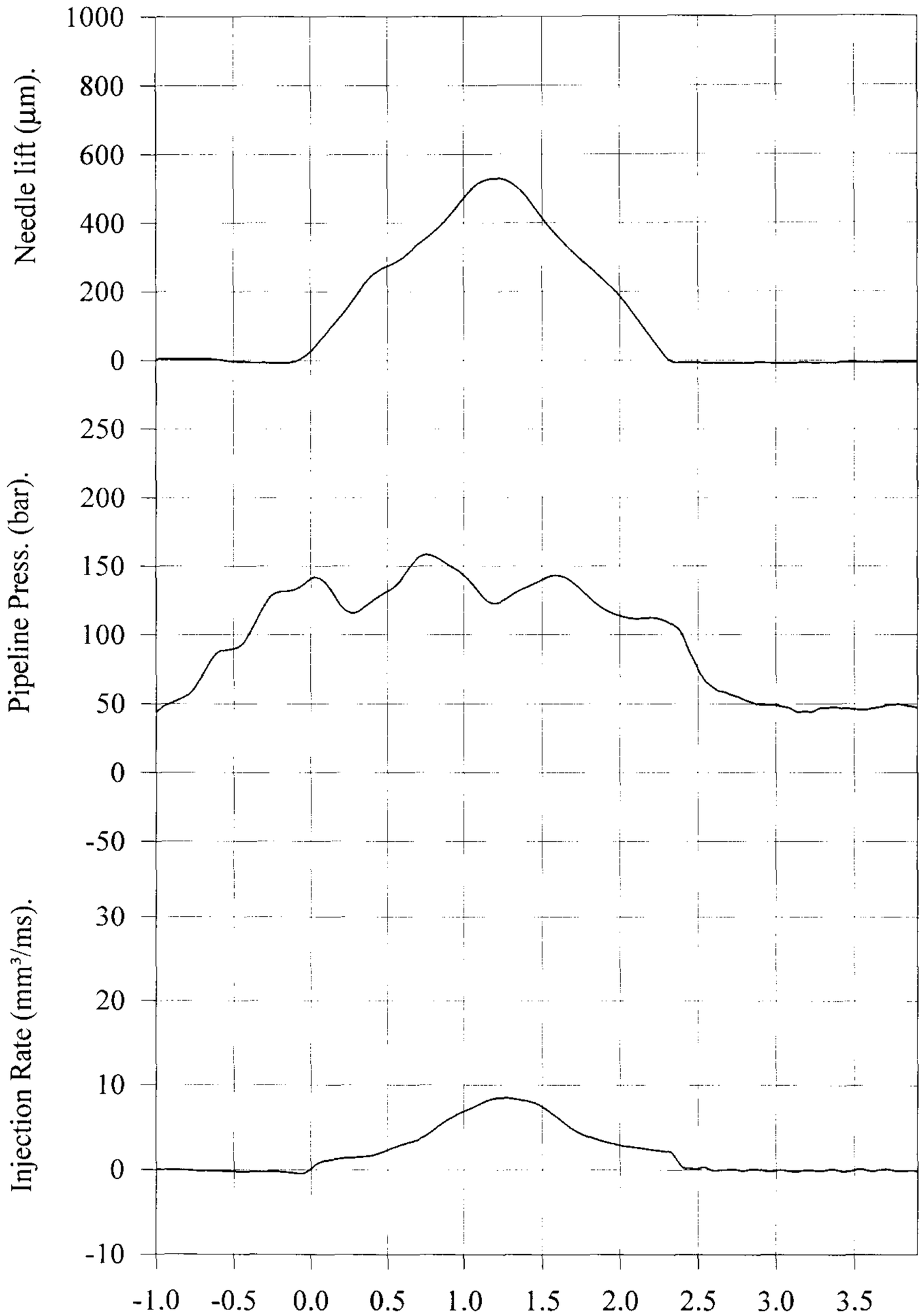


**Fig 3.4** Graphs of needle lift, line pressure and injection rate, of DPC pump FIE.
600 rpm, half load.

chamber of combustion products in-between successive injections, at normal pump speeds.

With electronic unit injectors (EUI) or the so called 'common rail' FIE, skip-firing is relatively simple [*Rao et al,* 1992], but in pump-pipe-nozzle systems, which still make up the bulk of injection systems in practice and hence also in research, the skip-firing of a Diesel injector is problematic. A commonly used technique is based on the fuel solenoid or cut-off, where the cut-off is held closed with the pump running at the required speed, but when an injection is required the cut-off is rapidly opened for one or more cycles. This is not very satisfactory, however, as in practice the delivery from the injector is always low immediately after the cut-off is opened, taking a number of injections to recover to full fuelling. Nonetheless this is a very simple method and can be used if a calibration is performed of the actual delivery using the cut-off. Despite that a better technique was thought necessary for use in the combustion chamber.

*Renner and Maly* [1994], have used a switching valve in the line to produce

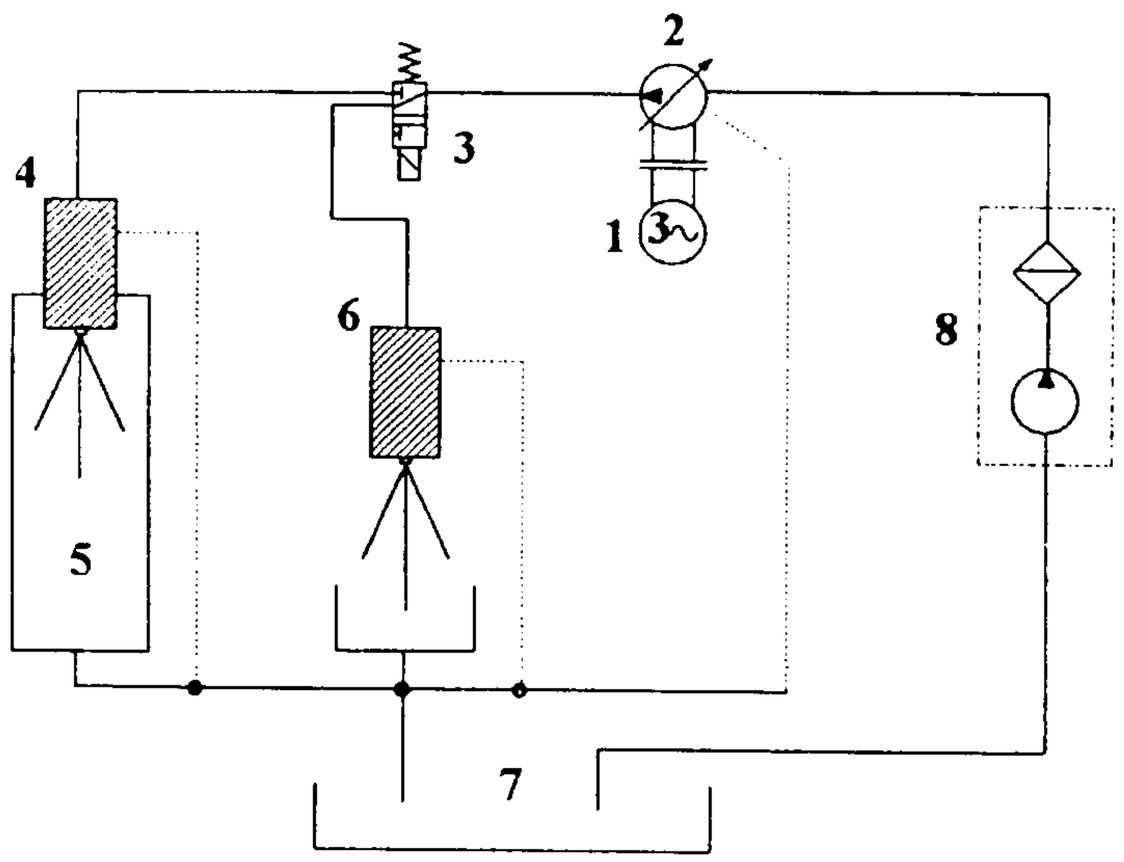


**Fig 3.5** Schematic diagram of skip-firing system using fifth injector and fast acting 'single injection valve'. The experimental set-up: 1 - electric motor: 2 - injection pump; 3 - single injection valve: 4 - injector: 5 - high pressure chamber: 6 - by-pass injector: 7 - fuel tank: 8 - fuel circulating pump. [*Renner and Maly*, 1994]

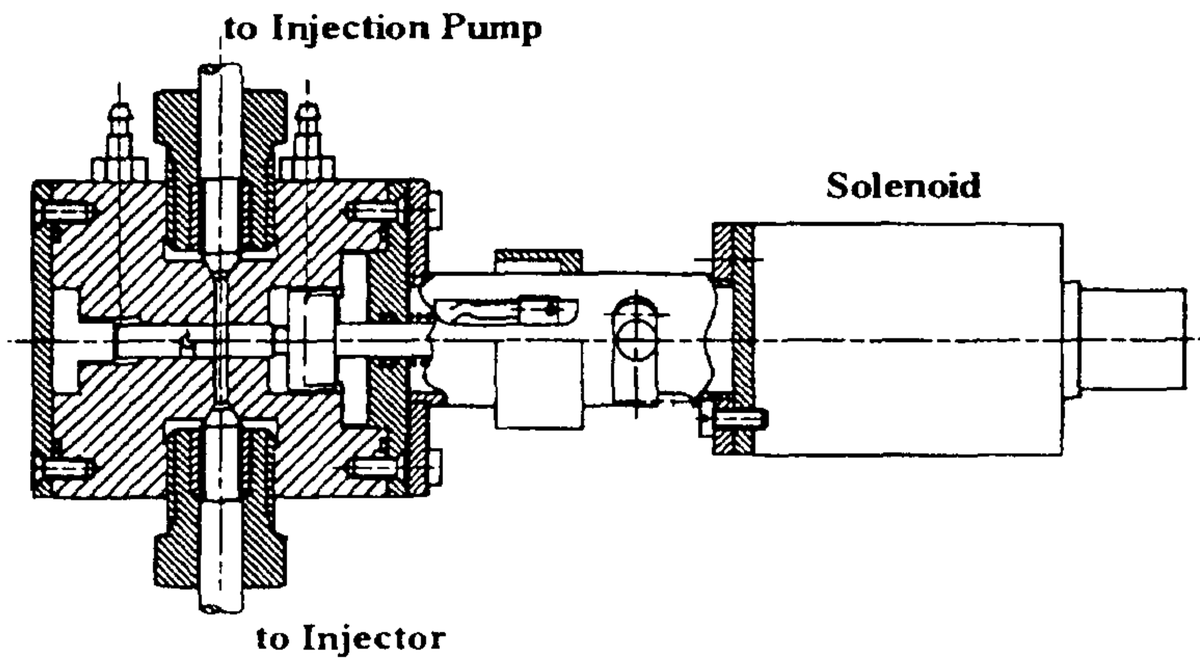


**Fig 3.6** Fast acting single injection valve. In the 'on' position shown, the electro-magnetically operated shift needle connects reflection-free the high pressure pipelines via a hole identical to the inner diameter of the pipelines used. [*Renner and Maly*, 1994]

much more realistic injections. The basic principle involves the use of a two way valve in the pipeline and a fifth injector or by-pass injector, as shown in Figures 3.5 and 3.6. The pump is run continuously, but with the fuelling cut-off open. Normally the delivery from the pump is directed via the two way-valve to the fifth injector. This, like the three dummy injectors discussed previously, discharges into a vessel. When an injection is needed for the experiment, the two-way valve is rapidly switched on directing a single pulse of fuel from the pump to the injector mounted in the test equipment. After the single injection is completed the valve switches back to its normal position and the fifth injector again takes the pump delivery.

Although this seems to be a straightforward method, there are a number of objections. Firstly, a great deal of complicated piping needs to be used; this extra piping changes the characteristics of the FIE and hence affects the validity of the experiments. Secondly, fast acting high pressure valves are expensive and along with the fifth injector the cost of the set-up becomes very high. Thirdly, and most importantly, the back pressure which builds up in the pipe line when the pump is injecting continually (this can be over 100 bar) will tend to leak out past the main injector while the pump is delivering to the fifth injector via the two-way valve. When the valve switches and directs one shot from the pump to the main injector, the first part of the delivery is used filling the pipe before an injection can take place. This

may only be a few percent of the delivery, but as with the fuel solenoid method, a calibration has to be made if accurate experiments are to be performed; pump timing may also be affected

What is thus needed is a simple and cheap device, which can be taken from system to system and simply bolted to the pipeline. At the same time it should introduce the minimum of changes to the injection characteristics; the design of such a device is described below.

### 3.1.2.2 Conceptual and detail design of Mk.1 skip-firing valve.

The two main requirements for the design are that there should be as little change to the production FIE system as possible and that the valve should be simple to fit and operate. The first idea was to fit a relief valve into the pipeline. The cracking pressure of this valve would be set to below the nozzle opening pressure of the injector, so that whenever a pressure pulse was delivered from the pump, to prevent an injection occurring, the relief valve would open thus preventing pipeline pressure from exceeding the nozzles opening pressure. On the other hand, when an injection is required, the relief valve is held down and prevented from opening. The pressure pulse from the pump will then travel down the pipe and open the injector in the normal manner. With this system it was hoped that a near perfect single-shot injection could be achieved.

The finished Mk.1 valve is shown in Plate 16, and disassembled in Plate 17. The valve has a main body into which an old pintle nozzle is fitted; the pintle has been ground off to reduce the obstruction caused to the flow. Screwed into the top of the body is a spring holder, the position of which can be adjusted up and down to vary the spring force on the needle. The whole assembly is bolted onto the pipeline close to the pump and a hole is drilled through the pipe at the point of contact between valve and pipeline. The pintle nozzle is firmly held to the bottom of the body affecting a seal. In this way the pipeline pressure acts on the underside of the needle. The only force stopping this pressure from lifting the needle being that exerted by the spring; this is

the arrangement of the relief valve. A solenoid bolts to the back of the valve body and, via a lever and push rod, holds the needle down when energised. Thus the relief valve

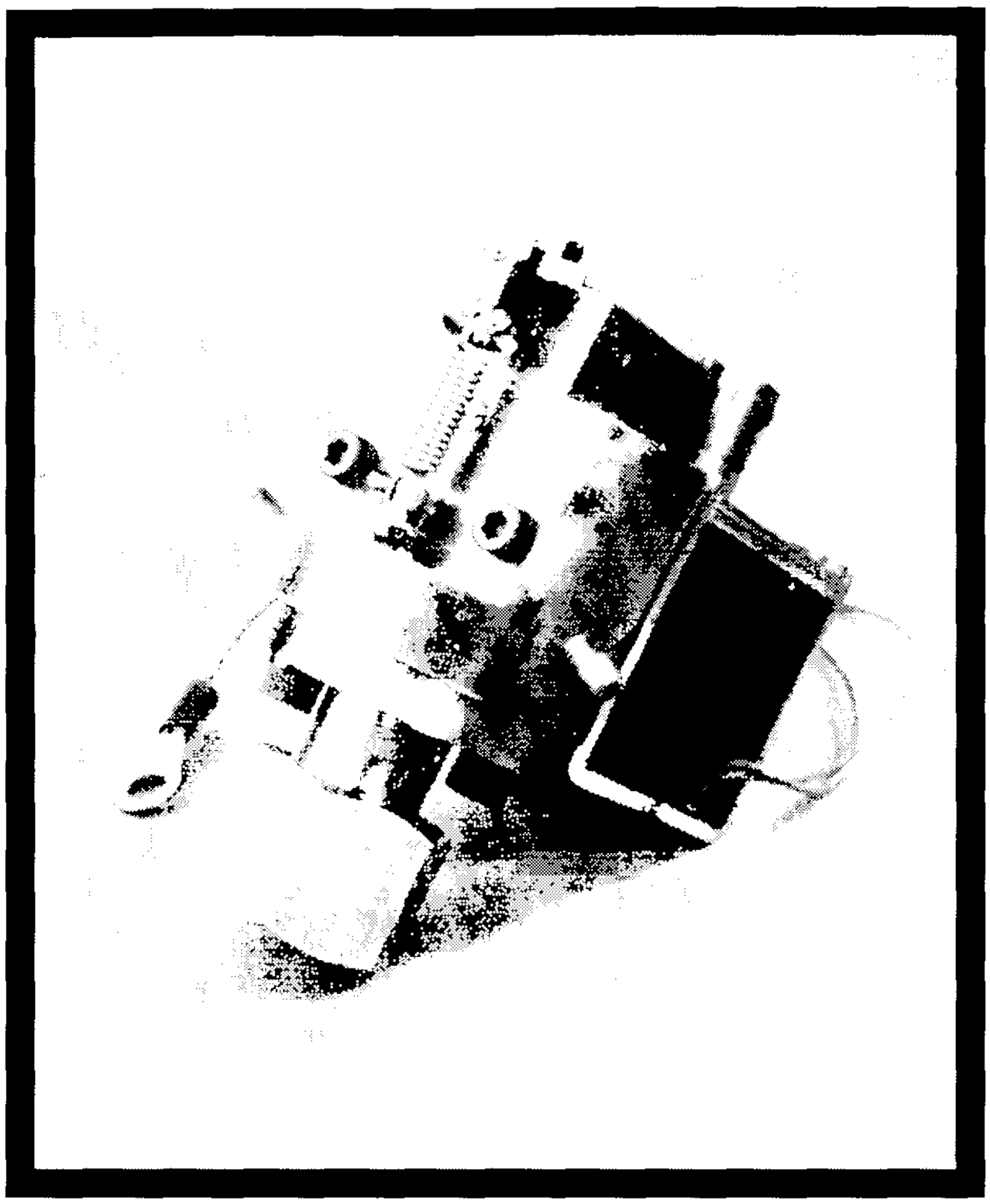

**Plate 16.** Mk.1 skip-firing valve.

is held closed by the lever and the injection proceeds as normal. A tension spring returns this lever to its rest position, after the solenoid is de-energised, so that its inertia does not stop the relief valve from opening. A screw on the lever provides for adjustment of the lever travel, and hence determines the maximum needle lift.

The final part of the system was the electronics controlling the solenoid. Here the once-per-revolution pulse is used to switch on a transistor for just one revolution.. A timer then starts which can be set to delays from 0.5s to 10s. When the timer delay is over, the electronics again waits for the once-per-revolution pulse and the cycle repeats; by this means regular but intermittent injections could be achieved.

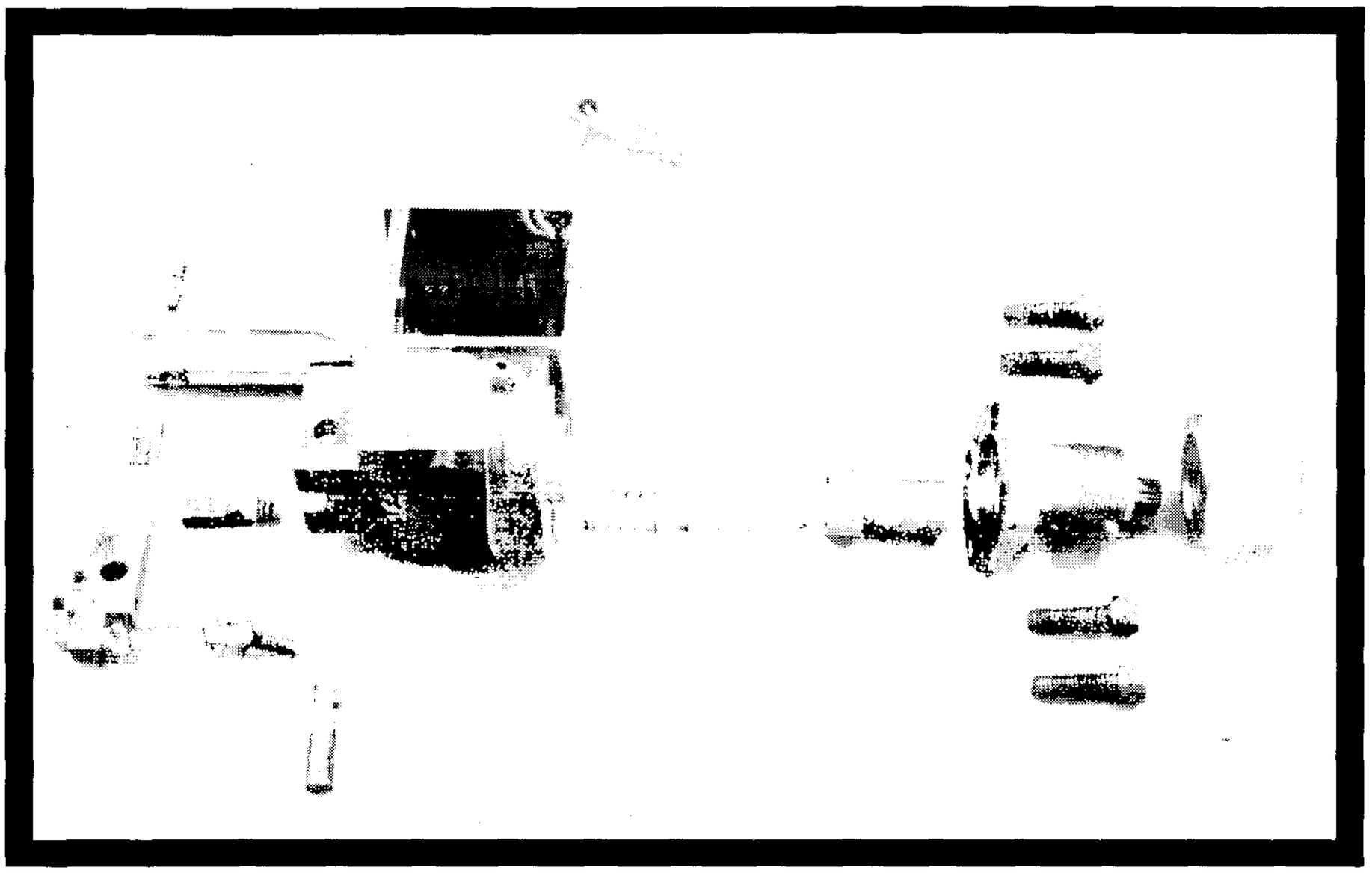

**Plate 17.** Exploded view of Mk.1 skip-firing valve.

### 3.1.2.3 Tests of Mk.1 skip-firing valve with DPC pump.

Once the valve had been completed all that remained was to test it in a real injection system. As the DPC pump was already set up, this was considered a good test case. The skip-firing valve was bolted to the pipeline and a series of tests completed at the same load and speed conditions at which the pump was calibrated. The goal was to produce single-shot injections identical to those of the calibration.

To allow comparison with and without the skip-firing valve, the needle lift, injection rate and line pressure were all sampled using the same data acquisition system as before. The single difference between this and the standard calibration was that injections were intermittent so that sampling during the period without injections was considered unnecessary. For this reason the data acquisition card was only triggered when the valve was energised. However, the subsequent two injections were also sampled in order to determine if the valve was functioning correctly and only producing single injections.

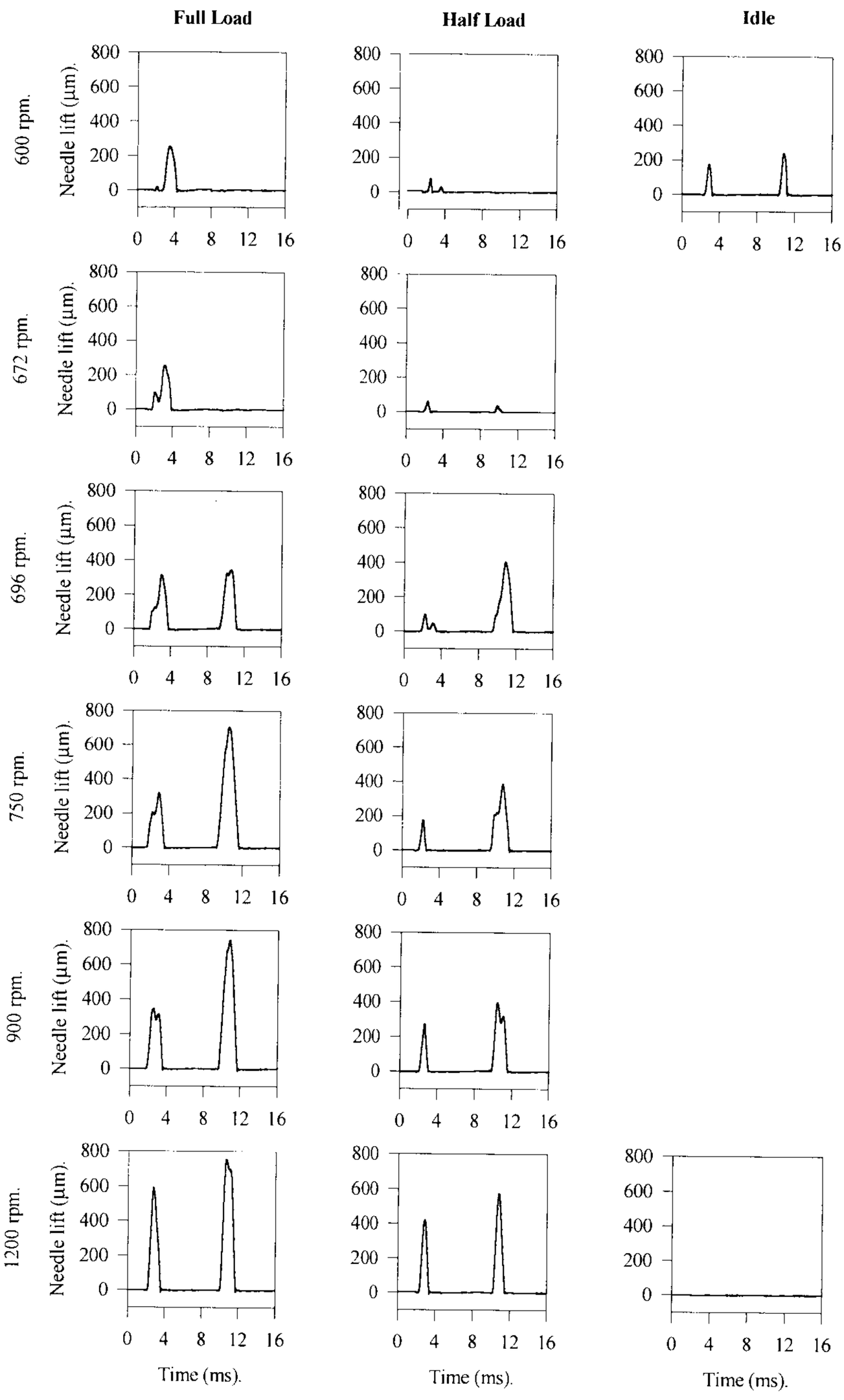


**Fig 3.7** Graphs of needle lift traces of pre, main and post injections, at different loads and speeds using Mk.1 skip-firing valve and DPC pump FIE.

The results of the tests are shown abridged in Figure 3.7; this figure shows the needle lift traces for the various tests. In each graph the main and the following injection are shown. Ideally the main injection would be identical to the original calibration with no 'follow on' injections. Unfortunately the results are far from satisfactory and there is very little similarity between these results and those of the original calibration. The main problem is that the valve does not seem to operate fast enough and this is manifested in the small needle lifts obtained at the higher speed condition where the first injection is little more than a dribble. Even at low speeds where the valve seems to operate fast enough, a stroboscopic light was used to check this and the result was an injection with a delivery far below that measured in the calibration. 'Follow on' injections were also a problem except at very low speeds.

The observed faults are probably caused by different factors. First, the speed of operation of the valve is clearly related to the design of the moving parts; the conclusion being that the solenoid has insufficient power to move the lever fast enough. The use of the lever itself was only necessary because of the inadequate power of this solenoid. On the other hand, the low delivery seems to be caused by a more fundamental problem which is related to the pipeline pressure trace. By comparing the two calibrations with and without the valve, it can be seen that the residual pressure left in the pipeline between injections is very low in the case of using the skip-firing valve, but has a high value without the valve under normal conditions. The conclusion that can be drawn from this is that, with the valve fitted, the pipeline is partially empty. This may be because gas has been sucked in through the relief valve or may be due to cavitation. In either case, even with the valve fully closed, the delivery from the pump must first fill the pipe before any injection can occur. Secondly, because of the low pressure on one of the outputs from the pump, cavitation is very likely to occur in the pumping chamber. There is anecdotal evidence of this as the characteristic 'hammering' noise caused by injections of the three dummy injectors was not present in this case.

### 3.1.2.4 Improved design of skip-firing valve.

Since the Mk1 valve failed to meet its design specifications, a new improved Mk.2 valve was designed and made which would hopefully solve the problems of the earlier design. The basis of the new design is still an old pintle nozzle, though almost every other detail has been changed.

To improve the speed of operation, a much more powerful solenoid was acquired; this solenoid is a special type with a very short stroke but can produce a force of up to 1 kn. It is much more expensive than the original solenoid, but can hold the valve closed without the use of a lever as an amplifier. The short stroke, only 3 mm, is not a restriction as the maximum valve lift needs only to be 1.5 mm for unrestricted flow.

The biggest problem with the first design was the low residual pressure in the pipe and to solve this it was decided to abandon the idea of a simple relief valve exhausting to atmospheric pressure. Instead, back pressure would be maintained on the downstream side of the valve, so that even with the valve fully open, pressure in the pipe could not fall below a pre-set back pressure. Back pressure is maintained by a 'Swagelok' relief valve, which can be adjusted to open at a particular pressure. To reduce pressure fluctuations, caused when the relief valve opens and closes, a long coil of piping is installed between the skip-firing valve and the relief valve. If this proves inadequate an accumulator could be installed in the system which would certainly eliminate any fluctuations. One beneficial consequence of the back pressure is that the pintle nozzle is forced open as soon as the solenoid de-energises, thus leaving an unrestricted passage for the pressure pulse in the line to discharge through. In the existing design, at high speed the spring operated valve could not open fast enough to prevent the pressure exceeding the nozzle opening pressure, consequently injections occurred continuously (This was a problem even at quite low pump speeds).

Plate 18 shows the Mk.2 valve in-situ on the EPVE pump system. The coil of pipe and relief valve can be seen clearly, the unconnected port is designed to accept a pressure gauge, this being used when setting the back pressure. The value of the back pressure would be obtained from an existing calibration of the particular FIE; surprisingly this value seems to vary quite considerably, typical values being from 10

to 100 bar, due to the degree of sealing at the delivery valve of the pump and the injector needle not being consistent for different FIE. The large cylindrical object on the top of the valve is the solenoid. Its plunger has a pip machined on the end which bears directly on top of the needle.

Power for the solenoid is produced by a specially designed power-pack. This contains an unregulated 165V DC power supply along with mains line filtering to reduce interference with any nearby sensitive electronics. A Mosfet transistor, also within the power-pack, is used to switch the power to the solenoid on and off. This is triggered from an external counter which only needs the outputs from a shaft encoder to operate. The counter allows the timing of the solenoid energisation to be controlled much more precisely than on the first design. In particular the length of energisation can be set to be as short as possible, giving the maximum time for the back pressure to lift the needle clear from its seat, ready for the next pressure pulse to be vented. A schematic diagram of the system is shown in Figure 3.8

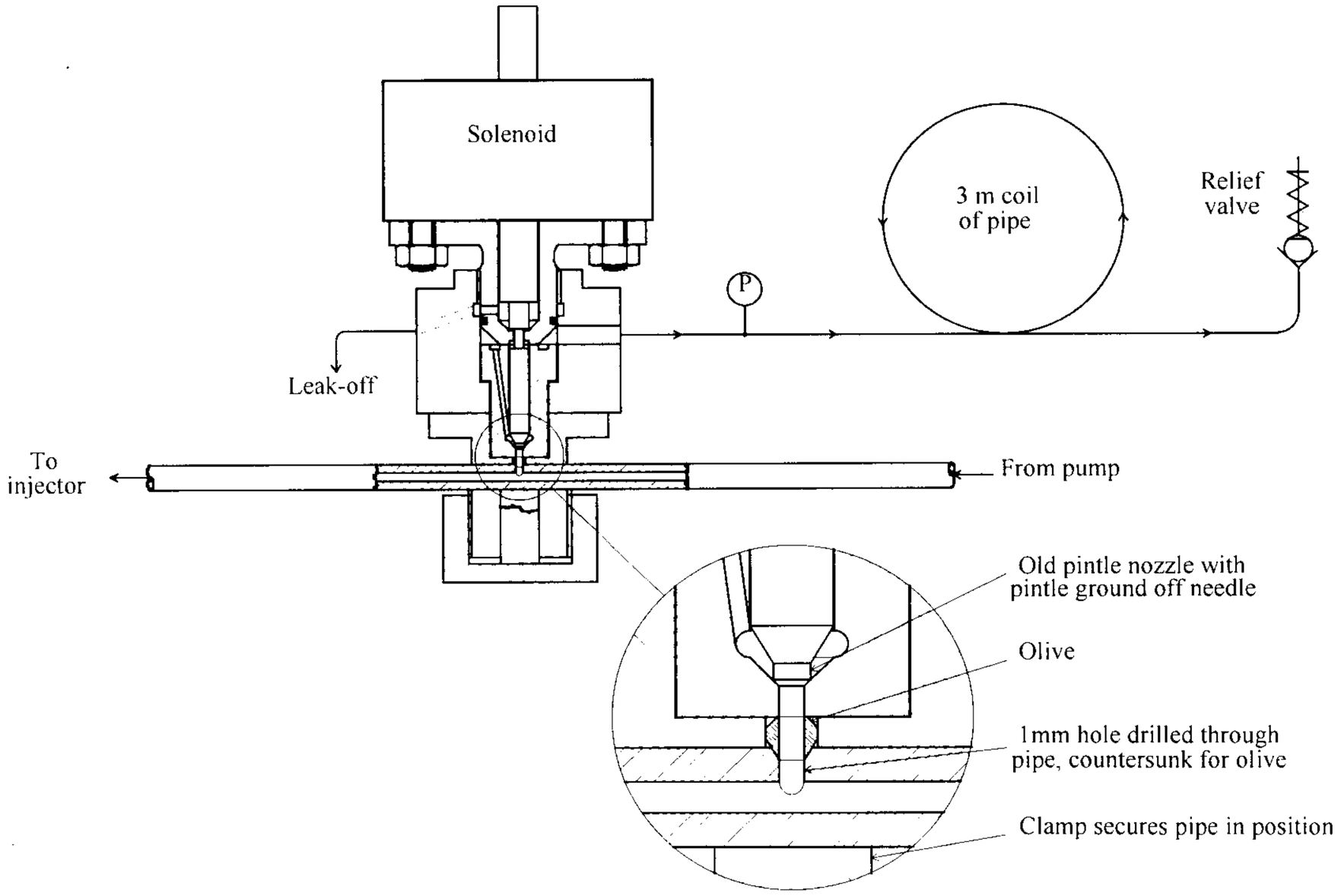


**Fig 3.8** Schematic diagram of Mk.2 skip-firing valve showing cross sectional detail.

### 3.1.2.5 Tests of Mk.2 skip-firing valve with EPVE pump.

Following preliminary tests with the DPC pump, the operation of the new valve was evaluated in detail in the EPVE pump. This was due to the fact that the EPVE pump operates at much higher pressures and deliveries and therefore provides a much 'tougher' test of the valve's operation. The high injection pressure in particular could easily lift the needle valve if the solenoid provides insufficient force.

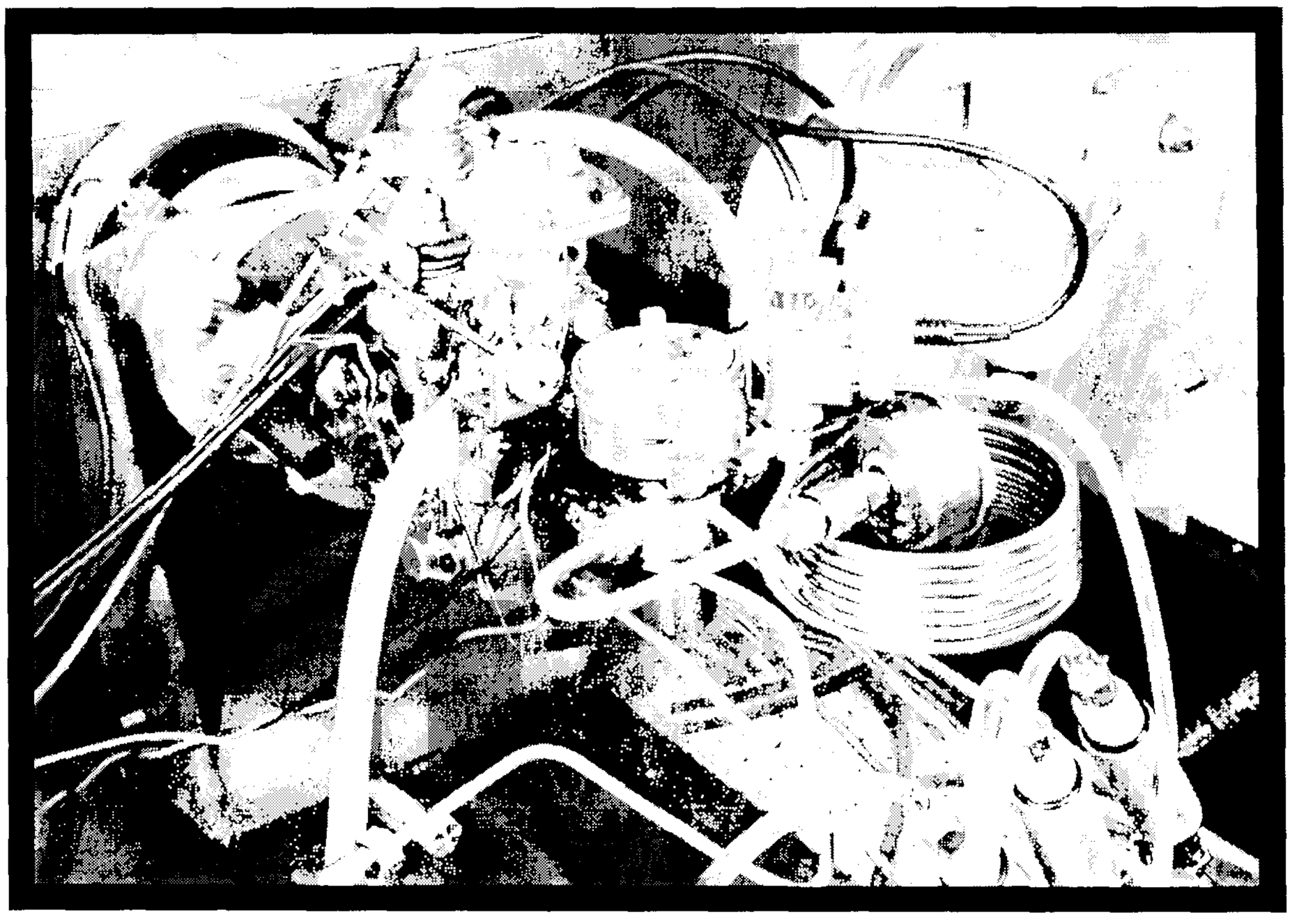

**Plate 18.** Mk.2 skip-firing valve fitted to EPVE pump FIE on Hartridge pump test machine.

The tests of the valve were carried out on a Hartridge pump test machine. The set-up for this will be described in the section concerning the EPVE pump's calibration. The only difference between the previous and the present set-up being that the Ono Sokki rate meter was not used since the rate measurement was considered unnecessary. If the needle lift and line pressure traces match closely those measured in

the ordinary calibration, this is an adequate proof of the operation of the valve. Delivery can be measured by the burettes fitted to the Hartridge. In particular the absence of 'dribbly' injections in the preceding and succeeding cycles can be easily confirmed from the needle lift trace.

Only tests at 800 rpm were recorded as the electronics driving the valve failed before the higher speed tests could be done. However, measurements at both high and low load were recorded. An idle test was not done as no comparison could be made with an ordinary calibration..

Figures 3.9 to 3.12 show a comparison of the needle lift and line pressure traces with and without the skip-firing valve, at the above two operating conditions. The most notable feature is the virtual disappearance of any small injection preceding the skip injection. The cycle prior to the skip injection seems to show a small needle lift, but, according to the pressure trace, the nozzle opening pressure, 250 bar, is never reached. This 'hump' in the needle lift trace could be explained by pressure effects in the sensor. This behaviour has been observed consistently in every calibration performed using a variety of different sensors. Normally this hump is disguised by the normal needle lift so it is missed if not actually looked for.

A second small injection was identified just after the skip injection. This is, however, sufficiently small to ignore as the main purpose of the valve is to prevent any injection prior to the skip injection. In this way the chamber will be clean and free of any fuel vapour or combustion products at the start of injection. If a small injection occurs after the main injection, consisting of only a few percent of the main delivery, this is not expected to influence the measurements, provided a sufficient time is left between injections to clear the exhaust products.

Close observation of the graphs shows that the duration of needle lift is shorter than that of the test calibration; this is at first sight a defect of the valve. There are two possible explanations; either there is some leakage past the skip-firing valve during the course of injection, or the delivery of the pump was actually lower than that of the calibration. Although this last explanation might be seen as convenient, it is quite plausible since, as will be explained in the section on calibration, the delivery is determined by measuring the rack position with an accurate potentiometer. The corresponding resistance was measured with an accurate multimeter once the

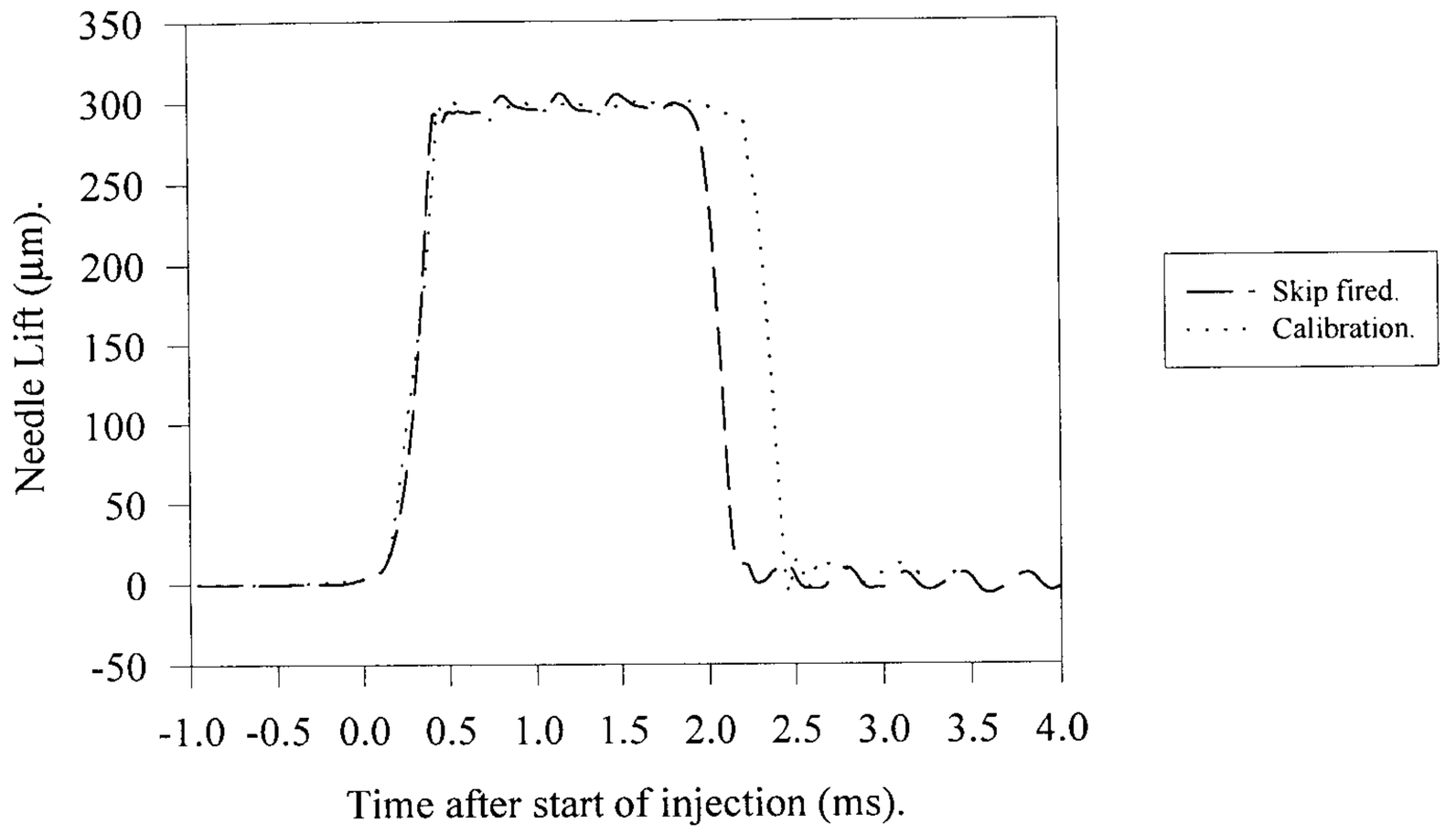


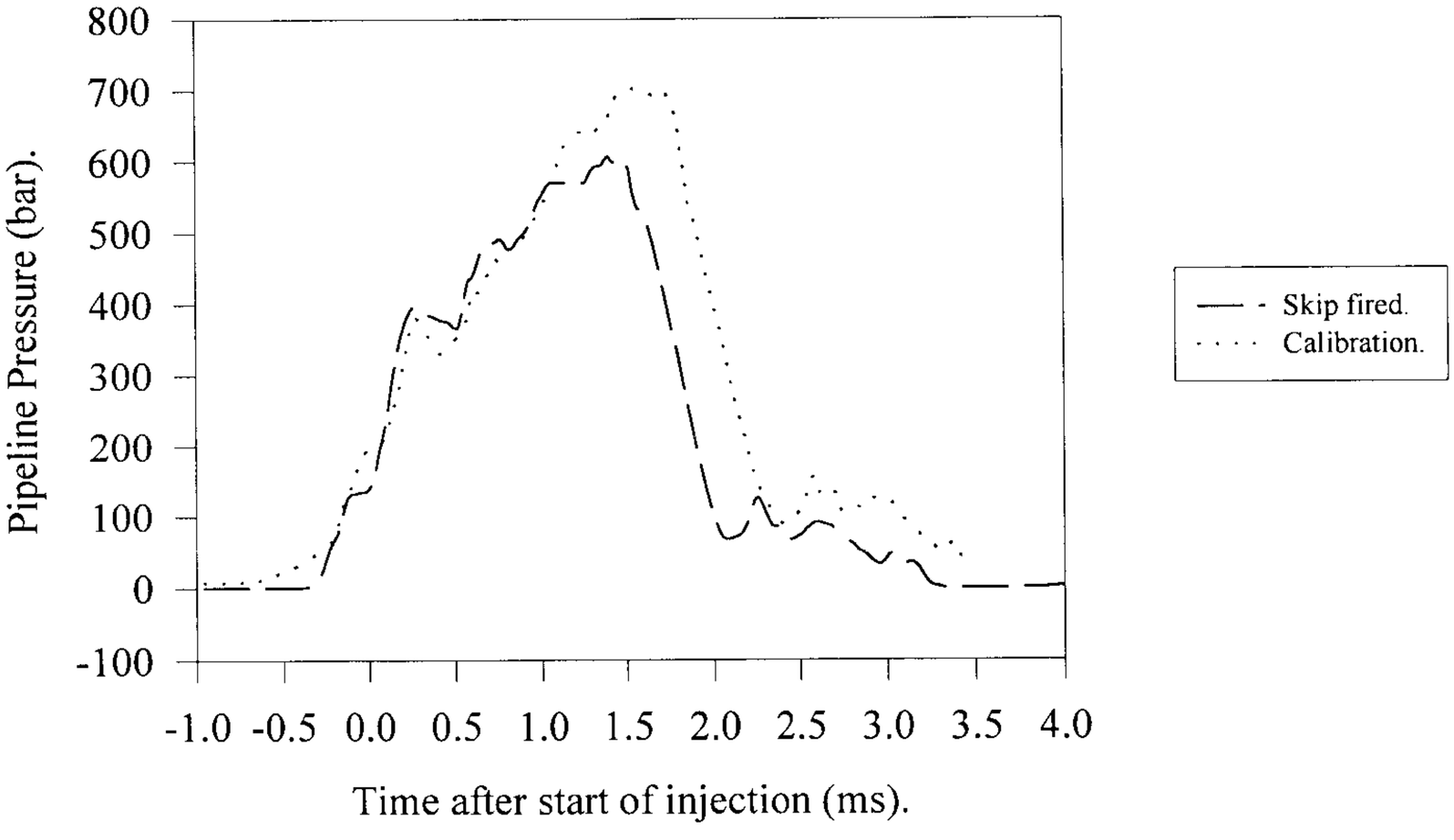


**Fig 3.9** Graphs comparing needle lift and pipeline pressure traces of skip-fired injection and calibration, using Mk.2 valve and EPVE pump FIE at 800 rpm, full load.

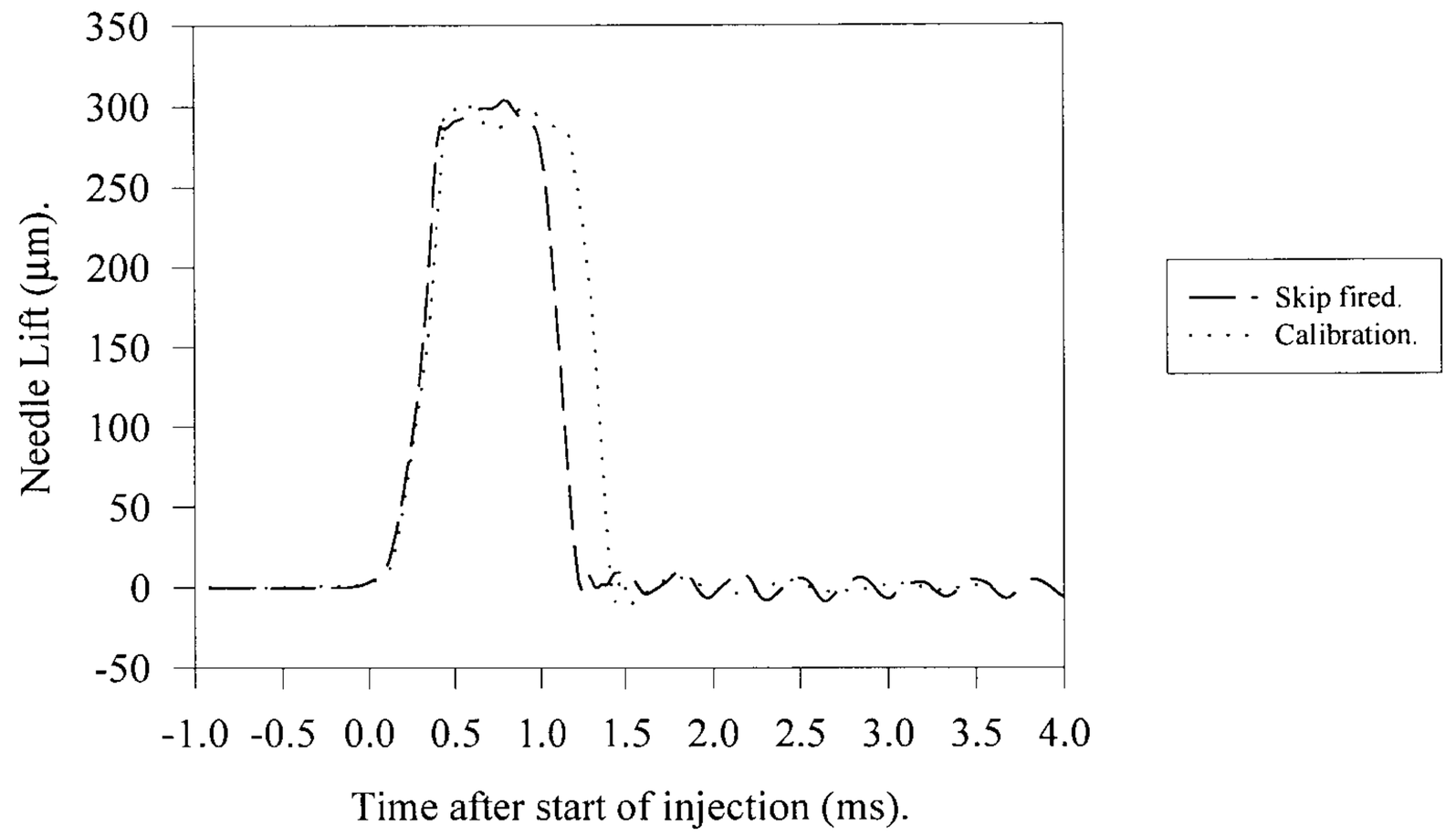


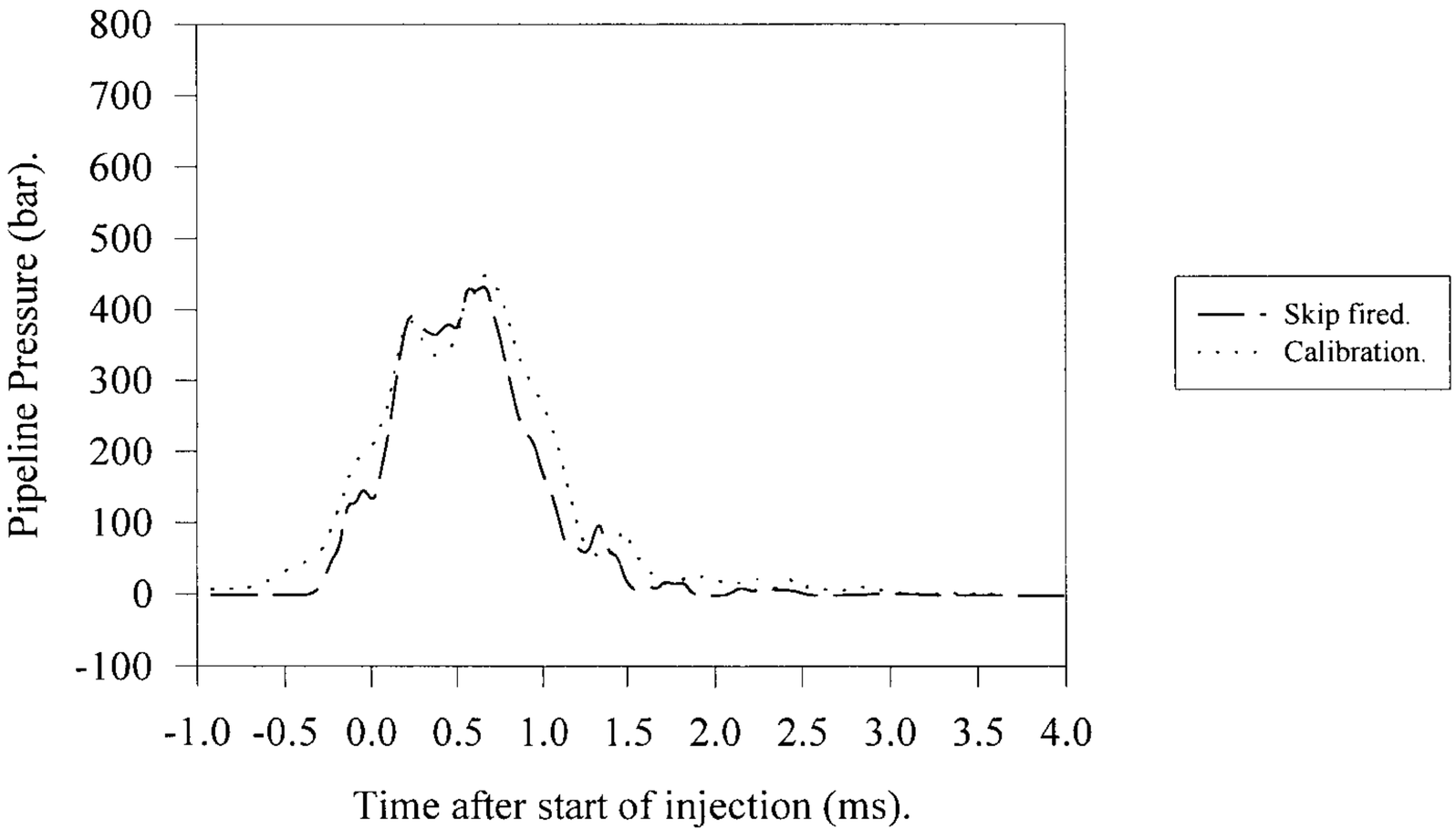


**Fig 3.10** Graphs comparing needle lift and pipeline pressure traces of skip-fired injection and calibration, using Mk.2 valve and EPVE pump FIE at 800 rpm, half load.

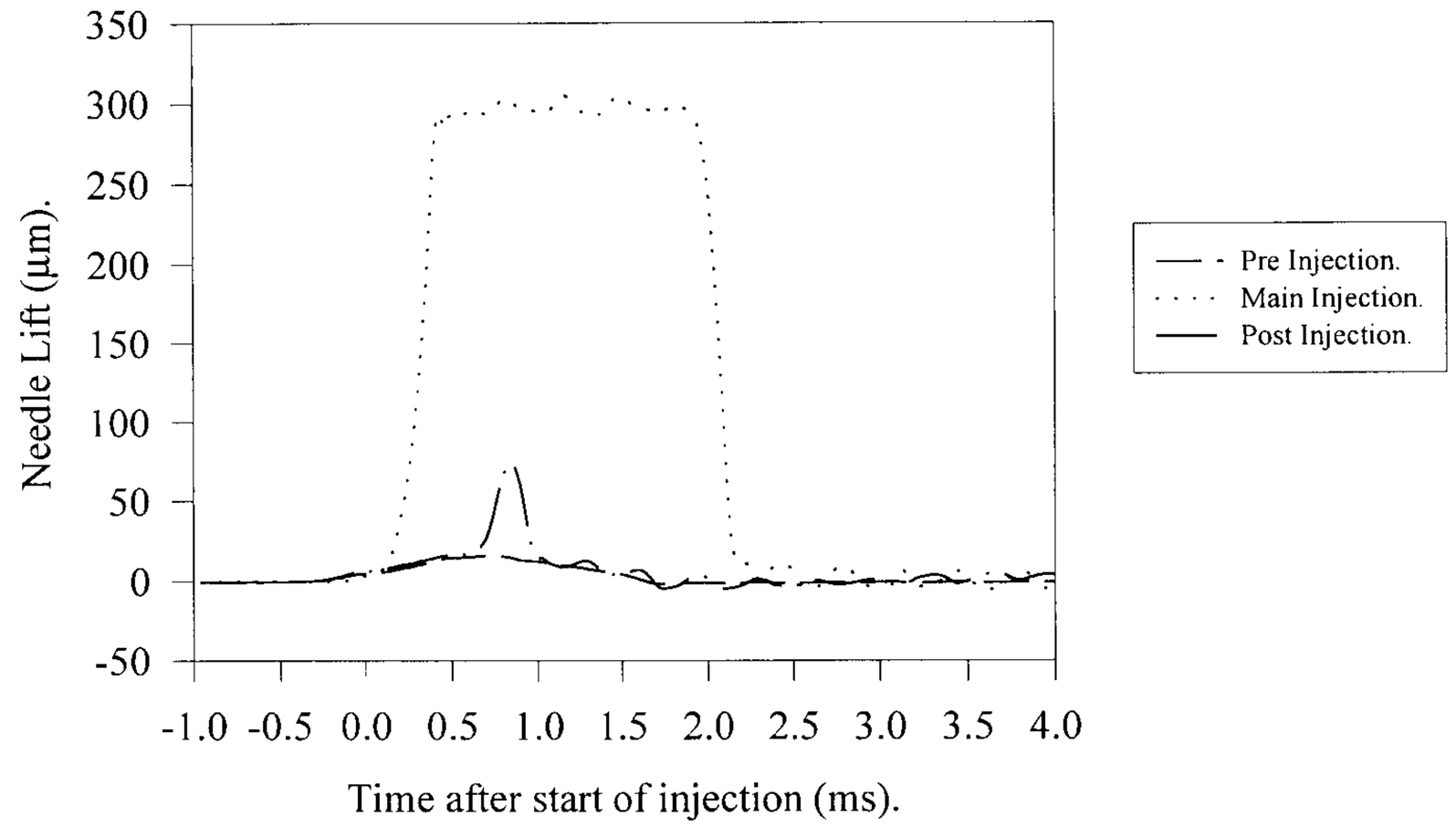


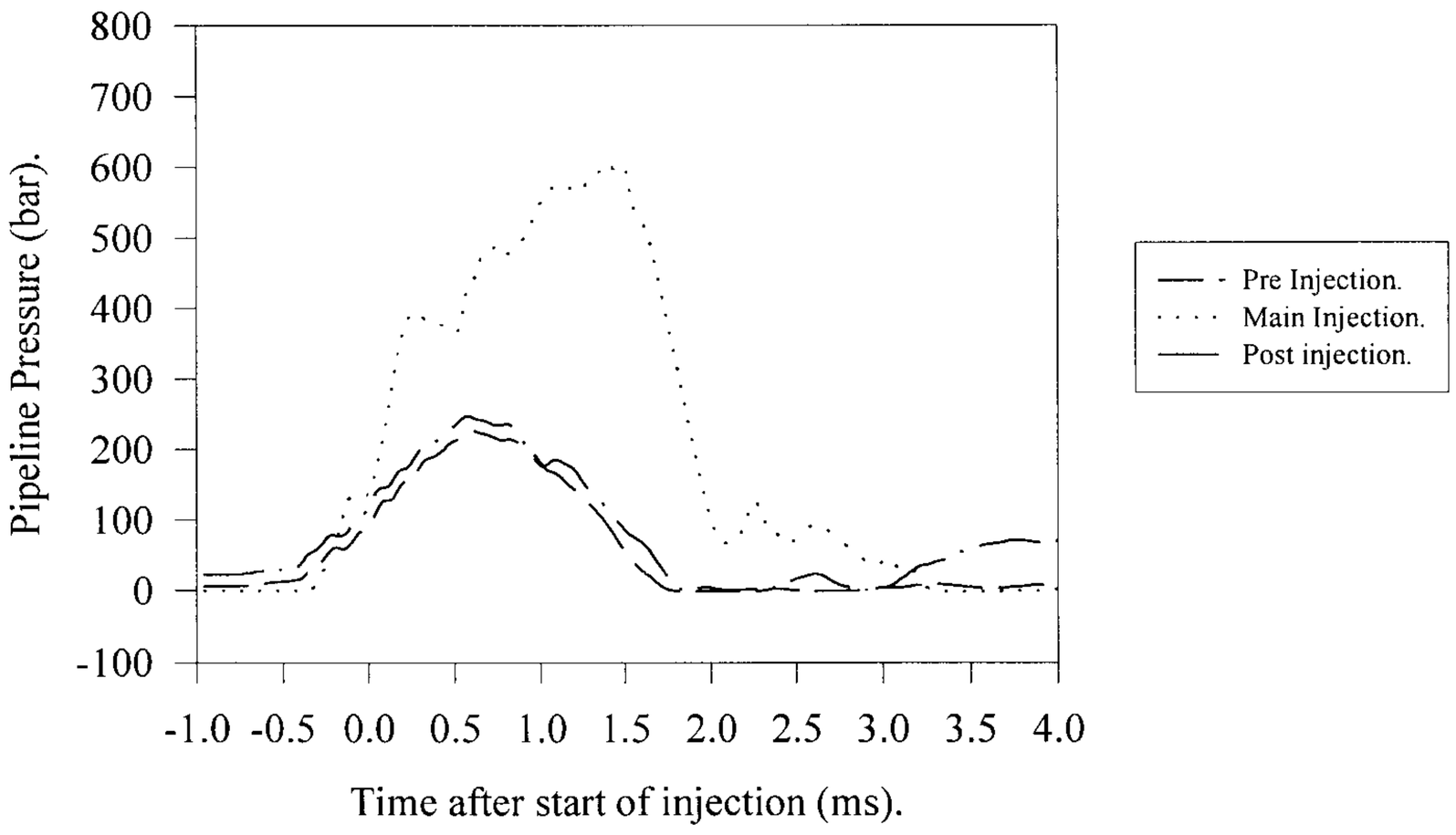


**Fig 3.11** Graphs comparing needle lift and pipeline pressure traces of pre, main and post skip-fired injections, using Mk.2 valve and EPVE pump FIE at 800 rpm, full load.

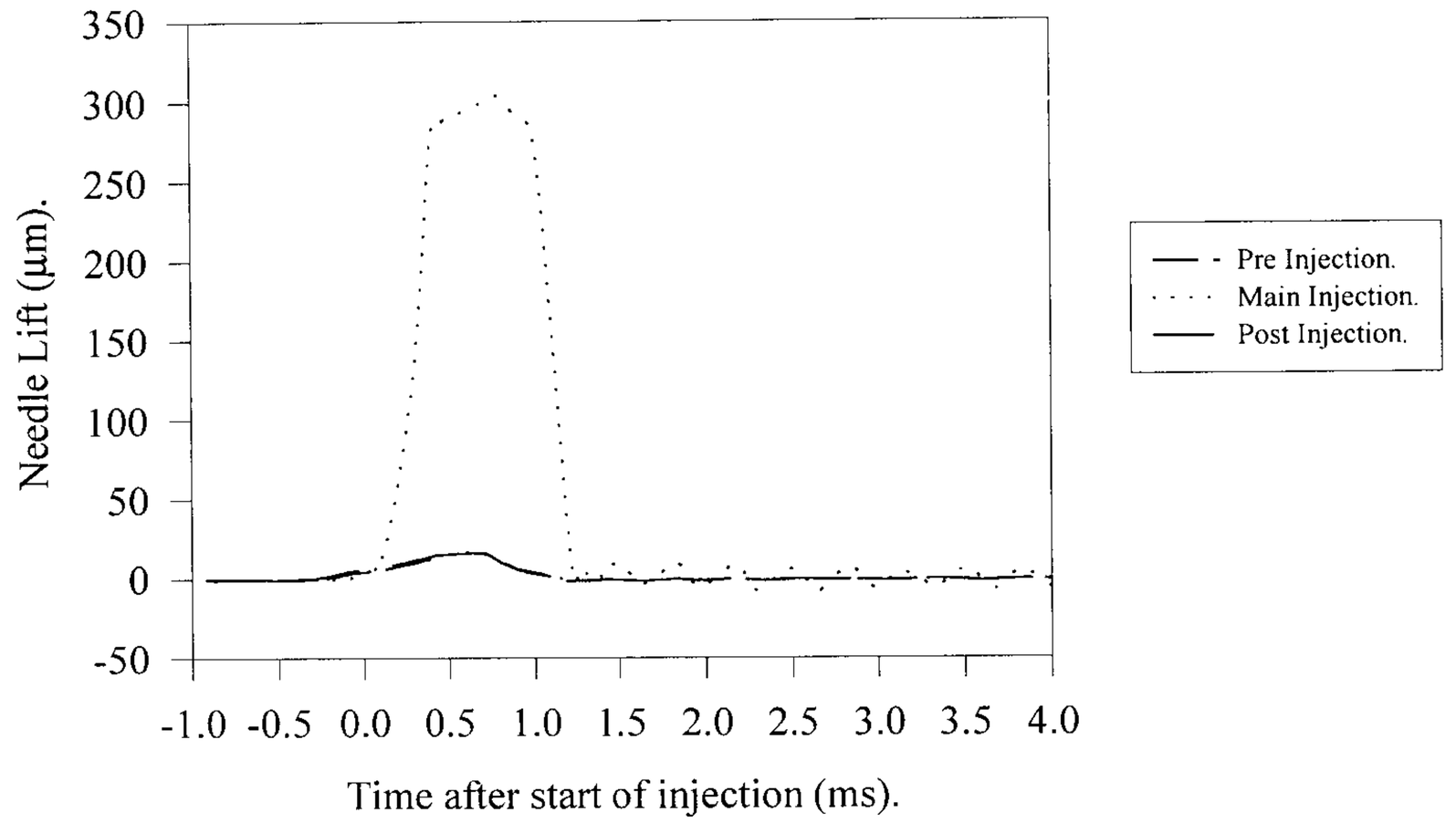


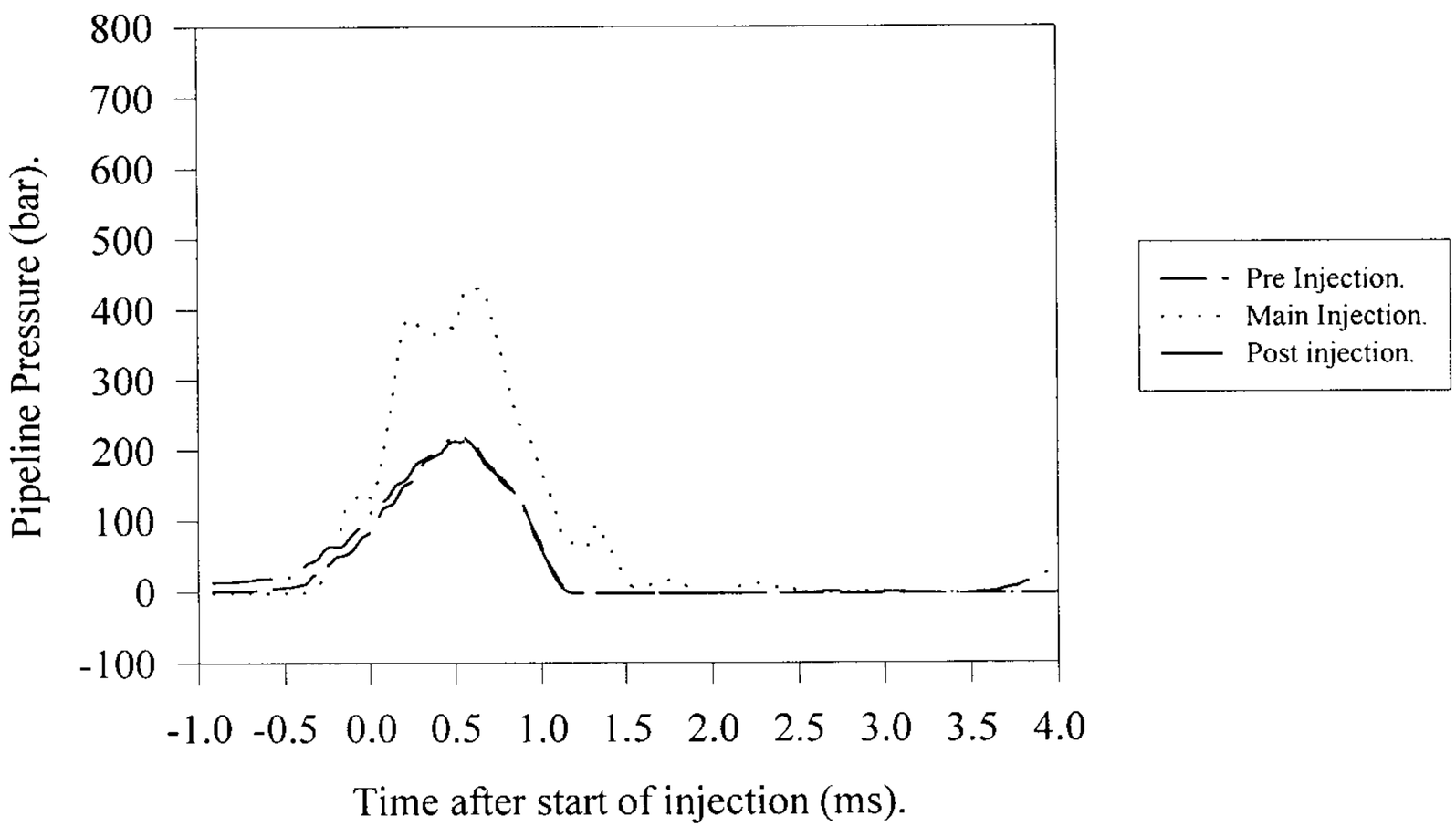


**Fig 3.12** Graphs comparing needle lift and pipeline pressure traces of pre, main and post skip-fired injections, using Mk.2 valve and EPVE pump FIE at 800 rpm, half load.

appropriate delivery had been achieved. By returning to the same value of resistance, a constant delivery could be maintained. This potentiometer may have moved explaining the discrepancy.

## 3.2 BOSCH MW PUMP CALIBRATION, IMAGING AND SPRAY CHARACTERISATION USING PDA.

### 3.2.1 Calibration of MW pump.

The remaining part of this thesis will consist of the characterisation of the Diesel spray produced by two different high pressure pump-pipe-nozzle systems. The characterisation was performed using the phase Doppler technique which will be described later in this chapter.

Prior to the PDA tests, a calibration of the pump had to be performed to provide essential data for further analysis. All of the measured parameters in a calibration are useful, in conjunction with the droplet size and velocity, in attempting to understand the atomisation process.

The calibration will not be described in too much detail as it is such a standard procedure; however, a brief account is necessary for reasons of completeness. An Ono Sokki rate meter [*Takamura,* 1992] was used for the rate measurement rather than a Bosch type. The Ono Sokki is a more convenient system compared to the Bosch type meter used for the DPC calibration. It also offers a major advantage in eliminating the pressure fluctuations present in the Bosch type, so it seems to yield more reliable data; the set-up is shown in Plate 19. The large white box is the Ono Sokki meter, the calibrated injector can be seen fixed into an adapter in the meter. An inductive type needle lift sensor is fitted which is identical to that used in the DPC calibration; the lead can be seen exiting the injector body. Finally a bridge type Kistler pressure sensor is fitted adjacent to the injector in the pipeline. All three of these sensors feed signals into a data acquisition system as described for the DPC test. The triggering was achieved using flywheel holes as a encoding ring as well as a once-per-revolution

hole, also drilled in the flywheel. This type of triggering is considered to give a very reliable measure of pump shaft position due to the rigidity of the flywheel mounting.

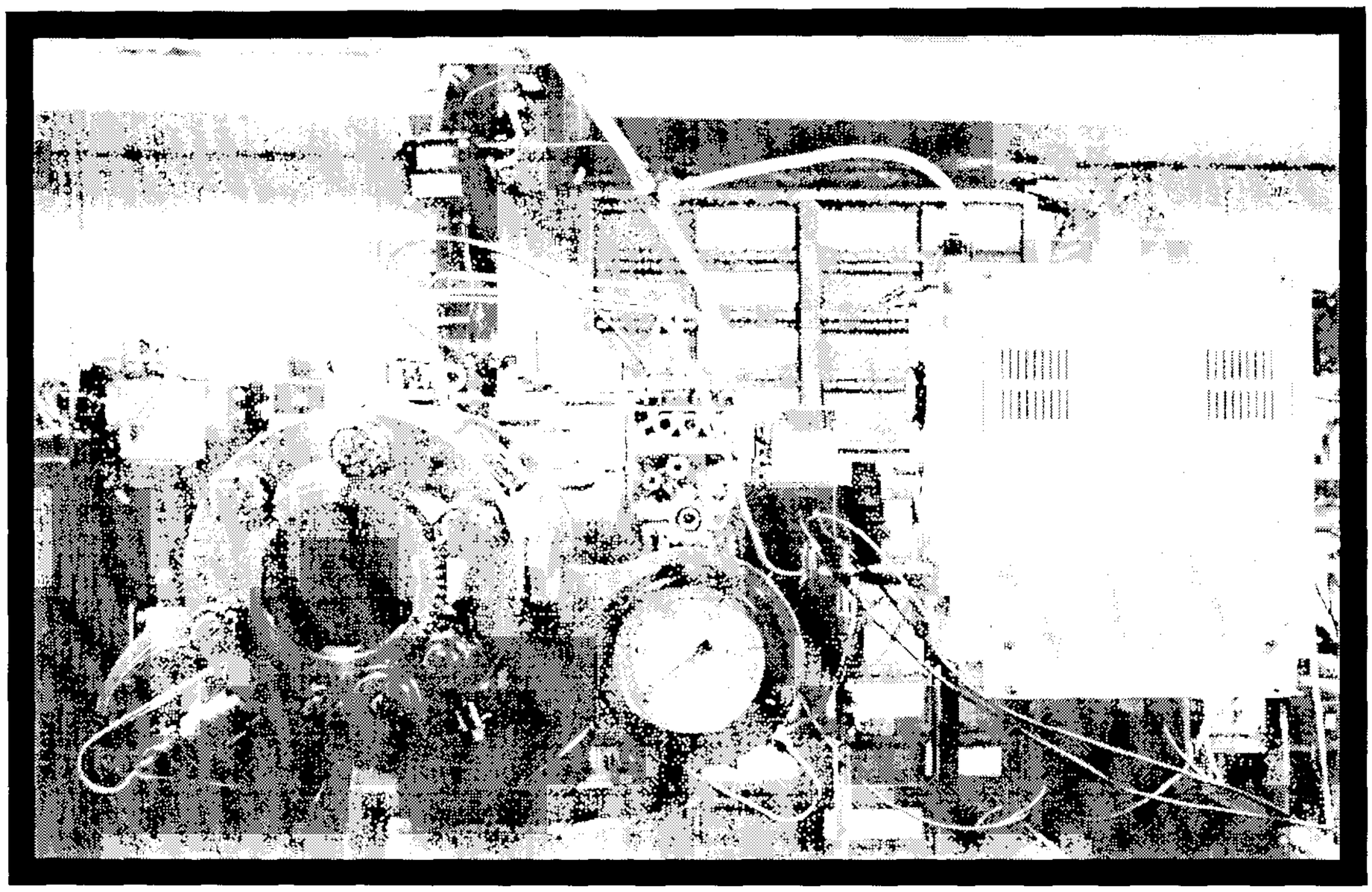

**Plate 19.** Front view of chamber with MW pump FIE fitted and Ono Sokki rate meter.

The three remaining dummy injectors are fitted into a tank with a return line to the main fuel tank. The leak-off connections on the injectors are also fed back to the fuel tank, in order to eliminate large quantities of fuel oil from lying in the tray under the pump which might constitute a fire risk.

Boost pressure was simulated by feeding the boost connection from an air regulator, supplied from the shop air supply. The pressure being set to the values supplied by Perkins which can be found in Table 3.2. Two additional features of the set-up are the fuel and oil pumps, unlike on a distributor pump; since these services are not provided internally in the injector pump, suitable external motor driven pumps had to be used.

Finally to turn the fuelling on and off a pneumatic cylinder was fitted to actuate the fuel shut-off lever. This was controlled via a solenoid valve switched by the control system which allowed for a convenient and rapid switching of fuelling.

As with the DPC pump calibration, 150 injections were recorded at each of the four conditions of speed and load which are summarised in Table 3.2.

| Speed (rpm) | Load | Delivery ($mm^3$/Inj). | Boost Press. (bar). | Chamber Press. (bar). |
|---|---|---|---|---|
| 1300 | Full | 84.5 | 1.02 | 33.0 |
| 1300 | Half | 46.9 | 0.74 | 27.0 |
| 800 | Full | 87.1 | 0.91 | 32.0 |
| 800 | Half | 44.4 | 0.45 | 25.0 |

**Table 3.2** Test conditions for calibration of MW pump.

The results are presented in Figures 3.13 to 3.16. The only processing of this data was the conversion of the raw voltages to actual values by multiplying by a constant factor. The rate measurement however was 'smoothed' by the use of Fourier analysis. It should be noted that on the rate meter itself there is the option of hardware low-pass filters; the highest frequency filter, 6 kHz, was selected which removes only part of the signal noise. The objection to using a lower frequency filter is the possibility of removing real information rather than noise. Fourier analysis was also used to smooth the averaged data using Microsoft Excel, with all frequencies above 4 kHz rejected by the software.

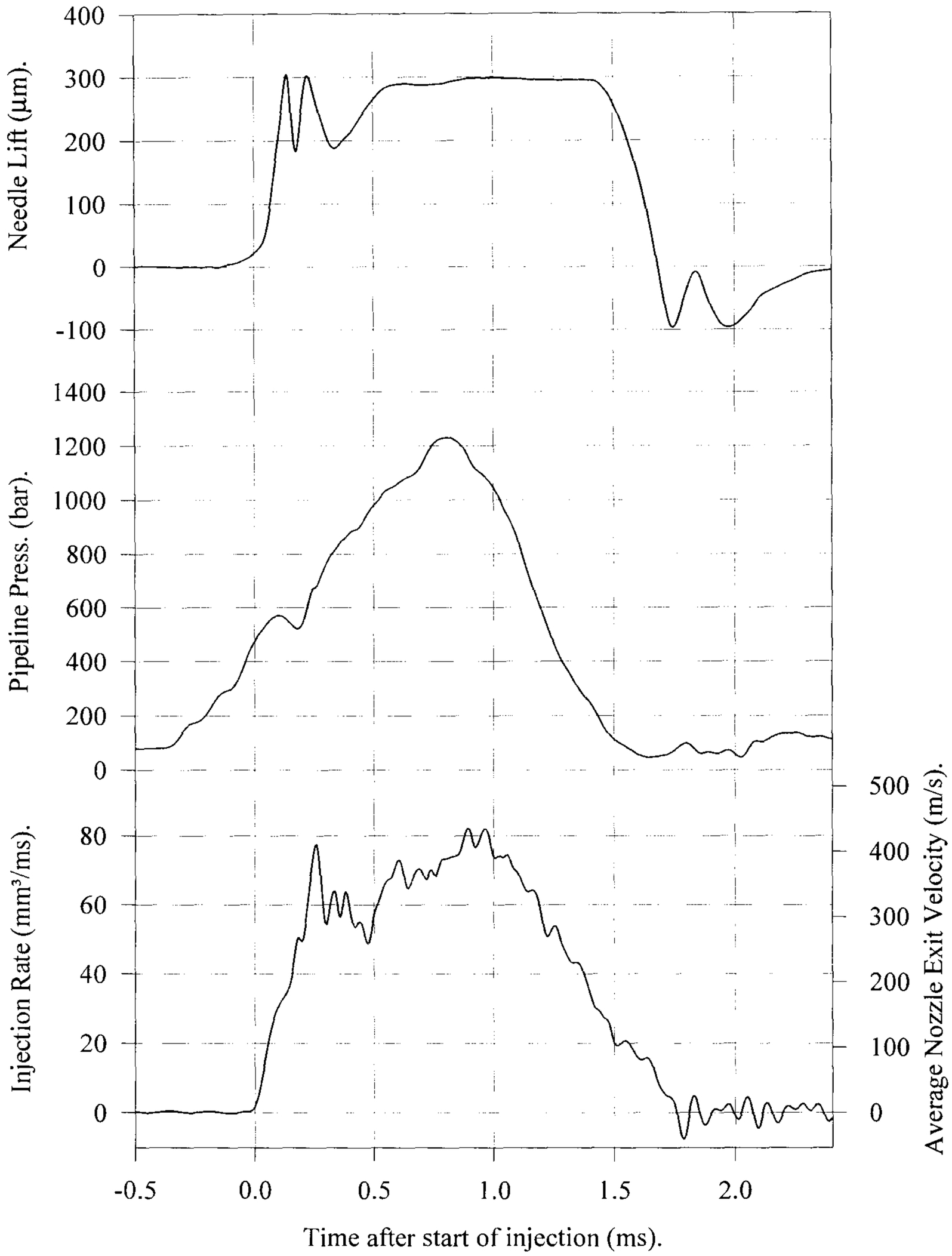


**Fig 3.13** Graphs of needle lift, line pressure and injection rate, of MW pump FIE.
1300 rpm, full load.

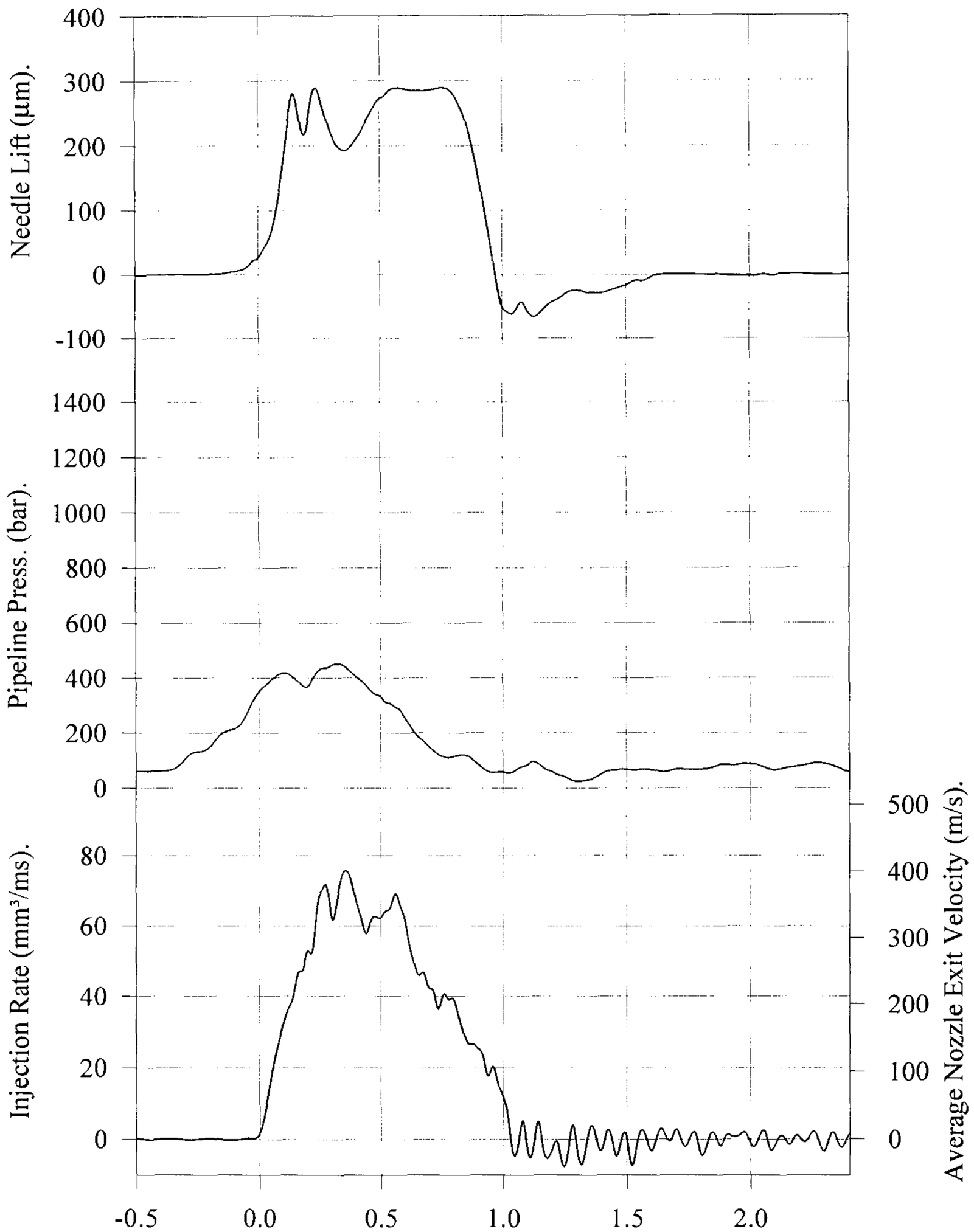


**Fig 3.14** Graphs of needle lift, line pressure and injection rate, of MW pump FIE.
1300 rpm, half load.

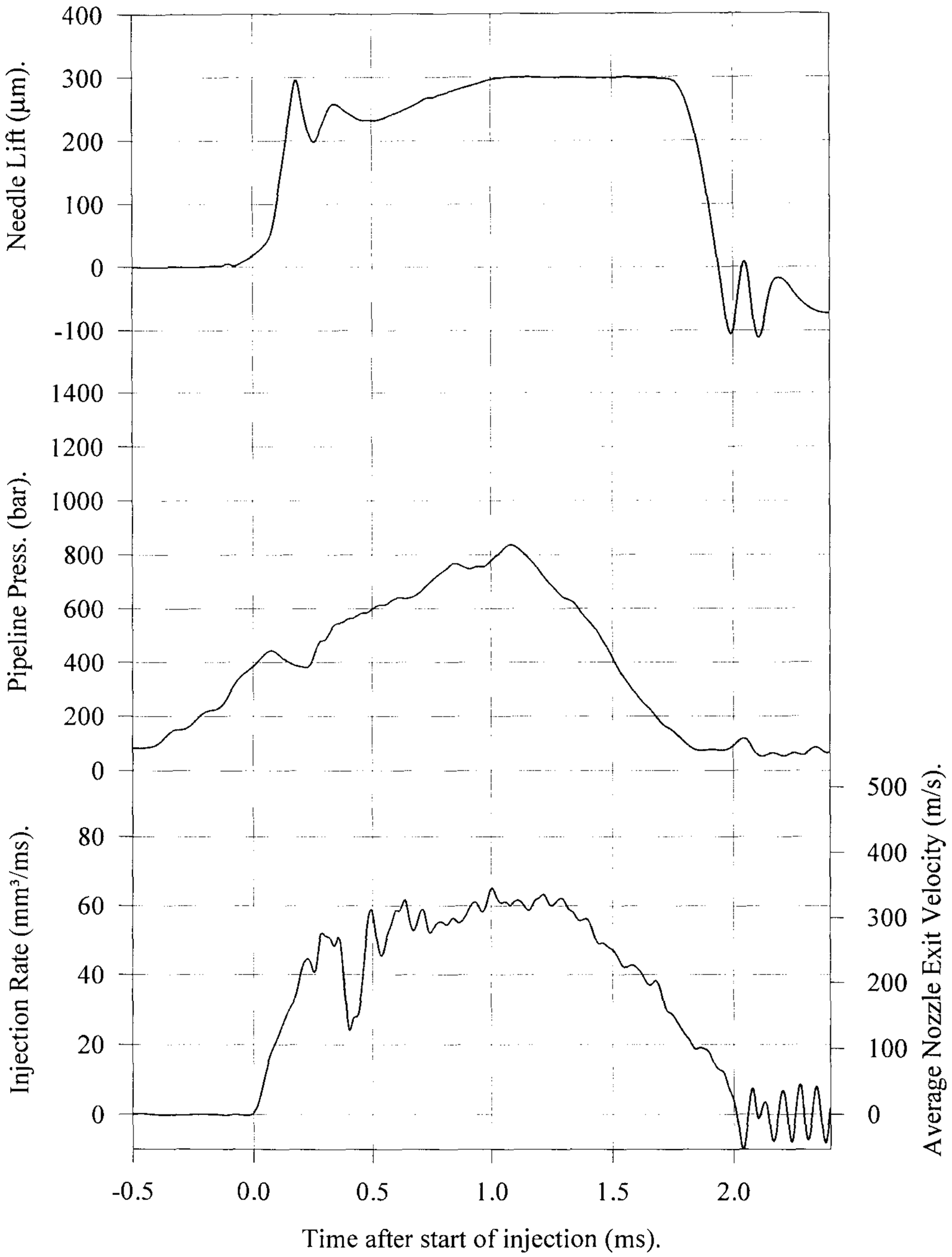


**Fig 3.15** Graphs of needle lift, line pressure and injection rate, of MW pump FIE. 800 rpm, full load.

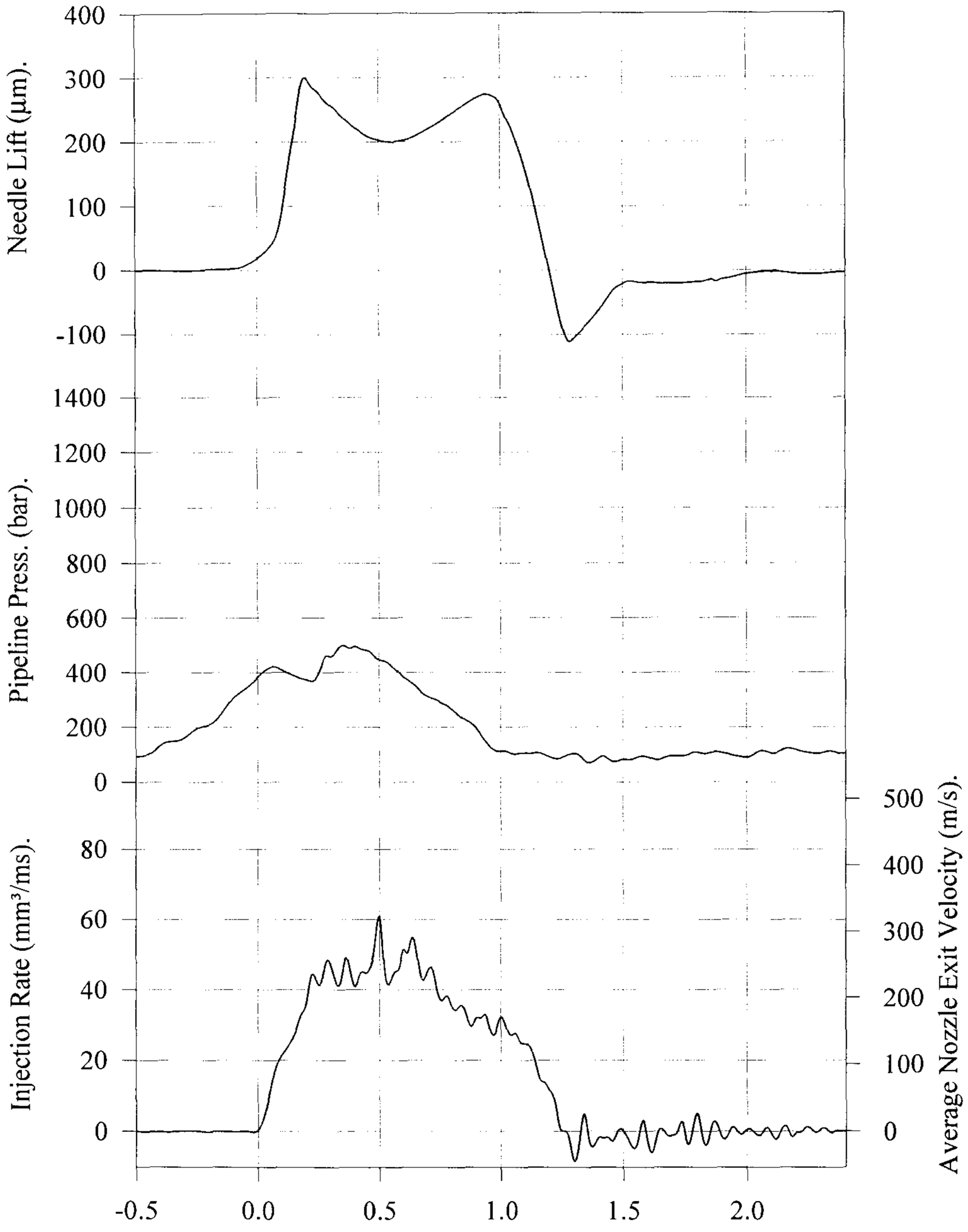


**Fig 3.16** Graphs of needle lift, line pressure and injection rate, of MW pump FIE.
800 rpm, half load.

### 3.2.2 Imaging.

Imaging of the sprays from the MW pump system was carried out using a high speed 'Imacon' camera capable of taking six images at shutter-speeds down to a few nanoseconds. The camera consists of a standard medium format camera lens, the image from this is directed by optics onto six separate photoarrays; each of these arrays is capable of producing a single image. In operation these arrays are triggered by internal electronics at which point they sample the image for the pre-set shutter-speed. Each photoarray can be triggered at any time, pre-set by the user via a dedicated software package. The images can all be taken at the same instant, normally, however, a series of images separated by say 0.1 ms is sampled, in this way the development of the diesel spray can be studied. As the images are sequential and obtained from the same injection, fewer injections need to be sampled to obtain statistically viable data; this is due to the variation in the starting times of each injection and will be explained in more detail when the results are discussed in Chapter 4.

Once the camera has been focused, all that remains is to adjust the aperture and shutter speed. Since there is no combustion, there is no problem with the photo arrays being overwhelmed, on the contrary the problem is more one of insufficient light and a flash light was used to illuminate the sprays through the head window. The duration of the 'flash' is sufficient to last for the whole of the injection and the flash was triggered 1 ms prior to the start of injection. With the maximum aperture possible a compromise has to be struck between the degree of electronic gain used to amplify the signal from the arrays and the length of the exposure. A short exposure would give sharp images but necessitates a high gain for a reasonably bright image, this in turn makes the images 'grainy'. In the end an exposure time of 10 μs was chosen; assuming that an average droplet in a spray has a velocity of 50 m/s, this equates to 0.5 mm of movement. This may seem quite high but the lowest gain setting could be used and this combination seemed to give the sharpest images. For each test case six images were taken separated by 0.1 ms; the conditions of chamber pressure, pump speed and load and the results are given in Chapter 4.

## 3.2.3 Phase Doppler anemometry.

### 3.2.3.1 General description of the technique.

Phase Doppler anemometry (PDA), has become the standard laser based technique for droplet sizing and has been applied to Diesel sprays by numerous authors [*Pitcher and Wigley,* 1994a; *Pitcher and Wigley,* 1991; *Koo and Martin,* 1990; *et al*]. Because the technique is well established and the principles widely understood, only a brief description will be given here.

PDA is an extension of laser Doppler anemometry (LDA) and requires identical transmitting optics. A laser beam is split into two beams of equal intensity and by a series of lenses these two beams are made to cross at some distance from the transmitter. The two beams are not parallel but arranged to converge so that the diameter of the crossing is very small. To ensure reliable measurements the axes of the beams must lie in the same plane so that they cross precisely with no misalignment.

In a simplified analysis it is assumed that there are fringes formed within the crossing caused by the interference of the two beams; these fringes are located at a fixed distance apart which can be determined simply from the crossing angle and the laser's wavelength. If a droplet passes through the crossing, which is usually referred to as the control volume or probe volume, light is scattered in all directions with a frequency which depends on the speed of the droplet passing through the fringes and their spacing. A photomultiplier focused on the control volume is used to collect the scattered light which arrives in bursts (called Doppler bursts), one for each droplet and a processor is used to measure the frequency of each burst and hence the velocity of the corresponding droplet. This frequency measurement can be done in a number of ways which, but for sake of brevity, are not described in detail here. However, one common requirement in all processors is that the signals from the photomultipliers must be processed before they reach the frequency measuring stages, for a number of reasons.. A graph of the intensity of the 'Doppler bursts' has a characteristic Gaussian shape (see Figure 3.17). Because of electronic difficulties in handling signals with widely varying amplitude, logarithmic amplifiers are needed in the input stages of the

processor to produce signals of more even amplitude. These logarithmic amplifiers also serve to reduce the variations in signal amplitude caused by the different sized droplets; as the intensity of scattered light varies with the square of droplet diameter, the log-amplifiers increase the diameter range by increasing the dynamic range of the processor, which is an important measure of the quality of a processor.

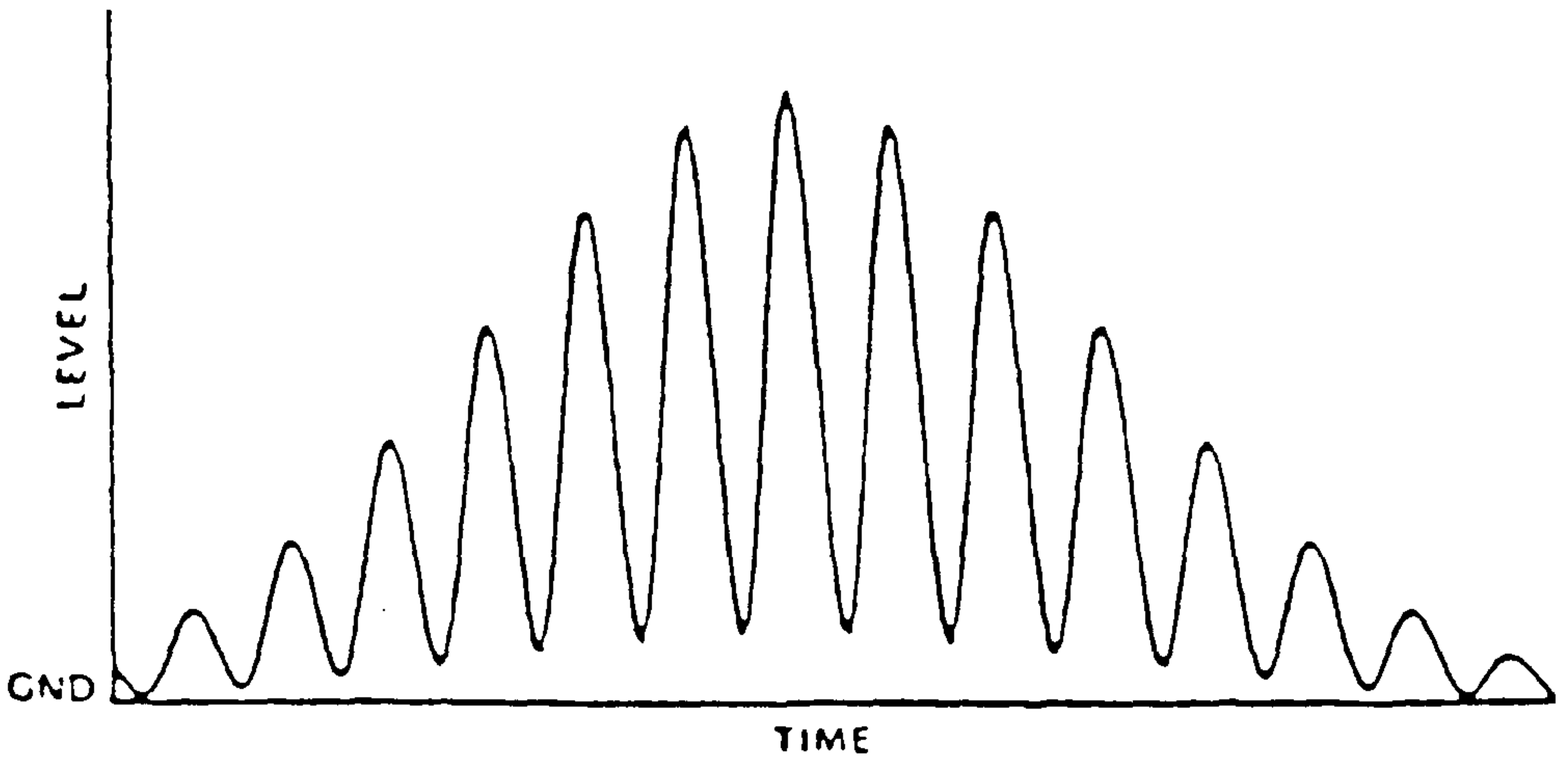


**Fig 3.17** Typical (ideal) Doppler burst from LDA receiver; showing characteristic Gaussian shape.

By comparison with LDA, PDA is more complicated. Instead of one photomultiplier there are at least two (see Figure 3.18) which are placed a fixed distance apart and accurately focused onto the same position within the control volume. Again they measure the Doppler bursts produced by droplets crossing the control volume but because of their position the bursts have a phase shift relative to one another (see Figure 3.19) which is proportional to the diameter of the droplet. So by simultaneously measuring the frequency and the phase shift of these signals, both the droplet's velocity and size can be determined.

Unfortunately there are significant practical difficulties in achieving the above. The quality of PDA optics needs to be even higher than for LDA. In particular, the different photomultipliers must focus on exactly the same area within the control volume, otherwise the detectors might be sampling from different droplets. Another problem is that the linear relationship between phase shift and diameter only exists

when the photomultipliers are at a few specific scattering angles relative to the crossing beams. Because there are only a limited number of possible angles and even fewer which yield good signal to noise ratios, difficulties can be found in providing optical access into combustion chambers and engines. Also the phase shifts, particularly for small diameter high velocity droplets, are very small and require electronics of the highest quality to be measurable.

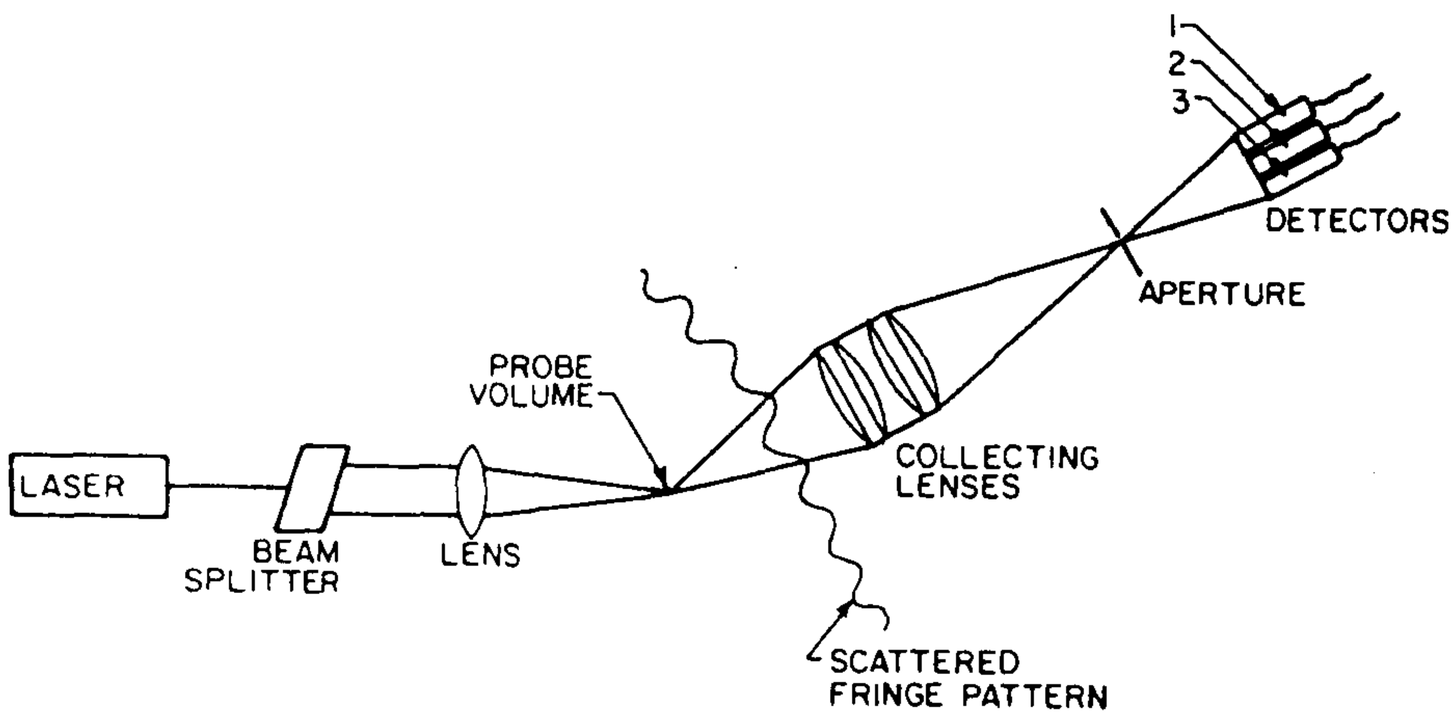


**Fig 3.18** Schematic diagram of PDA system with three detectors. This set-up shows forward scattering of refracted light; by virtue of the low scattering angle very little reflected light is received by the detectors. [*Aerometrics,* 1990]

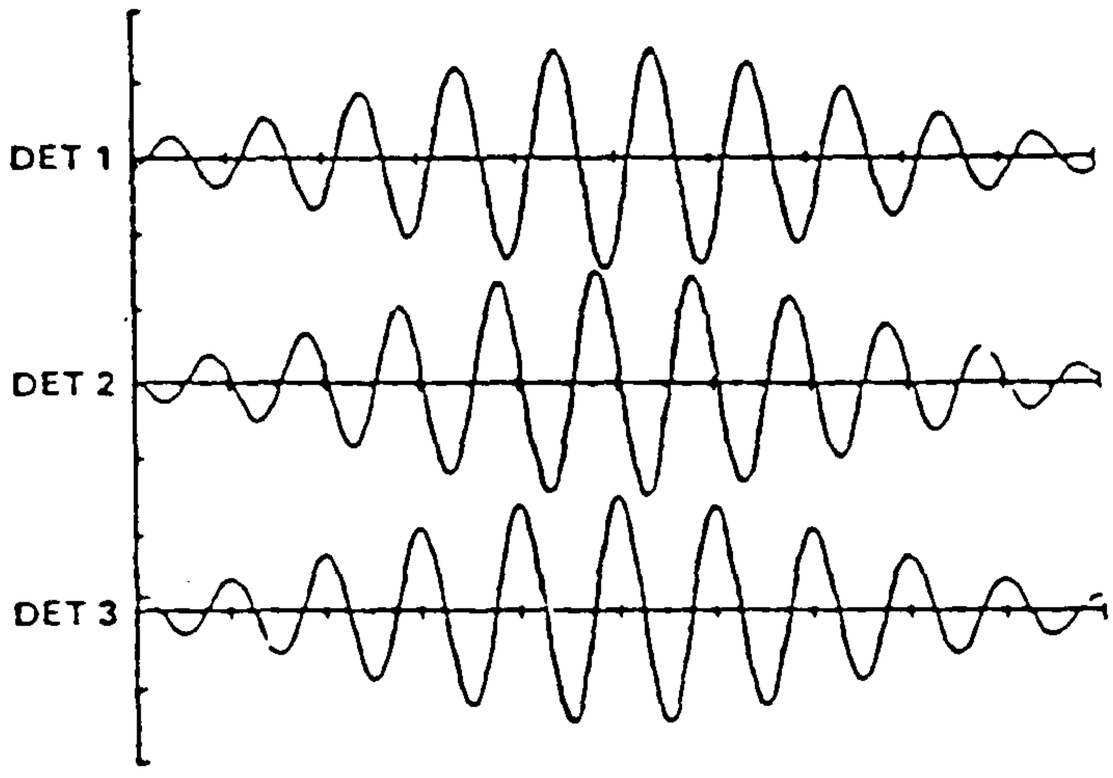


**Fig 3.19** Typical PDA signal from the three detectors showing the phase difference between the Doppler bursts which is linearly related to the droplet diameter. [*Aerometrics,* 1990]

### 3.2.3.2 Measurement of Diesel sprays with PDA.

Measurement using PDA in a Diesel spray such as that of interest in the present study presents some additional difficulties. The density of the droplets is such that there is a distinct possibility that several droplets will occupy the control volume at the same time. Even with the most sophisticated signal processors this makes measurements very difficult, with associated low validation rates. One partial solution is to use very small control volumes to reduce 'multiple occupancy', but there are problems associated with small control volumes. Firstly the fringe spacing needs to be small so that the processor has enough fringe crossings to allow accurate measurements. This in turn means that the signal frequency for a given velocity is proportionately higher. Given the finite frequency response of the processor, there is a limit on the velocity which can be handled, often well below the maximum droplet velocities found in sprays. In addition, the size range is affected as the higher frequencies make determination of the phase shift more difficult. Hence measuring small droplets, except at low velocities, is limited by the smallest phase difference, in time, that the processor can measure.

Thus a compromise has to be struck between the velocity and size range versus validation rate. The smallest possible control volume should be chosen which allows the full velocity range of the spray to be measured. As for the size range, this is not so crucial as long as the large drops are measurable. Measurements of small drops probably have to be sacrificed. This is acceptable only because in a spray the small droplets (under 10 μm) have little influence on the value of the Sauter mean diameter (SMD); while there is a reasonable number of large droplets (circa 50 μm). However, this has to be considered as a last resort since a full study of sprays, their atomisation and combustion would undoubtedly need information about these small droplets.

The choice of scattering angle is also important in determining the overall performance of the PDA equipment. Two scattering angles are popular in diesel spray work: 30° and 70°. The principle advantage of 30° is the high signal to noise ratio; due to the large amount of refracted light scattered in this direction and the corresponding small amount of reflected light received at this angle; reflected light causes errors in

the PDA measurement by producing different phase shifts to that of refracted light. Consequently if the signal intensities from reflection and refraction are comparable, PDA measurements are not really possible; at scattering angles much greater than 30° this becomes a serious problem.

At the 70° scattering angle, however, which is approximately the Brewster angle for diesel fuel, if the light is plane polarised in the plane of scattering, in theory no light should be reflected from the droplets towards the receiver; the only signal should come from refracted light. A second advantage in using 70° is that variations in the refractive index, which occur if the fuel temperature changes, have little effect on the slope of the calibration curves. For a thorough review of the merits of this scattering angle the reader is referred to *Pitcher* [1994b].

Because of the above advantages and because of the available optical access in to the chamber, 70° was chosen as the most suitable scattering angle for these experiments.

### 3.2.4 PDA measurements of MW pump based system.

#### 3.2.4.1 Layout of optical equipment.

The accurate, rigid mounting of the transmitter and receiver in a PDA system is crucial for its satisfactory operation. Slight misalignment of the optics can dramatically affect validation rates and often prevent measurement altogether. For this reason a purpose built optical bench has been used to maintain alignment even when there are many sources of vibration in the test cell; this bench also allows for rapid initial alignment and checking of the system's response.

The type of transmitter used was of a standard design made in the Thermofluids Section. No fibre optic link was available so the laser and transmitter had both to be mounted and aligned relative to one another on an optical rail. The receiver was mounted on a separate rail made specially to hold it at the 70° scattering

angle used in the present experiments. Both these rails were subsequently bolted to the milling table of the chamber mount and therefore held in accurate and permanent alignment to one another.

The receiver used was an Aerometrics RCV 2100, but the processor (counter) was built within the Section [*Hardalupas and Laker,* 1993]. The specifications of the counter are given in Table 3.3, which includes the specifications of the Aerometrics counter used in the experiments with the EPVE pump. As can be seen, the Imperial College counter has lower specifications in terms of dynamic range (this is the ratio of smallest to largest diameter measurable at any one setting) and data rate. The reason for using two different counters was so that a comparison of their relative performance could be made.

Due to the choice of the 70° scattering angle, optical access into the chamber presented difficulties; the main problem being that the lip of the head window mount partially obscured the receiver aperture. Any such obstruction is undesirable and can badly affect the PDA system's performance as it reduces the amount of scattered light received by the detectors. This is particularly problematic when using such a large scattering angle as 70°. As the angle is increased from what is probably the optimum of 30°, the intensity of scattered light falls dramatically. This can be partially offset by the use of higher laser power, but the price paid for this higher laser power is increased noise levels. Therefore any reduction in the amount of scattered light reaching the detectors must be avoided if possible. To solve this problem a useful feature of the chamber mounting was used. The chamber was swivelled around by 10° about a vertical axis. This still allows the beams to enter the chamber from the transmitter but eliminates the obstruction of the receiver lens. One objection to this is that the co-ordinate table is misaligned with the chamber, which results in the need for some complex trigonometry when positioning the beams crossing at a particular grid point.

| Counter | Max. sample frequency | High pass filter cut-off frequency | Dynamic range | Clock frequency | Resetable clock | Maximum data rate | Remarks |
|---|---|---|---|---|---|---|---|
| I.C 'Model 3' | 20 MHz | 1.5 MHz | 12.9 | 500 MHz | yes | 25 kHz | The main limitation of the counter for Diesel spray characterisation is the low data rate this limits the amount of droplets that can be sampled in the dense region of the spray. The minimum signal to noise ratio that the counter can handle is also appears to be quite low and hence validation rates when measuring in the interesting regions of the spray are also low |
| Aerometrics PDP-3100. | 20 MHz | Adjustable | 100 | 400 MHz | no | 50 kHz | This counter can handle a much higher data rate momentarily; the counter appears to have a temporary buffer which can store a number of samples at a much higher data rate than the 50 kHz figure quoted in the specification. Validation rates also seems to be much higher |

**Table 3.3** Comparison of two PDA systems used for Droplet sizing.

### 3.2.4.2 Mechanical details and injector mounting.

The injector is mounted in the chamber using a specially made adapter shown in Figure 3.20. The injector is offset from the centre of the chamber to allow the relevant part of the spray to pass in front of the side windows; the relevant part being from 10 mm to 25 mm away from the nozzle. It should be noted that these figures are not arbitrary, since long experience has shown that measurement closer than 10 mm to the nozzle is difficult due to the high droplet density, the non-sphericity of the droplets (these are more likely near to the nozzle due to the higher velocities and hence higher aerodynamic distortion of the droplets) and the possible presence of a liquid core in the spray. All three of these factors invalidate the principle of PDA, namely the need for single spherical droplets in the control volume. The upper 25 mm limit is set as this is the radius of typical piston bowls in small Diesel engines; any measurement past this point is of only academic interest as the spray/wall interaction will dramatically influence the spray characteristics.

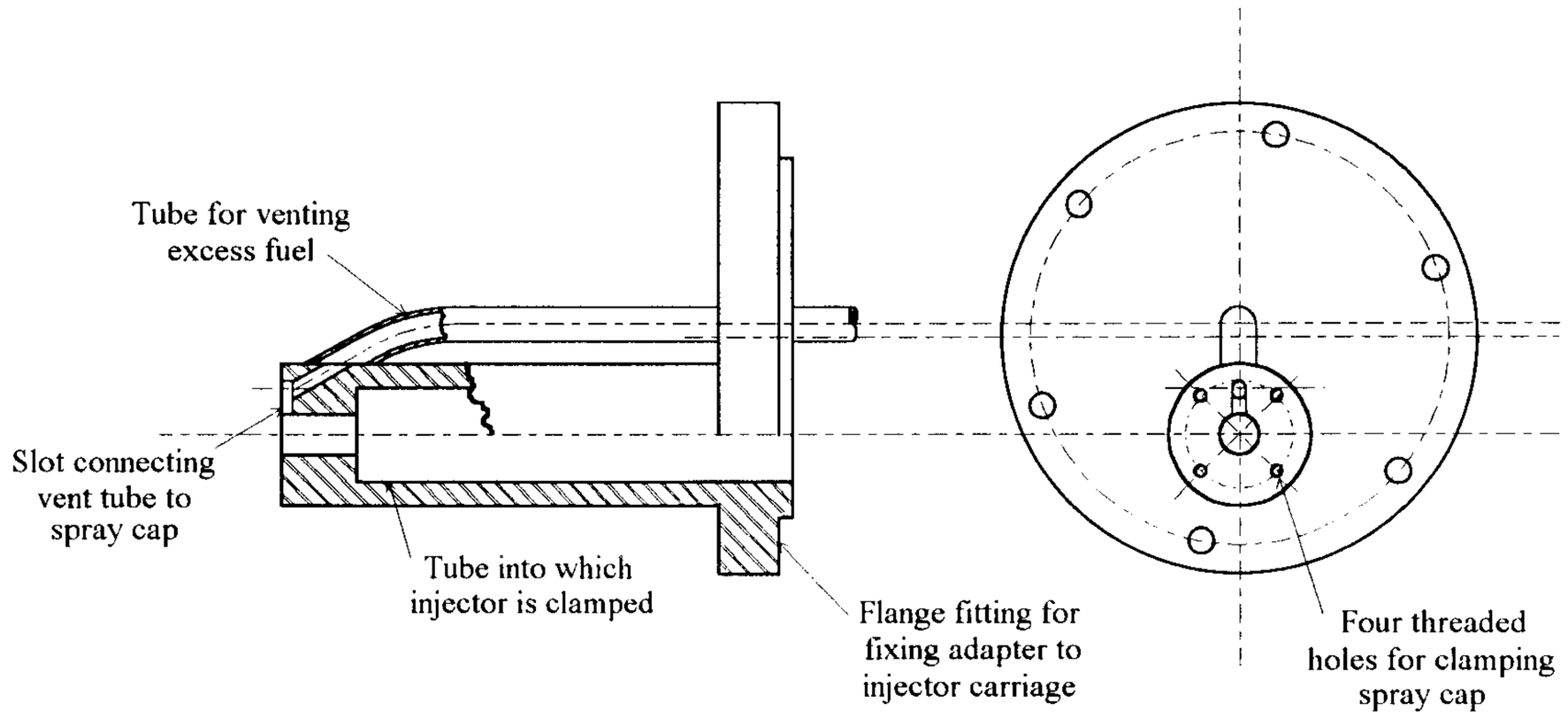


**Fig 3.20** Adapter designed for holding RT type injectors of MW pump system. The injector is held 17.5 mm eccentric of the chamber's centre line to facilitate the taking of PDA measurements.

The PDA measurements on the MW pump are to be done without combustion, this is to allow the spray structure to be studied for a considerable period prior to combustion. Measurements within a combusting spray are possible with PDA, but it was felt that a study of the fundamental break-up processes was needed first, without the added variables of vaporisation and combustion. One problem caused by this is that the fuel after being injected into the chamber's gas stream, because it does not combust will be free to foul the inside of the chambers and particularly the windows. Although the gas stream will tend to scavenge the fuel from the chamber, a percentage of the fuel will still reach the walls and windows; and if too much fuel is present in the chamber, measurements will be difficult or even impossible. To reduce the quantity of unburnt fuel inside the chamber, it was decided that only the fuel from the spray being characterised would be allowed into the chamber, the remaining five sprays were captured in a special 'spray cap' and the fuel vented outside the chamber in an air stream.

Figure 3.21 shows the spray cap for the MW pump's injectors; the one for the EPVE pump is almost identical. The cap is designed to direct all but one of the sprays into a small chamber, the cap bolts to the end of the injector adapter and the chamber is linked to a vent pipe by a slot milled in the end of the adapter. The chamber is sealed onto the injector nozzle so, if there is a slight pressure build-up within the chamber no fuel can leak across the hole; this is important as, if there is a film of fuel oil surrounding a hole when the injection takes place, a number of large drops can be produced uncharacteristic of the injection. This is problematic as large droplets tend to disproportionately affect the measured values of Sauter mean diameter, as will be explained in a later section. To aid the removal of the excess fuel, an air stream is created to carry the fuel along the vent pipe by allowing air to leak in around the flange of the cap (simply done by using no gasket). In operation, as soon as pressure rises in the chamber air leaks profusely out of the chamber through the vent pipe, so much so that a control valve has to be fitted to the end of the vent pipe to reduce the flow to manageable levels. In effect the atmosphere is used as a vacuum pump to 'suck' the fuel from the chamber. This type of spray cap has been used widely in the laboratory at Imperial College on atmospheric rigs, but here an actual vacuum pump is required.

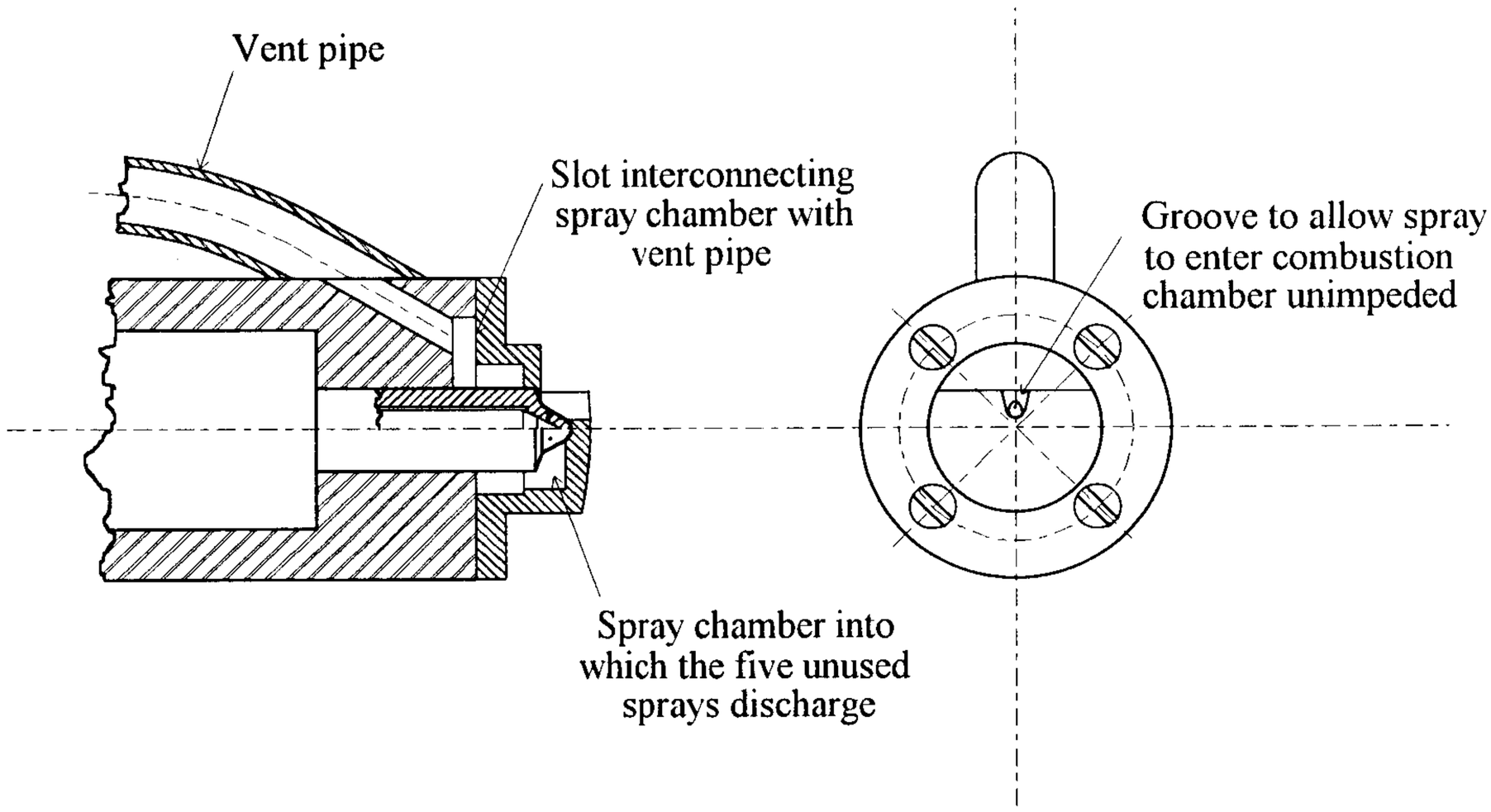


**Fig 3.21** Spray cap designed to allow just one spray into the chamber and vent the fuel from the five remaining sprays to outside the chamber.

One problem with the injector being offset in the adapter is that it is difficult to produce a realistic swirling flow field about the injector. Clearly the centre of swirl is likely to be on the axis of the chamber rather than on the axis of the injector. Nonetheless an attempt was made to produce a swirling flow, with the relevant bowl angular velocities provided from information in similar-size production engines. The swirl type inlet port was fitted to the chamber and LDA measurements were taken of the flow velocities, both radial and tangential; since it was assumed that the axial component of velocity is small. After numerous attempts with different levels of air flow through the chamber, it was found that only very low velocities were achievable. What seemed to happen was that the air past at high velocity around the wall while, towards the centre of the chamber, the velocities dropped to not more than 1m/s. Since this is about an order of magnitude below the required velocities, it was decided to fit a baffle inside the chamber which would effectively bring the wall of the chamber much closer to the injector; i.e. to within 35 mm from the nozzle. Again LDA measurements were taken, which showed that although there was a slight improvement, the high velocities still remained close to the new wall and a decision was made at this point to opt for quiescent conditions, since the low velocities present

in the centre of the chamber, even with the swirl port, were so low as to have an insignificant effect on the spray.

### 3.2.4.3 Measurement procedure.

PDA measurements were performed at four radial locations at each of three axial positions, 10, 17.5 and 25 mm from the nozzle exit. The radial locations were chosen to be roughly along imaginary lines emanating from the nozzle hole (see Figure 3.22). At each position the axial velocity and diameter of several thousand individual droplets was logged over a time period encompassing the whole of the injection and a short period afterwards. The time of arrival was registered for each validated droplet, so that a complete map in space and time could be constructed.

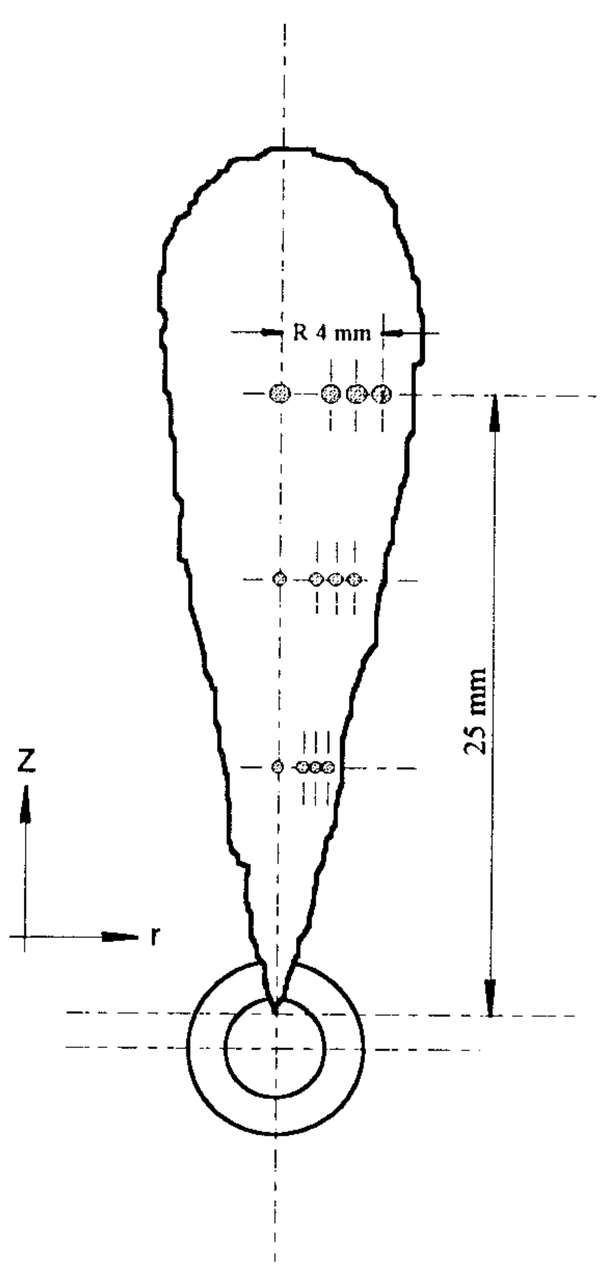


**Fig 3.22** Diagram of spray showing position of one measurement station, all the remaining stations are located using the same Cartesian notation.

The chamber was run with a gas pressure which gave an equivalent density to that of the real engine's combustion chamber; the densities and chamber pressures can be found in Table 3.2. All tests were done with unheated air flow as evaporation was not being studied. Sufficient air flowed through the chamber to allow the diesel pump to be run with continuous injection, the fuel being purged from the chamber by the high gas flow rate between injections.

Once the air valve was opened and the pump set running, after a small delay to allow the pressure to reach equilibrium, the PDA system was started, measurements being taken from successive injections. It was found that about three minutes of data acquisition were required to fill the computer's memory with measurements. Each time typically 1000 validated samples were collected. At each position a minimum of 6000 samples were taken, requiring typically six different experiments. These experiments were conducted successively to minimise any differences caused by changes in the operating conditions.

The validation rate was typically as low as 5%. To examine the statistical reliability of the data at such low validation rates, a check of validity additional to the PDA measurements was made using an LDA sample at each location and the same optical set-up. The velocities obtained from the PDA and LDA experiments were then compared. Because the validation rate in the LDA experiments was much higher, typically 70%, any discrepancy between the two measurements will indicate biasing of the PDA validation to a certain size class. For instance if the velocities taken by the PDA system were higher than those from the LDA system, this would probably indicate biasing towards larger droplets, as these tend to have higher velocities. The results of these tests are given in the next chapter.

## 3.3 BOSCH EPVE PUMP CALIBRATION, IMAGING AND SPRAY CHARACTERISATION USING PDA.

### 3.3.1 Calibration of EPVE pump.

The calibration of this pump followed the procedure of the MW pump's calibration and will not therefore be described here in detail. The only difference was the use of a Hartridge pump test rig rather than the top of the chamber as a mounting for the pump. The Hartridge was used due to the convenience it offered for the calibration in setting the initial delivery of the pump.

The conditions at which these tests were performed are given in Table 3.4 and the results of the calibration are shown in Figures 3.23 to 3.26.

| Speed (rpm) | Load | Delivery ($mm^3$/Inj). | Boost Press. (bar). | Chamber Press. (bar). |
|---|---|---|---|---|
| 1200 | Full | 109.7 | 1.42 | 40.9 |
| 1200 | Half | 55.2 | 1.16 | 30.8 |
| 800 | Full | 134.7 | 1.47 | 39.2 |
| 800 | Half | 63.6 | 0.80 | 35.4 |

**Table 3.4** Test conditions for calibration of EPVE pump.

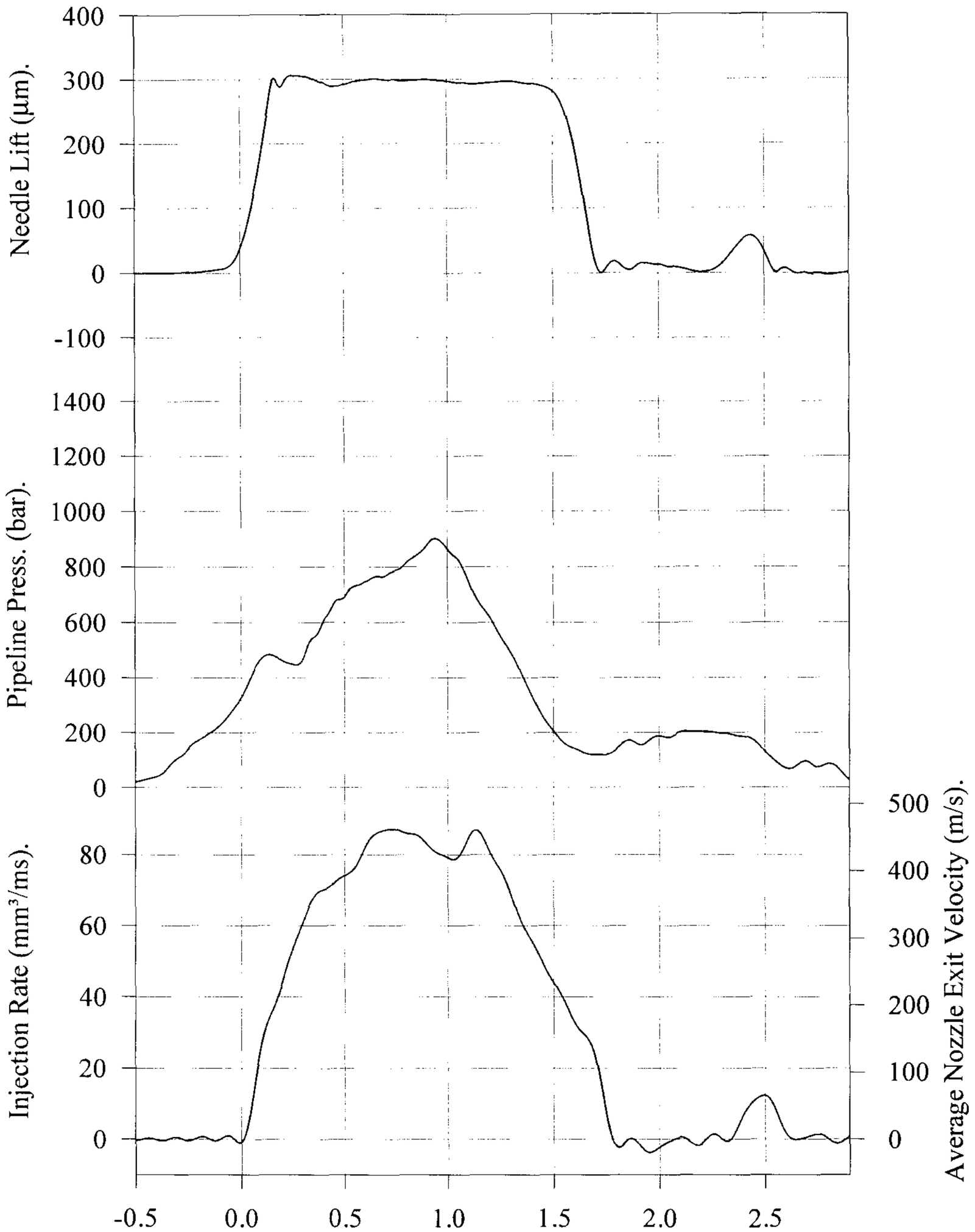


**Fig 3.23** Graphs of needle lift, line pressure and injection rate, of EPVE pump FIE.
1200 rpm, full load.

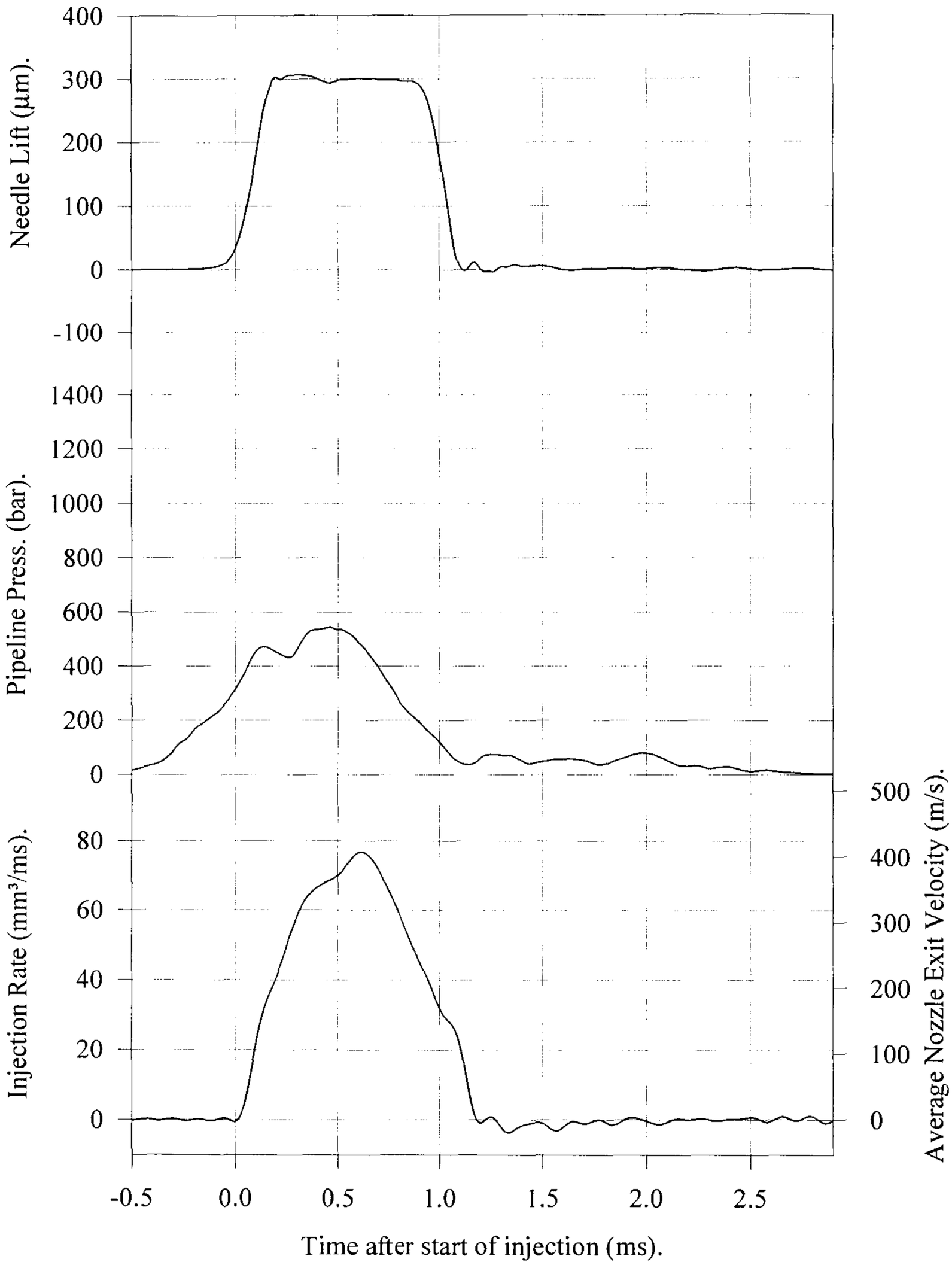


**Fig 3.24** Graphs of needle lift, line pressure and injection rate, of EPVE pump FIE.
1200 rpm, half load.

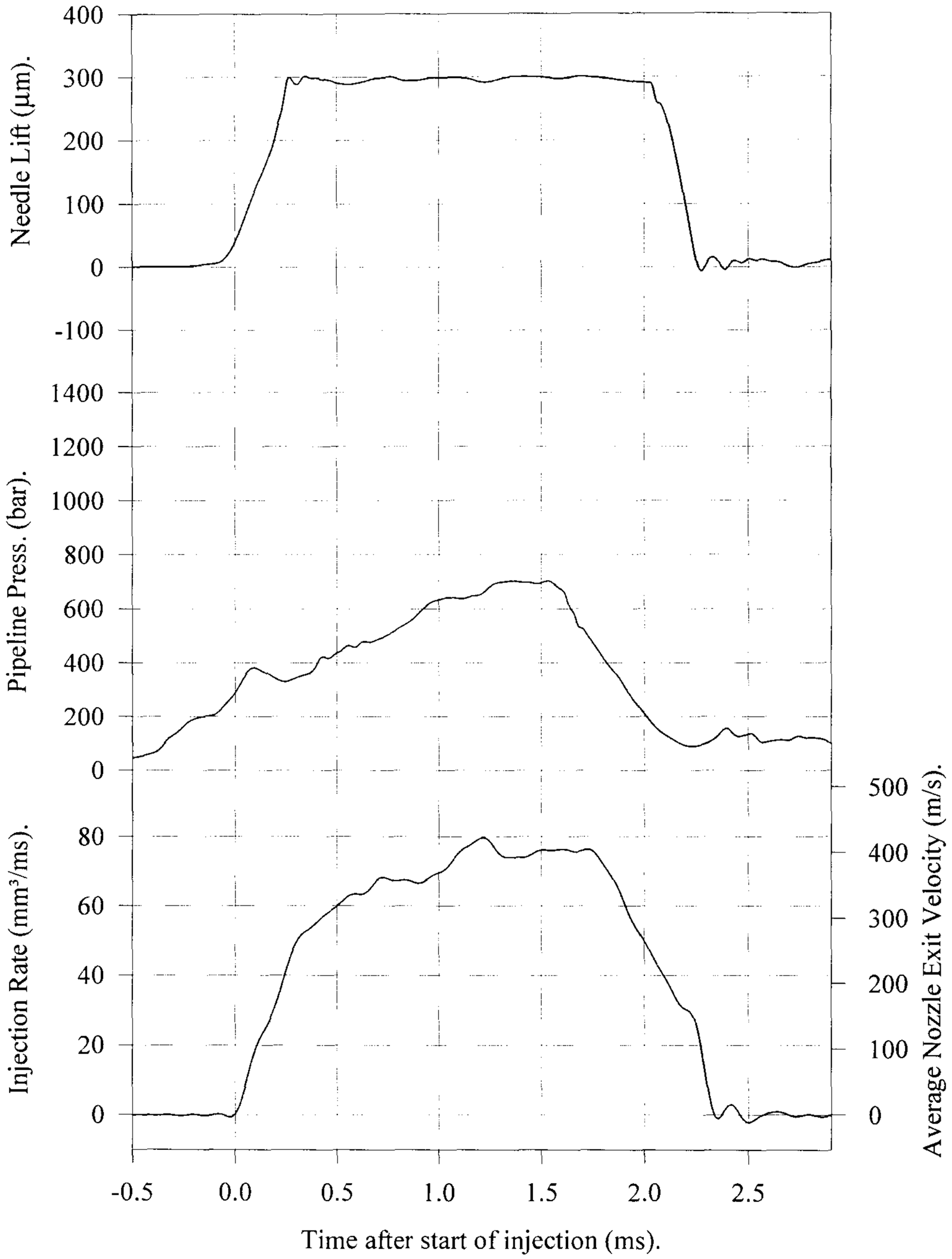


**Fig 3.25** Graphs of needle lift, line pressure and injection rate, of EPVE pump FIE.
800 rpm, full load.

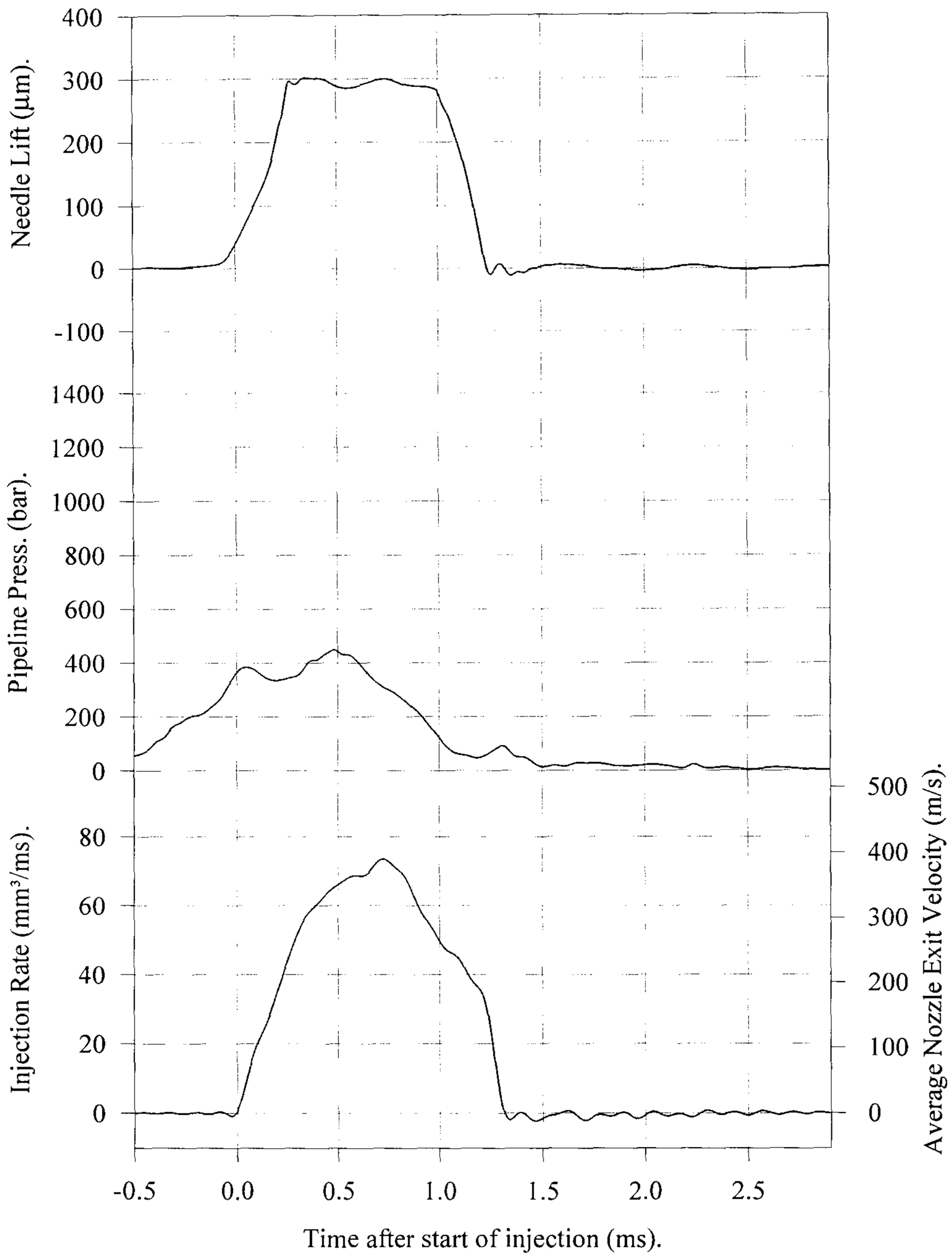


**Fig 3.26** Graphs of needle lift, line pressure and injection rate, of EPVE pump FIE. 800 rpm, half load.

### 3.3.2 Imaging.

Imaging of the sprays from the EPVE pump, unlike the MW pump, used a high speed closed circuit camera as the 'Imacon' was unavailable. The camera had a maximum sample rate of 50 Hz, consequently only one image per injection could be sampled. However, 15 images could be sampled at a time at each trigger point rather than just one with the 'Imacon' which enabled a larger statistical sample to be obtained so that variations in the time of the start of injection could be accounted for by averaging, although a lot more computer memory was needed to store the data.

A tungsten/halogen spotlight was used to illuminate the sprays through the head window. As with the imaging of the MW pump system a compromise between gain and exposure time was made to maximise the image quality. The camera was triggered by the same circuitry used for the calibration; a time delay was introduced with a pulse generator to enable the time at which the camera was triggered in each cycle to be varied. A preliminary run was done in which the delay of the start of the injection from the trigger point was established. This was performed with the pump running while a monitor displayed each image as it was recorded giving a series of images on screen at a specific point during the injection period. By adjusting the delay until the spray was seen to disappear, the delay to the start of injection could be ascertained. Once this reference time had been established, measurements at any specific time in the course of the cycle could be made simply by adding the required time to the reference time and setting the new delay on the pulse generator.

It is interesting to note that variations in chamber pressure had a marked effect on the reference time, indicating that high chamber pressures initially blocked the flow of fuel through the holes at low needle lifts. In addition there were apparently random cycle to cycle variations of the reference time of the order of 50 μs. This is unlikely to be due to triggering errors as from observations on the oscilloscope the flywheel holes used for the triggering circuit gave a very precise trigger, so the variations must be assumed to be caused in the FIE.

The test conditions and results of these tests are given in full in Chapter 4

### 3.3.3 PDA measurements of EPVE pump based system.

#### 3.3.3.1 Layout of optical equipment.

The general arrangement of the optical equipment is the same as that for the MW pump with the one central difference being the use of the Aerometrics counter rather than the Imperial College counter. The one difficulty in using this counter was that the timing clock used to tag measurements, could only be reset at the start of each experimental run; with no facility for resetting the clock after each revolution of the pump. As a consequence, the measurements could not be tagged relative to the start of injection, which is essential in dense Diesel sprays as the data rate is so low that many thousands of separate injections are required to allow statistically accurate measurements. Consequently, an alternative method of tagging the measurements had to be found.

The first option was to attempt to make an alteration to the counter's electronics to produce a resetting clock. A clock existed on the board already but this is simply reset at the start of the experiment and runs continuously. This counter consists of simple 74000 series TTL logic chips which have a reset pin that receives the required pulse at the start of the run. If an external TTL signal could be substituted for this reset pulse, a means of resetting the counter before each injection could be achieved. Such an alteration was made and a small circuit board added onto the Aerometrics board containing merely one logic gate to act as a buffer. The buffer would prevent damage to the Aerometrics board if a high voltage was applied to the reset input by mistake. A switch was also fitted so that the board could be switched between normal operation and resetable operation.

Unfortunately the trial of this device proved unsuccessful. Although the counters did reset, because of the design of the Aerometrics board this caused partial resetting of the counter. It appears that there are two levels of counting, the front high frequency end, consisting of the two TTL counters, that the alteration successfully reset and a low frequency adder in the microprocessor. This adder reads the value of the count from the high frequency counters at a low sampling frequency and adds this to a stored value. Consequently even if the TTL counters are reset, the value stored in

the microprocessor is not. Unfortunately there was no easy means of resetting this stored value as the source code of the computer program was unavailable.

After consultation with Aerometrics it became clear that to achieve a resetting counter would require a considerable investment of money in an additional board and new software. This was considered unjustified as the PDA processor in question was already at the end of its useful life. The method finally adopted to solve the problem can only be said to be a partial solution and unfortunately introduced a small error into the timing. The PDA processor does allow the measurements to be gated so that data is only acquired over a certain period of the cycle; this is a standard feature available in most processors. Normally this gate is set to simply cover the part of the injection of interest, if, however, the gate is set to take measurements over a longer period, then the data rate towards the end of the gate period will be much higher. This is due to the spray density and the velocities being much lower, thus facilitating a high validation rate. Because there are a large number of samples towards the end of the gate, as a first assumption it can be assumed that the last droplet measured during the gated period is in fact at the end of the gate. The time of this gate relative to crank angle position is known as it is produced by a pulse generator triggered by the once-per-revolution signal from the pump. Therefore, each droplet has a reference time from the start of the experiment, simply by subtracting the reference time of the last droplet from all the droplets in the previous gated period, which will have times relative to the end of the gate. It is then a simple matter to convert these into time 'after the start of injection' (ASI) by adding the gate length and any delay of the start of the gate relative to the start of injection. This requires the raw data to be post-processed by a simple 'C' program. As an added refinement to reduce timing errors, a simple check of the data is made in this program. The first and last droplets in the gate period should be exactly the gate's length apart if the timing is to be without error. In practice a small error is inevitable, so in the code this error is calculated and, if it exceeds a certain value, all droplets from that injection are rejected. The error chosen was 50μs, which seems quite high, but was selected as a compromise between the need for accuracy and the need to avoid rejecting much of the acquired data.

### 3.3.3.2 Mechanical details and injector mounting.

Apart from the change of pump there are very few differences between the mechanical set-up of the MW pump based system, which should be referred to. The adapter for mounting the injector in the chamber and the spray cap are similar to those used for the MW pump (see Figures 3.20 and 3.21). As with the MW pump the injector is offset from the centre of the chamber by 17.5 mm to facilitate the PDA measurements. The novel feature with this adapter is the ability to position the injector in six angular positions, one for each of the six holes. By this means all six sprays could be studied in turn if differences between the sprays needed to be looked at.

### 3.3.3.3 Measurement procedure.

A very similar procedure was adopted as for the MW pump. Measurements were taken at the same axial and radial positions as before but, because of the change in the PDA counter, a longer gate (typically 8 ms) was used to facilitate the timing. This meant that a great deal more data could be acquired, most of which was subsequently rejected in the post-processing. So a great deal more space was required in storing the raw data, which is an unfortunate consequence of the timing method.

# CHAPTER 4

# RESULTS AND DISCUSSION.

## 4.1 IMAGING OF SPRAYS FROM MW AND EPVE PUMP SYSTEMS.

### 4.1.1 Penetration.

As described in the last chapter, images of the sprays produced by the MW and EPVE pump based systems were obtained with two different imaging systems. These images have revealed much useful information about the sprays and their development. Measurements of spray tip penetration were deduced from the images by using the computer package 'Photostyler'. The length of the spray was measured by counting its length in pixels, but a subjective judgement has to be made as to the position of the tip of the spray. To reduce errors caused by this, at least ten images at each condition were measured and an average taken. Figures 4.1 to 4.2 show the geometry of the injectors and the orientation of the holes, while Figure 4.3 is a schematic representation of the sprays emanating from an injector, which also shows the numbering sequence of the holes used throughout this text. A selection of the images is shown in Figures 4.4 to 4.7. The measured tip penetrations are shown in Figures 4.8 to 4.10 for the MW pump and Figures 4.11 to 4.13 for the EPVE pump.

Figures 4.8 and 4.11 show a comparison of the tip penetration with and without the spray caps fitted, in order check if the use of the caps affected the sprays development. As can be seen there is a very good correlation between the two traces for both pump systems and it has been assumed that the single sprays produced when using the caps are representative of the multi-hole injection system.

Figures 4.9 and 4.12 show the tip penetration for the MW and EPVE pump systems respectively for each of the four conditions of speed and load used in the PDA experiments, while Figures 4.10 and 4.13 show the effect of varying chamber pressure

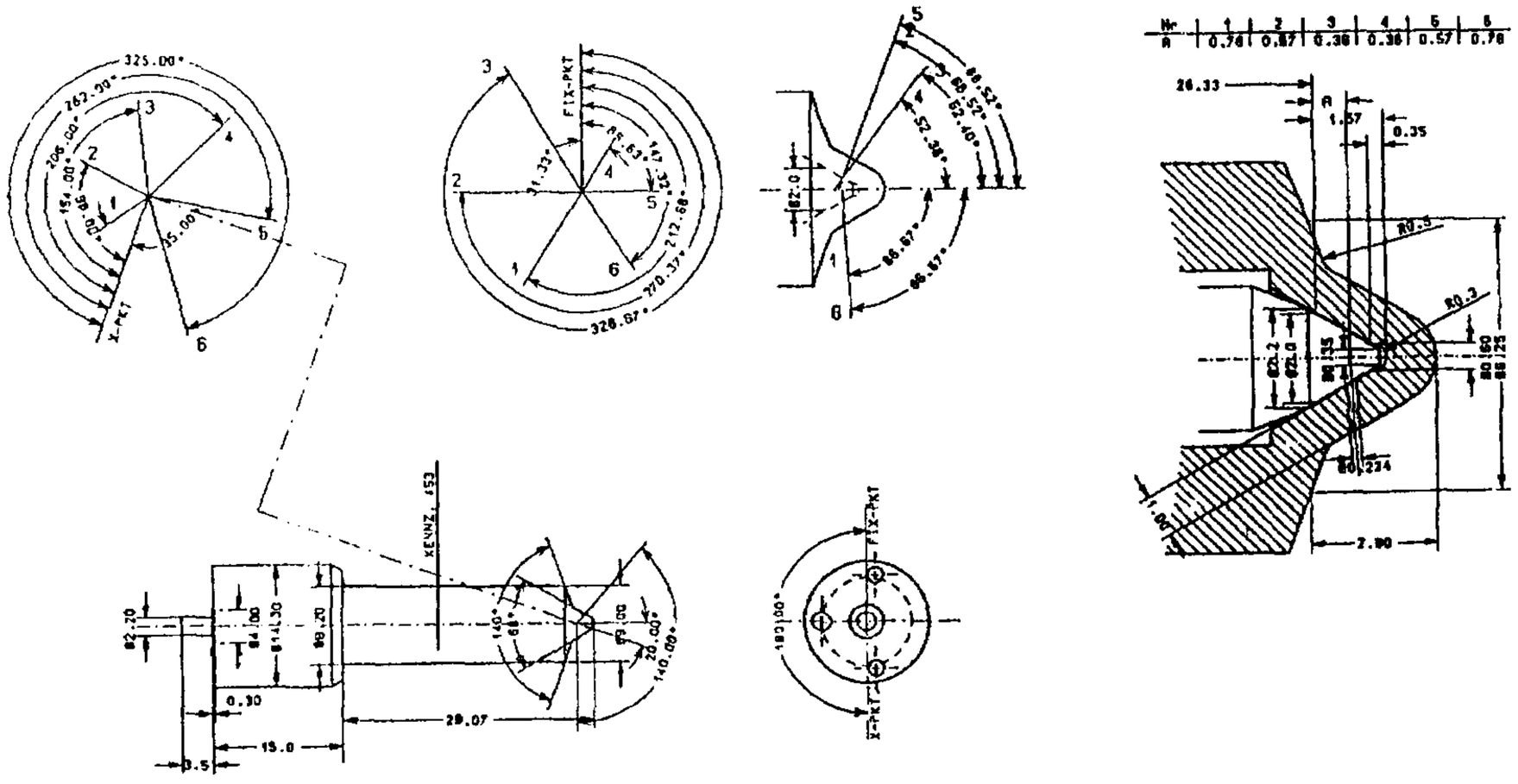


**Fig 4.1** Diagram of RT injector nozzles used in MW pump based FIE system, showing angles of sprays.

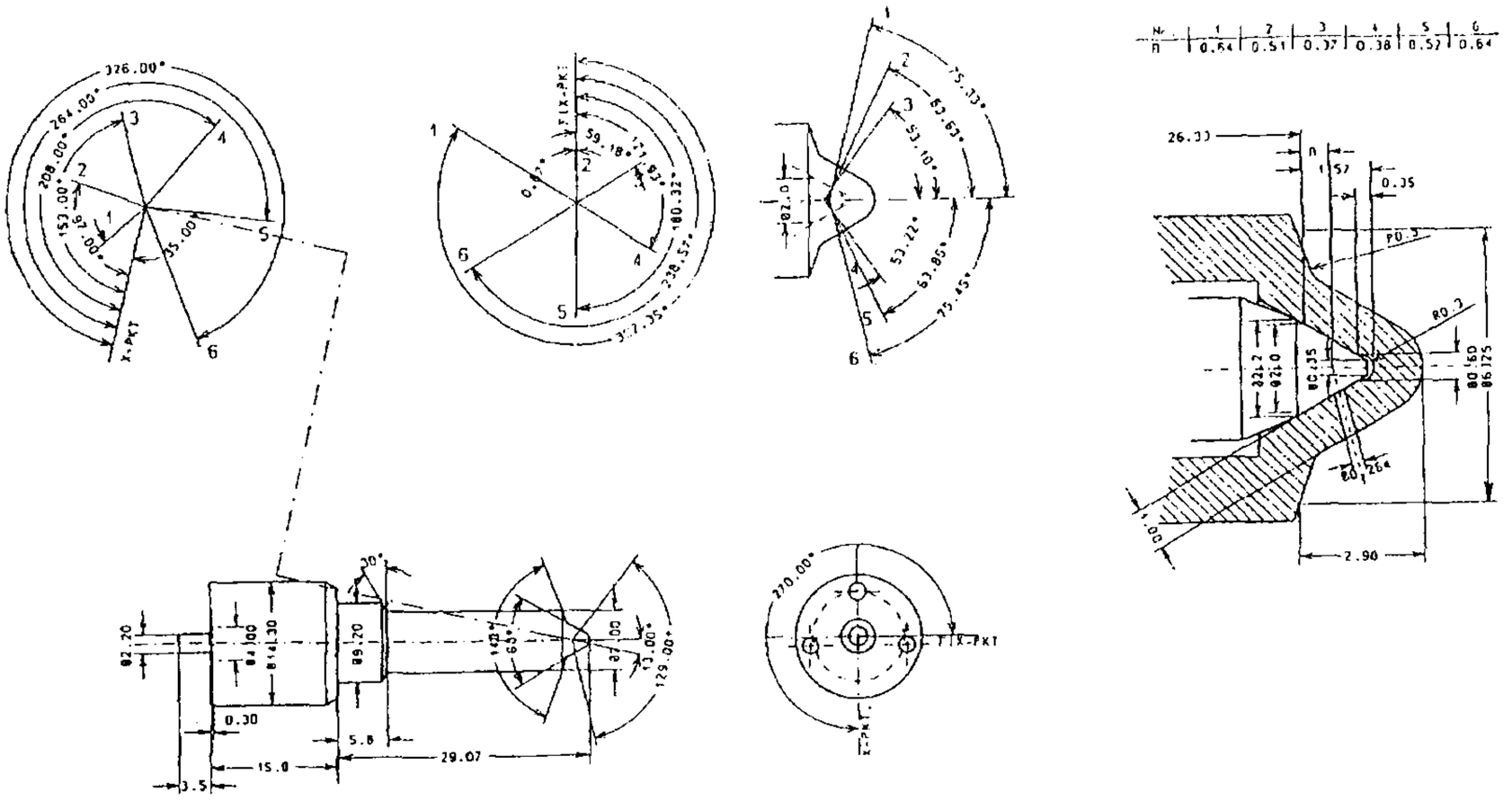


**Fig 4.2** Diagram of KDAL injector nozzles used in EPVE pump based FIE system, showing angles of sprays.

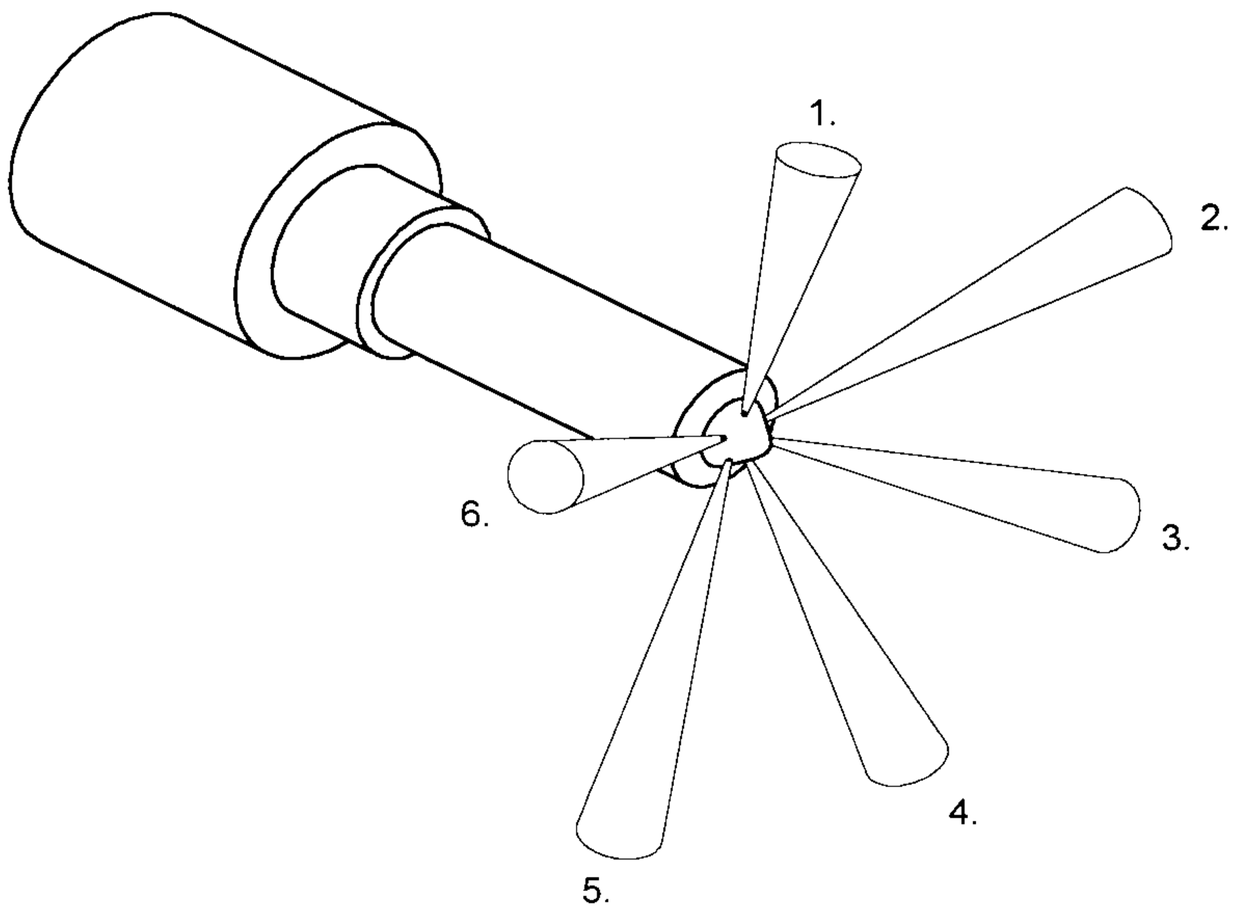


**Fig 4.3** Isometric view of injector nozzle showing all six sprays and their orientation.

on spray tip penetration. These graphs also show predictions of penetration using Hiroyasu's correlation; given as Equation 4.1 below [*Hiroyasu and Arai,* 1990]. A number of other correlations have been examined which give the same general trend [*Dent,* 1971; *Naber and Siebers,* 1996], but these have not been plotted for the sake of clarity. The results show, as would be expected, that higher chamber pressure, or more specifically density, reduces tip penetration.

$$S = 2.95 \cdot \sqrt{\sqrt{\frac{P_{inj} - P_{cha}}{\rho_{cha}}} \cdot d_o \cdot t} \qquad (4.1)$$

Injection pressure is also an important determinant of tip penetration and it is interesting to note that the graphs and images show that higher load and pump speed (and hence higher injection pressure) does not necessarily result in greater tip penetration. This is partly because the increase in injection pressure is offset by an

increase in chamber density (pressure) at the higher speeds and loads (this was done to match the conditions found in a typical production engine). Even taking this effect into account the graphs indicate that injection pressure does not have as large an effect on tip penetration as the various correlations in the literature would indicate. An additional problem with the correlations is that they tend to over-predict the initial penetration. One possible solution which might solve both of these problems is to take account of the low injection pressures which occur at the beginning of injection; typically the correlations use a constant value for the pressure acting across the hole during the whole injection period, which is usually calculated from the peak injection pressure found in the calibration of the FIE. This is quite unrealistic since due to the gas pressure in the chamber, the pressure drop may be momentarily negative at very low needle lifts, which might explain the apparent delay in injection when comparing needle lift and injection rate measurements.

It was decided that a better prediction of penetration could be achieved by taking account of this low pressure drop in the early stages of injection. To model this Hiroyasu's correlation was modified, by using instead of a fixed value for the injection pressure, a more realistic ramp from zero to full pressure for the first half of the injection period. This involves an additional term in Hiroyasu's correlation, the result of which is given below:

$$S = 2.95 \cdot \sqrt{\sqrt{\frac{\left(\frac{2 \cdot P_{Inj} \cdot t}{t_{Inj}}\right) - P_{cha}}{\rho_{cha}}} \cdot d_o \cdot t} \qquad (4.2)$$

$$\text{where} \quad t \le \frac{t_{inj}}{2}$$

Predictions using this correlation are also shown on the graphs and, as can be seen, a much closer approximation is achieved throughout the course of the injection than with Hiroyasu's correlation.

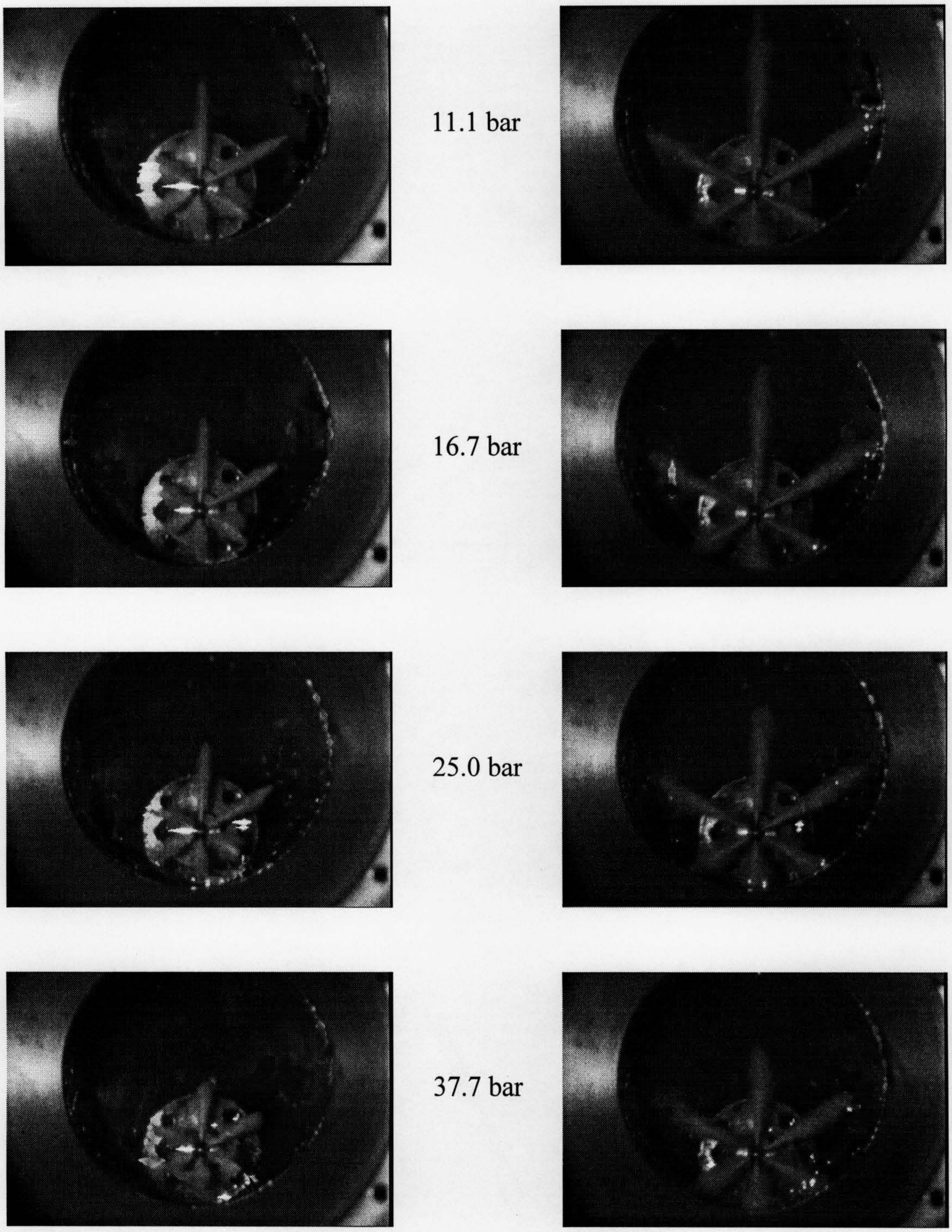


**Fig 4.4** Images of sprays at 0.2 ms and 0.5 ms ASI at different chamber pressures, without spray cap fitted. MW pump based system at 800 rpm, half load.

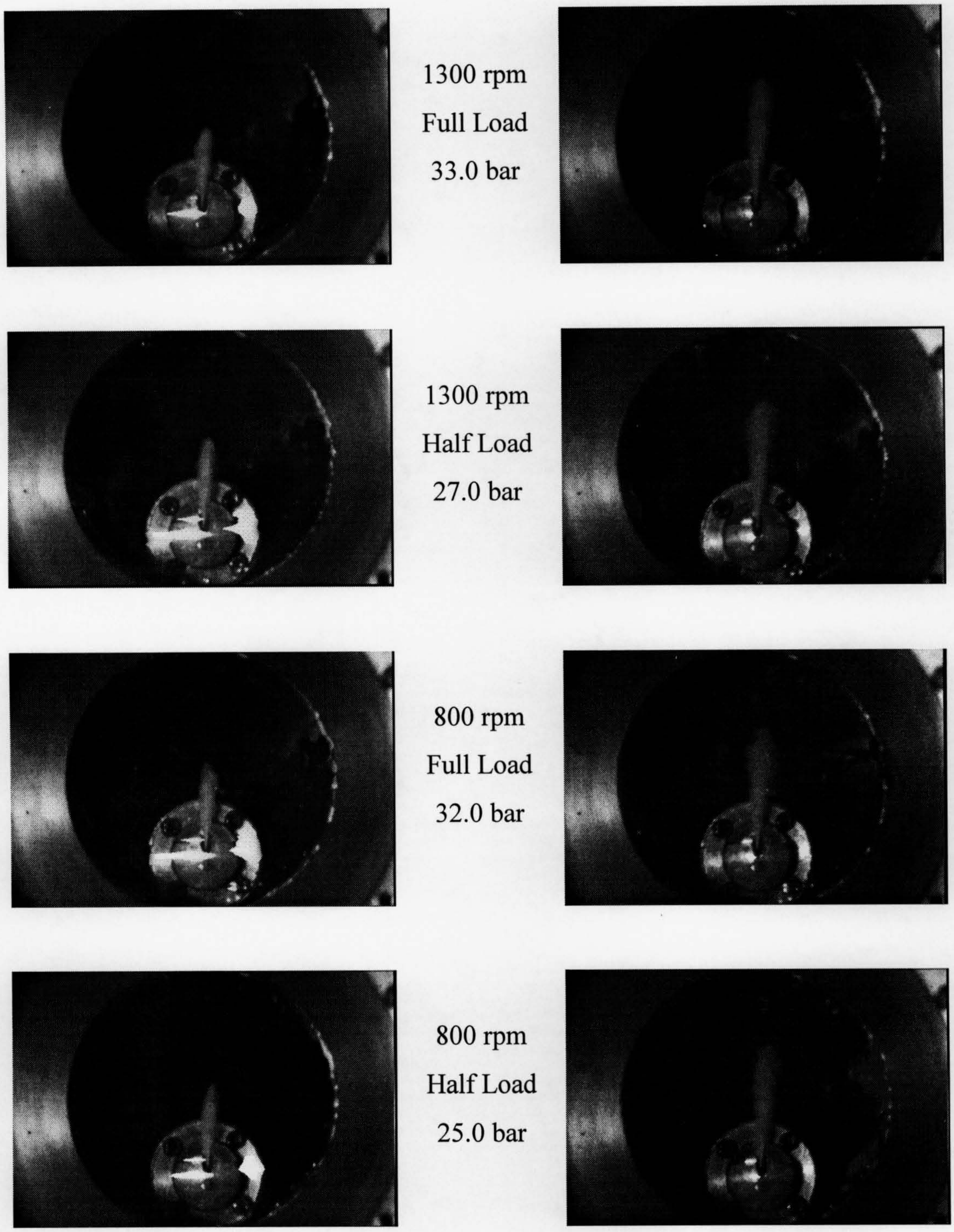


**Fig 4.5** Images of sprays at 0.2 ms and 0.5 ms ASI at four different conditions of load and speed used in the PDA studies, with spray cap fitted. MW pump based system.

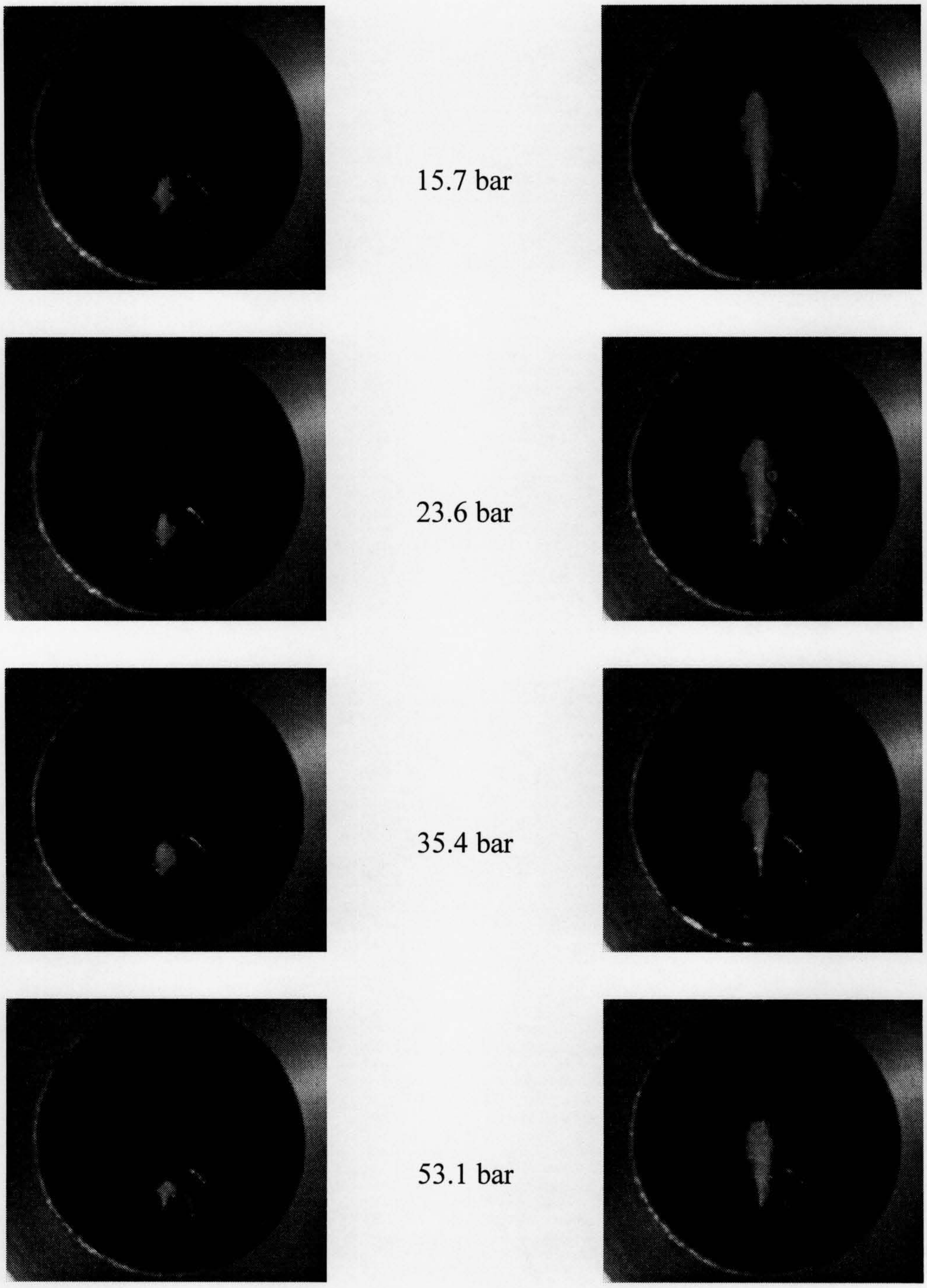


**Fig 4.6** Images of sprays at 0.2 ms and 0.5 ms ASI at different chamber pressures, with spray cap fitted. EPVE pump based system at 800 rpm, half load.

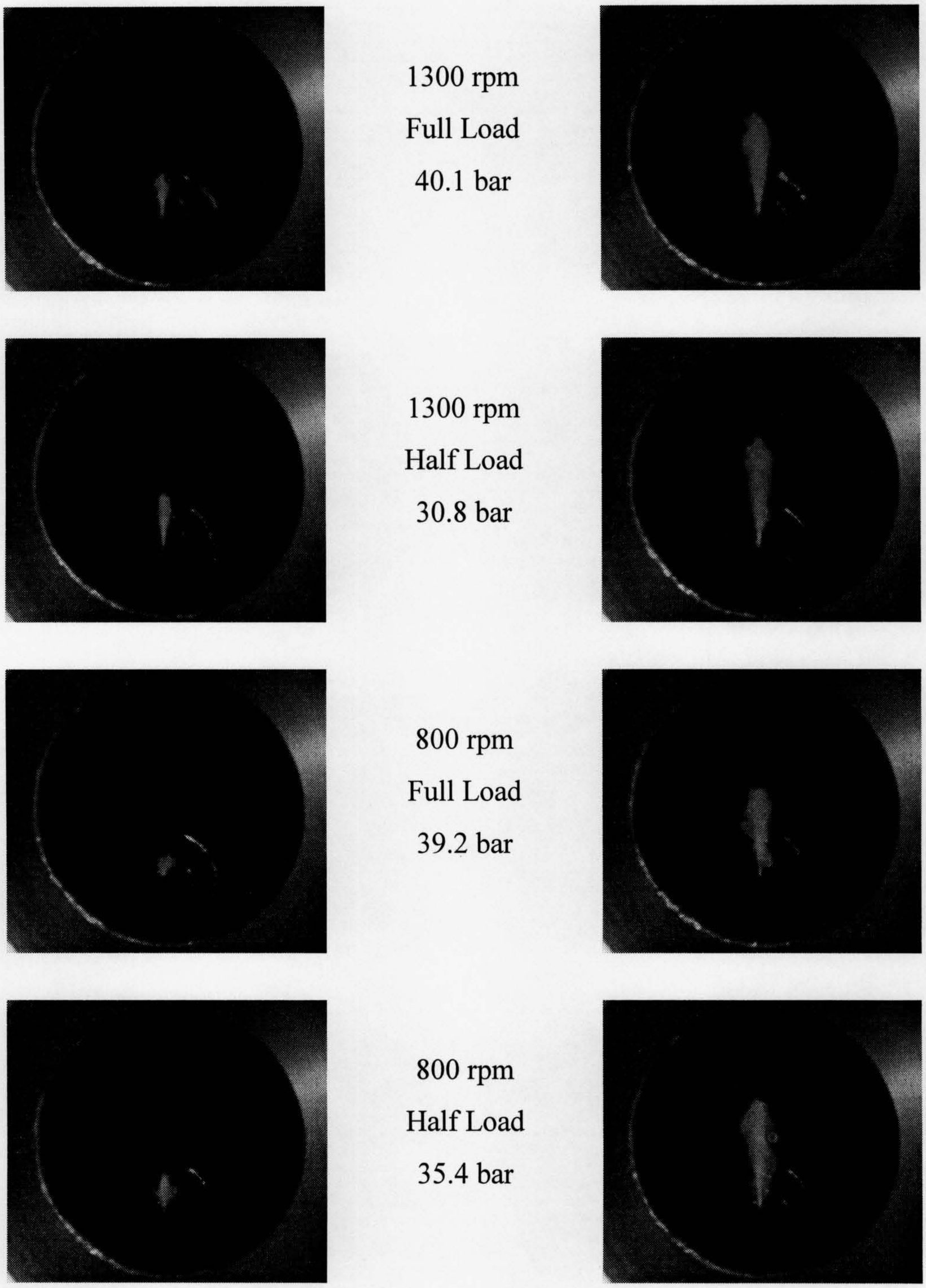


**Fig 4.7** Images of sprays at 0.2 ms and 0.5 ms ASI at four different conditions of load and speed used in the PDA studies, with spray cap fitted. EPVE pump based system.

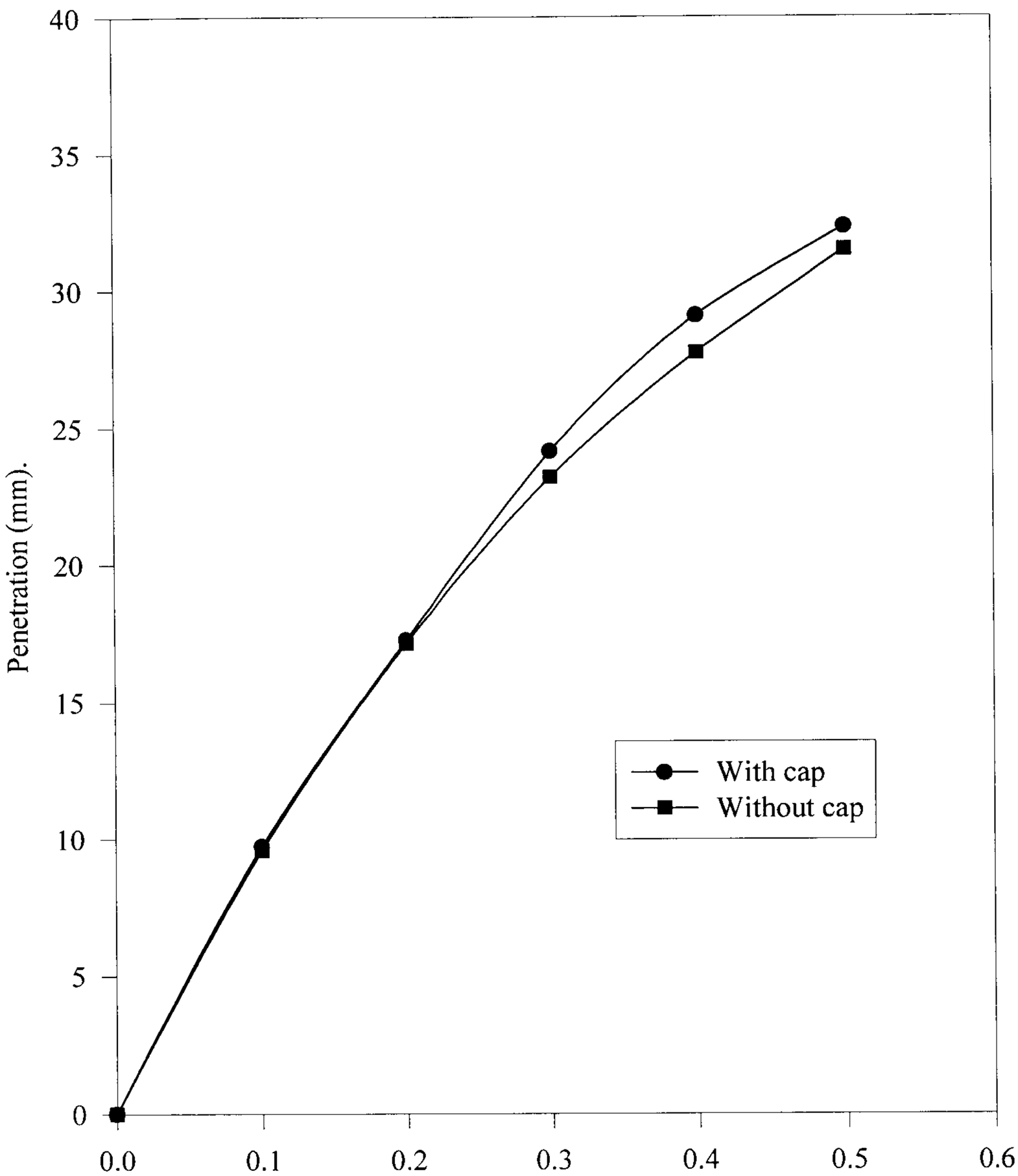


**Fig 4.8** Graphs of penetration vs. time with and without spray cap fitted.
MW pump based FIE at 1300 rpm, full load.

**1300 rpm Full Load.**
**Chamber pressure 33bar.**

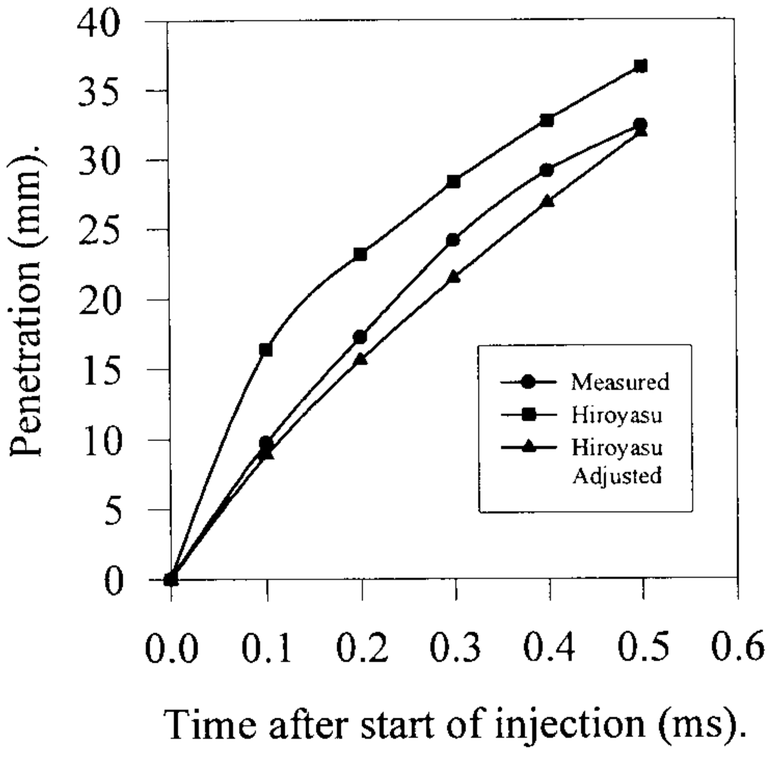


**1300 rpm Half Load.**
**Chamber pressure 27bar.**

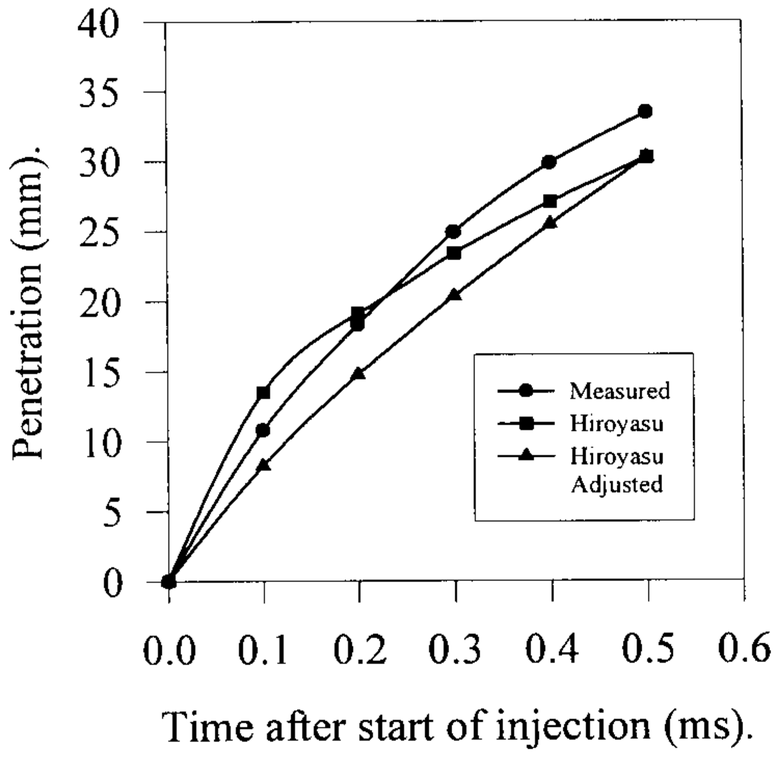


**800 rpm Full load.**
**Chamber Pressure 32bar.**

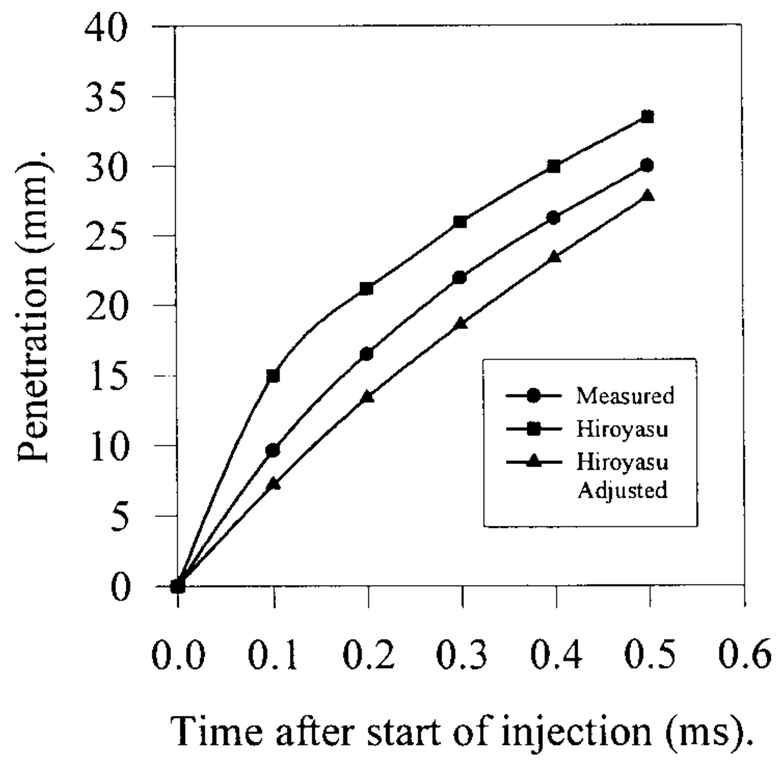


**800 rpm Half load.**
**Chamber pressure 25bar.**

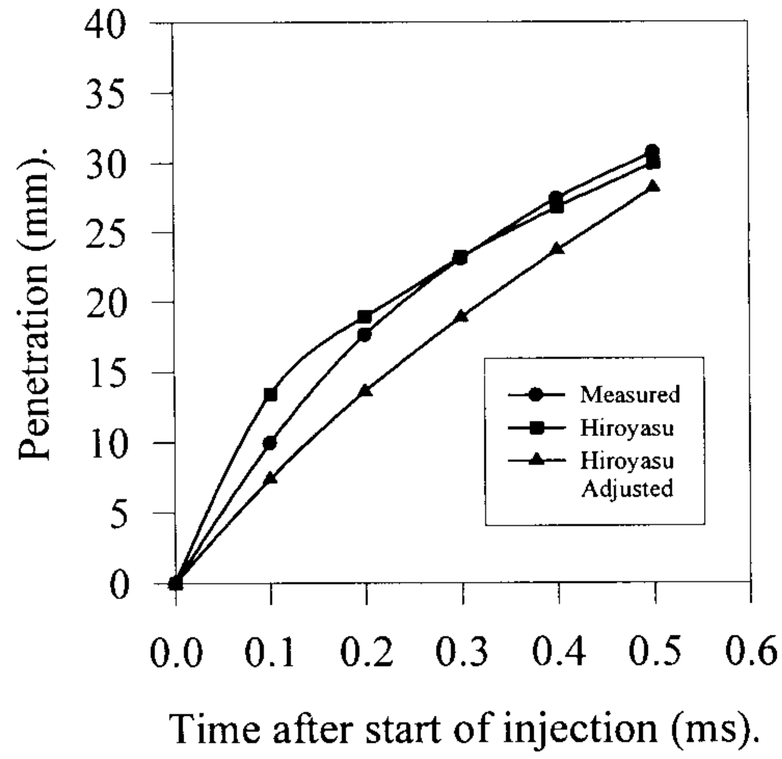


**Fig 4.9** Graphs of penetration vs. time at different loads and speeds.

MW pump based FIE.

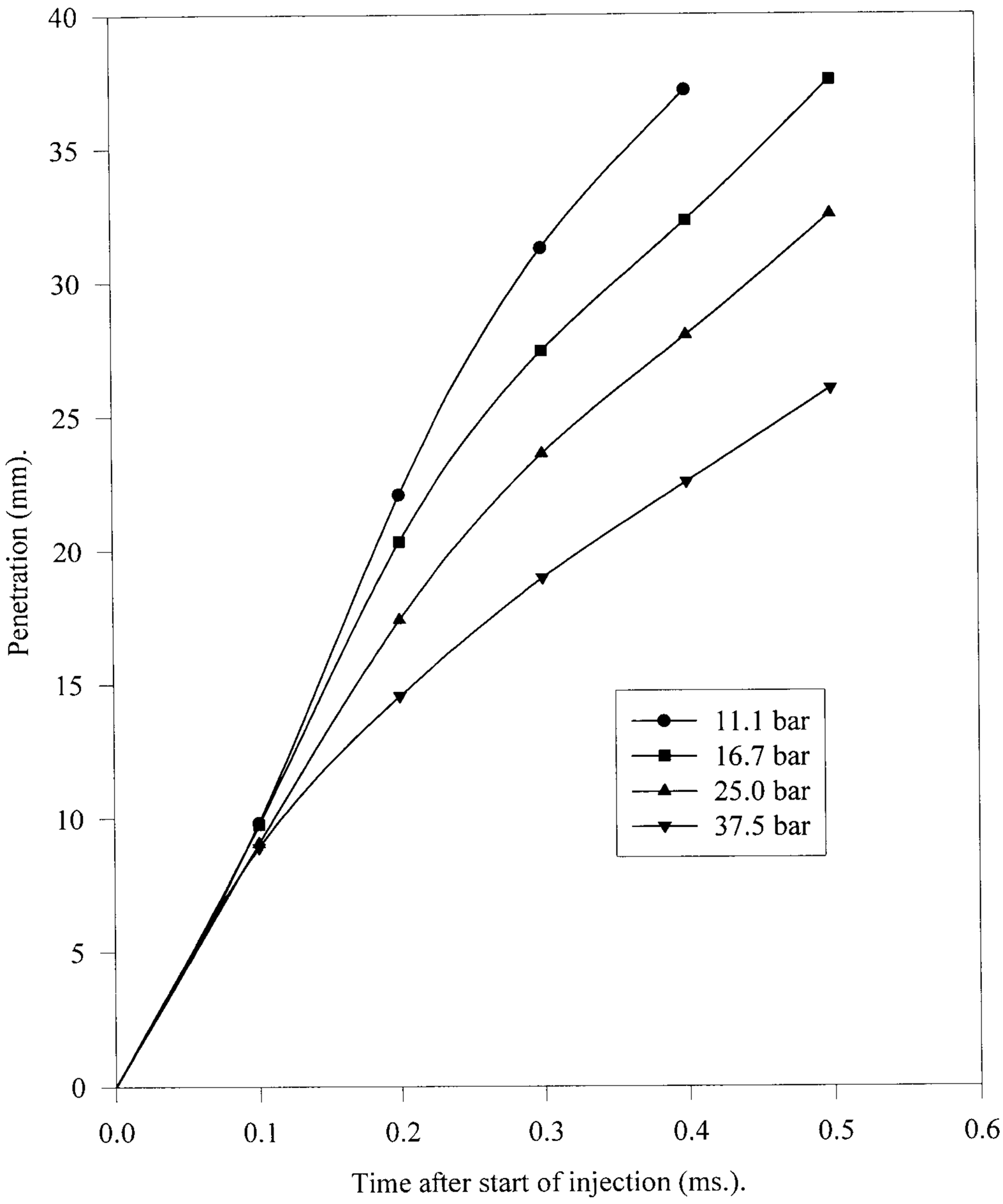


**Fig 4.10** Graphs of penetration vs. time for different chamber pressures.
MW pump based FIE at 800 rpm, half load.

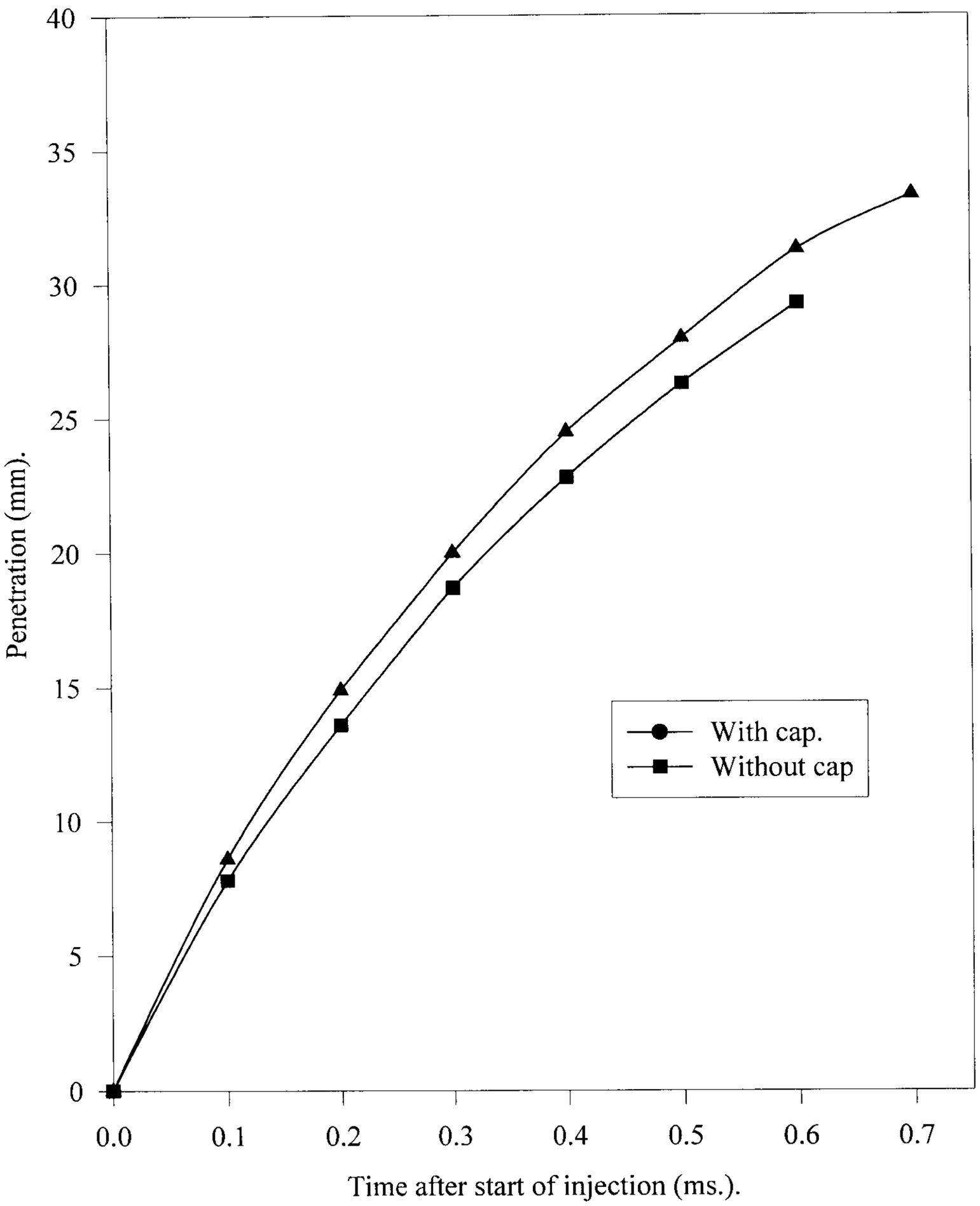


**Fig 4.11** Graphs of penetration vs. time with and without spray cap fitted.
EPVE pump based FIE at 1300 rpm, full load.

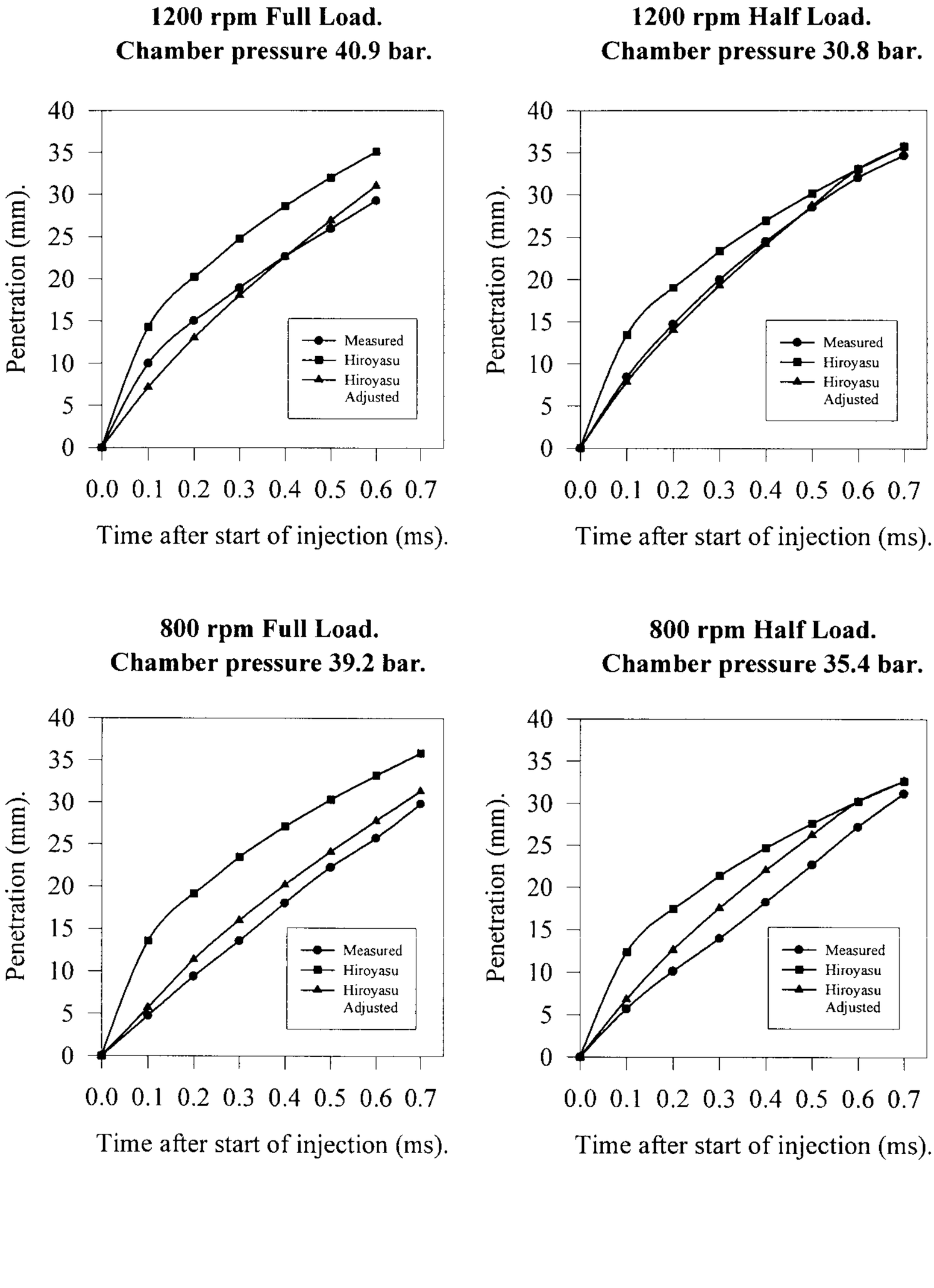


**Fig 4.12** Graphs of penetration vs. time at different loads and speeds.
EPVE pump based FIE.

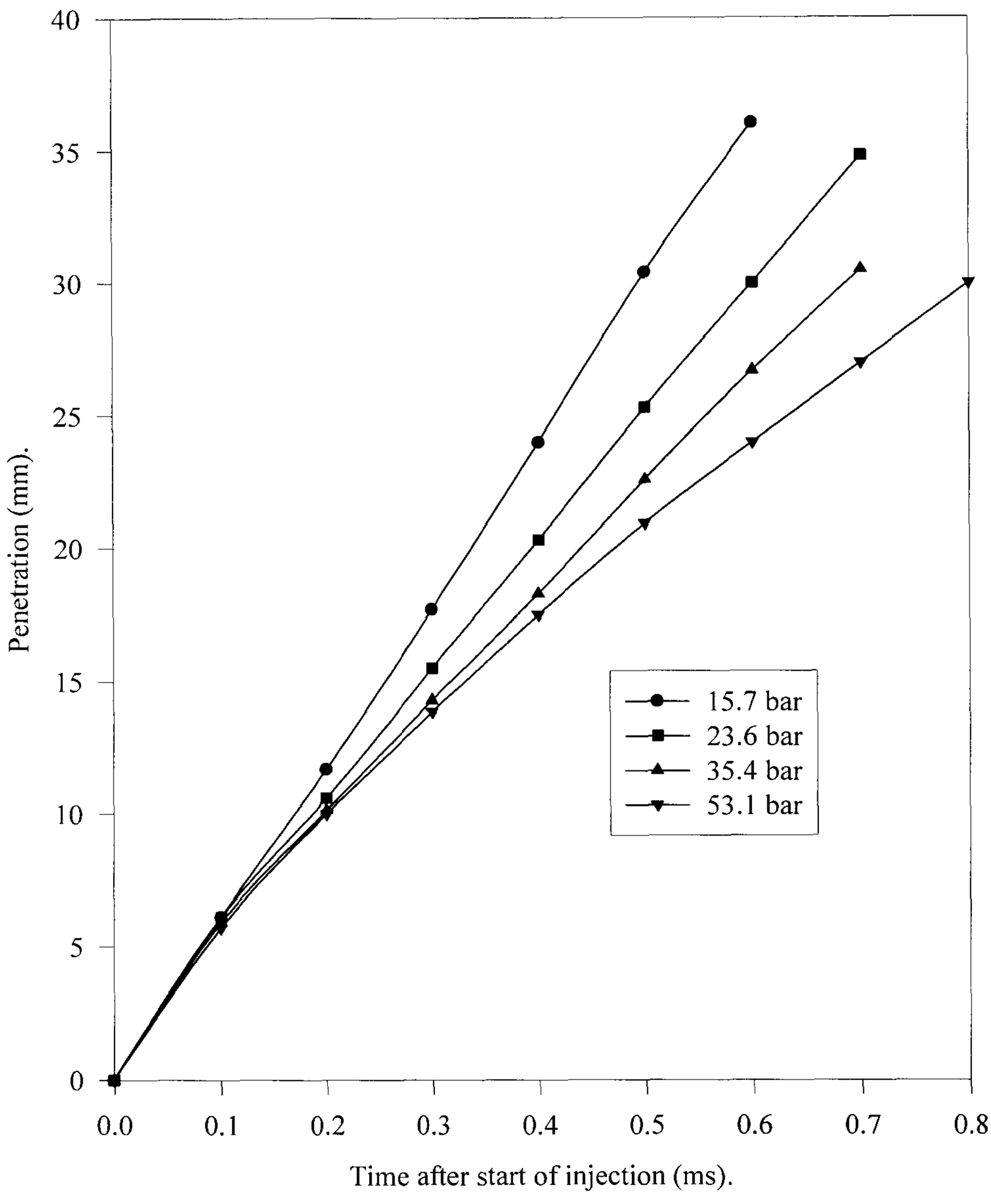


**Fig 4.13** Graphs of penetration vs. time for different chamber pressures.

EPVE pump based FIE at 800 rpm, half load.

## 4.1.2 Cone Angle.

### 4.1.2.1 Sprays of MW Pump Based System.

Figure 4.14 along with Table 4.1 shows the spray cone angle at different pressures for each of the six sprays injected by the MW pump based system. These are measurements based on one spray image with the spray cap removed in each case.

A study of these results reveals some interesting features. First of all a wide variation in spray angle from spray to spray is evident, which occurs even at high needle lifts. Concentrating on the MW pump first, holes 1,2,3 and 6 produce what might be described as typical sprays. These are sprays where there is cavitation in the holes and which atomise at the exit from the hole; see for example Hole 4 exhibits a much larger cone angle, this can be explained in a number of different ways. In general wide cone angle implies a lack of cavitation combined with a swirling flow into the hole [*Soteriou et al,* 1995]. The lack of cavitation is easily explained as hole 4 is the most inline with the injector axis, see Figure 4.1, and is therefore the least likely to cavitate as the degree of cavitation is a function of, amongst other factors, the acuteness of the 'turn' which the fuel has to make as it enters the hole. On the other hand, the swirling inlet flow normally stems from an eccentric needle at low needle lifts [*Iiyamu,* 1992]. At high needle lifts, however, it is unlikely that the needle is sufficiently close to the hole to induce swirl. A possible explanation is that the large spray cone angle is a remnant of the early part of injection caused during the low needle lift period. This cone may then obscure the central, more typical part of the spray, produced at a higher needle lift. Alternatively, the geometry of the flow passages around the needle may tend to produce swirling inlet flow even at high needle lifts.

The large cone angle of spray 5 lies in-between that of spray 4 and the other sprays. If hole orientation and the consequent degree of cavitation was the only explanation for the presence of high cone angles, then spray 3 would be expected to be of similar shape to spray 5, as this hole has an almost identical inclination to hole 3. The fact that this is not the case could indicate either that geometric factors or alternatively needle eccentricity play an important part in causing these hollow cone

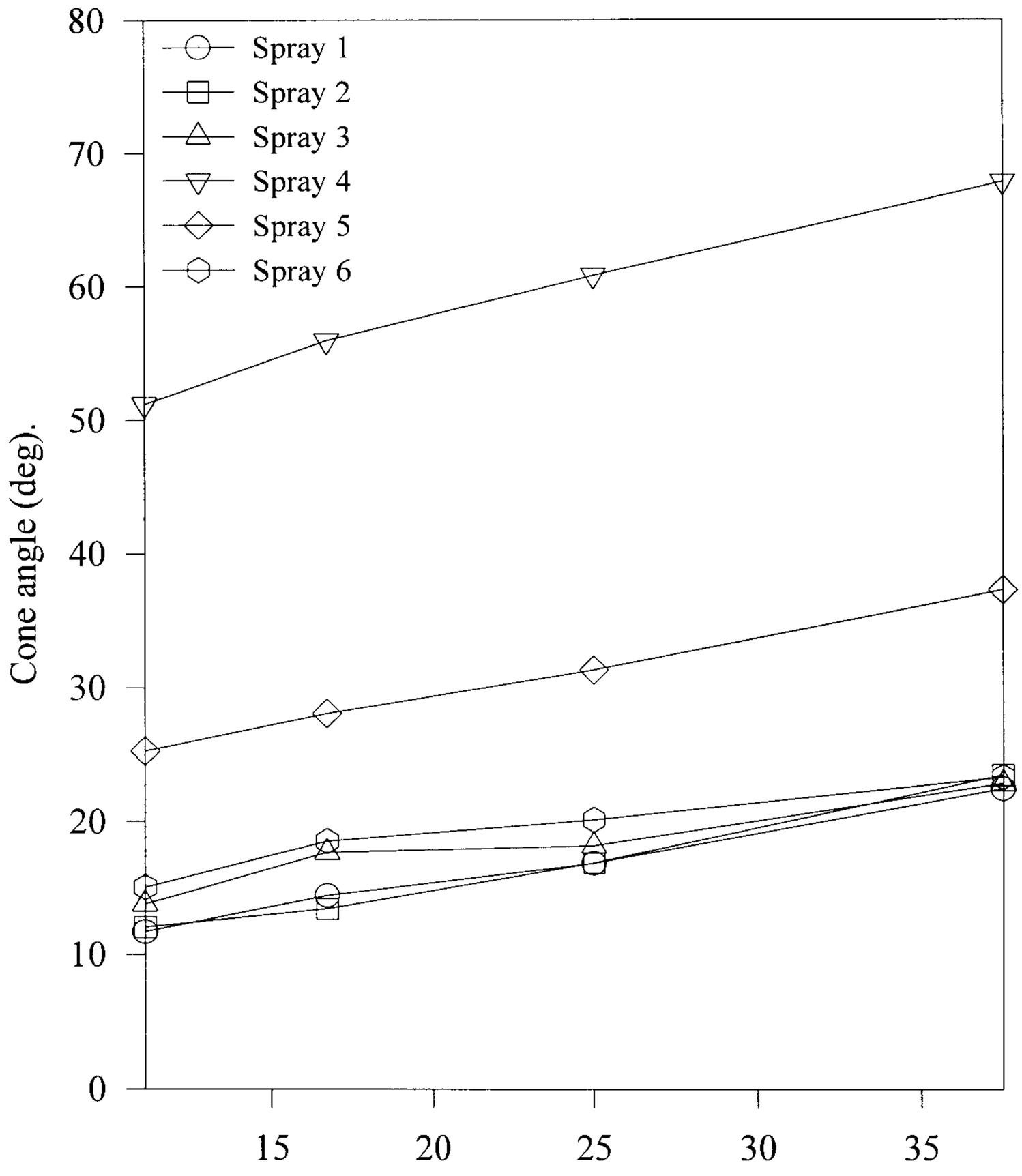


**Fig 4.14** Graph of spray cone angle vs. chamber pressure for each of the six nozzle holes. MW pump based FIE at 800 rpm, half load.

| Pump speed (rpm) | Load | Spray | Chamber Pressure (bar) | Cap | CN | Far angle @ 0.5 ms ASI |
|---|---|---|---|---|---|---|
| | | | | | | |
| 800 | half | 1 | 25 | yes | 22.1 | |
| 800 | half | 1 | 32 | yes | 17.2 | |
| 1300 | full | 1 | 27 | yes | 20.4 | |
| 1300 | full | 1 | 33 | yes | 16.6 | |
| 1300 | full | 1 | 33 | no | 16.6 | |
| | | | | | | |
| 800 | half | 1 | 11.1 | no | 48.6 | 11.7 |
| 800 | half | 2 | 11.1 | no | 48.6 | 12.0 |
| 800 | half | 3 | 11.1 | no | 48.6 | 13.8 |
| 800 | half | 4 | 11.1 | no | 48.6 | 51.2 |
| 800 | half | 5 | 11.1 | no | 48.6 | 25.3 |
| 800 | half | 6 | 11.1 | no | 48.6 | 15.0 |
| | | | | | | |
| 800 | half | 1 | 16.7 | no | 32.9 | 14.4 |
| 800 | half | 2 | 16.7 | no | 32.9 | 13.4 |
| 800 | half | 3 | 16.7 | no | 32.9 | 17.7 |
| 800 | half | 4 | 16.7 | no | 32.9 | 56.0 |
| 800 | half | 5 | 16.7 | no | 32.9 | 28.1 |
| 800 | half | 6 | 16.7 | no | 32.9 | 18.5 |
| | | | | | | |
| 800 | half | 1 | 25 | no | 22.1 | 16.9 |
| 800 | half | 2 | 25 | no | 22.1 | 16.9 |
| 800 | half | 3 | 25 | no | 22.1 | 18.2 |
| 800 | half | 4 | 25 | no | 22.1 | 60.9 |
| 800 | half | 5 | 25 | no | 22.1 | 31.3 |
| 800 | half | 6 | 25 | no | 22.1 | 20.1 |
| | | | | | | |
| 800 | half | 1 | 37.5 | no | 14.6 | 22.5 |
| 800 | half | 2 | 37.5 | no | 14.6 | 23.5 |
| 800 | half | 3 | 37.5 | no | 14.6 | 22.9 |
| 800 | half | 4 | 37.5 | no | 14.6 | 67.8 |
| 800 | half | 5 | 37.5 | no | 14.6 | 37.3 |
| 800 | half | 6 | 37.5 | no | 14.6 | 23.4 |

**Table 4.1** Table of spray cone angles at various conditions of speed and load for MW pump based system.

sprays, even at high needle lifts. During these tests, therefore, the centre of eccentricity might have been oriented towards sprays 4 and 5 (precession of the centre of eccentricity with time is expected to take place, making these experiments difficult to repeat).

The dependence of cone angle on chamber pressure is clearly illustrated in Figure 4.14. The cone angle can be seen to increase more or less linearly with pressure. However, since there are very few correlations in the literature of the effect of chamber pressure on cone angle and most are empirical, it was decided to construct a correlation to predict the cone angles of the sprays from the two systems.

A simple way of predicting cone angle might be to assume that the spray as it exits the hole develops a constant radial velocity, regardless of the chamber pressure; the droplets would then travel along a curved path, something like an artillery shell, as they decelerate. This assumes that atomisation alone is the cause of the radial velocity and that subsequently there are no collisions between the droplets, also that this process is not affected by changes in the chamber pressure. Another assumption is that the radial velocities are so low that the decelerating effect of the chamber pressure on this component of velocity will be insignificant. Axial velocity (penetration), on the other hand, is of sufficient magnitude to be influenced by the chamber pressure.

So as a basis for the prediction of cone angle, the measured penetration values were used and the radial velocity assumed to remain constant over the injection period. The following simple expression can thus be used to predict the cone angle for the various experiments:

$$\vartheta = 2 \cdot \arctan\left(\frac{V \cdot t}{S}\right) \tag{4.3}$$

Figure 4.15 shows a comparison between this prediction and the experimental results for the MW pump based system. The constant value of the radial velocity was calculated for the 11.1 bar case using the above formula rearranged. The graph shows that the prediction underestimates the cone angle as chamber pressure increases. In other words the radial velocity seems to increase with increasing chamber pressure. This is doubly so as the effect of deceleration on the radial spray velocity, although small, would become more significant at higher chamber pressures and if this

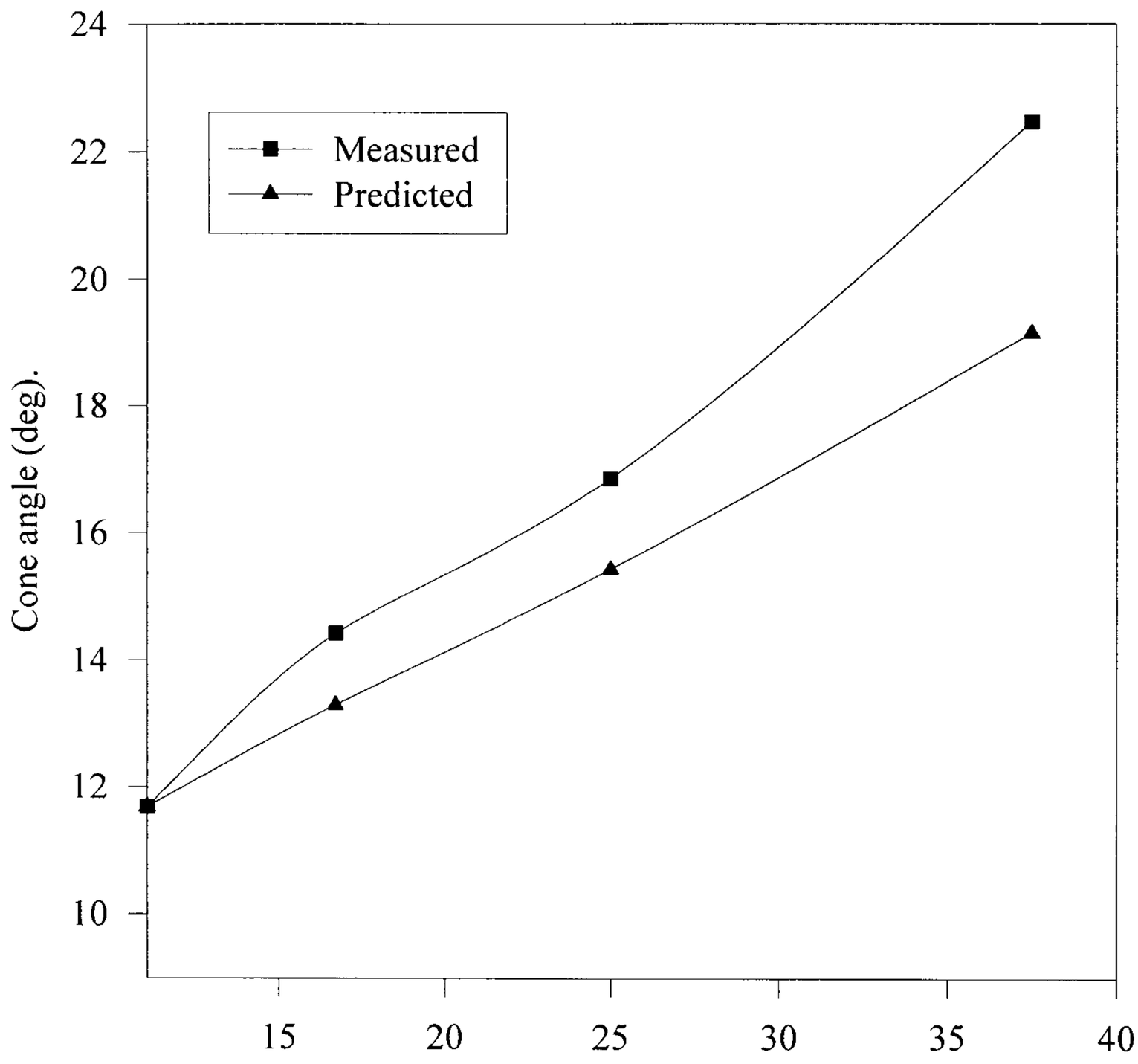


**Fig 4.15** Graph of measured and predicted spray cone angle vs. chamber pressure. MW pump based FIE at 800 rpm, half load.

deceleration was accounted for, an even smaller cone angle would be predicted by Equation 4.3 at these higher pressures.

A possible explanation for this is the influence of cavitation. If there is any swirling flow caused in the sac volume, this may reach the hole exit. Such swirling flow will cause a radial velocity even in the absence of atomisation. It might be assumed that cavitation in the hole dissipates much of this angular momentum. Whether this dissipation is complete in cavitating sprays has not been demonstrated and will depend upon the extent of cavitation. So to explain the discrepancy between

the prediction and the measurements, the degree of cavitation must fall as chamber pressure increases thereby lessening the dissipation of angular momentum and leading to sprays with more angular momentum and, hence, higher cone angle. As will be shown in the next section, the degree of cavitation does indeed fall with rising chamber pressure.

So far only typical atomising sprays have been considered. Much work has been done on atypical sprays which regularly occur in Diesels [*Soteriou et al,* 1995]. This paper categorises sprays into three types, 'A', 'B' and 'C'. Type 'A' sprays can be said to be typical and occur at higher needle lifts where there is cavitation in the hole. Type 'B' sprays, or so called hollow cone sprays, occur mostly at low needle lifts when there is no cavitation and because of the asymmetry of the inlet to the hole at low needle lifts, there is a swirling inlet flow into the hole. This angular momentum is conserved along the hole and causes the characteristic high cone angle and the resulting hollow spray configuration.

Sprays of type 'C' exhibit hydraulic flip, which is characterised by sprays with a great deal of cavitation. Consequently the fluid pressure in the hole falls to such a degree that gas from the chamber is able to force itself along the hole until it reaches the recirculation region where it causes the fuel to separate from the edge of the entrance to the hole. The fuel then flows through the hole as a solid stream surrounded by a jacket of gas, without touching the sides. It exits as a smooth column of liquid and the consequent spray is poorly atomised and has a low cone angle. Once hydraulic flip has occurred in the hole the cavitation ceases but the spray does not revert to a more typical type as the condition becomes stable. Hydraulic flip can also occur at low needle lifts where the fuel pressure is sufficiently low to allow the influx of chamber gas.

Partial hydraulic flip has also been described by *Soteriou et al* [1995]; here the conditions for hydraulic flip exist but the spray does contact at least part of the holes surface during injection. This can occur when the fuel has to enter the hole with an acute turn (as in most injectors), the fuel being 'flung' to one side of the hole by the high centrifugal forces. This type of spray is more likely to occur than the more conventional 'total' hydraulic flip in sprays from multi-hole injectors, like those investigated here.

As would be expected, type 'C' sprays have higher velocities and hence penetration than the other spray types. This is partly due to the nature of the spray, having a great deal of momentum and relatively small frontal area; the spray is, in this case, 'streamlined'. Further to this, there is an effect on sprays of type 'A' where the cavitation reduces the density of the 'fluid' exiting the hole and there is a consequent reduction in the speed of sound, see Figure 4.16. The graph shows that, as the gas to liquid ratio increases, the mixture begins to behave as a gas with sonic velocities within the range of injection velocity. As a consequence, with strong cavitation, a choked flow can occur in the holes which sets a ceiling on the liquid exit velocities. However, in a hydraulically flipped spray there is no cavitation once the hydraulic flip has occurred and the sonic velocity becomes very high; approaching 1000 M/s or so, although such velocities are unlikely to be achieved by a Diesel spray. Another explanation for the greater penetration of type 'C' sprays is that the smaller droplets in the more atomised sprays of type 'A' and 'B' will be decelerated more rapidly than the larger droplets and ligaments present in sprays of type 'C', due to the greater degree of air entrainment and consequent drag.

One might ask under what specific conditions does hydraulic flip occur and whether this is predictable. *Soteriou et al* [1995] have described a critical value of cavitation number (CN, defined in Equation 4.4) at which there is a sudden drop in the coefficient of discharge. This critical value of CN is not affected by changes in injection pressure or chamber pressure, but is merely a function of hole shape, hole size, the sharpness of the hole inlet and other geometric factors, such as the sac volume shape and hole orientation.

$$CN = \frac{P_{inj} - P_{cha}}{P_{cha} - P_{vap}} \qquad (4.4)$$

Table 4.1 shows the calculated values of CN versus spray cone angle (and penetration). These values are calculated making the assumption that the sac volume pressure is the same as the measurement of the pipeline pressure in the calibration. As

the pressure varies throughout the course of injection, the peak value was taken, which will, of course, only give the highest value of CN, but since the shape of the pressure trace can often be assumed to be triangular, this value can still be seen as characteristic of the injection as a whole. Hence even if the degree of cavitation varies throughout injection, the value of CN will still identify the conditions where transition to hydraulic flip is most likely to occur.

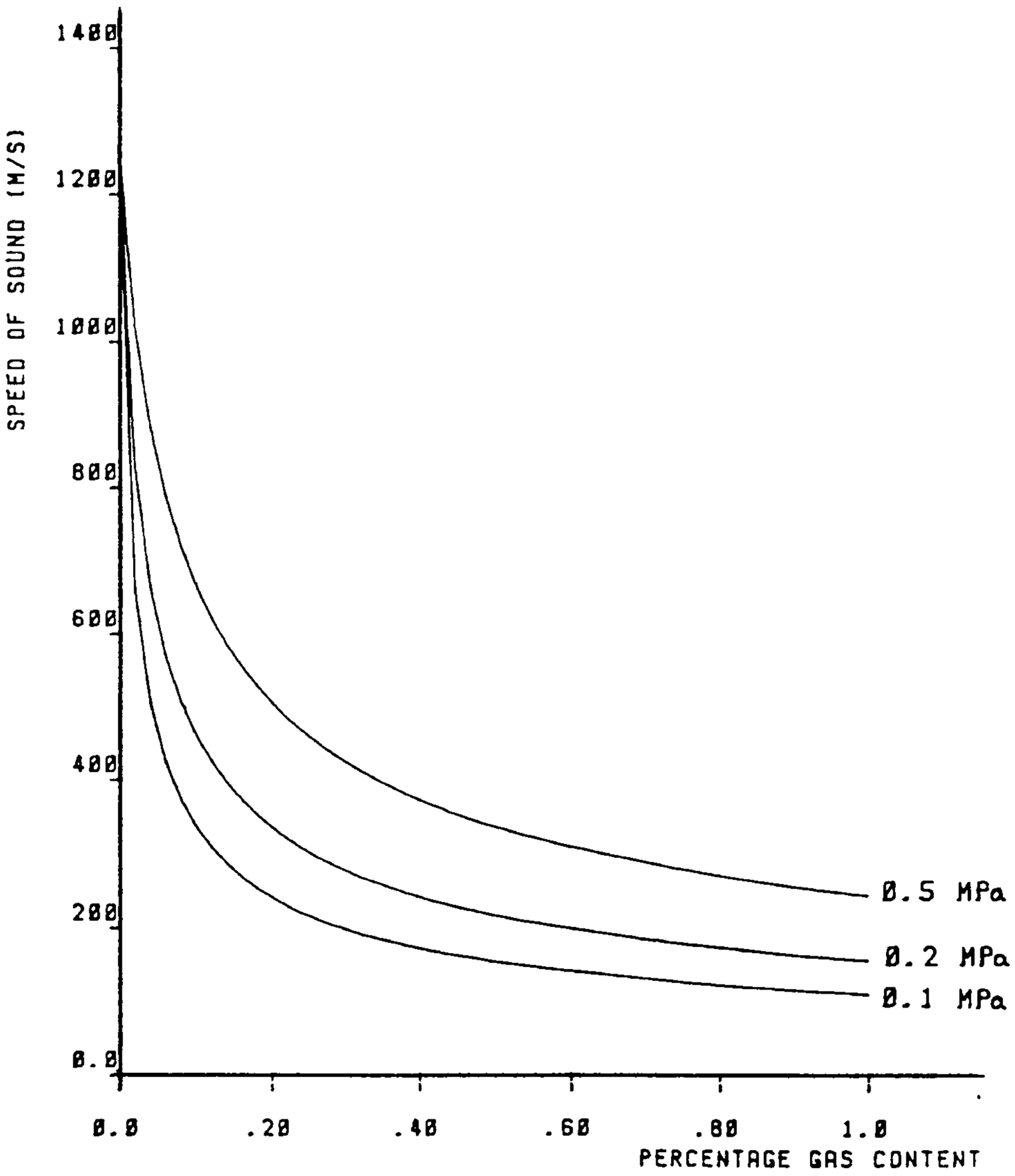


**Fig 4.16** Graph of the speed of sound vs. gas/liquid ratio for Diesel air mixture, at three different chamber pressures.

The value of CN can also be used to identify the transition between sprays of type A and B or large cone sprays. As explained earlier, sprays of type 'B' occur when there is little or no cavitation and particularly at low needle lifts. Therefore, there should be a cavitation number below which sprays with large cone angles occur. This value will vary from hole to hole but should remain constant for varying chamber pressure conditions. Another notable feature of the results from the MW pump is the absence of low cone angles characteristic of hydraulic flip; as will be seen later this does not appear to be the case for the EPVE pump.

### 4.1.2.2 Sprays of EPVE Pump Based System.

The test matrix used for the imaging of the EPVE pump based system was much more extensive. As a consequence a good deal more data was acquired on cone angle for this pump. which is shown in Figure 4.17 and Table 4.2.

Unlike the MW pump, both the near and far cone angle are given. The definition of near and far spray cone angle can be found in a number of references e.g. *Montgomery et al* [1996]. The definitions are to some degree arbitrary but it was felt that for completeness both should be tabulated; the graphs, however, show just the far angle.

The first section of Table 4.2 gives details of the cone angle at the four conditions of speed and load at which the PDA results were taken. Looking first at the far cone angle at 0.5 ms ASI, the same measurements as for the MW pump, there is only a small variation in cone angle; the angles increase with load at each speed probably due to the increase in chamber pressure rather than any effect of higher load, although there may be a slight dependence of spray cone angle on injection pressure [*Su et al,* 1995].

At 0.2 ms ASI the far angle shows a slight anomaly, as at the 1200 rpm half load condition there is a very low cone angle. This spray is probably showing hydraulic flip. If this is so what is interesting is that the transition between the two different spray regimes has occurred simply by changing the load and chamber pressure, thus indicating that these transitions may occur regularly in an engine. Of particular interest would be a study of these transitions under transient conditions.

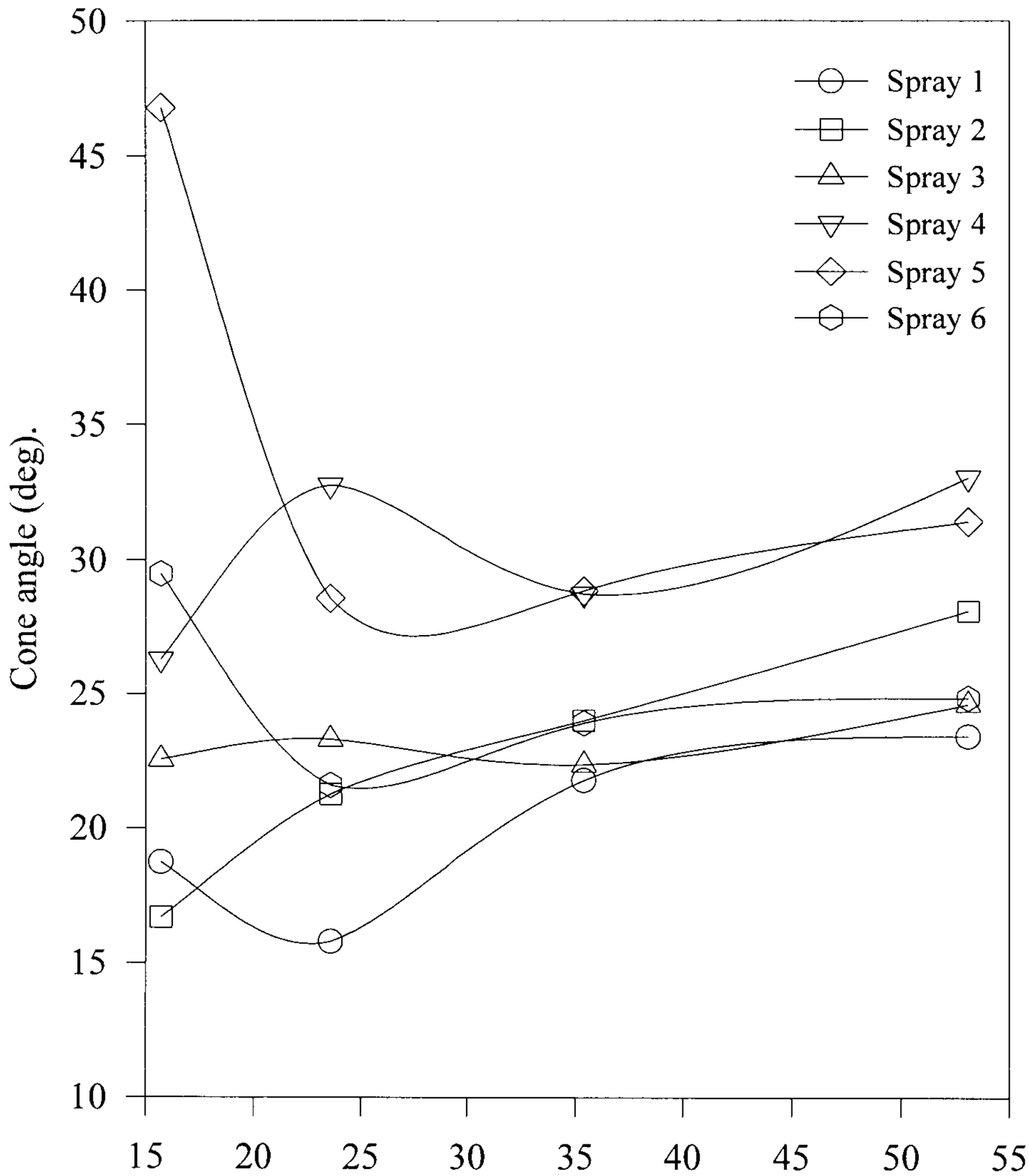


**Fig 4.17** Graph of spray cone angle vs. chamber pressure for each of the six nozzle holes. EPVE pump based FIE at 800 rpm, half load.

| Pump Speed (rpm) | Load | Spray | Chamber Pressure (bar) | Cap | CN | Time ASI | | | |
|---|---|---|---|---|---|---|---|---|---|
| | | | | | | Near cone (deg) | | Far cone (deg) | |
| | | | | | | 0.2 ms | 0.5 ms | 0.2 ms | 0.5 ms |
| | | | | | | | | | |
| 800 | half | 1 | 35.4 | yes | 11.34 | 63.4 | 15.8 | 28.1 | 24.1 |
| 800 | full | 1 | 39.2 | yes | 16.46 | 66.8 | 17.6 | 29.5 | 27.2 |
| 1200 | half | 1 | 30.8 | yes | 16.11 | 26.6 | 22.7 | 11.3 | 22.6 |
| 1200 | full | 1 | 40.9 | yes | 20.53 | 24.5 | 20.1 | 31.6 | 25.4 |
| 1200 | full | 1 | 40.9 | no | 20.53 | 38.3 | 19.5 | 17.0 | 25.2 |
| | | | | | | | | | |
| | | | | | | | | | |
| 800 | half | 1 | 15.7 | no | 25.89 | 66.3 | 13.8 | 23.1 | 18.8 |
| 800 | half | 2 | 15.7 | no | 25.89 | 18.5 | 14.0 | 17.9 | 16.7 |
| 800 | half | 3 | 15.7 | no | 25.89 | 25.3 | 22.1 | 19.8 | 22.5 |
| 800 | half | 4 | 15.7 | no | 25.89 | 26.0 | 27.5 | 29.0 | 26.3 |
| 800 | half | 5 | 15.7 | no | 25.89 | 81.5 | 22.0 | 26.8 | 46.8 |
| 800 | half | 6 | 15.7 | no | 25.89 | 36.9 | 21.4 | 28.3 | 29.5 |
| | | | | | | | | | |
| 800 | half | 1 | 23.6 | no | 17.25 | 57.0 | 18.0 | 17.5 | 15.8 |
| 800 | half | 2 | 23.6 | no | 17.25 | 18.4 | 20.8 | 16.4 | 21.3 |
| 800 | half | 3 | 23.6 | no | 17.25 | 20.9 | 15.2 | 22.8 | 23.3 |
| 800 | half | 4 | 23.6 | no | 17.25 | 27.7 | 23.9 | 34.0 | 32.8 |
| 800 | half | 5 | 23.6 | no | 17.25 | 66.9 | 21.1 | | 28.6 |
| 800 | half | 6 | 23.6 | no | 17.25 | 48.3 | 18.3 | 32.5 | 21.6 |
| | | | | | | | | | |
| 800 | half | 1 | 35.4 | no | 11.34 | 62.7 | 17.2 | 30.3 | 21.8 |
| 800 | half | 2 | 35.4 | no | 11.34 | 30.1 | 19.1 | 34.9 | 27.2 |
| 800 | half | 3 | 35.4 | no | 11.34 | 24.5 | 24.6 | 26.2 | 22.4 |
| 800 | half | 4 | 35.4 | no | 11.34 | 32.4 | 20.3 | 36.8 | 28.7 |
| 800 | half | 5 | 35.4 | no | 11.34 | 85.0 | 24.2 | 40.4 | 28.9 |
| 800 | half | 6 | 35.4 | no | 11.34 | 43.5 | 19.1 | 40.1 | 23.9 |
| | | | | | | | | | |
| 800 | half | 1 | 53.1 | no | 7.30 | 26.6 | 22.0 | 29.8 | 23.4 |
| 800 | half | 2 | 53.1 | no | 7.30 | | 30.6 | 21.0 | 28.1 |
| 800 | half | 3 | 53.1 | no | 7.30 | 19.0 | 13.9 | 23.0 | 24.6 |
| 800 | half | 4 | 53.1 | no | 7.30 | 23.0 | 20.1 | 21.5 | 33.0 |
| 800 | half | 5 | 53.1 | no | 7.30 | 34.1 | 32.1 | 37.0 | 31.4 |
| 800 | half | 6 | 53.1 | no | 7.30 | 34.0 | 28.7 | 31.2 | 24.8 |
| | | | | | | | | | |
| 800 | half | 1 | 15.7 | yes | 34.93 | 67.9 | 13.2 | 17.8 | 25.6 |
| 800 | half | 1 | 23.6 | yes | 23.39 | 68.4 | 14.6 | 23.8 | 19.4 |
| 800 | half | 1 | 35.4 | yes | 15.48 | 63.4 | 15.8 | 28.1 | 24.1 |
| 800 | half | 1 | 53.1 | yes | 10.09 | 57.0 | 24.0 | 18.3 | 26.2 |

**Table 4.2** Table of spray cone angles at various conditions of speed and load for EPVE pump based system.

A worrying aspect here is the paucity of research reported in the literature on the atomisation of 'hydraulically flipped' sprays, particularly as these are likely to be rather badly atomised and more likely to hit the piston bowl before vaporisation is complete. One might argue that such sprays are more likely to lead to smoke than the 'typical' atomised spray. Despite this there seems to be no references in the literature giving the characteristics of such a spray.

In the last section a relationship between cone angle and chamber pressure was shown to exist and hence a prediction of the spray cone angle was postulated that only takes account of drag. However, increasing the chamber pressure will also result in a lower CN, this may result in higher spray cone angles due to a partial transition to type 'B' sprays at values of CN slightly above the critical value. Therefore the effect of increasing chamber pressure may not simply be to increase aerodynamic drag on the droplets, but also to change the nature of the nozzle flow. This might explain why the spray cone angle prediction (Equation 4.3) tends to underestimate the cone angle at higher pressures as the consequent lower CN means that the spray would tend to have a higher cone angle than this simple formula predicts. An empirical adjustment of Equation 4.3 can be made using the value of CN, in the modified form of the equation.

$$\vartheta = \frac{K \cdot 2 \cdot \arctan\left(\frac{V \cdot t}{S}\right)}{CN^{n}} \qquad (4.5)$$

If Equation 4.4 is substituted into Equation 4.5 and the small values are cancelled, the chamber pressure (raised to a power) appears in the numerator of the equation and the hence predicted cone angle would rise with increasing chamber pressure . This fits with the various graphs of cone angle already presented. Figure 4.18 shows a graph of measured cone angle for the EPVE pump.; also shown are predictions using both Equations 4.3 and 4.5.

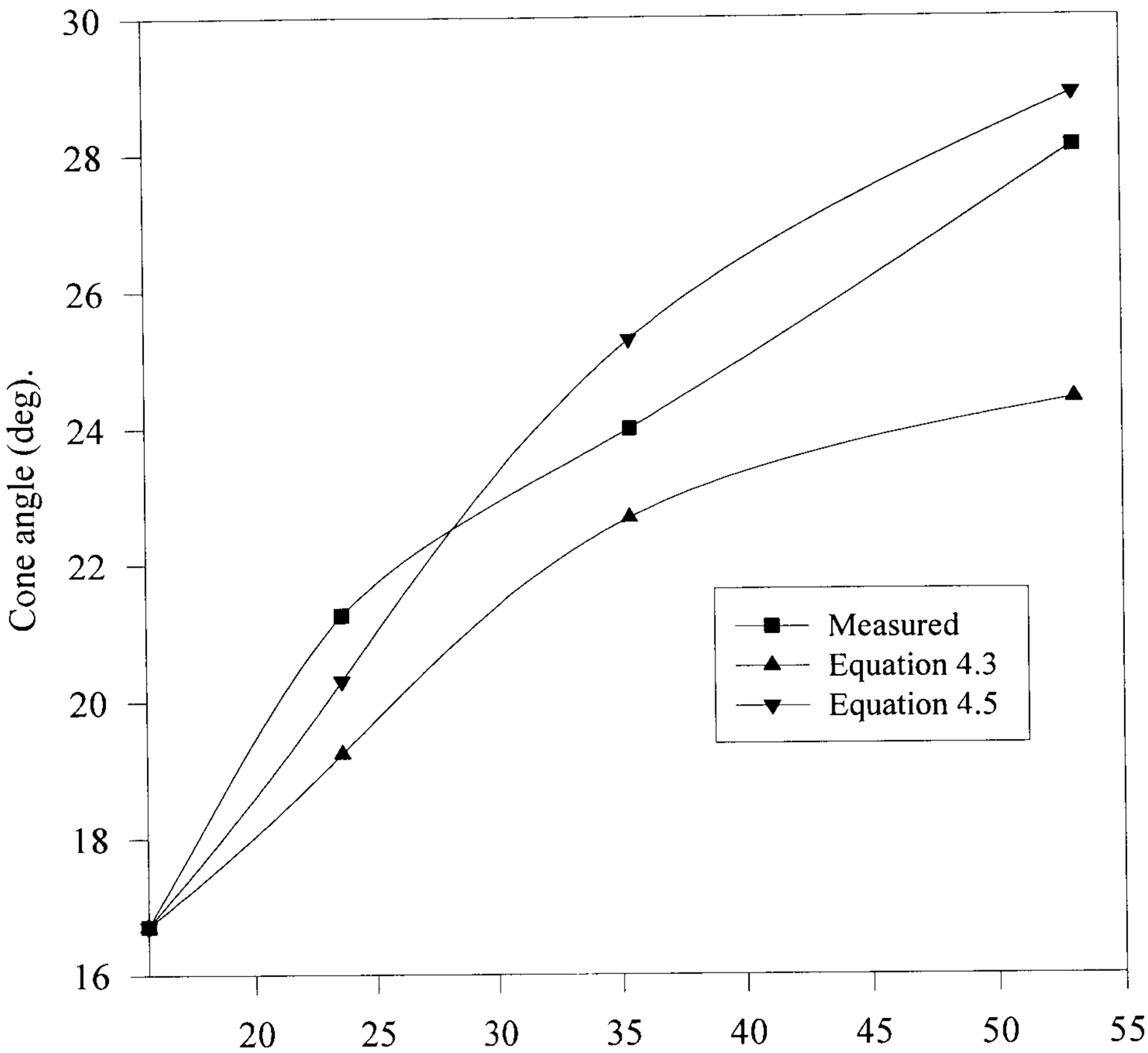


**Fig 4.18** Graph of measured and predicted spray cone angle vs. chamber pressure using two different correlations. EPVE pump based FIE at 800 rpm, half load.

The value of the exponent, 'n', in Equation 4.5 was evaluated using spray cone angles measured from the MW pump system, by producing a least squares fit of the data. This value should be universal as it relates to the effect of changes in CN and the same value of 'n' was used to produce Figure 4.18, even though this was a different FIE. The value of 'K', however, will change from pump to pump, or even from hole to hole as 'K' is related to the initial radial velocity which is not predicted; measurement of the spray cone angle at one condition of speed and load is therefore needed for each hole in each FIE system.

As can be seen from Figure 4.18, the modified correlation gives an improved fit to the measured data, as compared with the original correlation, and because the value of the exponent n was calculated from the results of a different pump this would tend to confirm the validity of the correlation. Clearly however, a great deal more tests would be needed to confirm this.

## 4.2 PDA RESULTS.

The PDA technique was described in the previous chapter along with the experimental set-ups used for both pumps, and this section will present and discuss the acquired data. To reduce the number of graphs to manageable levels, only a few scatter plots of the data will be presented. However, all of the raw data has been averaged, graphs of which represent the main bulk of the results. Figures 4.19 to 4.30 are the averaged plots for the MW pump, while Figures 4.31 to 4.42 are the averaged plots for the EPVE pump. Also given in the figures are the velocity and diameter pdfs along the centre line.

An important part of this section is the comparison between the results obtained by the two different PDA systems. The differences, particularly in the value of SMD, are a little disconcerting and need some explanation before the PDA results can be looked at with confidence. This subject was touched upon in Chapter 3, but will be discussed in greater detail later in this chapter.

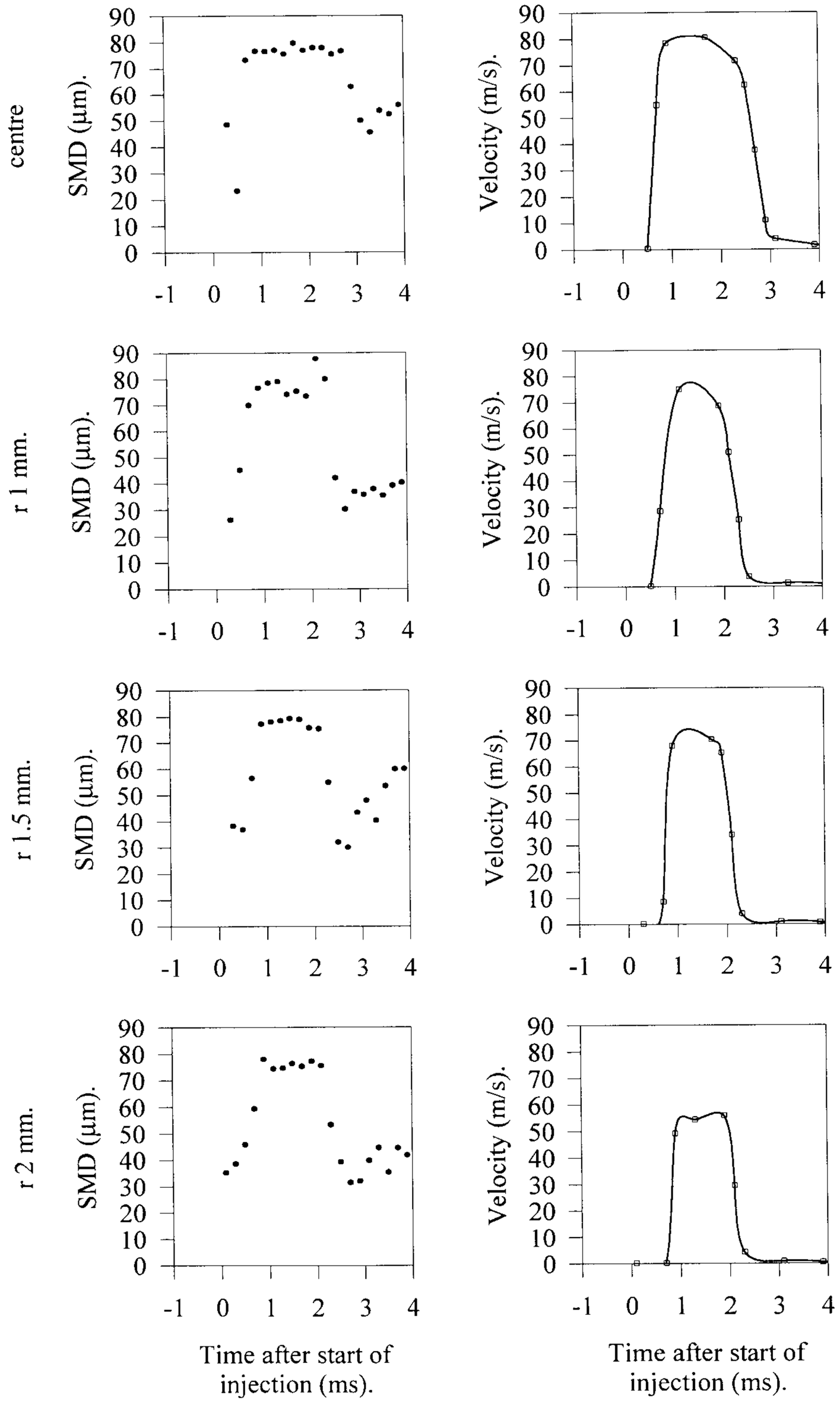


**Fig 4.19** Graphs of droplet Sauter mean diameter and average axial droplet velocity at different radial positions. MW pump based FIE at 1300 rpm, full load, measured 10 mm from nozzle.

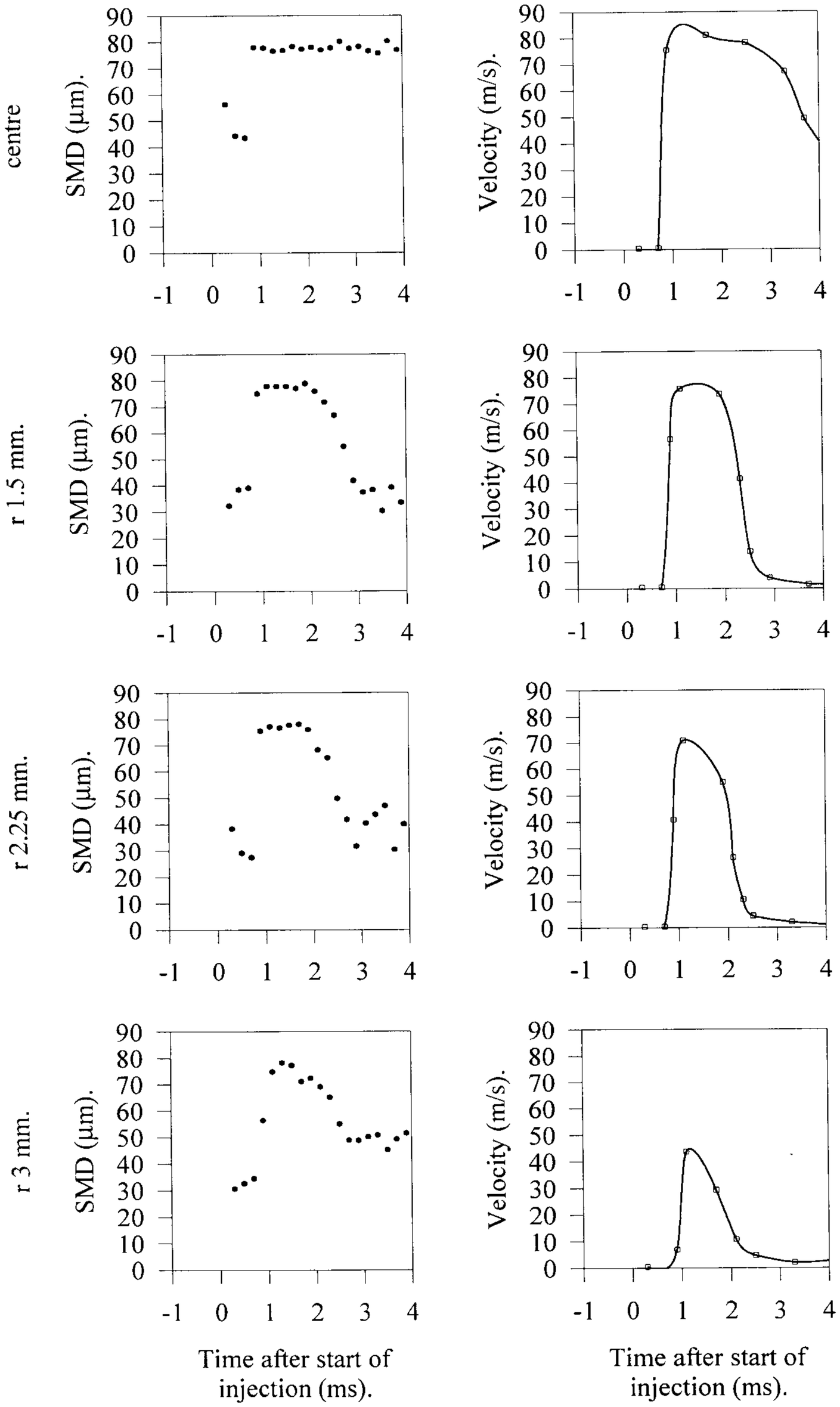


**Fig 4.20** Graphs of droplet Sauter mean diameter and average axial droplet velocity at different radial positions. MW pump based FIE at 1300 rpm, full load, measured 17.5 mm from nozzle.

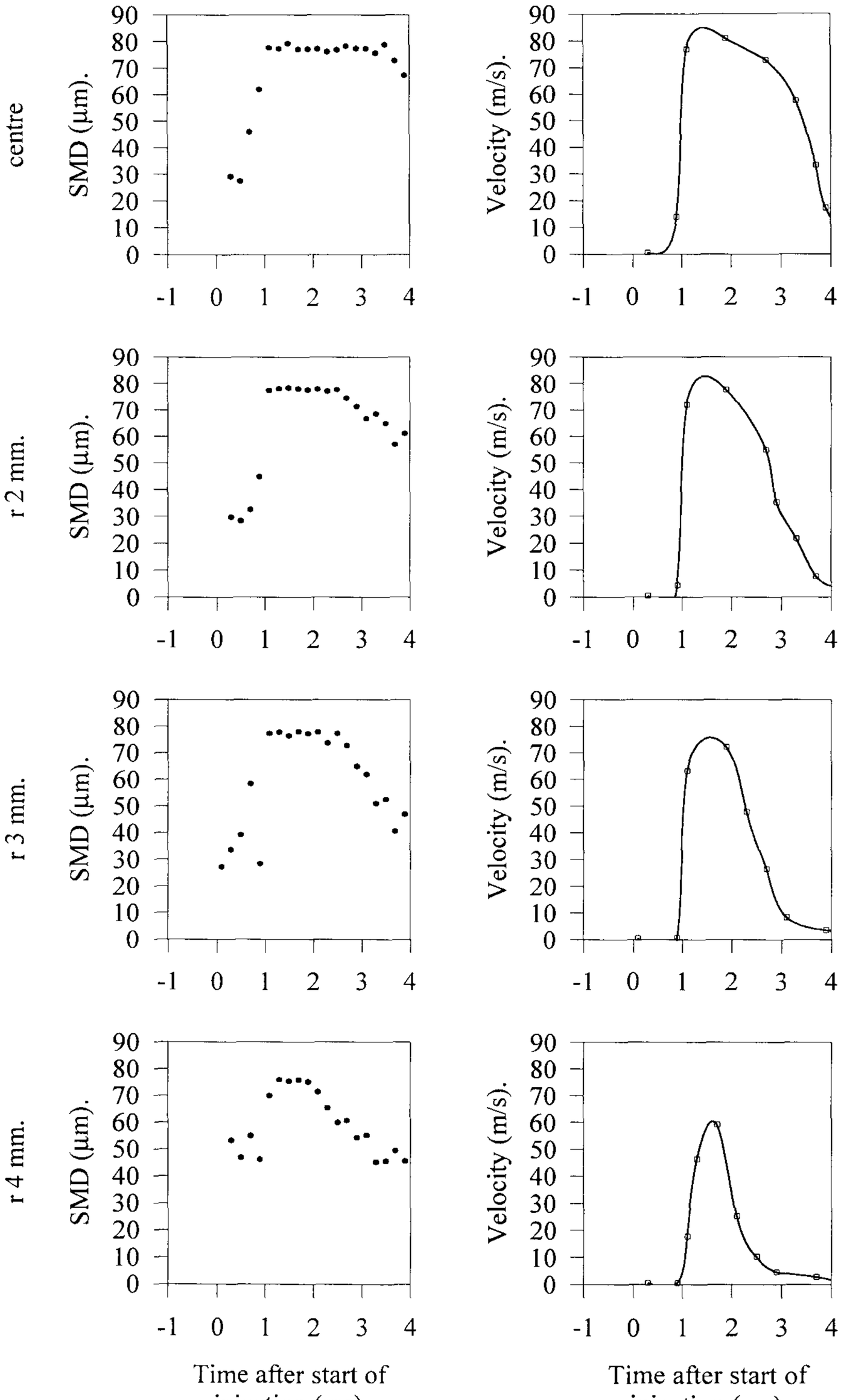


**Fig 4.21** Graphs of droplet Sauter mean diameter and average axial droplet velocity at different radial positions. MW pump based FIE at 1300 rpm, full load, measured 25 mm from nozzle.

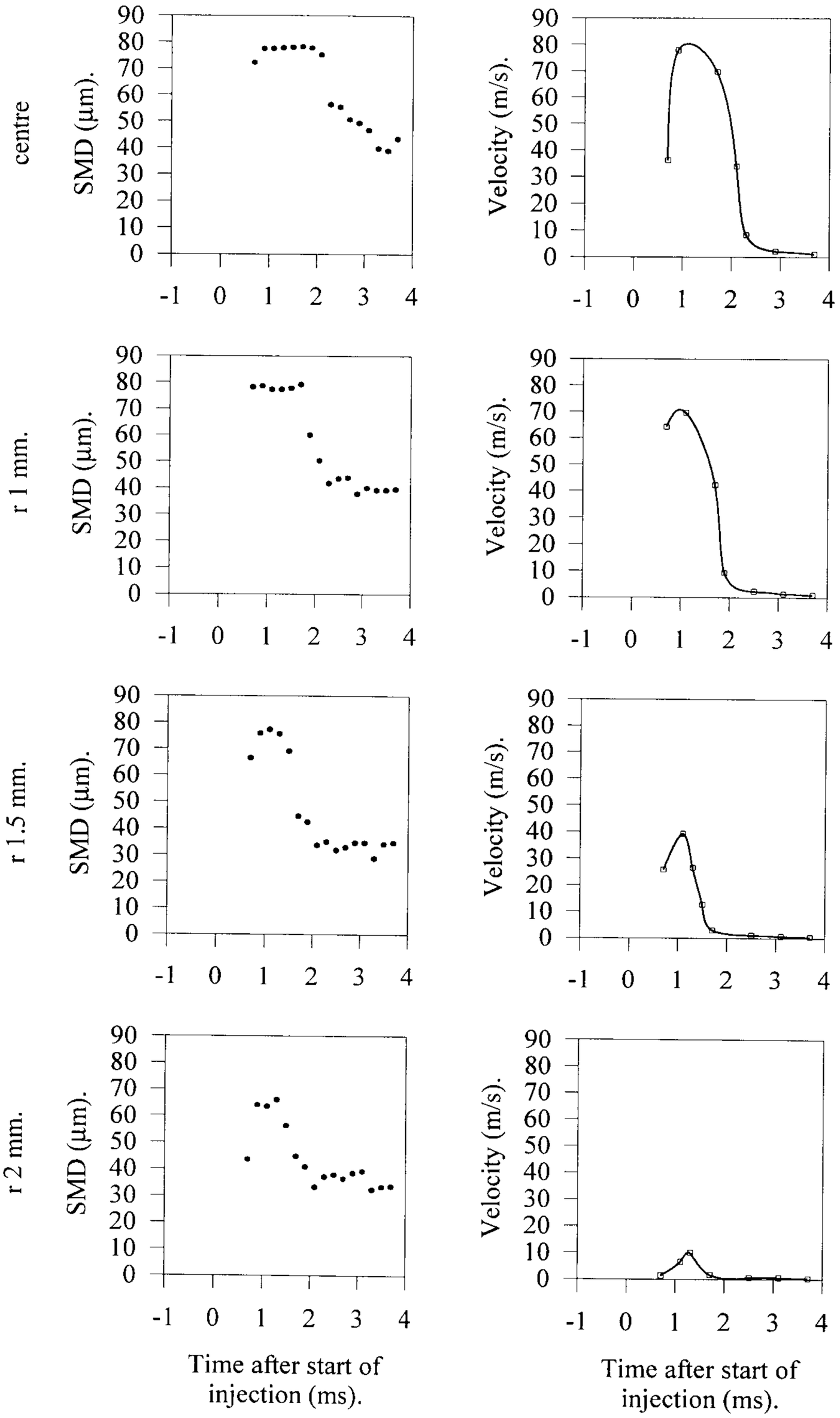


**Fig 4.22** Graphs of droplet Sauter mean diameter and average axial droplet velocity at different radial positions. MW pump based FIE at 1300 rpm, half load, measured 10 mm from nozzle.

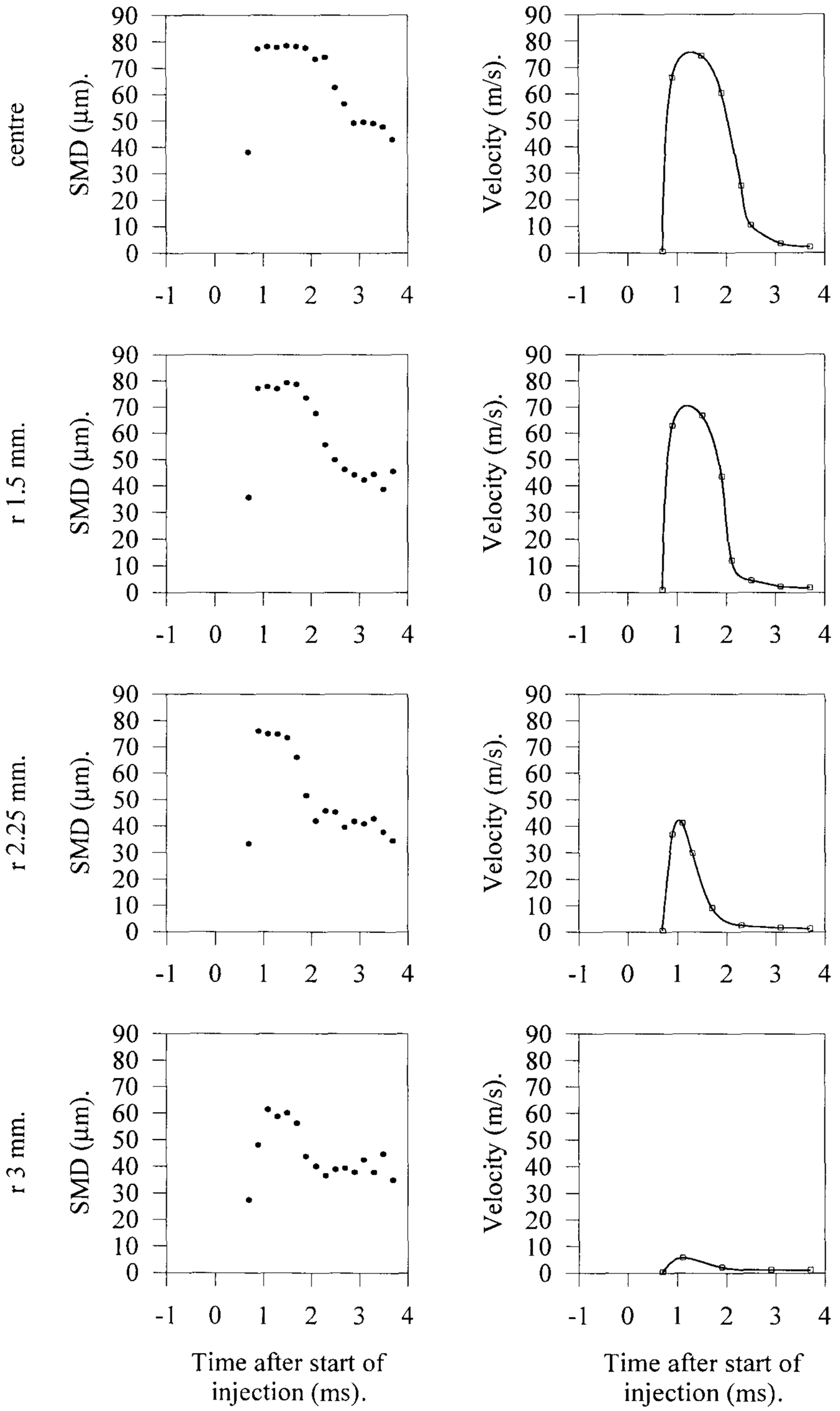


**Fig 4.23** Graphs of droplet Sauter mean diameter and average axial droplet velocity at different radial positions. MW pump based FIE at 1300 rpm, half load, measured 17.5 mm from nozzle.

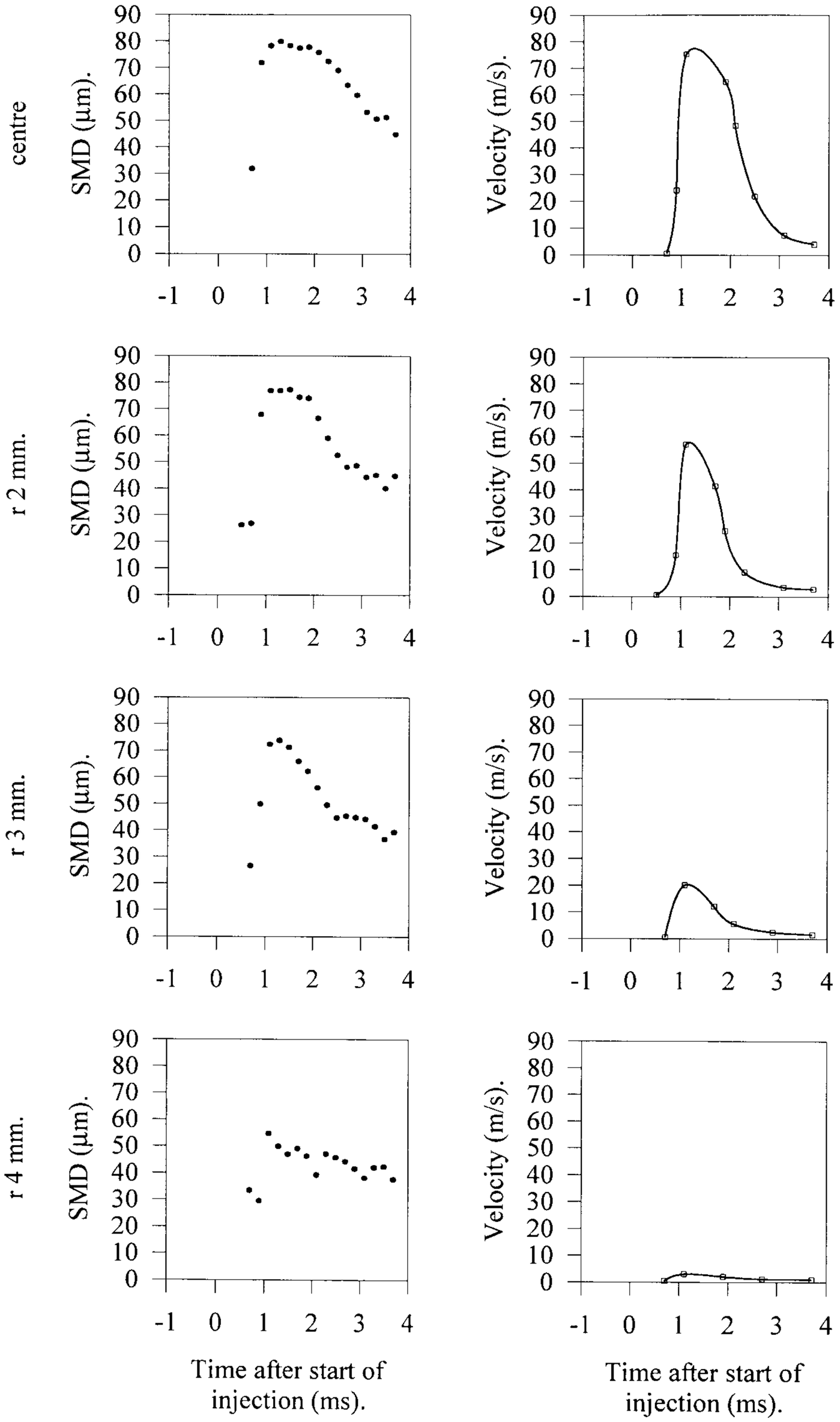


**Fig 4.24** Graphs of droplet Sauter mean diameter and average axial droplet velocity at different radial positions. MW pump based FIE at 1300 rpm, half load, measured 25 mm from nozzle.

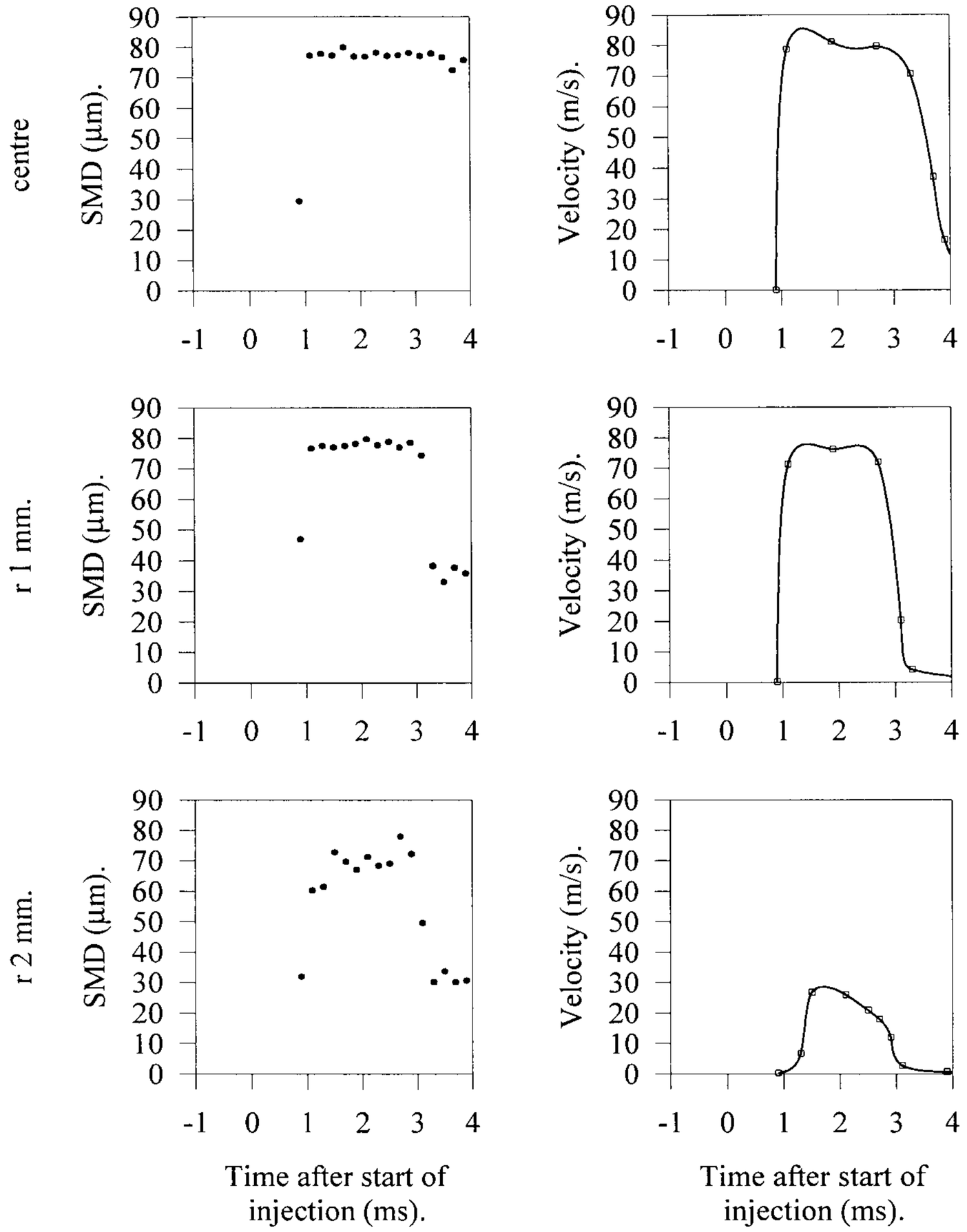


**Fig 4.25** Graphs of droplet Sauter mean diameter and average axial droplet velocity at different radial positions. MW pump based FIE at 800 rpm, full load, measured 10 mm from nozzle.

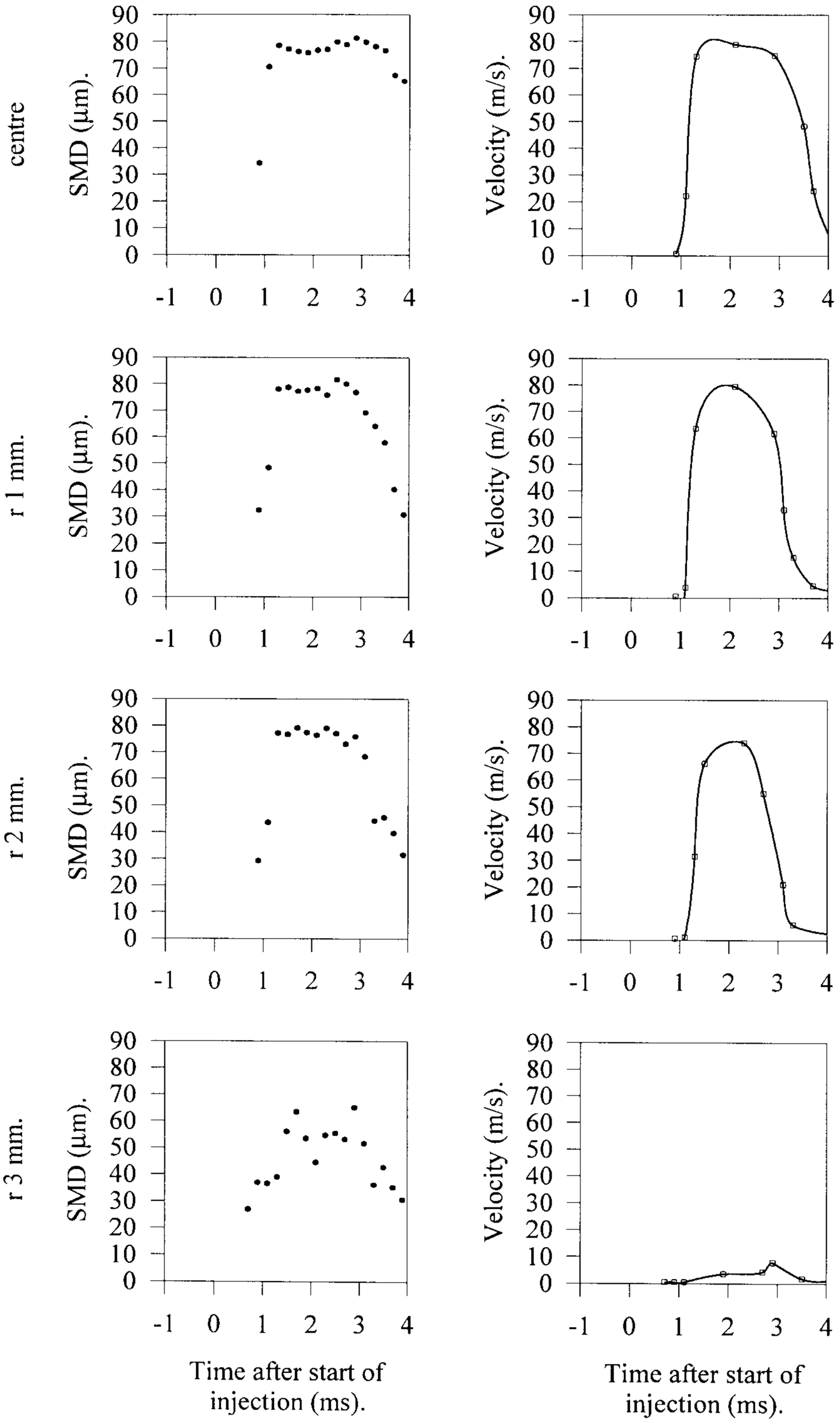


**Fig 4.26** Graphs of droplet Sauter mean diameter and average axial droplet velocity at different radial positions. MW pump based FIE at 800 rpm, full load, measured 17.5 mm from nozzle.

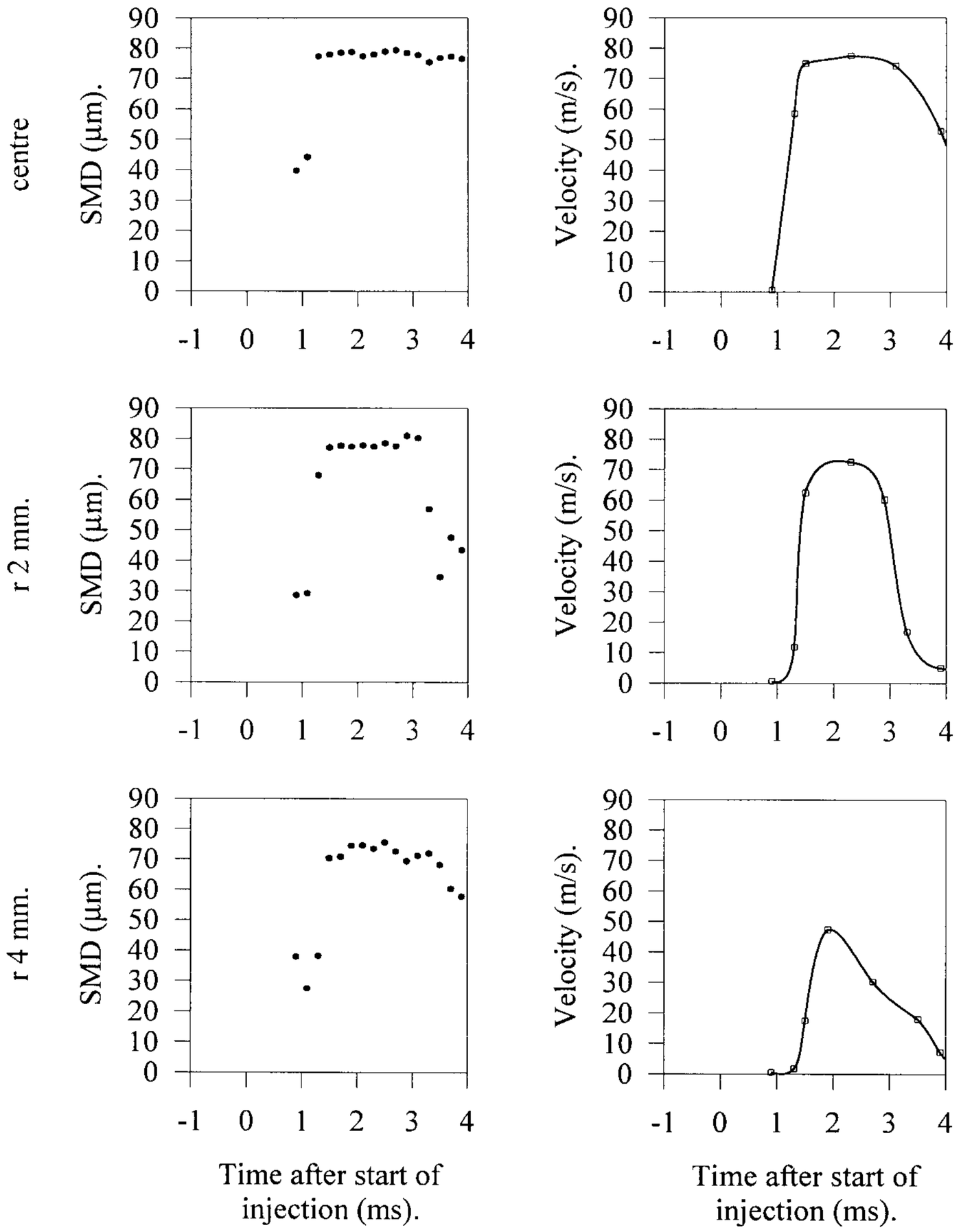


**Fig 4.27** Graphs of droplet Sauter mean diameter and average axial droplet velocity at different radial positions. MW pump based FIE at 800 rpm, full load, measured 25 mm from nozzle.

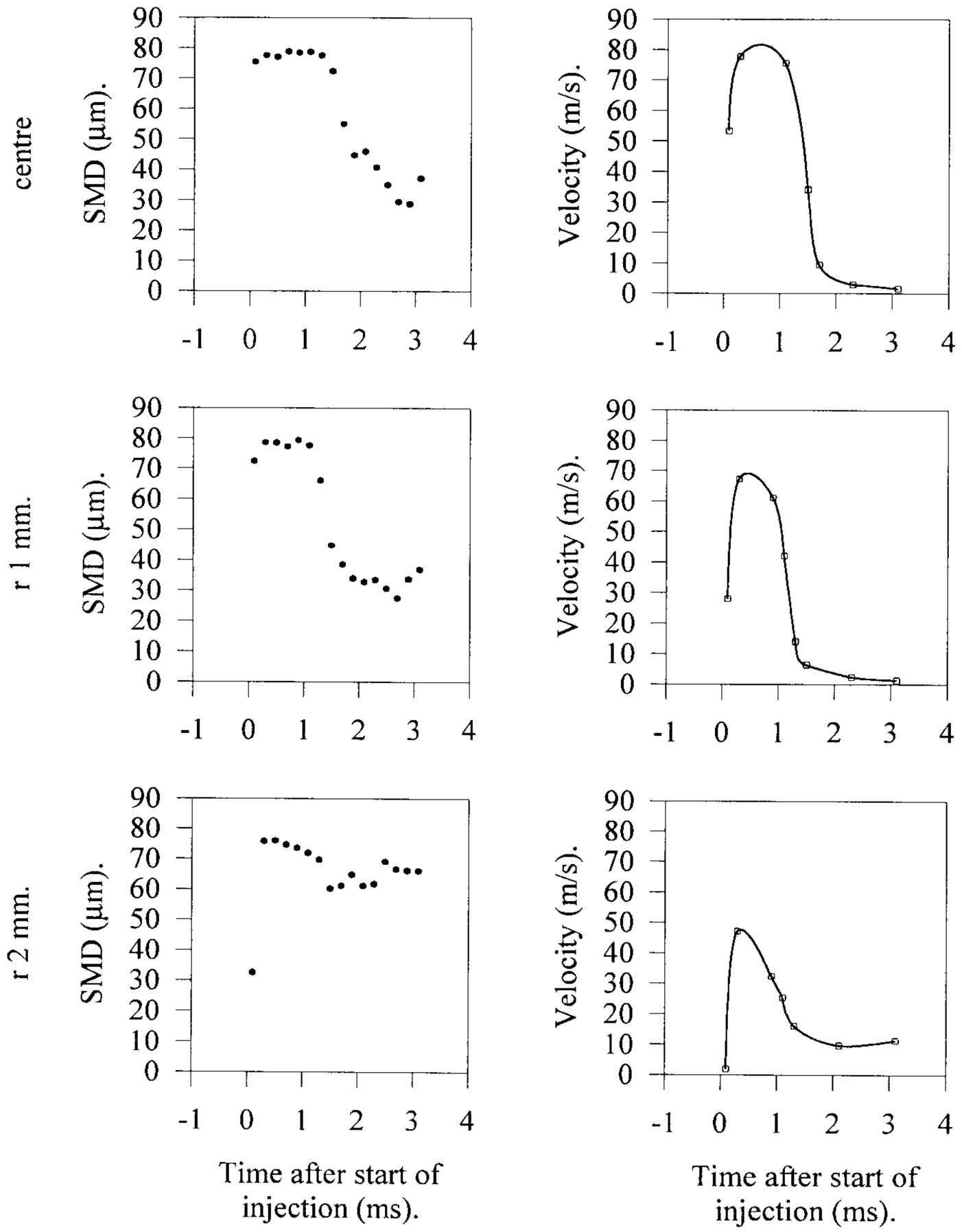


**Fig 4.28** Graphs of droplet Sauter mean diameter and average axial droplet velocity at different radial positions. MW pump based FIE at 800 rpm, half load, measured 10 mm from nozzle.

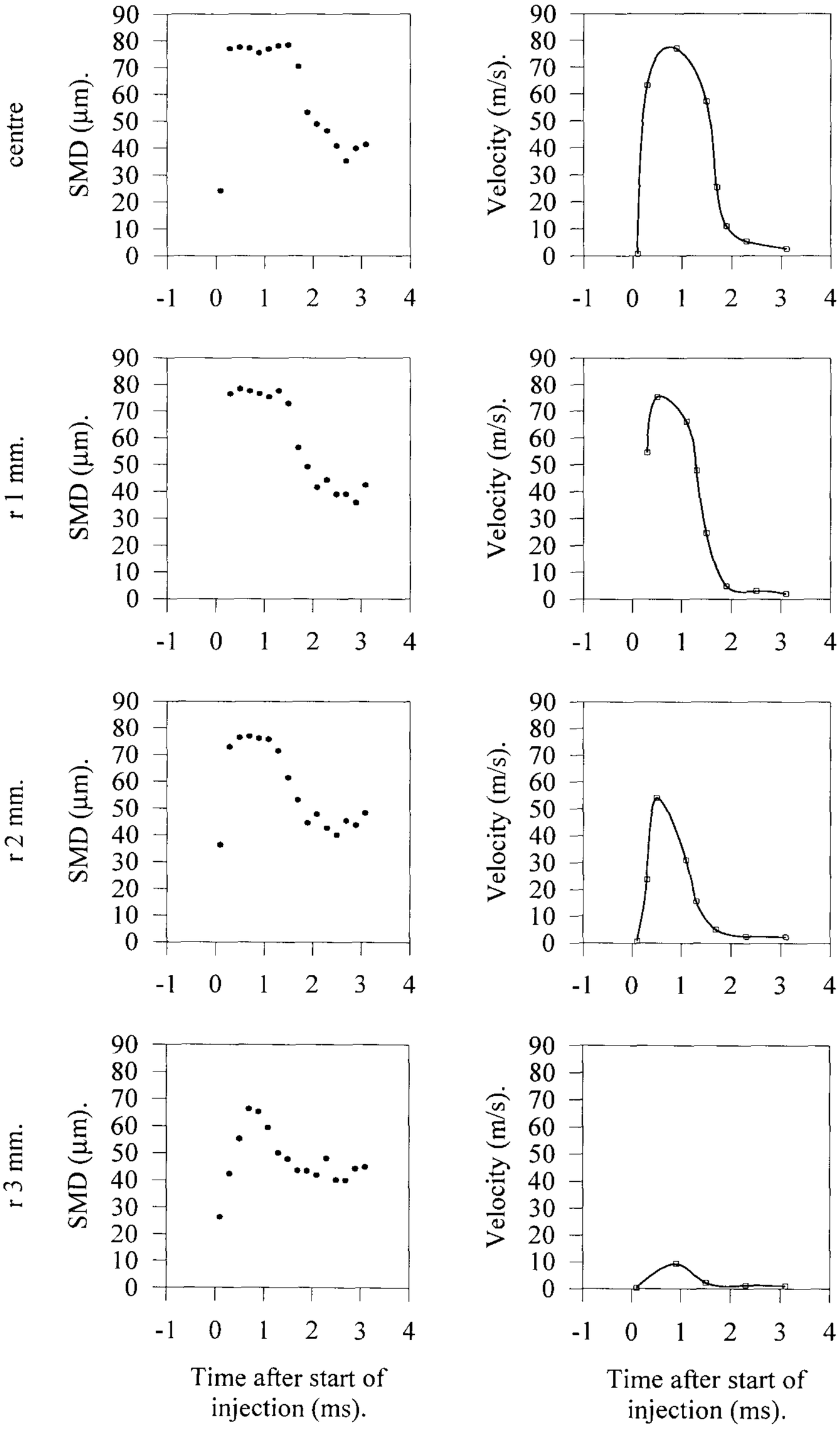


**Fig 4.29** Graphs of droplet Sauter mean diameter and average axial droplet velocity at different radial positions. MW pump based FIE at 800 rpm, half load, measured 17.5 mm from nozzle.

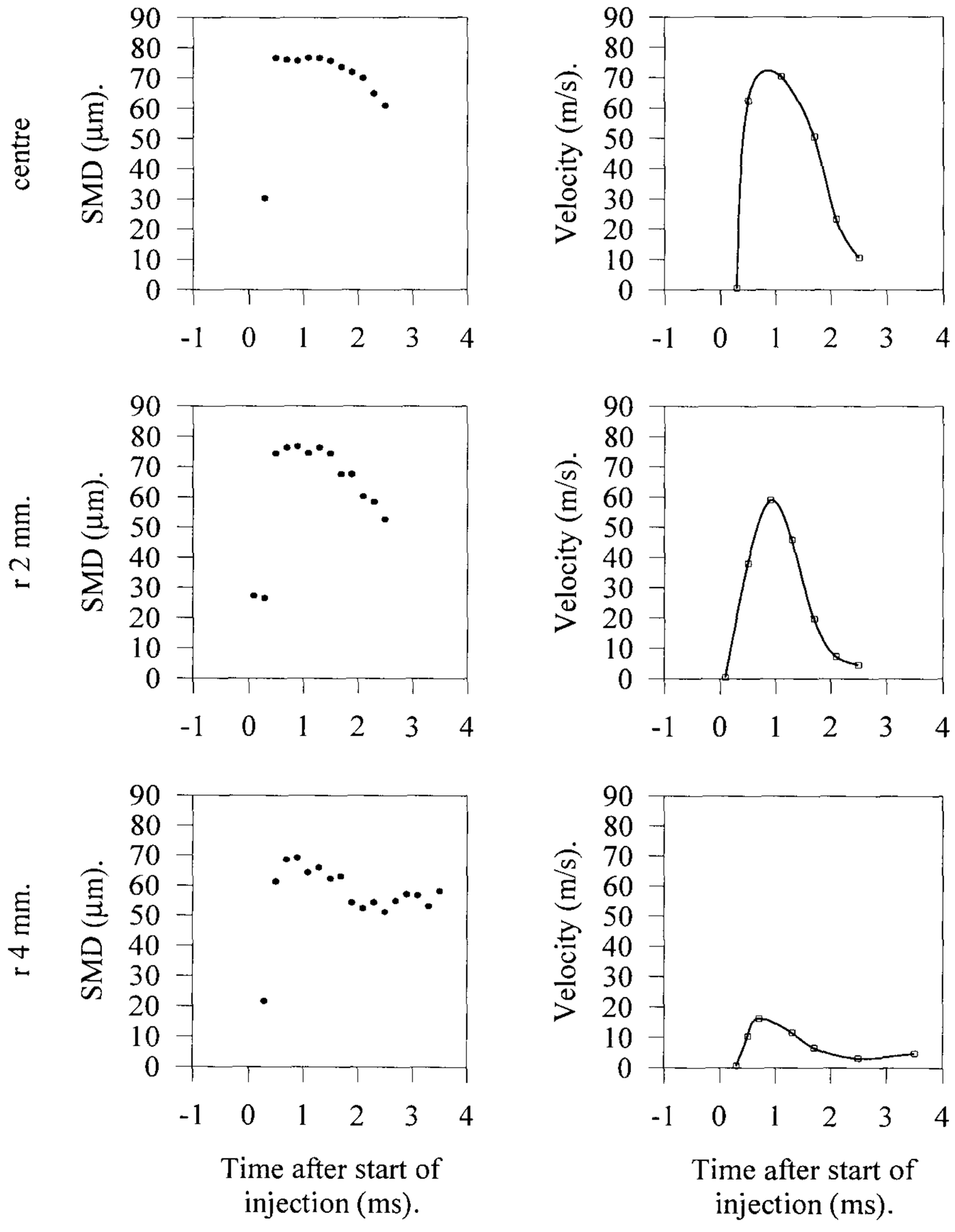


**Fig 4.30** Graphs of droplet Sauter mean diameter and average axial droplet velocity at different radial positions. MW pump based FIE at 800 rpm, half load, measured 25 mm from nozzle.

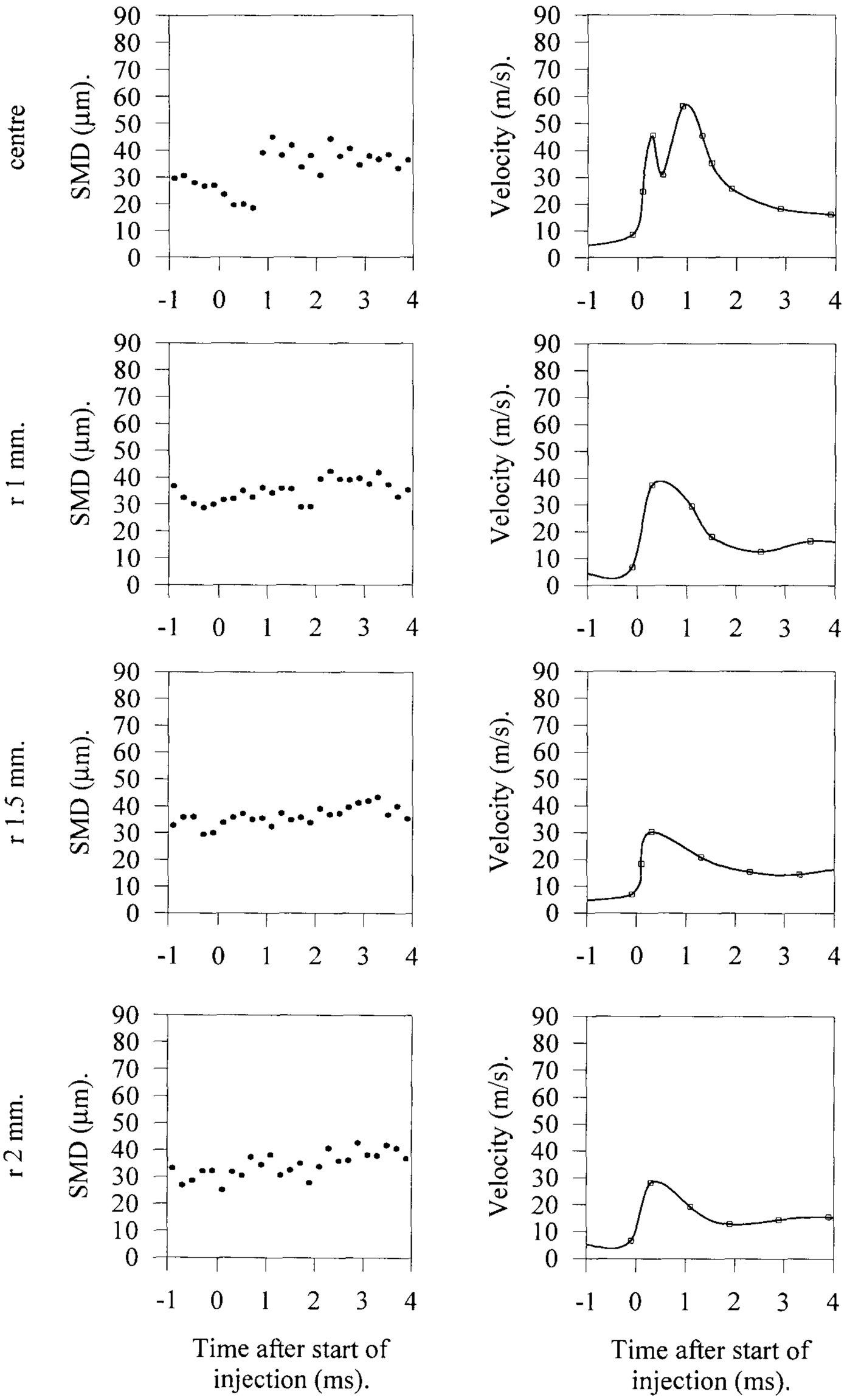


**Fig 4.31** Graphs of droplet Sauter mean diameter and average axial droplet velocity at different radial positions. EPVE pump based FIE at 1200 rpm, full load, measured 10 mm from nozzle.

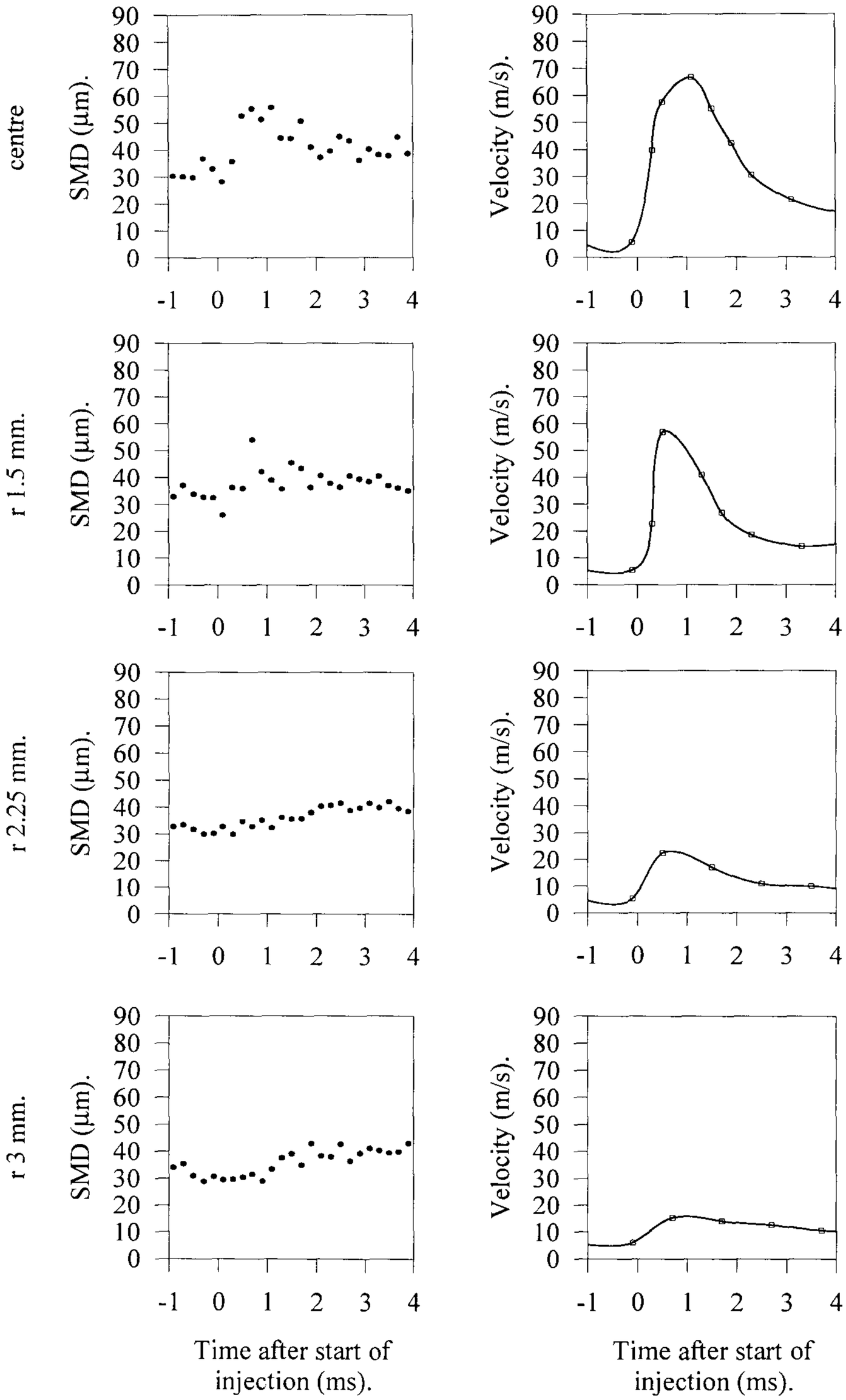


**Fig 4.32** Graphs of droplet Sauter mean diameter and average axial droplet velocity at different radial positions. EPVE pump based FIE at 1200 rpm, full load, measured 17.5 mm from nozzle.

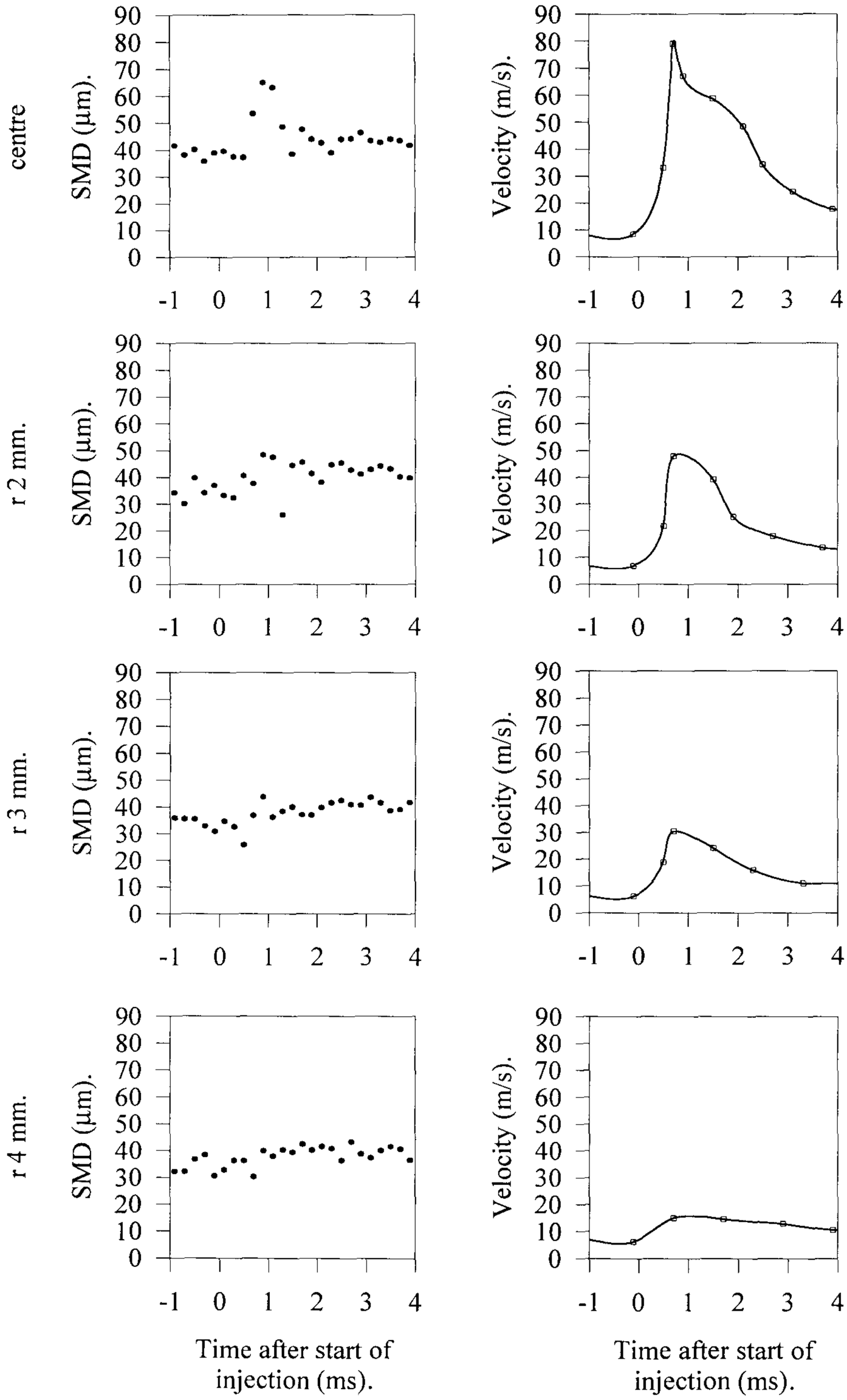


**Fig 4.33** Graphs of droplet Sauter mean diameter and average axial droplet velocity at different radial positions. EPVE pump based FIE at 1200 rpm, full load, measured 25 mm from nozzle.

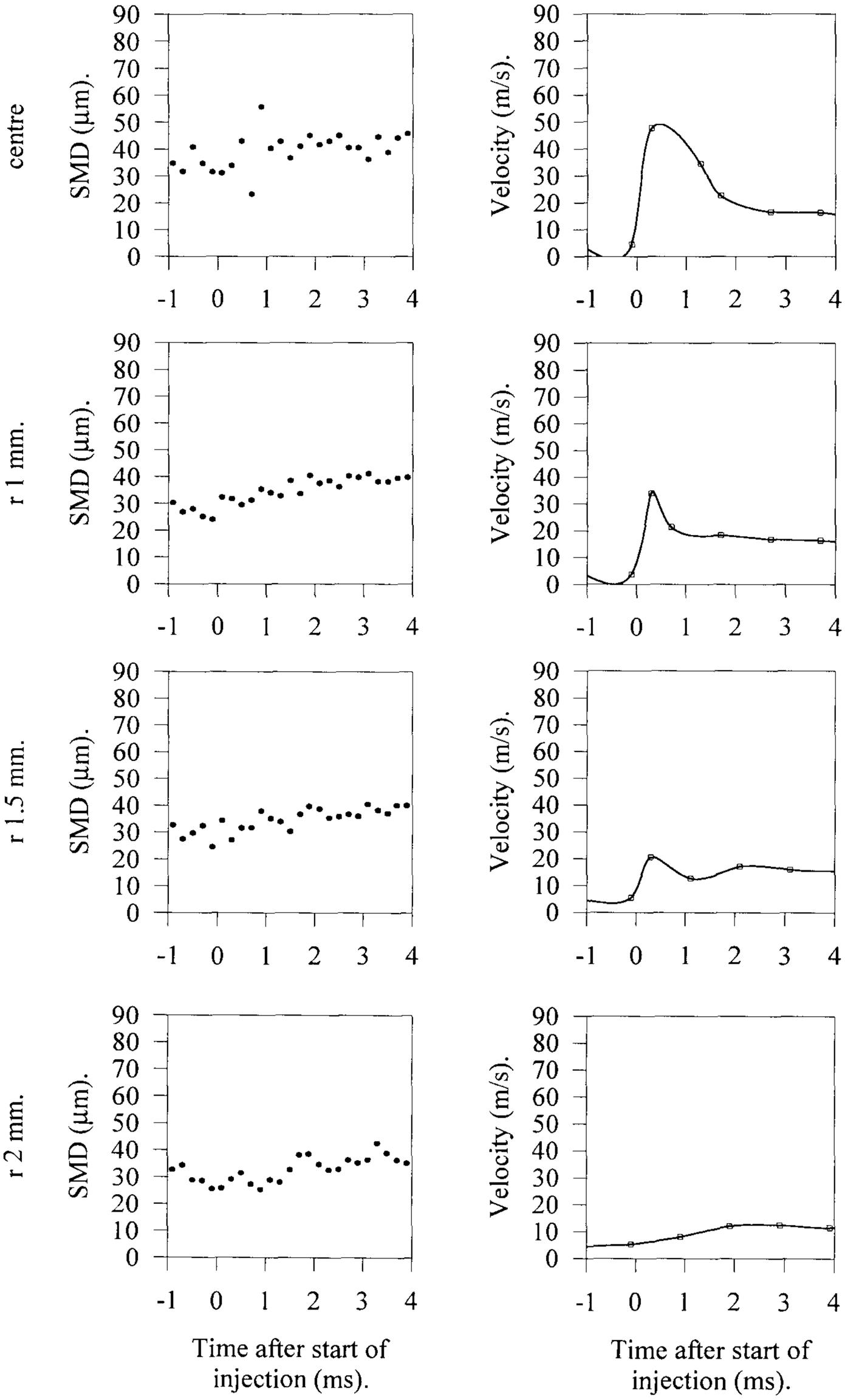


**Fig 4.34** Graphs of droplet Sauter mean diameter and average axial droplet velocity at different radial positions. EPVE pump based FIE at 1200 rpm, half load, measured 10 mm from nozzle.

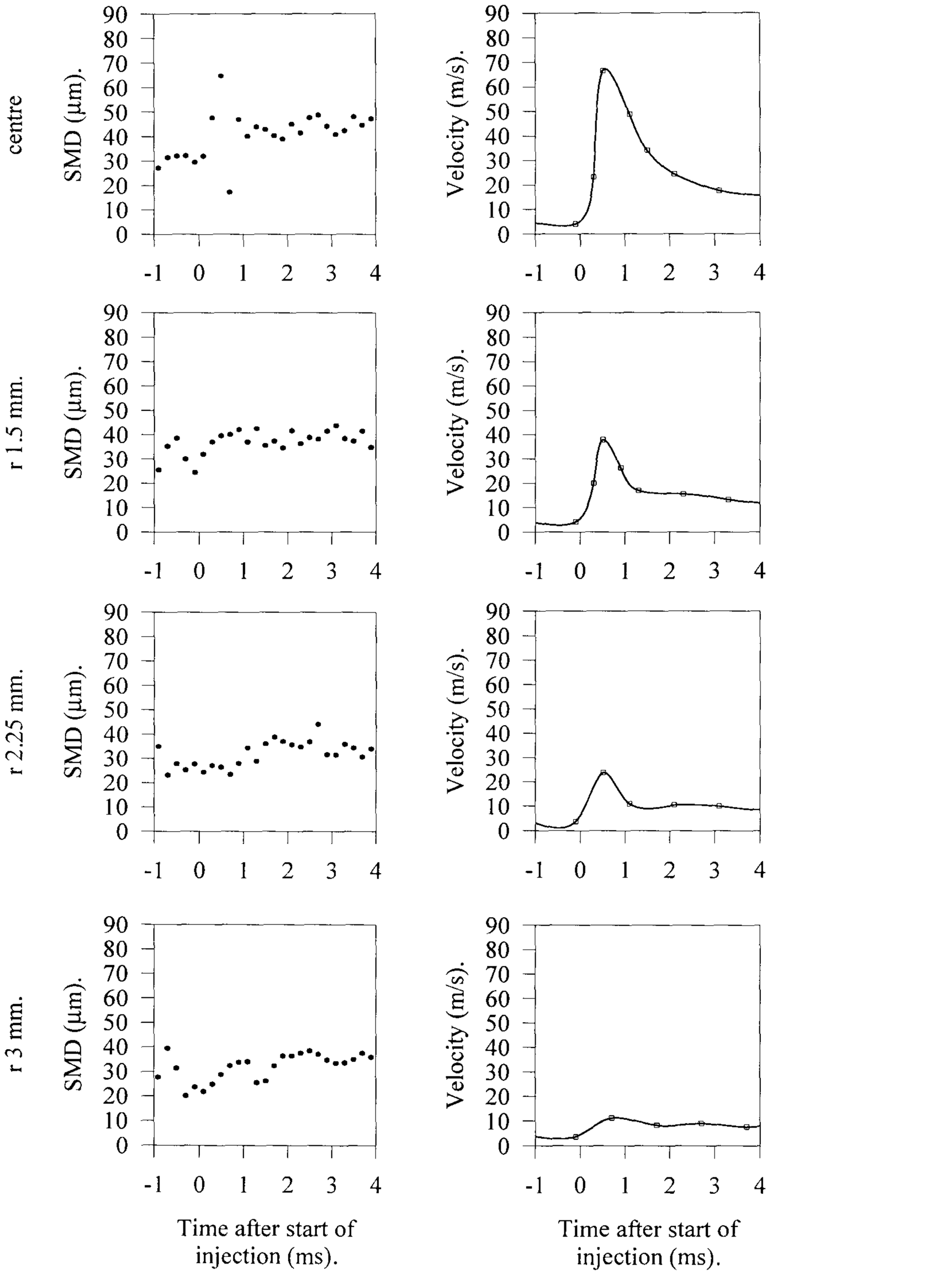


**Fig 4.35** Graphs of droplet Sauter mean diameter and average axial droplet velocity at different radial positions. EPVE pump based FIE at 1200 rpm, half load, measured 17.5 mm from nozzle.

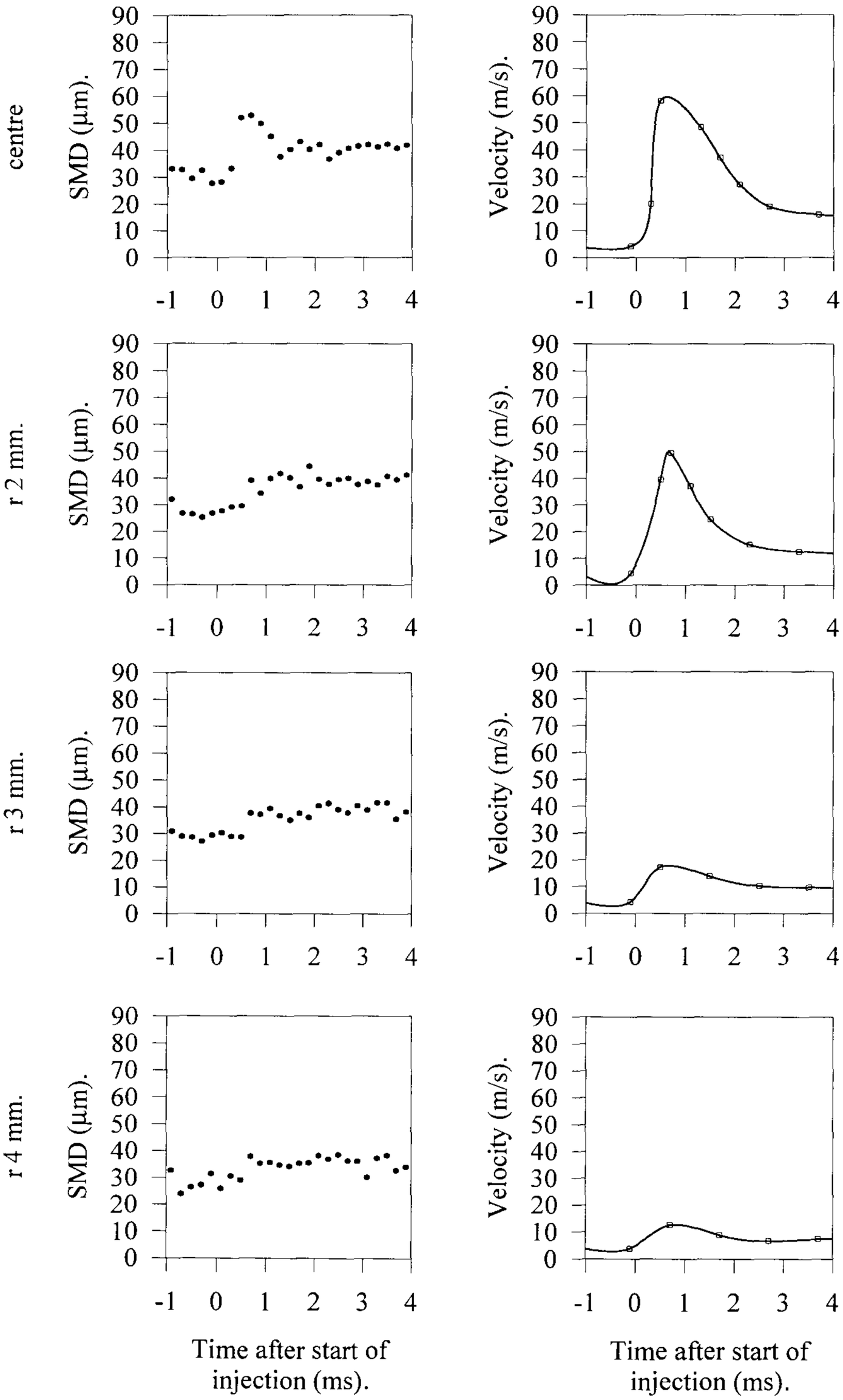


**Fig 4.36** Graphs of droplet Sauter mean diameter and average axial droplet velocity at different radial positions. EPVE pump based FIE at 1200 rpm, half load, measured 25 mm from nozzle.

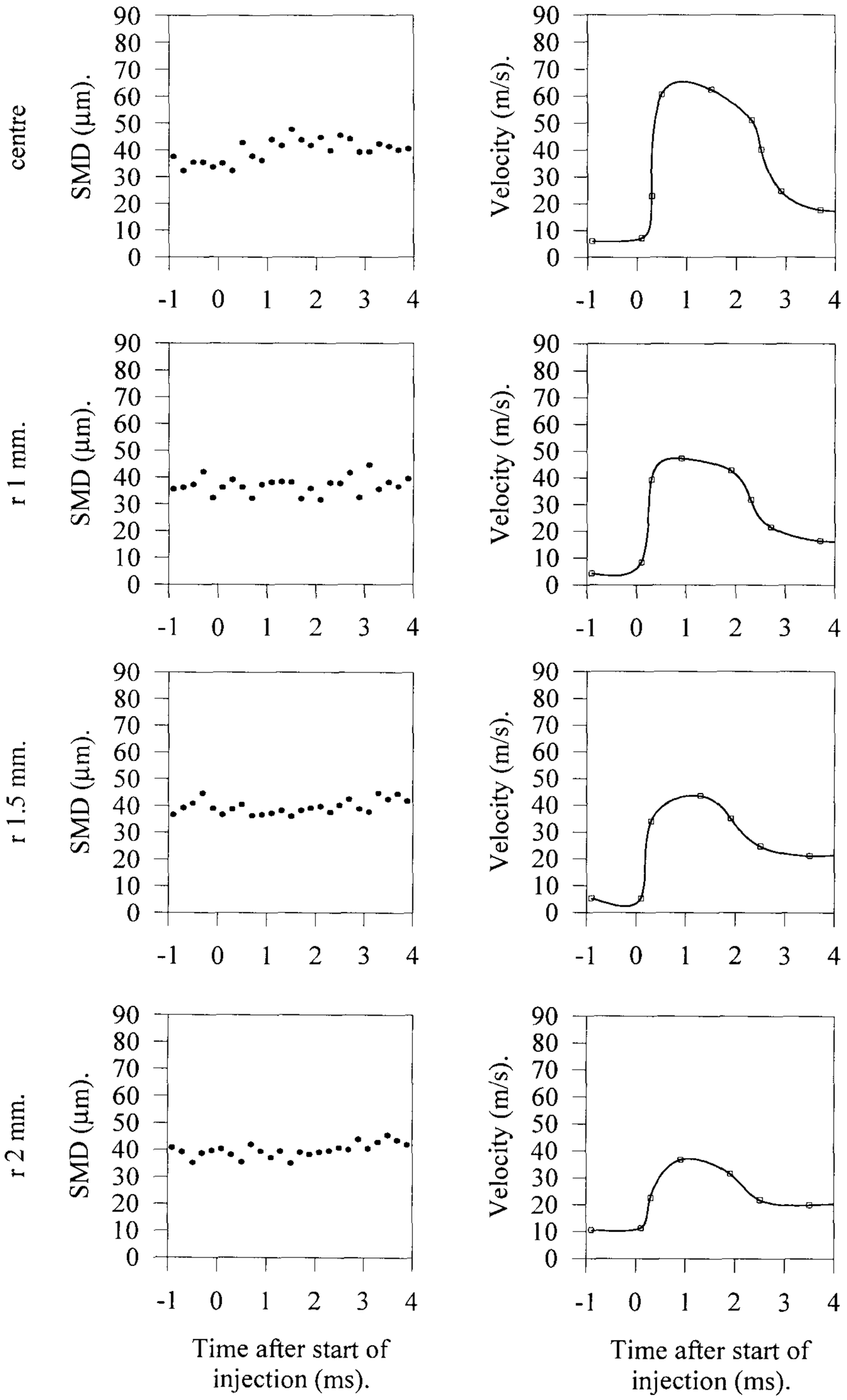


**Fig 4.37** Graphs of droplet Sauter mean diameter and average axial droplet velocity at different radial positions. EPVE pump based FIE at 800 rpm, full load, measured 10 mm from nozzle.

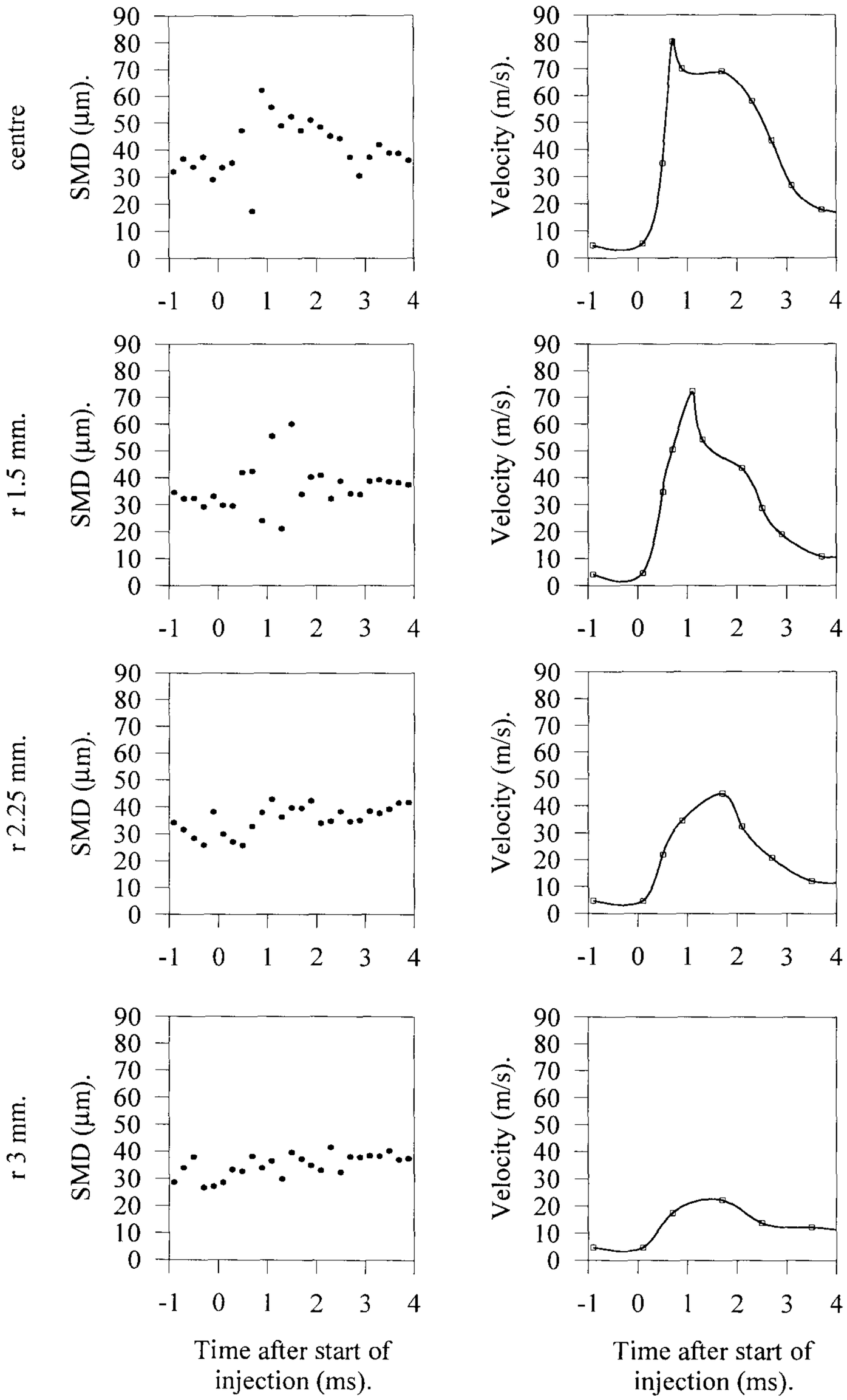


**Fig 4.38** Graphs of droplet Sauter mean diameter and average axial droplet velocity at different radial positions. EPVE pump based FIE at 800 rpm, full load, measured 17.5 mm from nozzle.

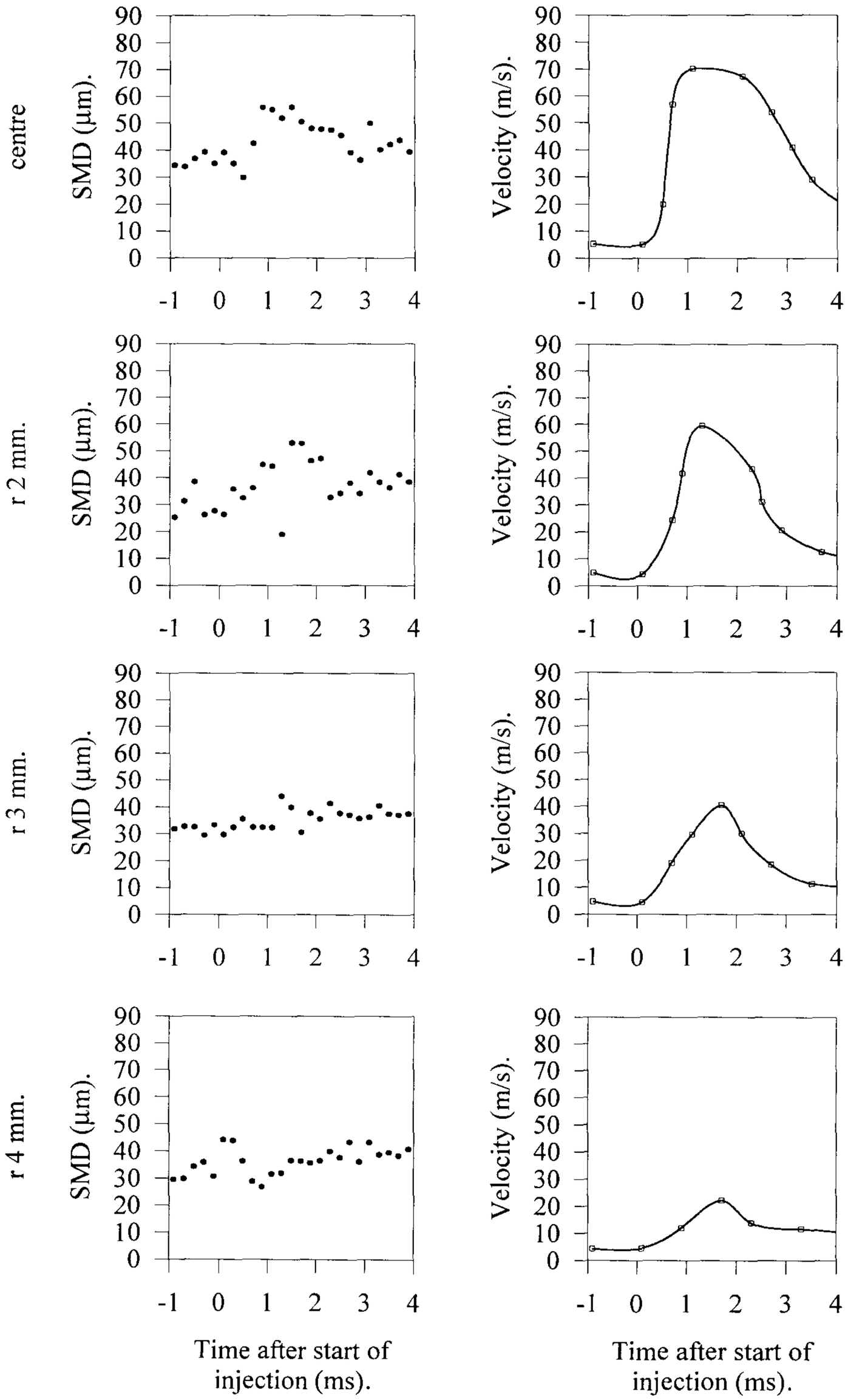


**Fig 4.39** Graphs of droplet Sauter mean diameter and average axial droplet velocity at different radial positions. EPVE pump based FIE at 800 rpm, full load, measured 25 mm from nozzle.

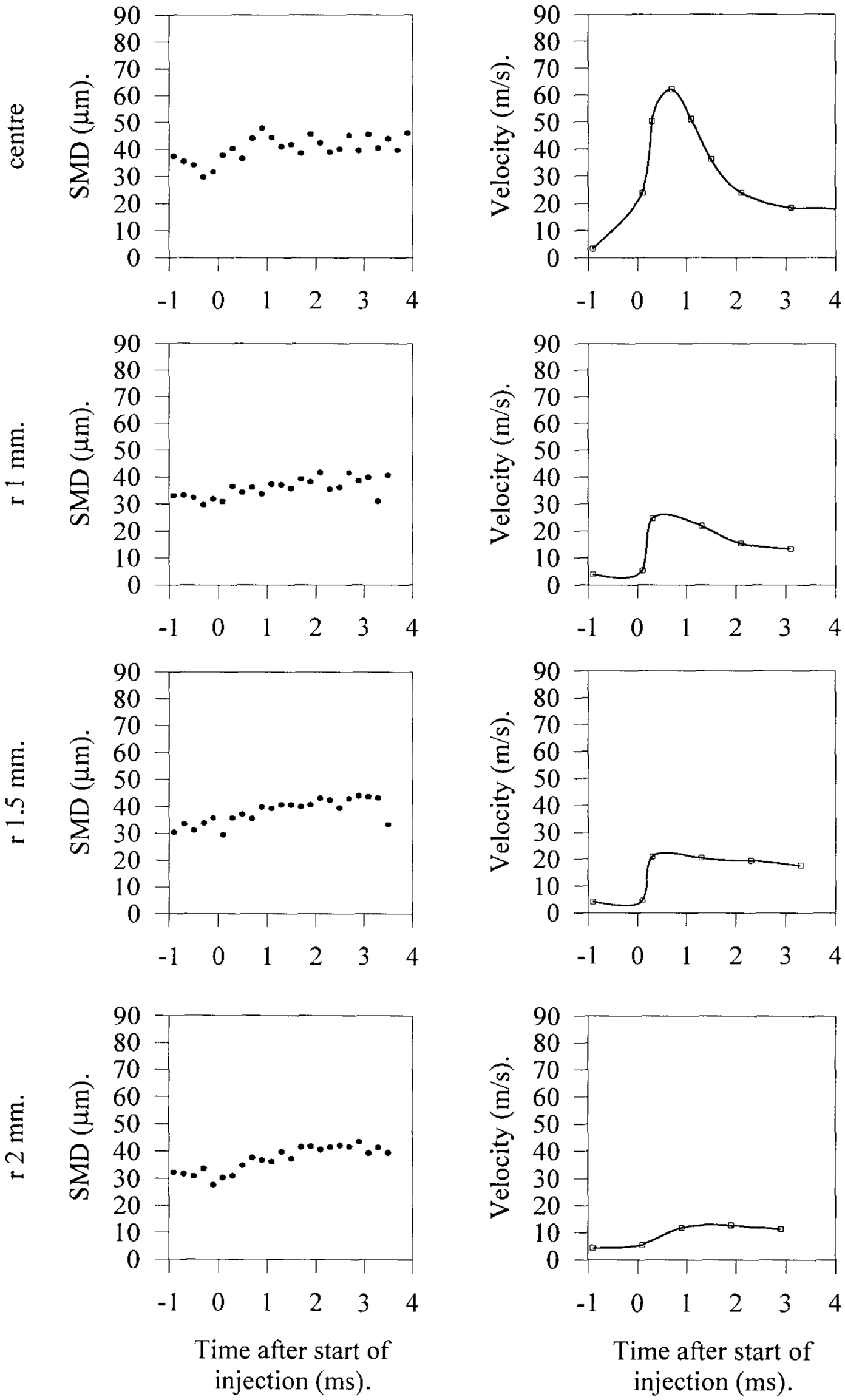


**Fig 4.40** Graphs of droplet Sauter mean diameter and average axial droplet velocity at different radial positions. EPVE pump based FIE at 800 rpm, half load, measured 10 mm from nozzle.

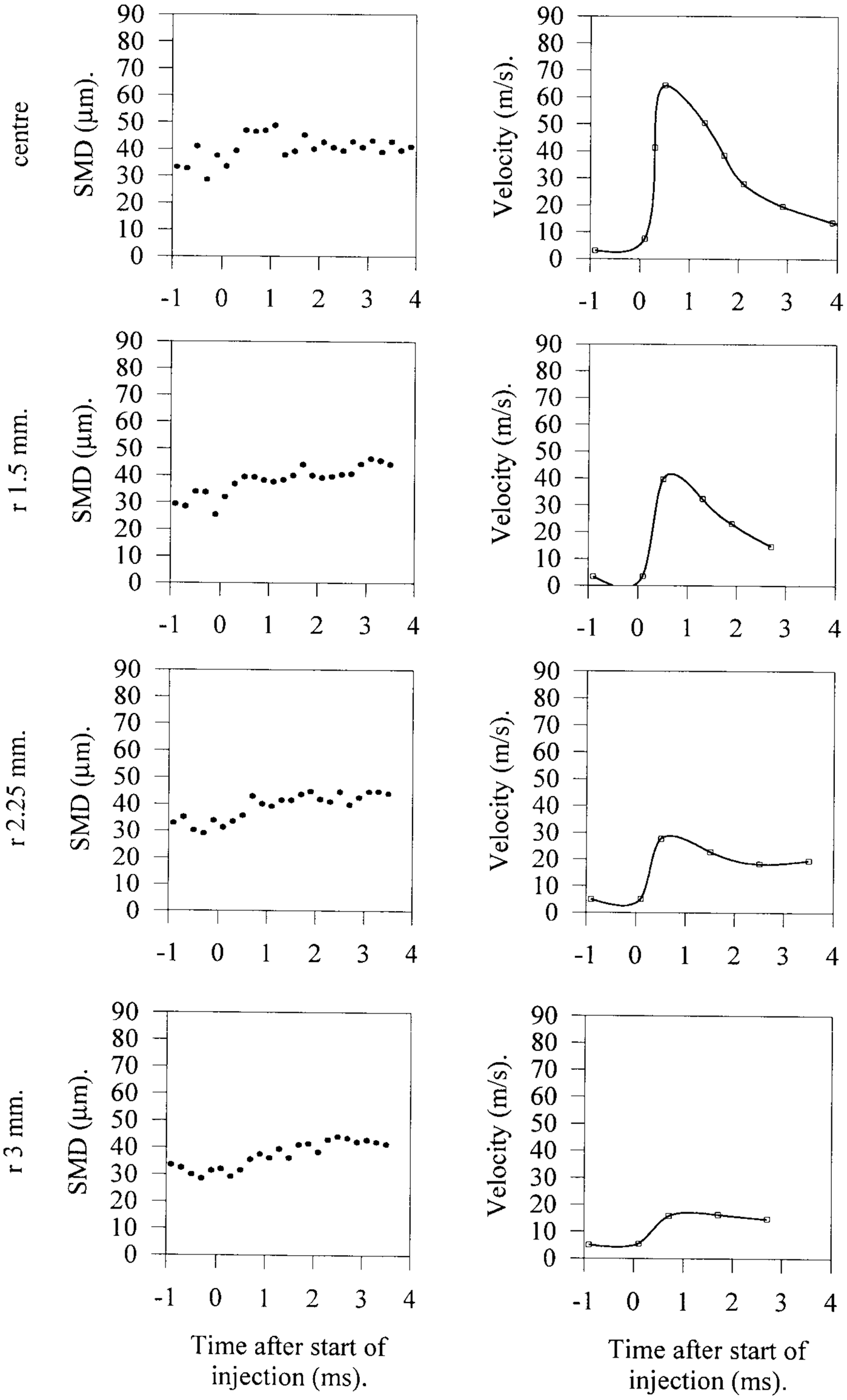


**Fig 4.41** Graphs of droplet Sauter mean diameter and average axial droplet velocity at different radial positions. EPVE pump based FIE at 800 rpm, half load, measured 17.5 mm from nozzle.

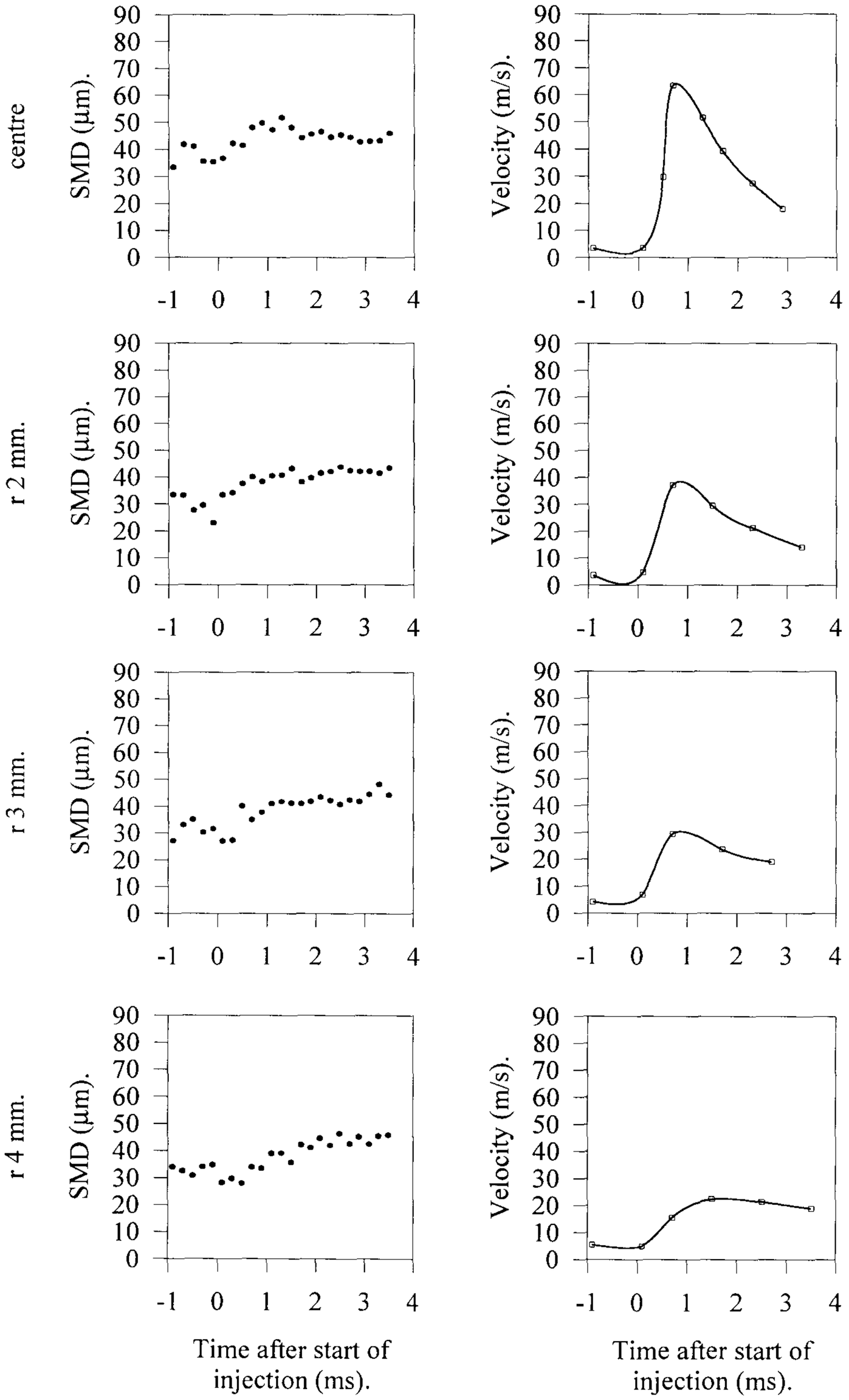


**Fig 4.42** Graphs of droplet Sauter mean diameter and average axial droplet velocity at different radial positions. EPVE pump based FIE at 800 rpm, half load, measured 25 mm from nozzle.

### 4.2.1 Droplet Velocities.

The reader is first referred to the averaged plots of velocities which follow the general trends found in the literature. Firstly, even at quite different loads and chamber pressures, peak average droplet velocities are around 70-80 m/s for both pumps. This ties up with the finding from the images that the penetration is not greatly affected by variations in injection pressure. The value of peak velocity appears to be similar both close to and far from the injector. At first sight this is unexpected and one could be forgiven for concluding that droplet velocities would increase with increasing load and pump speed (and hence injection pressure), falling chamber pressure and be proportionately higher closer to the nozzle than at a greater distances. In reality very close to the nozzle, where PDA measurements are all but impossible, the change in injection pressure probably does yield an increase in velocities (assuming that there was no transition in the spray type leading to, say, choked flow in the nozzle which did not exist before). However, at any appreciable distance downstream of the nozzle (even 10 mm) the velocities appear to be much lower. This first section will explain the reasons for the observed similarity in the magnitude of the velocities.

The first reason for the similarity is due to the drag on the droplets following approximately a square law. If very high initial velocities exist the drag is very large, rapidly decelerating the droplets to a low figure; if, however, the initial velocity is lower then the droplets will decelerate less. Thus the tip velocities eventually reached will tend to be similar regardless of the initial velocity; this characteristic velocity will be a function of the gas properties, principally the density, in the chamber.

This still fails to explain fully why the peak velocity and the penetration are relatively constant with changing injection pressure, as it is unlikely that the characteristic velocity would be so similar when initial velocities vary considerably. Another effect on the sprays is air entrainment, increased amount of which, in sprays with higher pressure, may lead to increased levels of drag. Evidence for increased entrainment can be found by looking at the velocity traces at the edges of the spray. Figure 4.43 shows two plots of the peak average velocity at the same radial positions but at two different load and speed conditions. As can be seen the high pressure spray

(high load) has much more of a 'top hat' velocity profile in section than the low pressure spray, although the velocity in the centre is similar. This can be explained by the increased mass flux at the edge of the spray which will mean that there is more momentum in that region of the spray to maintain higher velocities despite the decelerating effect of the high density air. The best evidence for such an increase in mass flux would be an actual flux measurement using a PDA system; unfortunately such measurements although possible are unreliable in such dense sprays [*Domnick,* 1997]. However, the increased mass flux can be inferred by considering the fact that the cone angle does not increase appreciably at higher injection pressures. Clearly if more mass is being delivered through the nozzle, and the average velocities and injection duration do not increase appreciably then simple conservation of mass says that the average mass flux of the spray must be higher. If there is an increase in the mass flux in the middle of the spray, then higher velocities would be found in this region; as this is not the case the increased mass flux must be towards the spray's edges.

To summarise, the higher values of velocity and momentum at the edge of the spray are likely to lead to increased air entrainment, probably in the spray in general, combining this with the square law drag effects tending to decelerate droplets regardless of initial velocity to similar values, explains the similar values in peak average droplet velocity, despite the higher initial velocity and momentum at high injection pressure. Indeed the small differences in the peak velocity could be seen as evidence of increased air entrainment alone. It is interesting to postulate as to whether this increased air entrainment explains why diesel engines with high pressure FIE produce less soot, rather than because of smaller droplets formed in the sprays.

A study of the droplet velocity profiles, yields a further interesting and fundamental point about diesel sprays. Although the peak velocity is largely unaffected by load, pump speed and chamber pressure, these parameters do seem to affect the velocity profile of the spray during the course of injection. For those injections with high injection pressures and hence high initial velocity, the profile of the velocity trace is more square and the velocity graphs rise more sharply. In other words the peak velocity is reached very quickly, while with lower initial injection velocities this peak is reached much more slowly. This can be explained by assuming

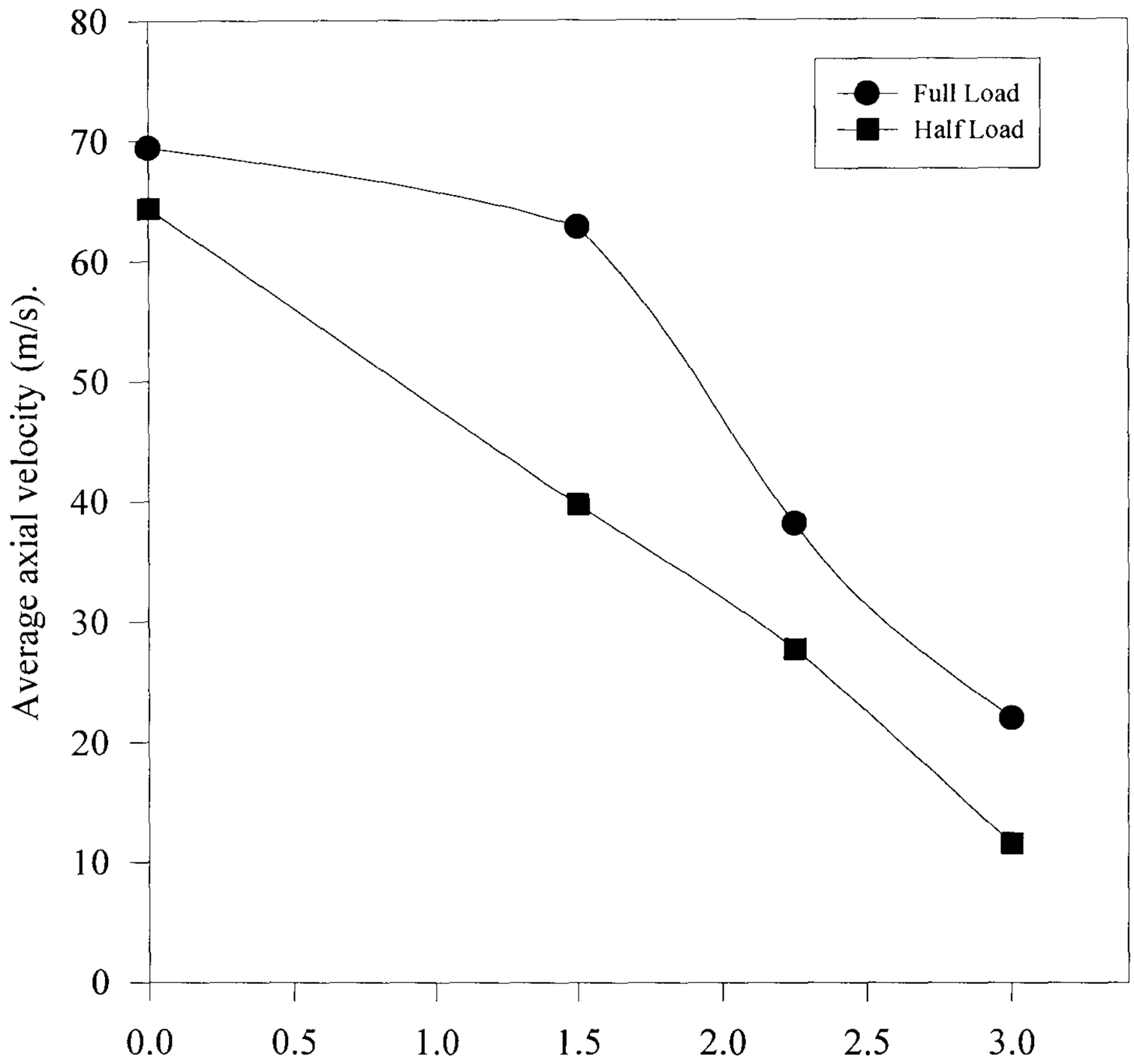


**Fig 4.43** Graph of average axial droplet velocity at different radial positions at high and low load, showing the more 'top hat' velocity profile found in the high load case. MW pump based FIE at 800 rpm, measured 25 mm from the nozzle.

that the first drops exiting the injector, however fast they are travelling, will be decelerated rapidly, but in so doing they will accelerate a portion of the air. Fuel sprayed after the initial phase will then be injected into this jet stream of air, and as a consequence the relative velocity between the air and droplets will be much less and the droplets will be decelerated less. These drops will of course 'catch up' those first injected and overtake them. Once this happens they will then be entering relatively quiescent air and once again be decelerated rapidly. This is an explanation for the

'mushroom' head of sprays as the fuel injected is continually 'catching up' and then 'falling over' fuel injected earlier.

### 4.2.2 Droplet Diameters.

The velocity profiles of the sprays from each pump show a fairly close correlation, this would be expected as the two FIE are very similar; both FIE are pump-pipe-nozzle systems, both sets of injectors are multi-hole of the VCO type and crucially have the same hole dimensions, and the injection pressures are also similar, although slightly lower for the EPVE pump. However, at first sight the graphs of SMD have little or nothing in common. The first part of this section explains the reasons for this discrepancy.

As was explained in Chapter 3, the two sets of data were obtained with different PDA systems and the differences between the two systems and principally the different values of laser power and photomultiplier (PMT) voltage may explain the discrepancies in the results. These last two parameters have an important impact on the values of SMD produced for a number of reasons, but before these are explained, a brief explanation will be given of the manner by which the two parameters are set. Clearly if laser power is increased while PMT voltage is maintained at a constant value or vice-versa if PMT voltage is increased while maintaining a constant laser power, the strength of the PMT signal reaching the decoding electronics will increase. A point will be reached where the PMTs are saturated and the signal will show an almost constant value. At this point the PMTs are likely to be damaged and continued operation will quickly lead to their failure. However, even when partial saturation exists, the signal produced will tend to be little more than noise, equally if too low a combination is selected then the signal will be so small as to fail to register in the electronics and no measurements at all will be possible. A balance must thus be struck between achieving a sufficiently large signal amplitude and avoiding noise. Put simply, a low laser power could be used if a high PMT voltage was chosen and vice versa.

This simple approach to setting the values works reasonably well for LDA work on non-dense sprays with low velocities and a small range of diameters. Diesel sprays are, however, dense, have high velocities and a large range of diameters (typically varying by over a factor of 100 which is well beyond the dynamic range of most PDA counters) and because of this the laser power must be set first to suit the prevailing conditions. The importance of laser power probably stems from its effect on the size of the control volume, as high laser power leads to larger control volumes.

| **Laser** | | |
|---|---|---|
| Wavelength (l) | 0.5145 | μm |
| Beam diameter at $e^{-2}$ ($b_0$) | 1.25 | mm |
| **Transmitting Optics** | | |
| Grating lens ($f_1$) | 80 | mm |
| Collimating lens ($f_2$) | 300 | mm |
| Focusing lens ($f_3$) | 600 | mm |
| Beam order (p) | 1 | |
| Grating track | 2 | |
| Number of grating line-pairs | 8192 | |
| Grating line-pair width ($d_r$) | 11.47 | μm |
| Diffraction angle ($q_p$) | 2.57 | deg |
| Beam diameter after $L_2$ ($b_0'$) | 4.6875 | mm |
| Beam separation (s) | 26.95 | mm |
| Beam intersection angle (f) | 2.57 | deg |

| **Frequency Shift** | | |
|---|---|---|
| Grating speed | 213.1 | rev/s |
| Frequency shift | 3.49143 | MHz |
| Velocity shift | 40.00 | m/s |
| **Signal Processors** | | |
| Maximum Doppler frequency | 20 | MHz |
| Maximum velocity | 189 | m/s |
| Velocity/frequency conversion | 0.0873 | $MHz/ms^{-1}$ |
| **Size Measurement** | | |
| Maximum diameter | 424 | μm |
| Phase/diameter conversion | 0.589 | μm/deg |
| **Control Volume** | | |
| Fringe spacing ($d_f$) | 11.46 | μm |
| Diameter at $e^{-2}$ ($b_x$) | 83.87 | μm |
| Length at $e^{-2}$ ($b_y$) | 3.73 | mm |
| No. stationary fringes ($N_f$) | 7 | |

**Table 4.3** Various parameters of PDA system, including: Laser, transmitting and receiving optics and control volume dimensions.

A large control volume is undesirable in Diesel work because of the droplet density. If this is high, the likelihood of multiple occupancy is also high; because of this large control volumes reduce the validation rate, as the signal to noise (S/N) ratio is lower. In addition small droplets will be discriminated against as only the larger droplets will reflect sufficient light to reduce S/N ratio sufficiently for the validation logic to accept the signal. Put another way, assuming that multiple occupancy is inevitable, the signal

from a large droplet will tend to overwhelm those signals from the other smaller droplets in the control volume; there is thus an in built bias to larger droplets and for this reason alone as small a control volume as possible should be used.

As was explained in the last chapter, the control volume must still contain the required number of fringes to make measurement possible. Thus if a very small control volume is used then the fringe spacing will have to be very small; this in turn will make the signal frequency of the Doppler bursts from droplets with even moderate velocity out of the range of the counter. Hence, a compromise must be made and the control volume is usually made as small as possible whilst still allowing the full velocity range of the spray to be measured. Unfortunately the bandwidth of both the counters used was only 20 MHz and this resulted in a relatively large control volume (the details of the various parameters are given in Table 4.3 above)

Increasing laser power undoubtedly increases the effective size of the control volume, but more importantly at high laser power the beams will have a much more top hat profile than at the very low powers used in some of the experiments. Such a top hat profile will again effectively make the control volume larger as droplets from the fringes will produce signals almost as strong as those in the middle. There is another effect of higher laser power, as the laser beams have to pass through he middle of the spray there is a great deal of light scattered in all directions by the 'body' of the spray and hence noise levels in a diesel spray are inherently high, however small the control volume is, however, as laser power is increased the amount of noise will also increase leading to a biasing towards droplets which are large enough to scatter sufficient light to overwhelm the background noise. Evidence for the above effects can be found by reference to Figures 4.44 to 4.45, which show scatter graphs of the results of both pump systems, as can be seen during the main part of the injection when only a very few small (sub 30 μm) droplets are measured since their signals are too weak to register; this despite the fact that Diesel sprays are known to be dominated by droplets of this size class However, once the main part of the injection has past, small droplets are sampled quite readily.

This is why any attempt to measure flux using PDA is futile as, although there are means of correcting the measurements to take account of the small droplets whose signals are not validated, such corrections are only feasible when validation rates are

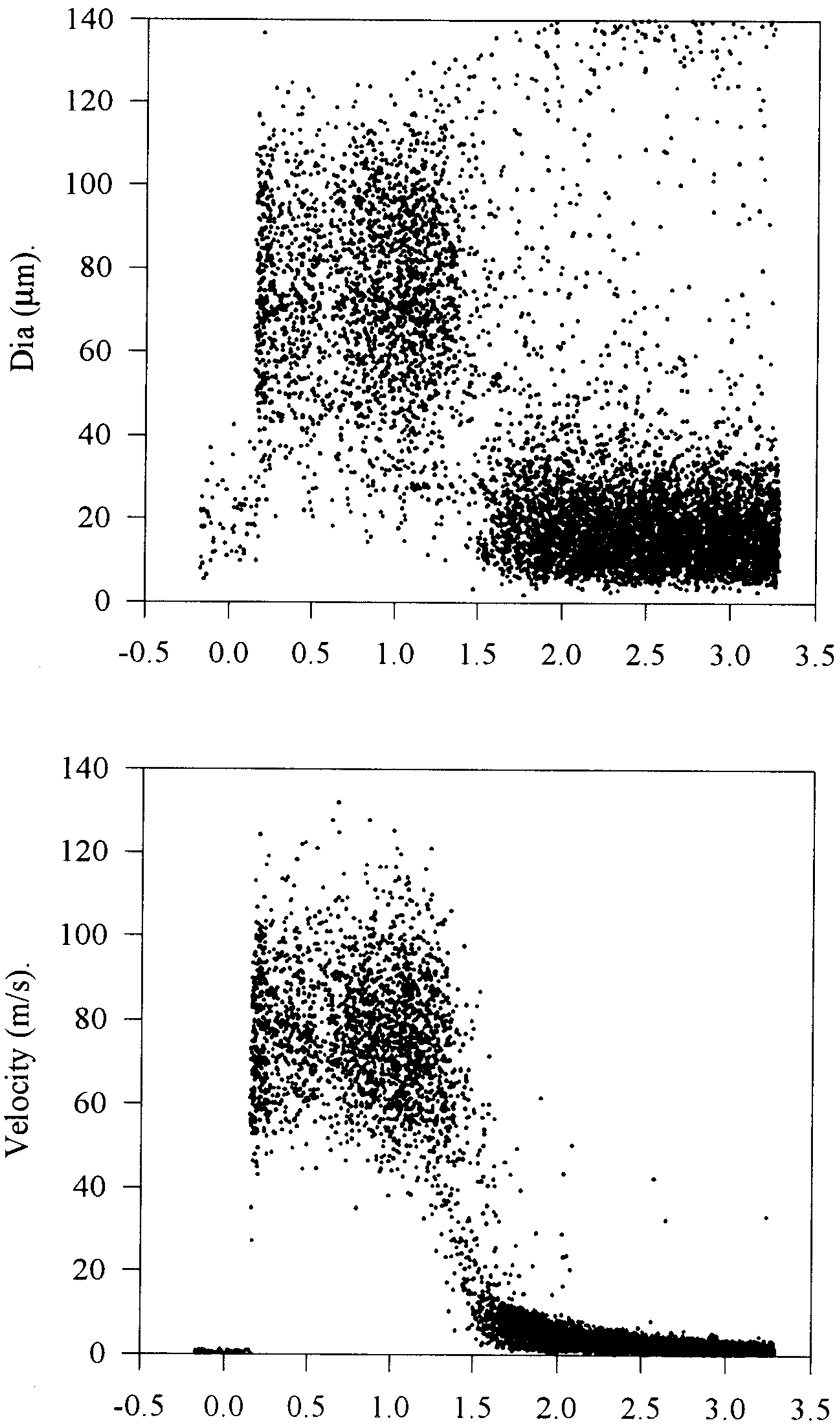


**Fig 4.44** Scatter plots of droplet diameter and velocity vs. time ASI. MW pump based system at 800 rpm, half load, measured on spray centre line, 10 mm from the nozzle.

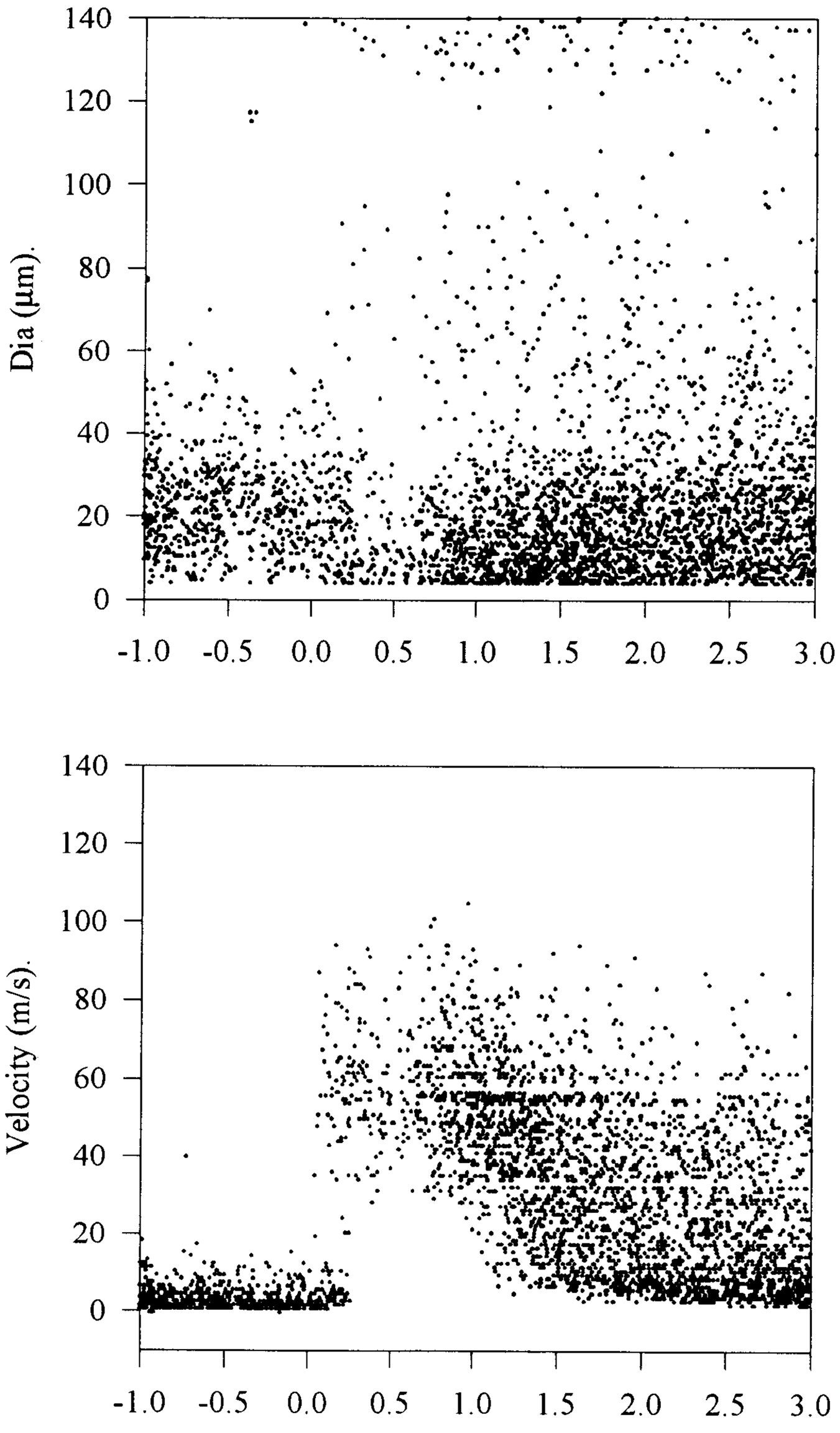


**Fig 4.45** Scatter plots of droplet diameter and velocity vs. time ASI. EPVE pump based system at 800 rpm, half load, measured on spray centre line, 10 mm from the nozzle.

reasonably high [*Domnick,* 1997]; in this case validation rates of about only 2.5% were achieved in the core of the spray.

The scatter plots might give a false impression of the number densities of droplets at various stages of the injection period as there are seemingly more droplets in the tail of the spray than in its core. This is clearly not the true picture and is simply due to the much higher validation rates due to the higher signal to noise ratios in the more sparsely populated tail of the spray.

For the reasons given above, high laser power is undesirable when measuring in the middle of any dense spray and during the experiments on the MW pump system the laser power was kept as low as possible, being compensated by using a high PMT voltage. One might argue that such high voltages will inevitably increase the magnitude of the background noise and have the same effect as using high laser power; this is untrue simply because changes in laser power determine which size classes of droplets scatter sufficient light to rise above the background noise. The PMT voltage, on the other hand, apart from a small increase in electrical noise, simply controls the amplitude of this signal and doesn't affect its 'shape'. Thus, when setting up the two parameters, laser power was adjusted to be as low as practically possible (the laser's minimum output was 50 mW) and PMT voltage was then set to maximise the validation rate, usually at a point with a high degree of PMT saturation.

Although the explanation given above tends to suggest that the biasing to larger droplets is overcome by using low laser power, this is optimistic as despite the use of very low laser power the results from the MW pump system show hardly any small droplets in the core of the spray. Small droplets are known to exist in sprays and hence the conclusion is that despite the use of laser powers and PMT voltage conducive to measuring small droplets, the signal to noise ratio at which the counter could validate droplets was still too high for valid measurement of small droplets to be made in this region. This fits in with the preliminary experiments when various levels of laser power and PMT voltage were tried, with high laser power the results were even more biased to larger droplets; an interesting study of the effect of various parameters is given by *Koo and Martin* [1991].

One interesting possibility which has not been explored is whether by saturating the PMTs, but still using low laser power, that the larger droplets could be

discriminated against as their signal would be above the threshold of the counting logic; however, the PMTs would need to be able to withstand a high degree of saturation without damage.

A further check to see if the results of the MW pump system tests are biased to particular size classes was done by taking LDA measurements in the spray and comparing the results with the PDA measurements. This is effective because of the much higher validation rates achieved when taking LDA measurements, of the order of 50 to 80%. Such high validation rates indicate that the biasing to particular size classes and particularly to large droplets is unlikely, because as most of the droplets are small, even when the measurements are biased to large droplets, such a high validation rate means that most of the samples must consist of smaller droplets. Figure 4.46 shows a scatter plot comparing LDA and PDA measurements at the same condition. These two measurements are in fact coincident as the program running the decoder was reprogrammed to output all droplets passing the LDA validation criterion into a separate file; the PDA results are simply a sub-set of those droplets passing the additional PDA validation checks. Bearing in mind what has already been said about the importance of variations in laser power and PMT voltage, this is clearly a great advantage when making such a comparison.

As was alluded to in Chapter 3, the PDA system used for the tests on the EPVE pump system used the same transmitting and receiving optics, the only difference between the hardware being the use of an Aerometrics counter rather than the Imperial College counter. As was also discussed in Chapter 3, the Aerometrics counter lacked a resetable clock and, to enable a time reference for the samples to be obtained, the PDA counter had to be set up to discriminate towards those droplets at the end of the injection after the main part of the spray had past. Unfortunately to achieve this, higher laser power had to be used as simply increasing the PMT voltage eventually led to more noise. This enabled more droplets in the tail end of the spray to produce a signal, as normally these parameters are optimised to facilitate measurements in the core of the spray. Once the main part of the spray had past, the signal amplitude falls off due to a reduction in the level of background noise, consequently less measurements are made at the tail end of the spray under this condition. Consequently, the validation rates of measurements in the spray core were

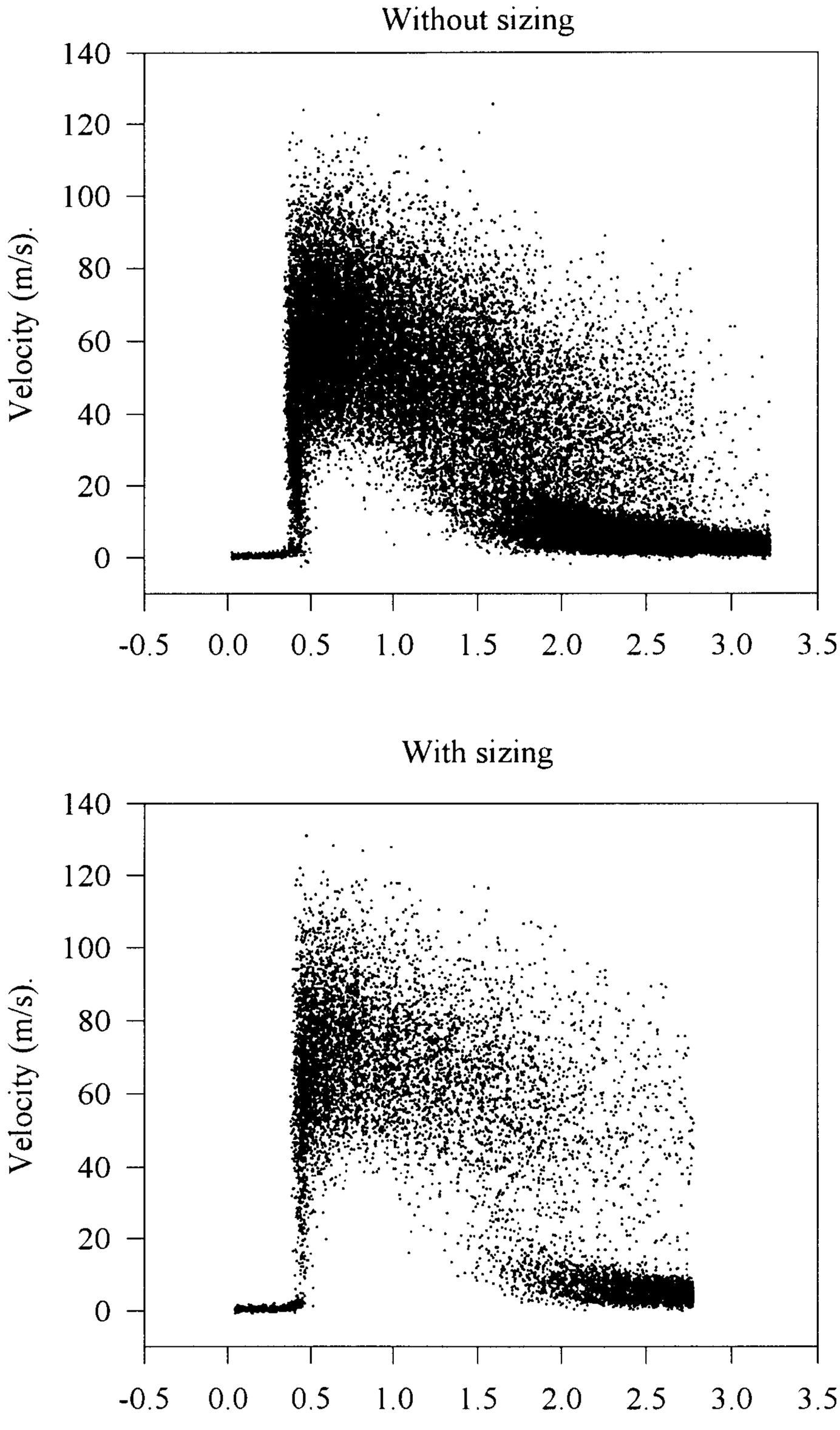


**Fig 4.46** Graphs of droplet velocities measured using PDA system with and without sizing and under identical conditions of speed and load. MW pump based system at 800 rpm, half load, measured on spray centre line, 25 mm from the nozzle.

much reduced, but fortunately the Aerometrics counter seemed to be able to cope with much lower signal to noise ratios and sufficient numbers of samples in the spray core were obtained. The lower signal to noise ratios possible with the Aerometrics counter may also explain why quite a few small droplets were sampled in the core of the spray with this counter, despite the use of higher laser powers (see Figures 4.44 to 4.45).

Reference to the graphs of SMD for both pumps shows that the SMD measured with the EPVE pump system's spray is lower in general than that for the MW pump. This is partly due to the reasons detailed above and the biasing of the results of the MW pump towards larger droplets. It seems unlikely that there would be any fundamental difference between the two systems as the conditions are very similar in terms of, the line pressures, hole size, sack volume geometry and chamber pressure; further to this, a study of the images of the sprays shows similar cone angles and general structure indicating a similar degree of cavitation. This is by no means conclusive proof that the droplet sizes should be similar but simply adds weight to the assumption that any differences in SMD are attributed to the uncertainties associated with the two different PDA systems rather than any fundamental difference between the sprays.

A comparison of two different PDA systems working on similar sprays has been detailed above; to look at this point further a survey was conducted in which the results of a number of different Diesel spray characterisations by different researchers were compared (see Table 4.4). Most of the entries are for PDA measurements, but there are also some Malvern measurements for comparison. The interesting column here is the normalised SMD, which is simply the average SMD divided by the hole size, and this should be reasonably comparable between different systems under similar conditions. The basis of using hole size as a normalising factor is due to the fact that various models of spray break-up assume that a column of liquid of roughly the same diameter as the hole exits the nozzle and subsequently breaks up producing droplets of the order of the size of the hole; indeed even with other models it is a fair assumption that droplet sizes are related to the hole size more or less linearly. A number of points arise from a close look at this column. Firstly, the disparity between PDA and Malvern; typically results from a Malvern detector are lower than those of the PDA measurements. This is a well known fact and Malvern has consequently

| Paper | Authors | Hole size (mm) | Delivery ($mm^3$/inj/ hole) | Pump Speed (rpm) | Peak Inj Press. (bar) | Peak Vel. (m/s) | SMD 0.5 ms ASI. (μm) | SMD 1.0 ms. ASI. (μm) | SMD 2.0 ms. ASI (μm) | SMD Normalised (μm/μm). | Measurement Technique or Instrument. | Remarks. |
|---|---|---|---|---|---|---|---|---|---|---|---|---|
| *"Experimental Investigation of the Sprays of an Axi-Symetric Nozzle of a Common-Rail High Pressure Electro-Injector"*. SAE 970054 | A. Ficarella, D. Laforgia, G. Starace and V. Damiani. | 0.194 | Low | 150 | 150 | 48 | | 90 | 90 | 0.464 | PDA:- Aerometrics DSA4000. | Common Rail Injection System. |
| *"Droplet Sizes and Velocities in a Transient Diesel Fuel Spray"*, SAE 900397 | Ja-Ye Koo and Jay K. Martin | 0.406 | 23 | 800 | 170 | 150 | 110 | 70 | 40 | 0.246 | PDA:- Aerometrics PDPA counter. | Atmospheric test. |
| *"Effect of Injector Nozzle Hole Size and Number on Spray Characteristics and the Performance of a Heavy Duty D.I. Diesel Engine"*, SAE 962002 | D.T. Montgomery, M. Chan, C.T.Chang, P.V. Farrell and R.D. Reitz. | 0.225 | 75% | 1600 | 900 | | 25 | 23 | 23 | 0.102 | Light extinction. | Common Rail Injection System |
| *"Characteristics of the Spray from a Diesel Injector"*, Int. J. Multiphase Flows Vol 18, pp 159-179. 1992 | Y. Hardalupus, A.M.K.P. Taylor and J.H. Whitelaw. | 0.18 | 2.35 | 600 | | 55 | | 75 | 20 | 0.417 | PDA:- Imperial College- counter. | |
| *"The Droplet Dynamics of Diesel Fuel Sprays Under Ambient and Engine Conditions"*, Laser Anemometry Vol 2. ASME. pp 571-586, 1991. | G. Pitcher and G. Wigley. | 0.2 | 7.5 | 250 | 400 | 120 | 10 | 10 | 15 | 0.05 | PDA:- Dantec 60X. | Ethyl Alcohol Fuel. |
| *"Flow and Heat Transfer Characteristics of Impinging Diesel Sprays Under Cross-Flow Conditions"*, SAE 950448 | C. Arcoumanis, P. Cutter. | 0.22 | 4 | 600 | 315 | 190 | 50 | | | 0.227 | PDA:- Aerometrics PDPA counter. | Atmospheric test. |
| *"Nozzle Effect on High Pressure Diesel Injection"*, SAE 950083. | T.F. Su, P.V. Farrel and R.T. Nagarajan. | 0.259 | 203 | | 724 | | | | 35 | 0.135 | Light extinction | Common Rail Injection System. |
| *"Investigation of Drop Size Distribution in the Spray of a Five-Hole, V.C.O. Nozzle at High Feeding Pressure"*, SAE 950087. | F.Di Giorgio, D. Laforgia and V.Damiani. | 0.19 | 8 | 150 | 900 | | 10 | 11 | 11 | 0.052 | Malvern.. | |

**Table 4.4** Survey of various Diesel spray droplet sizing measurements found in the literature, using PDA and other sizing techniques. The table gives the injection system parameters (where these were available) as well as a typical values of SMD and peak velocity from the measurements.

being largely discredited for Diesel measurements [*Chang*, 1993]. The reasons for this are that Malvern is a scattering technique which looks at the scattered light from the spray along a typically 9 mm wide beam and assumes a particular droplet distribution (typically Rosin-Rammler). From this droplet distribution a calibration curve is produced and the SMD can be read off directly. Figure 4.47 and 4.48 show a typical probability density function (pdf) from each pump; the pdf, in particular from the MW experiments, shows why the Rosin-Rammler distribution cannot adequately describe a Diesel spray as it fails to take account of the larger droplets which seem to occur in the middle of the range. These larger droplets are important when considering the mass fraction and will thus have a strong influence on the SMD. Even if a distribution could be constructed to fit these pdfs, and assuming that this new distribution could be applied to different Diesel sprays, the calibration curve of the instrument would be almost flat at points and make measurements unreliable.

The normalised SMD produced by the various PDA systems also show anomalies with the results seeming to vary widely from 0.16 μm/mm to 0.416 μm/mm; the values produced by the tests on the MW and EPVE pumps fall within this range. There are a number of possible explanations for this and at this point it is worth discussing a correction which was applied when the average SMDs were calculated for both the MW pump and EPVE pump systems. A study of the pdfs of both pumps show that towards the upper end of the measuring range (in both cases the maximum diameter that could be measured was about 140 μm) there are a number of large droplets, this is shown particularly well in the pdf from the EPVE pump system. These droplets are probably erroneous or so called 'ghost' droplets which numerous authors have described, but offering little explanation for their cause; in this context the paper by *Koo and Martin* [1990]is useful, where despite the use of a diameter range of over 300 μm there were still a handful of large droplets, completely detached from the rest of the results. These droplets would totally dominate the calculations of SMD and, assuming that the measurements are erroneous, completely invalidate the values of SMD obtained. The authors have suggested that simply by deleting any droplets above 200 μm (this spray is from a large injector with a hole of 0.406 mm) reasonable results could be obtained.

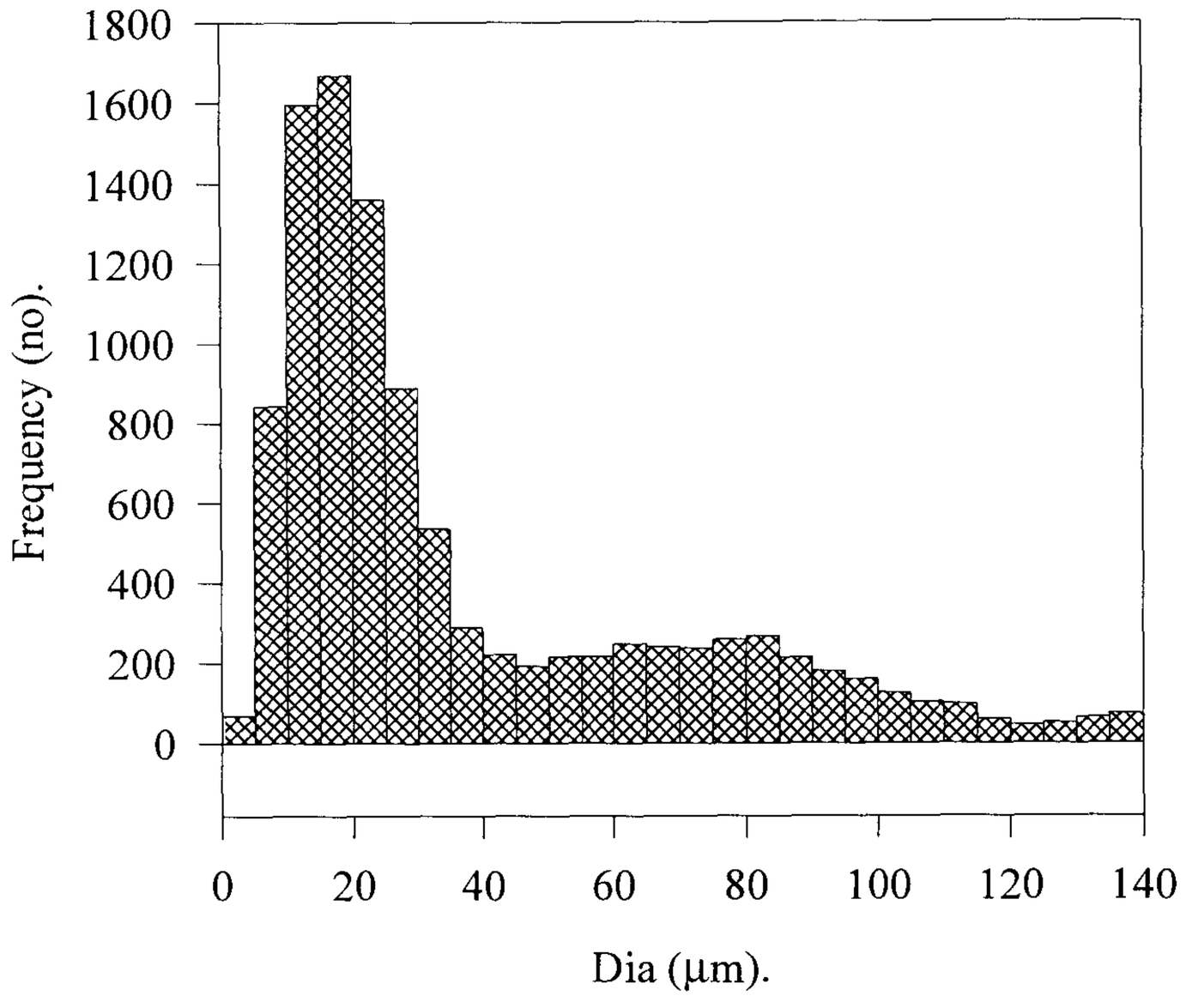


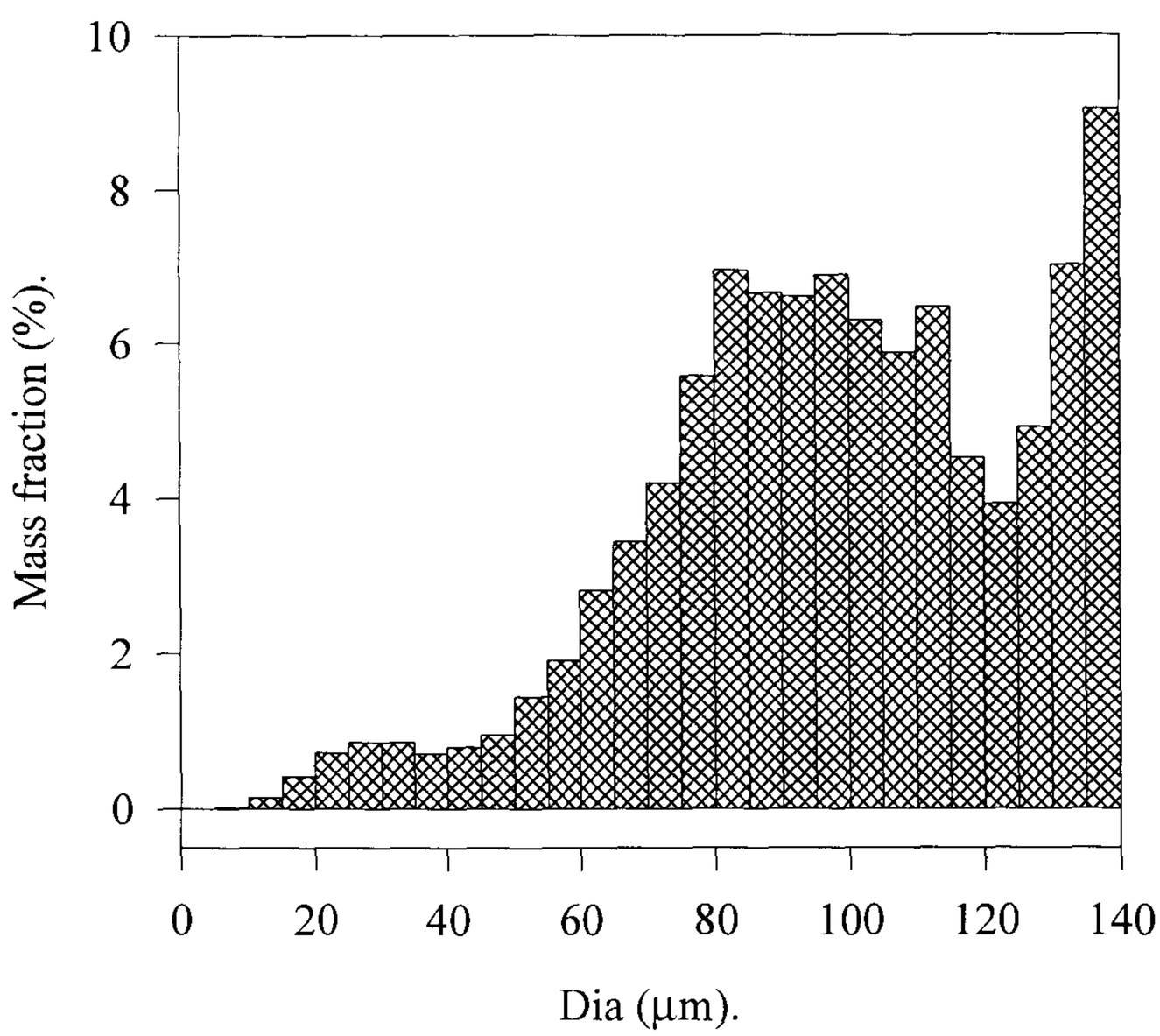


**Fig 4.47** Graph showing droplet diameter and mass fraction pdfs.

MW pump based FIE at 1300 rpm, half load, measured on spray centre line, 25 mm from nozzle.

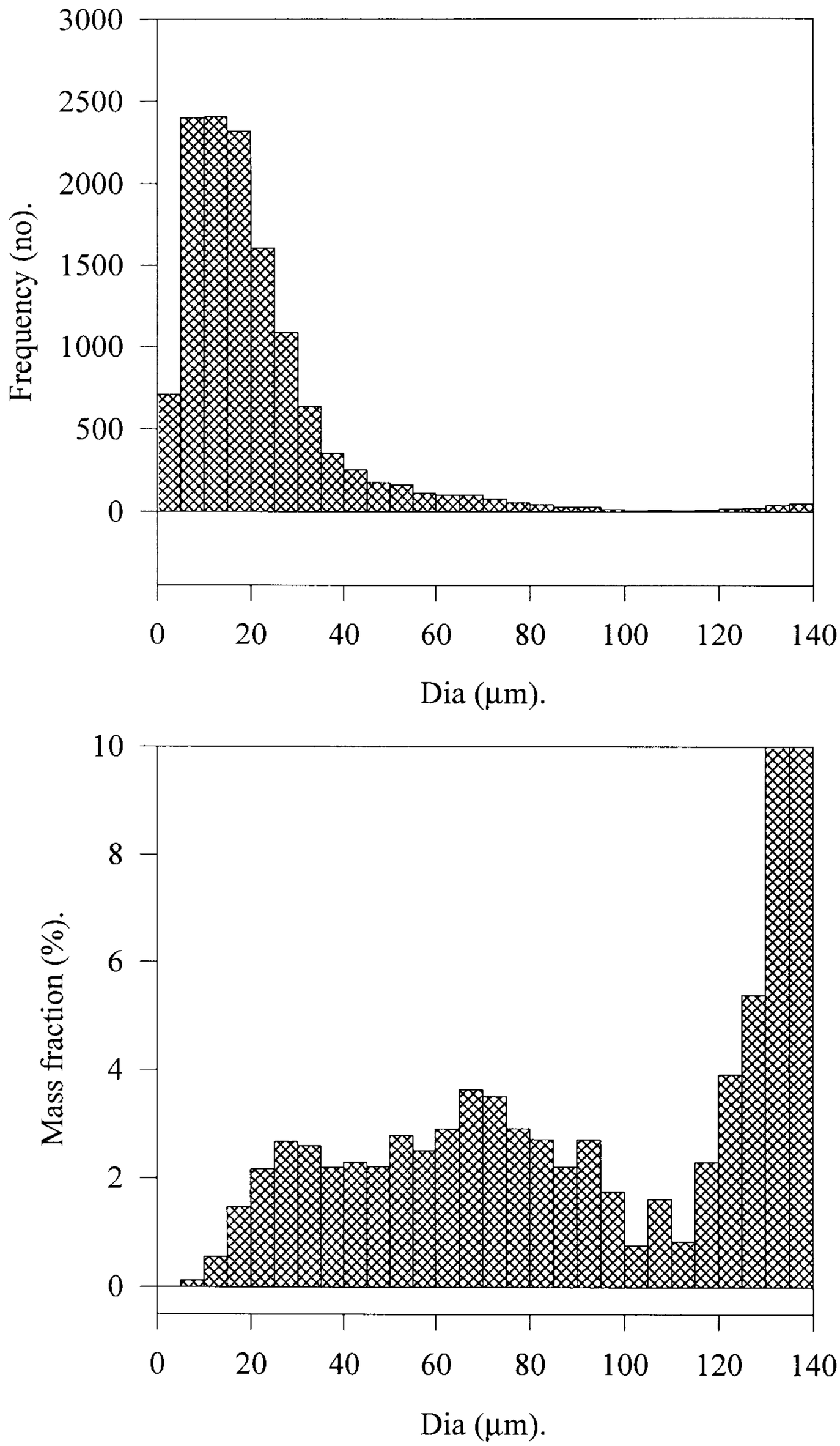


**Fig 4.48** Graph showing droplet diameter and mass fraction pdfs.

EPVE pump based FIE at 1200 rpm, half load, measured on spray centre line, 25 mm from nozzle.

As to the likely cause of these erroneous measurements, one explanation is that they are small droplets mistaken for large droplets. This is plausible as a small droplet only produces a tiny positive phase difference (maybe only a few degrees) and particularly if the droplet is travelling with a high velocity, any slight timing error in measuring the phase difference might transform this small positive phase angle into a small negative phase angle. Unfortunately a negative phase angle is the same as a large positive phase angle close to 360 degrees and these small droplets may therefore be confused for larger droplets.

Both of the PDA counters used have validation checks which can minimise this problem. Firstly, an intensity check is made by comparing the size determined by the phase difference with the intensity; since large droplets scatter more light than small droplets. Secondly, the sequence of the signals from the three PMTs is checked to ensure that they arrive in the correct sequence. If a phase error is introduced, as described above, then the signals will be out of sequence and consequently rejected.

Despite these two validation checks, due to the shear number of droplets measured in a Diesel spray characterisation, an occasional erroneous measurement may pass and be falsely validated; because of the effect that these false measurements may have on the value of SMD, a cut-off of 120 μm was applied when calculating the SMD; all droplets above 120 μm were discounted when processing the data. The value of this cut-off was chosen to be high enough to ensure that only the 'ghost' droplets were removed.

To perform an additional check on the validity of the PDA measurements from the Aerometrics counter, an additional test was conducted using a short gate of 50 μs at specific times during the injection; because this gate was very short the variations in the SMD during this period could be ignored. In this way the droplet SMD during any part of the injection could be measured by taking a series of measurements at different times during the injection period. This was a slow and laborious process but was completed for two typical test conditions; the results are shown in Figures 4.49 and 4.50. The graphs in this figure also show the results obtained from the original measurements for comparison. Of particular interest was to look at the SMD on the centre line, where most observers have noticed higher values than in the rest of the

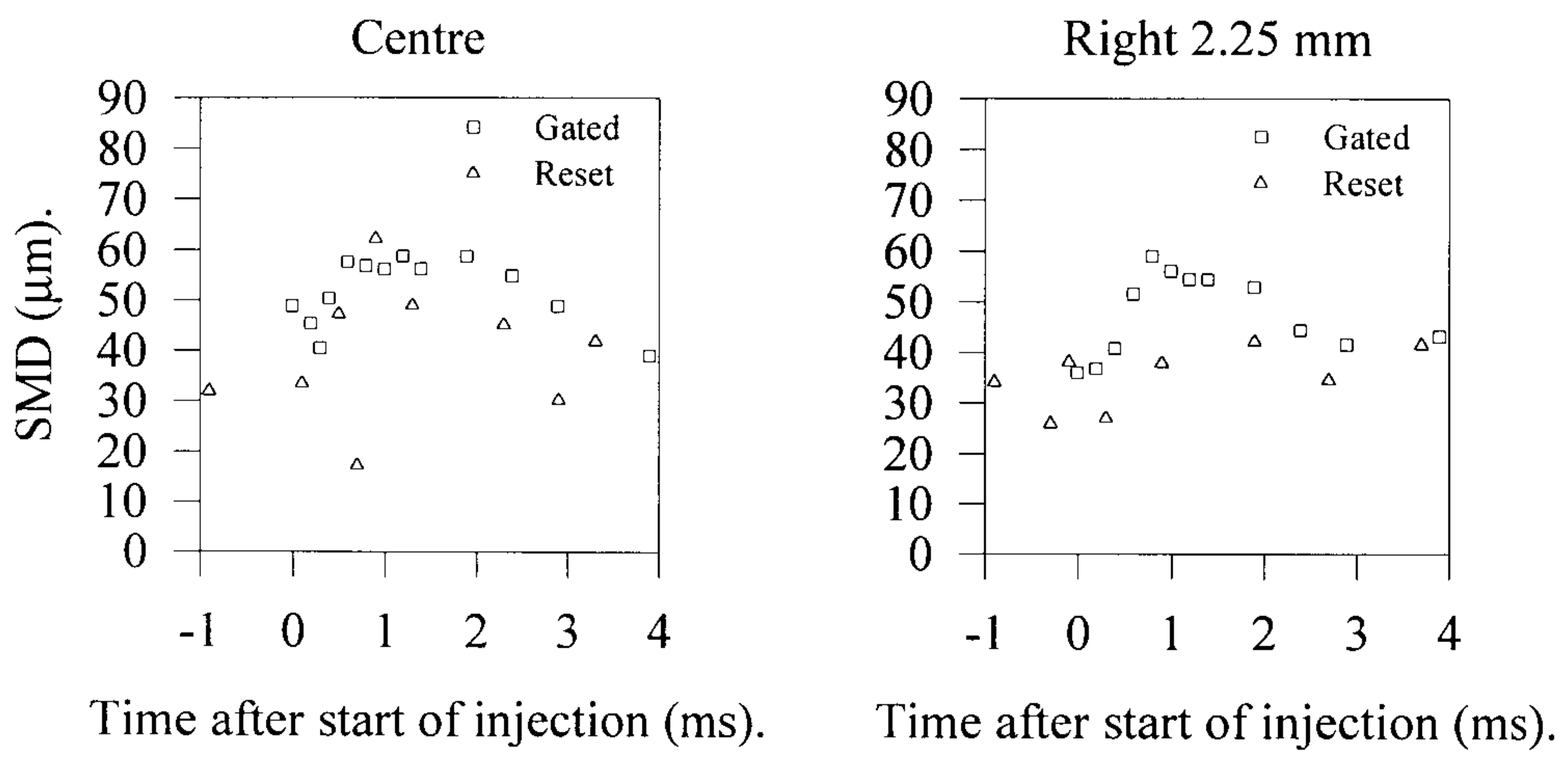


**Fig 4.49** Graphs showing comparison of SMD measured by using PDA system with different timing methods. EPVE pump based FIE at 800 rpm, full load, measured 17.5 mm from nozzle

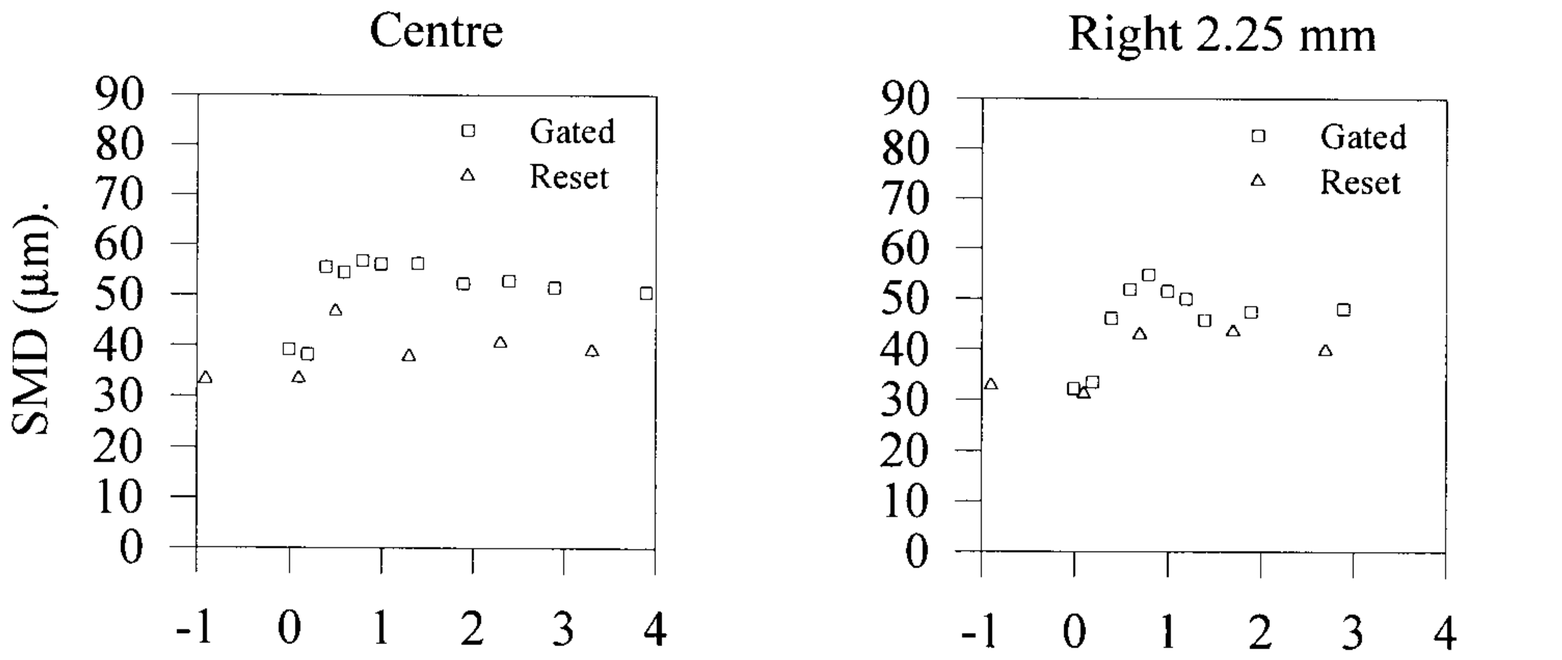


**Fig 4.50** Graphs showing comparison of SMD measured by using PDA system with different timing methods. EPVE pump based FIE at 800 rpm, half load, measured 17.5 mm from nozzle

spray, as this rise has not been observed in the tests described so far. The results seem to indicate that the SMD has been underestimated in the first run of experiments, but, there is no indication that SMDs are higher in this central part of the spray, confirming the validity of the original measurements. The difference between the two sets-of measurements can be explained because the laser power and PMT voltage, were optimised for each one of these short gates to give the best data rate. This would suggest then that the differences between the results from the two pump's systems can indeed be explained, at least partly, by the differences in the laser power and PMT voltage used.

Another possible explanation of the differences in the results is the presence or absence of cavitation which is thought to have a strong influence on spray atomisation [*Arcoumanis et al,* 1997]. It is by no means certain that the degree of cavitation is uniform when comparing different FIE systems and consequently the differences in the values of SMD could be attributed to such differences. It is also likely that there are hole to hole variations in the degree of cavitation expected from different sprays; this may be particularly relevant in the case of inclined injectors where the degree of cavitation is known to vary depending on the inclination of the hole relative to the injector's axis. This leads to one interesting possibility for future work to check on the influence of cavitation by relying on these very differences and characterising each of the sprays from each hole in an inclined injector. Clearly the influence of other variables, such as PDA system and sack volume geometry, can be reduced to a minimum with the only difference between the sprays being the degree of cavitation.

One issue raised during the experiments was the concern that the results could be falsified by stray droplets or fuel remaining in the chamber from previous injections. This obviously takes place to an extent, as there are measurements before the start of injection which can only come from fuel already present in the chamber. The question is to what degree do these 'background' droplets affect the measurements of the spray and particularly whether they consist overwhelmingly of large droplets which are more likely to influence the values of the measured SMD.

To check whether there was a problem, a number of tests were done measuring the 'background' droplets at a sufficiently large radial distance from the spray to be sure that any measurements were not from an actual injection. These tests were

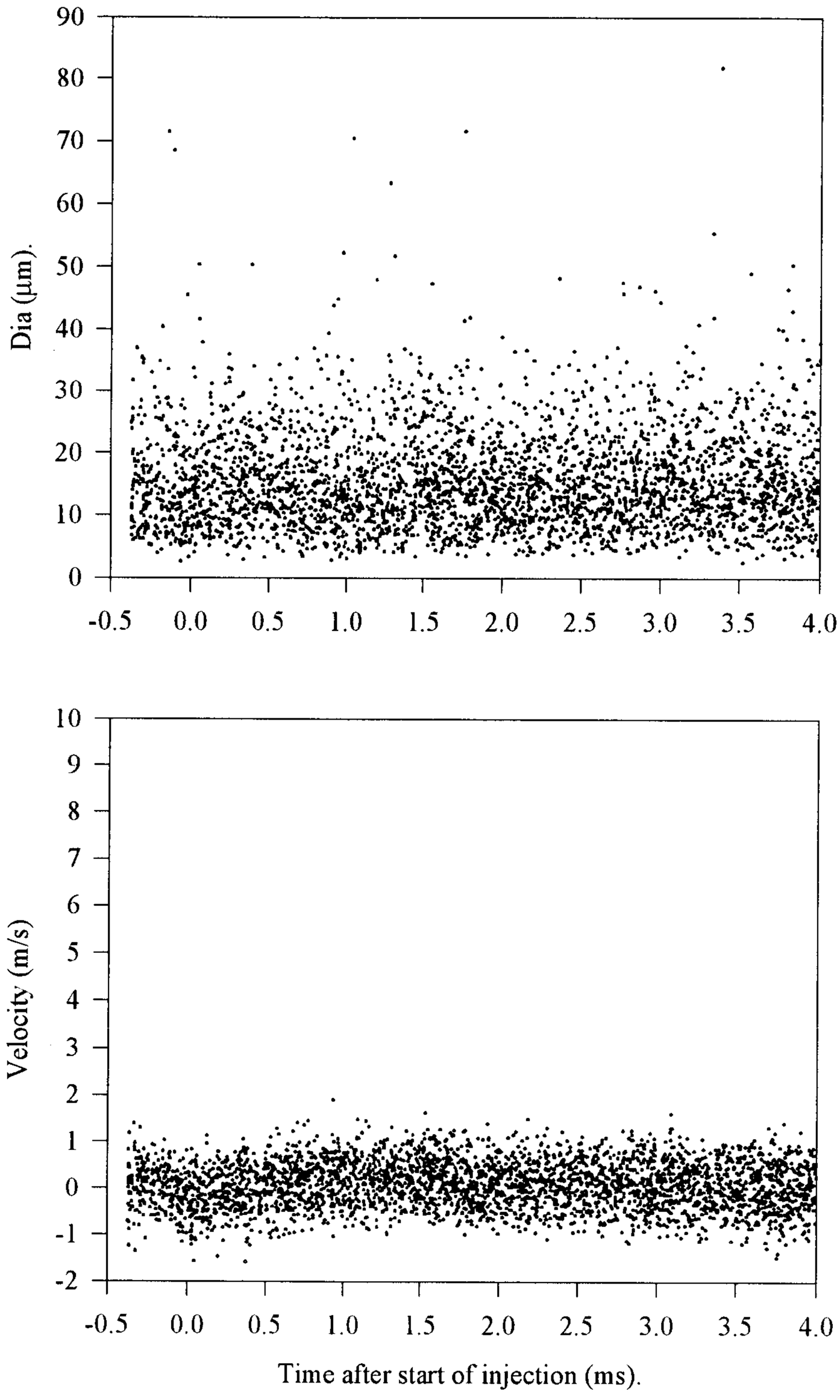


**Fig 4.51** Scatter plot of droplet diameter and velocity outside the spray envelope, to show background level of droplets. MW pump based FIE at 800 rpm, half load, measured 5 mm from the spray's centre line, 10 mm from nozzle.

conducted under the same conditions as the PDA measurements on the spray except for the laser power and PMT voltages which were adjusted to optimise the data rate. This should not invalidate the measurements as the droplet densities are so low that the influence of these parameters on the size class of the measured droplets is small.

Figure 4.51 shows the scatter plot of a typical test conducted at a distance of 5 mm from the spray's axis. The most notable feature is that there are relatively few large droplets which indicates that those measured in the core of the spray are indeed caused by the atomisation processes. In addition all the droplets have very low velocities, unlike those during the injection. An important point to stress here is that to obtain the measurements the laser power and PMT voltages used were very high which is itself an indication of the low droplet densities; despite this and the very high validation rate obtainable under these conditions, relatively few samples were taken. For these reasons the background level of droplets is not considered a problem that effects the interpretation of the spray results.

Much of the last section has discussed the practical difficulties in using PDA to measure Diesel sprays and the likelihood that some measurements, particularly in the core of the spray, may have large uncertainties. Why then use PDA at all? Quite simply it is better than existing alternatives, because PDA measures droplets individually and no assumptions are made about the nature of the size distribution; this is an advantage that cannot be overstated. However, as has been demonstrated, the selection of droplets actually validated by the particular PDA counter may not be statistically representative of the spray as a whole and this fact probably has to be accepted; the centre of a Diesel spray is so dense and the droplets so close together that even with the smallest control volume only a low percentage of the droplets are validated. Anecdotal evidence that this is the case comes from PDA experiments on atmospheric rigs where, because of the higher velocities, the sprays are more 'spread out' and the droplet densities are lower; consequently, as would be expected validation rates are higher. Thus PDA results from a Diesel spray must be looked at in the context of knowledge of the uncertainties involved in the measurements and the values, particularly of SMD, at certain locations and times must be treated with caution.

Despite the above comments, PDA has proved to be a valuable technique in providing understanding of the structure and characteristics of Diesel sprays, while at the same time allowing the testing of the performance of the high pressure chamber under realistic density conditions and with production fuel injection systems.

# CHAPTER 5

# CONCLUSIONS AND RECOMMENDATIONS FOR FURTHER WORK

## 5.1 ACHIEVEMENTS AND CONCLUSIONS.

To improve combustion in modern Diesel engines and hence reduce harmful exhaust emissions, requires a thorough understanding of the processes involved in during fuel injection such as atomisation, droplet break-up and vaporisation and the subsequent combustion of the fuel. The study of this in a modern research environment involves, amongst other techniques, the use of laser diagnostics, which in turn requires the design and construction of specialised tools with a provision of optical access, such as optical engines and constant-volume chambers. Constant-volume chambers in particular offer a flexible measuring tool capable, if well designed, of simulating a variety of different chamber conditions from high pressure to low pressure, high temperature to low temperature and with either quiescent or swirling flow fields. The first part of this thesis has described the design, construction and testing of a particularly advanced type of chamber along with its auxiliary equipment. This chamber allows for the continuous flow of high pressure air through the chamber which can also be heated if work on vaporisation and/or combustion is required.

The study of sprays and combustion in constant-volume chambers is often hampered by the inability to produce single injections into the test equipment. This is necessary as continuous injection at normal running speeds results in too much fuel being injected, with insufficient flow of air through many chambers to allow proper scavenging of the combustion products. The thesis has described the development of a skip-firing valve which can be fitted to any pump-pipe-nozzle injection system and which can produce single injections, when required. An additional feature of the valve is that it allows the pump to be run at normal operating speeds and hence the

injections produced have very similar line pressure and needle lift traces to those of the standard system..

Before the Diesel sprays could be characterised in the constant-volume chamber, the pump and injectors needed to be calibrated, so that the variation of injection pressure, injection rate and needle lift with time, were known at each test condition used in the subsequent optical experiments in order to assist in the interpretation of the spray results. The calibration of two different Diesel injection pumps with their injectors has been completed using standard techniques.

The first experiments conducted in the chamber were those of imaging the sprays; this was done using both an 'Imacon' camera and a CCD camera. These experiments were conducted at the same conditions of the subsequent PDA measurements, but some additional tests at varying chamber pressure and the same load and speed were completed to study the effect of this variable on the spray development. The results of this imaging exercise were used to measure the tip penetration and cone angle under various conditions of pump speed, load and chamber pressure. This data was analysed and two predictive correlations were suggested which predict with reasonable accuracy the tip penetration and 'far' cone angle. The correlation for spray tip penetration was developed on the basis of Hiroyasu's correlation [*Hiroyasu and Arai,* 1990], whereas that for spray cone angle was developed from first principles.

Lastly, extensive PDA measurements of the sprays generated by both MW and EPVE pump based systems were obtained. The velocities of the droplets from these experiments followed the expected trends and it was shown that sprays injected at high pressure have much higher velocities towards the edge, with a 'top-hat' type velocity profile. This implies that there is a larger amount of air entrainment into these sprays due to the higher relative velocity between the spray and the surrounding air. The most interesting result from these tests was the lack of any substantial differences in the droplet diameters either in different regions of the spray or even at different loads and pump speeds (and hence injection pressure) which seems contradictory to relevant work in the literature that suggests injection pressure strongly influences the droplet SMD.

## 5.2 RECOMMENDATIONS FOR FURTHER WORK.

Since Chapter 2 detailed a number of suggested mechanical improvements to the high pressure chamber designed, manufactured and tested during this research program, this section will focus on recommendations for future study of Diesel sprays.

The constant-volume chamber detailed in Chapter 2 of this thesis was designed for combustion studies as well as non-combustion work. Clearly to prove the full capabilities of the chamber requires that both type of experiments are made and once this has been done there are many experiments which can be completed using higher temperatures. In general studies of vaporising sprays using PDA are not very common and often limited due to the number of cycles that can be completed before window fouling occurs. Of particular importance are the PDA measurements, with combustion or at least vaporising sprays, of the high-pressure injection systems used for the experiments so far, as there are few studies in the literature which have looked at high pressure injection system whose sprays may have quite different characteristics to those of more traditional injection systems.

As was alluded to in Chapter 4, very little work has been reported in the literature on the differences between hydraulically flipped sprays and more typical cavitating sprays. Hydraulically flipped sprays may be very poorly atomised and, if they occur regularly in production Diesel engines, may lead to poor combustion. To study such sprays would first require images of the sprays from the injector to be taken and the sprays with particularly low cone angle could then be investigated; however, it would probably be of interest to characterise all of the sprays as this would not involve a great deal of extra work and would also allow consistent differences between the holes to be measured.

Alternatively an investigation could be made of the effect of cavitation on spray characteristics by studying just one spray, but controlling a parameter which in turn effects the Cavitation number and hence the degree of cavitation. The two parameters that can be controlled easily are chamber pressure and injection pressure; the latter can be varied by changing pump speed and load or, more simply, by using a common-rail injection system where the injection pressure can be controlled (such common rail systems are ideal as they can produce perfect single shot injections).

Another point of interest is the amount of air entrainment into the spray and its effect on combustion. Anecdotal evidence suggests that this has a strong effect on the soot levels produced by Diesel engines and that dramatic reductions of the latter can be made by increasing the amount of air entrained in the spray. This may be difficult to measure using PDA as measurements of gas velocity close to the spray are likely to be difficult as stray droplets from the injection may overwhelm the measurements from seeding particles. It may be possible to look at the velocity of very small (< 2 μm) droplets near to the spray as these are likely to follow the air motion, this however, requires a very sophisticated PDA system to cope with such small diameters although the optical set-up could be tailored to suit these small droplets as the remaining part of the size range is of no interest. A further study of air entrainment could be made by enhancing the amount of air entrained in the spray by directing a jet of air into its core. A study could then be made of the amount of soot produced by the engine when this parameter was varied.

Multiple-stage injection systems, which can be electronically controlled to allow simultaneous reduction of NOx and particulates in Diesel engines, are expected to play an important part in enabling the DI Diesel engine to satisfy future emissions standards. Therefore an investigation of the spray characteristics and the subsequent combustion would be useful in providing a data base for designers of multiple-stage FIE and the engines to which they are fitted.

# REFERENCES

Aerometrics, (1990) *"Manual of PDPA system",* Aerometrics Inc., Sunnyvale, California, USA.

Arcoumanis, C., Whitelaw, J. H., Hentschel, W., Schindler, K-P., (1994) *"Flow and Combustion in a Transparent 1.9 Litre Direct Injection Diesel Engine",* Proc. Inst. Mech. E., Vol. 208.

Arcoumanis, C., Cutter, P. A., (1995) *"Flow and Heat Transfer Characteristics of Impinging Diesel Sprays Under Cross-Flow Conditions",* SAE 950448.

Arcoumanis, C., Bae, C., Nagwaney, A., Whitelaw, J.H ., (1995) *"Effect of EGR on Combustion Development in a 1.9L DI Diesel Optical Engine",* SAE 950850.

Arcoumanis, C., Gavaises, M., French, B., (1997) *"Effect of Fuel Injection Processes on the Structure of Diesel Sprays",* SAE 970799.

Bates, S. C., (1988) *"A Transparent Engine for Flow and Combustion Visualisation Studies",* SAE 880520.

Bickford, J. H., (1990) *"An Introduction to the Design and Behaviour of Bolted Joints",* Second edition, Marcel Dekker Inc.

Bosch, W., (1966) *"The Fuel Rate Indicator: A New Measuring Instrument for Display of the Characteristics of Individual Injection",* SAE 660749.

CompAir Reavell, (1990) *"Handbook on Reveall TC 3.5 Mk 7 Compressor",* Compair Reavell Ltd., Ipswich.

Carabell, K. D., Farrell, P. V., (1993) *"Air Fuel Ratio Visualisation in a Diesel Spray",* Paper Presented at Winter Anual Meeting, ASME.

Chang, J.-C., (1993) *"Diesel Spray Characteristics and Spray/Wall Heat Transfer",* PhD Thesis, Imperial College, University of London.

Dec, J. E., Espey, C., (1995) *"Ignition and Early Soot Formation in a DI Diesel Engine Using Multiple 2-D Imaging Diagnostics",* SAE 950456.

Dent, J. C., (1971) *"A Basis for the Comparison of Various Experimental Methods for Studying Spray Penetration",* Transactions of the SAE, Vol. 80, pp 1881-1884.

Domnick, J., (1997) *"Some Comments Concerning the State-of-the-art of Phase Doppler Anemometry Applied to Liquid Sprays",* Proceedings of 13th Annual Conference on Liquid Atomisation and Spray Systems, 9-11th July, Florence, Italy.

Ficarella, A., Laforgia, D., Starace, G.,Damiani V., (1997) *"Experimental Investigation of the Sprays of an Axi-Symetric Nozzle of a Common-Rail High Pressure Electro-Injector",* SAE 970054.

Giorgio, F. Di., Laforgia, D., Damiani, V., (1995) *"Investigation of Drop Size Distribution in the Spray of a Five-Hole, V.C.O. Nozzle at High Feeding Pressure",* SAE 950087.

Hallberg, M., Ångström, H-E., (1996) *"Design of Combustion Bomb used for High Resolution Photography of Diesel Sprays",* Royal Institute of Technology.

Hardalupas, Y., Taylor, A. M. K. P., Whitelaw, J. H., (1992) *"Characteristics of the Spray from a Diesel Injeector",* Int. J. Multiphase Flows, Vol 18, pp 159-179.

Hardalupas, Y., Laker, J. R., (1993) *"Description of the Thermofluids Section 'Model 3' Phase Doppler Counter",* Imperial college of Science, Technology and Medicine, Mechanical Engineering Dept., Thermofluids Section, London, June.

Hiroyasu, H., Arai, M., (1990) *"Structure of Fuel Sprays in Diesel Engines",* Transactions of the SAE, Vol.99, Sect 3, pp 1050-1061.

Iiyama, A., Matsumoto, Y., Kawamoto, K., Ohishi, T., (1992) *"Spray Formation Improvements of VCO Nozzle for DI Diesel Smoke Reduction",* I.Mech.E Seminar Diesel Fuel Injection Systems, April.

Karimi, E. R., (1989) *"High-Speed Photography of Fuel Spray and Combustion Events in a Production Diesel Engine and Combustion Bomb",* Proc I.Mech.E., Vol 203, pp269.

Koo, J-Y., Martin, J. K., (1990) *"Droplet Sizes and Velocities in a Transient Diesel Fuel Spray",* SAE 900397.

Koo, J-Y., Martin, J. K., (1991) *"Comparison of Measured Drop Sizes and Velocities in a Transient Fuel Spray with Stability Criteria and Computed PDF's",* SAE 910179.

Montgomery, D. T., Chan, M., Chang, C. T., Farrel, P. V., Reitz, R. D., (1996) "*Effect of Injector Nozzle Hole Size and Number on Spray Characteristics and the Performance of a Heavy Duty D.I. Diesel Engine*", SAE 962002.

Naber, F. S., Siebers, D. L., (1996) *"Effects of Gas Density and Vaporisation on Penetration and Dispersion of Diesel Sprays",* SAE 960034.

Nazha, M. A. A., Crookes, R. J., (1992) *"Design and Operation of a High-Pressure Combustion System for Study of Soot Formation",* SAE 922206.

Oren, D. J., Wahiduzzaman, S., Ferguson. C. R., (1984) *"A Diesel Combustion Bomb: Proof of Concept"*, SAE 841358.

Pitcher, G., Wigley, G., (1994a) *"Velocity and Dropsize Measurements in Fuel Sprays in a Diresl Injection Diesel Engine"*, International Symposium on LDA applied to Fluid Mechanics.

Pitcher, G., Wigley, G., (1994b) *"Sensitivity of Dropsize Measurements by Phase Doppler Anemometry to Refractive Index Changes in Combusting Fuel Sprays"*, International Symposium on LDA applied to Fluid Mechanics.

Pitcher, G., Wigley, G., (1994c) *"Two Componet Velocity and Size Measurements for a Non-Combusting Fuel Spray in a Diesel Swirl Combustin Chamber"*, Sixth International Conference on Liquid Atomisation and Spray Systems, 18-22 July.

Pitcher, G., Wigley, G., (1991) *"The Droplet Dynamics of Diesel Fuel Sprays Under Ambient and Engine Conditions"*, Laser Anemometry, Vol 2, ASME.

Rao, K. K., Winterbone, D. E., Clough, E., (1988) *"Laseer Illuminated Photographic Studies of the Spray and Combustion Phenomenon in a Small High Speed DI Diesel Engine"*, SAE 922203.

Reitz, R. D., (1988) *" Effects of Ambient Gas Conditions and Turbulence on Vaporising Sprays"*, GM Research Laboratories, Fluid Mechanics Dept, January 28.

Renner, G., Maly, R. R., (1994) *"Spray Structure of Automotive Injectors", International Symoposium on Advanced Spray Combustion"*, July 6-8, Hiroshima, Japan,.

Richman, R. M., Reynolds, W. C., (1984) *"The Development of a Transparent Cylinder Engine for piston Engine Fluid Mechanics Research"*, SAE 840379.

Rife, J., Heywood, J.B., (1974) *"Photographic and Performance Studies of Diesel Combustion with a Rapid Compression Machine"*, SAE 740948.

Roark, R. J., Young, W. C., (1975) *"Formulas for Stress and Strain"*, McGraw-Hill Inc.

Schmidt, Th., Esser-Schmittmann, W., Roosen, P., Hssel, E., Xu, H., Reuter, U., Scheid, E., (1988) *"Pressure Chamber Experiments for Fuel Spray Model Development"*, Report to the European Energy Commission.

Soteriou, C., Andrews, R., Smith, M., (1995) *"Direct Injection Diesel Sprays and the Effect of Cavitation and Hydrraulic Flip on Atomisation"*, SAE 950080.

Su, T. F., Farrel, P. V., Nagarajan, R. T., (1995) *"Nozzle Effect on High Pressure Diesel Injection"*, SAE 950083.

Takamura, A., Takashi, O., Fukushima, S., Kamimoto, T., (1992) *"A Study on Precise Measurement of Diesel Fuel Injection Rate"*, SAE 920630.

Wahiduzzaman, S., Ferguson, C. R., (1986) *"The Effects of Aspect Ratio on Heat Loss fom a Swirling Flow Within a Cylinder"*, Journal of Heat Transfer, Paper No. 86-F-172.

Warrick, C. B., Su, T. F., Farrell, P. V., (1996) *"Temperature Effects on Fuel Sprays from a Multi-Hole Nozzle Injector"*, SAE 962005.

Weiderhorn, S. M., Evans, A. G., Roberts, D. E., (1974) *"Fracture Mechanics of Ceramics"*, pp 829, Vol. II, Plenum Press, NY.

Wiartalla, A., Backer, H., Durnholz, M., (1995) *"Influence of Injection Parameters on Spray Development Combustion and Soot Formation by Optical Measurement Techniques in a Model Combustion Chamber"*, SAE 950233.

Wrangham, D. A., (1960) *"The Theory and Practice of Heat Engines"*, 2nd Edition, Cambridge Univ. Press, pp 577.

Zarzycki, J., (1982) *"Glasses and the Vitreous State"*, Cambridge Univ. Press.